

Optimization and prediction of a geofoam-filled trench in homogeneous and layered soil

Mehran Naghizadehrokni

▶ **To cite this version:**

Mehran Naghizadehrokni. Optimization and prediction of a geofoam-filled trench in homogeneous and layered soil. Environmental Sciences. RWTH Aachen, 2022. English. ⟨NNT : ⟩. ⟨tel-04033534⟩

HAL Id: tel-04033534

https://hal.science/tel-04033534v1

Submitted on 17 Mar 2023

HAL is a multi-disciplinary open access archive for the deposit and dissemination of scientific research documents, whether they are published or not. The documents may come from teaching and research institutions in France or abroad, or from public or private research centers.

L'archive ouverte pluridisciplinaire **HAL**, est destinée au dépôt et à la diffusion de documents scientifiques de niveau recherche, publiés ou non, émanant des établissements d'enseignement et de recherche français ou étrangers, des laboratoires publics ou privés.



HAL Authorization

Optimization and prediction of a geofoam-filled trench in homogeneous and layered soil

Von der Fakultät für Bauingenieurwesen der Rheinisch-Westfälischen Technischen Hochschule Aachen zur Erlangung des akademischen Grades eines Doktors der Ingenieurwissenschaften genehmigte Dissertation

vorgelegt von

Mehran Naghizadehrokni

Berichter: Univ.-Prof. Dr.-Ing. Martin Ziegler
Univ.-Prof. Dr.-Ing. Raul Fuentes
Univ.-Prof. Dr.-Ing. habil. Christos Vrettos

Tag der mündlichen Prüfung: 19.12.2022

- Diese Dissertation ist auf den Internetseiten der Universitätsbibliothek online verfügbar.

Table of Contents

List of Figures **V**

List of Tables **XI**

List of Symbols **XIV**

Abstract **XV**

Kurzfassung **XVII**

1 Introduction **1**

1.1 Background 1

1.2 Scope and objectives 3

1.3 Structure of thesis 3

2 Literature Review **5**

2.1 Wave 5

2.1.1 Seismic wave 7

2.2 Sources of ground-born vibration 11

2.3 Effect of vibration 13

2.4 Vibration mitigation 14

2.4.1 Measures at the source 14

2.4.2 Measures at the receiver 15

2.4.3 Measures at the transmission path 15

2.5 Wave interaction by trench 16

2.6 Vibration isolation through wave barriers 17

2.7 Geofoam 26

3 Genetic Algorithm and Artificial Neural Network **27**

3.1 Genetic Algorithm . . . 27
3.1.1 Fitness function . . . 29
3.1.2 Genetic operators . . . 30
3.1.3 Replacement . . . 37
3.2 Application of genetic algorithms . . . 38
3.3 Artificial Neural Network . . . 39
3.3.1 Neurons . . . 41
3.4 Feedforward networks . . . 44
3.4.1 Backpropagation . . . 45
3.4.2 Data preparation . . . 46
3.5 Application of ANN . . . 46
3.6 Response Surface Methodology . . . 47

4 Vibration screening in homogeneous soil 49
4.1 Problem definition . . . 49
4.2 Field test . . . 49
4.2.1 Site investigation . . . 49
4.2.2 Field test method and equipment . . . 50
4.2.3 Test results and discussion . . . 53
4.3 Numerical modelling . . . 56
4.3.1 Validation of finite element method . . . 58
4.4 Near field isolation (soft barrier) . . . 60
4.4.1 Single wall system . . . 61
4.4.2 Double wall system . . . 65
4.4.3 Triangular wall system . . . 70
4.4.4 Comparison of different systems . . . 72
4.5 Far field isolation (soft barrier) . . . 74
4.5.1 Single-wall study . . . 74
4.5.2 double-wall barrier . . . 76
4.5.3 Triangular wall barrier . . . 78

4.5.4 Comparison of different systems . . . 79
4.6 Near field isolation (stiff barrier) . . . 81
4.6.1 Single wall barrier . . . 81
4.6.2 Double wall barrier . . . 82
4.6.3 Triangular wall barrier . . . 83
4.7 Conclusion . . . 84

5 Shape optimization of the trench by genetic algorithm 87
5.1 Introduction: . . . 87
5.2 Problem definition . . . 87
5.3 Finite element model . . . 87
5.4 Effect of cross-sectional area . . . 88
5.5 Genetic algorithm . . . 90
5.5.1 Implementation of genetic algorithm . . . 91
5.6 Genetic algorithm model for near field isolation . . . 91
5.6.1 Comparison between different systems (near field) . . . 93
5.7 Genetic algorithm model for far field isolation . . . 94
5.8 Conclusion . . . 95

6 Vibration screening in layered soil 97
6.1 Problem definition . . . 97
6.2 Homogeneous soil versus layered soil . . . 99
6.3 Single parametric study . . . 101
6.3.1 Influence of the depth and width of the barrier . . . 104
6.3.2 Influence of the shear wave velocity of the first layer . . . 106
6.3.3 Influence of the thickness of the first layer . . . 107
6.3.4 Influence of the location of the barrier . . . 107
6.3.5 Influence of the density of the geofoam . . . 108
6.4 Interaction between different parameters . . . 109
6.4.1 Interaction of D and V_s . . . 114
6.4.2 Interaction of V_s and L . . . 116

6.4.3 Interaction of X and V_s . . . 117
6.4.4 Interaction of X and D . . . 119
6.4.5 Interaction of X and L . . . 119
6.4.6 Interaction of three parameters on each other . . . 120
6.5 Conclusion . . . 121

7 Optimization and prediction of the trench in layered soil 123
7.1 Implementation of genetic algorithm . . . 123
7.1.1 Results . . . 124
7.1.2 Implementing feedforward neural network . . . 127
7.1.3 Results . . . 128
7.1.4 Validating ANN model . . . 131
7.2 Conclusion . . . 132

8 Summary, conclusions, and recommendations 135
8.1 Summary and conclusion . . . 135
8.2 Recommendations for future work . . . 139

9 Bibliography 141

Publications 151

A Guidelines for Python scripting 155

B Genetic algorithm code for homogeneous soil 165

C Plaxis script for layered soil 173

D Artificial Neural Network 175

E Genetic algorithm code for layered soil 179

F Developing an app for predicting and optimizing the vibration 185

G Diagrams of parametric study for layered soil 195

List of Figures

Figure 2.1 Harmonic load as a function of time [E Richart, 1970] 5
Figure 2.2 Different types of motion [E Richart, 1970] 6
Figure 2.3 Particle motion of body waves; a: P-wave b: S-wave [Developers, 2017] . 7
Figure 2.4 Particle motion of surface waves; a: Rayleigh-wave b: Love-wave [Developers, 2017] 8
Figure 2.5 Distribution of displacement waves from a circular footing on a homogeneous, isotropic and elastic half-space [Woods, 1968] 9
Figure 2.6 Variation of damping ratio with frequency [Orcaflex, 2010] 11
Figure 2.7 Wave interference phenomena 17
Figure 2.8 Stress-strain response of EPS [Stark et al., 2012] 26

Figure 3.1 Example of gene, chromosome and population in vibration isolation problem 28
Figure 3.2 Binary encoding representation 28
Figure 3.3 Floating encoding representation 29
Figure 3.4 Generate an initial population randomly for GA between the defined ranges 29
Figure 3.5 Calculated efficiency of each chromosome 30
Figure 3.6 Roulette wheel selection 31
Figure 3.7 Stochastic universal method 32
Figure 3.8 Tournament selection method 33
Figure 3.9 Example of single point crossover and create children 33
Figure 3.10 Example of two points crossover and create children 34
Figure 3.11 Example of uniform crossover and create children 34
Figure 3.12 Selected parents and new generated children after applying crossover . . 35
Figure 3.13 Example of flipping mutation and create child 36
Figure 3.14 Example of reversing mutation and create child 36
Figure 3.15 Example of uniform mutation and create child 36

Figure 3.16 Example of gaussian mutation and create child 37

Figure 3.17 Mating pool, selected children for applying mutation and the mutated children 37

Figure 3.18 New mating pool 37

Figure 3.19 Initial population and the new generated population 38

Figure 3.20 Classification of artificial intelligence [Kim, 2017] 39

Figure 3.21 Evaluating a model based on field data [Gurney, 1997] 40

Figure 3.22 A biological neuron [W and WM, 2002] 41

Figure 3.23 A single perceptron [Gurney, 1997] 42

Figure 3.24 Activation functions in artificial neural networks 43

Figure 3.25 A multi-layered feedforward neural network 44

Figure 4.1 Shear wave velocity profile of the site [Sprengel, 2017] 50

Figure 4.2 Vibration source: (A) Shaker structural dynamics Heiland & Mistler GmbH, (B) Vibration sensor 51

Figure 4.3 Measuring arrangement 51

Figure 4.4 Wheel trench device and injection of geofoam 52

Figure 4.5 Representation in the frequency domain: Measuring points C, D, E, G (Near field Isolation) 54

Figure 4.6 Representation in the frequency domain: Measuring points C, D, E, G (Far field Isolation) 54

Figure 4.7 Influence of normalized barrier depth on $\overline{A}_r$ ($X = 0.5$) 55

Figure 4.8 Automation process of FE model through connecting Plaxis to Python . 58

Figure 4.9 Validation of numerical modelling based on the result of field test, near field isolation, (D=3m, W=0.25m, L=10m, X=2m) 59

Figure 4.10 Validation of numerical modelling based on the result of field test, far field isolation (D=3m, W=0.25m, L=10m, X=12m) 59

Figure 4.11 Near field isolation case, comparative study of vibration isolation by open trench ($W = 0.06$, $D = 0.5$, $X = 0.4$) 60

Figure 4.12 Far field isolation case, comparative study of vibration isolation by open trench ($W = 0.1$, $D = 1$, $X = 5$) 61

Figure 4.13 Normalized soil particle velocity amplitude of ground surface with and without barrier, at the line parallel to the vibration source ($D = 1$, $W = 0.075$, $L = 2.5$, $X = 0.5$, Frequency= $50Hz$) 62

Figure 4.14 Influence of normalized barrier length on $\overline{A}_r$ ($X = 1.25$, $D = 1.25$) 62

Figure 4.15 Influence of normalized barrier depth on $\overline{A}_r$ ($X = 0.5$) 63

Figure 4.16 Influence of normalized barrier depth on $\overline{A}_r$ ($X = 2$) 63

Figure 4.17 Influence of normalized barrier width on $\overline{A}_r$ ($X = 0.5$) 64

Figure 4.18 Influence of normalized barrier location on $\overline{A}_r$ ($W = 0.1875$) 64

Figure 4.19 Influence of normalized barrier spacing on $\overline{A}_r$ ($D = 1$, $W = 0.075$, $L = 2.5$ and $X = 1.25$) 65

Figure 4.20 Normalized soil particle velocity amplitude of ground surface with and without barrier, at the line parallel to the vibration source ($D = 1$, $W = 0.075$, $L = 2.5$, $X = 0.5$, Frequency= $50Hz$) 66

Figure 4.21 Influence of normalized barrier length on $\overline{A}_r$ ($X = 1.25$, $D = 1.25$) 66

Figure 4.22 Influence of normalized barrier depth on $\overline{A}_r$ ($X = 0.5$) 68

Figure 4.23 Influence of normalized barrier width on $\overline{A}_r$ ($X = 0.5$) 69

Figure 4.24 Influence of normalized barrier width on $\overline{A}_r$ ($X = 1.25$) 69

Figure 4.25 Influence of normalized barrier location on $\overline{A}_r$ ($W = 0.0625$) 70

Figure 4.26 Influence of normalized barrier depth on $\overline{A}_r$ ($X = 0.5$) 71

Figure 4.27 Influence of normalized barrier depth on $\overline{A}_r$ ($X = 2$) 72

Figure 4.28 Influence of normalized barrier width on $\overline{A}_r$ ($X = 0.5$) 72

Figure 4.29 Influence of normalized barrier width on $\overline{A}_r$ ($X = 2$) 73

Figure 4.30 Comparison between different systems ($X = 2$) 73

Figure 4.31 Normalized soil particle velocity amplitude of ground surface with and without barrier, along the line parallel to the vibration source ($D = 1$, $W = 0.075$, $X = 3$, Frequency= $50Hz$) 75

Figure 4.32 Influence of normalized barrier depth on $\overline{A}_r$ ($X = 4$) 75

Figure 4.33 Influence of normalized barrier width on $\overline{A}_r$ ($X = 3$) 76

Figure 4.34 Influence of normalized barrier depth on $\overline{A}_r$ ($X = 4$) 77

Figure 4.35 Influence of normalized barrier width on $\overline{A}_r$ ($X = 3$) 77

Figure 4.36 Influence of normalized barrier depth on $\overline{A}_r$ ($X = 3$) 78

Figure 4.37 Influence of normalized barrier depth on $\overline{A}_r$ ($X = 4$) 79

Figure 4.38 Comparison of different systems 79

Figure 4.39 Influence of normalized barrier width on $\overline{A}_r$ ($X = 4$) 80

Figure 4.40 Normalized soil particle velocity amplitude of ground surface with and without concrete barrier, at the line parallel to the vibration source ($D = 1$, $W = 0.075$, $L = 2.5$, $X = 0.5$) 81

Figure 4.41 Influence of normalized barrier depth on $\overline{A}_r$ ($X = 0.5$) 82

Figure 4.42 Influence of normalized barrier depth on $\overline{A}_r$ ($X = 0.5$) 83

Figure 4.43 Influence of normalized barrier width on $\overline{A}_r$ ($X = 0.5$) 83

Figure 4.44 Influence of normalized barrier depth on $\overline{A}_r$ ($X = 0.5$) 84

Figure 4.45 Influence of normalized barrier width on $\overline{A}_r$ ($X = 0.5$) 84

Figure 5.1 Different shapes of trench 87

Figure 5.2 Mesh convergence study 89

Figure 5.3 Proposed FE model and material properties 89

Figure 5.4 Calculated value of efficiency of the geofoam-filled trench for different trench dimensions ($X = 5$ m, $L = 10$ m), near field system 90

Figure 6.1 Reflection and refraction process of the incident elastic waves 98

Figure 6.2 Penetration of R-wave in different layers 99

Figure 6.3 Vertical amplitude of ground vibration for homogeneous and layered soil 100

Figure 6.4 Proposed vertical harmonic load as vibration source 101

Figure 6.5 Schematic view of Plaxis model and selected parameters 102

Figure 6.6 Influence of depth on the efficiency ($X = 0.75$, $L = 0.5$, EPS= 15) 104

Figure 6.7 Influence of depth on the efficiency ($X = 1.5$, $L = 0.5$, EPS= 15) 105

Figure 6.8 Influence of shear wave velocity of the first layer ($X = 0.75$, $W = 0.075$, EPS= 15) 106

Figure 6.9 Influence of shear wave velocity of the first layer ($X = 2.25$, $W = 0.075$, EPS= 15) 108

Figure 6.10 Influence of normalized thickness of the first layer ($W = 0.075$, EPS= 15) 109

Figure 6.11 Influence of normalized location of the trench ($W = 0.075$, $V_s = 200m/s$, EPS= 15) 110

Figure 6.12 Influence of normalized location of the trench ($W = 0.075$, $V_s = 350m/s$, EPS= 15) 111

Figure 6.13 Calculated results obtained by FEM versus predicted results obtained by model 115
Figure 6.14 Interaction of D and V_s on the response of the trench ($X = 2.25$) 115
Figure 6.15 Interaction of D and V_s on the response of the trench ($X = 3.75$) 116
Figure 6.16 Interaction of V_s and L on the response of the trench ($X = 0.75$) 117
Figure 6.17 Interaction of V_s and L on the response of the trench ($X = 2.25$) 118
Figure 6.18 Interaction of V_s and X on the response of the trench ($D = 1.125$, $L = 1.5$) 118
Figure 6.19 Interaction of X and D on the response of the trench ($V_s = 200m/s$) . . 119
Figure 6.20 Interaction of X and L on the response of the trench 120
Figure 6.21 Interaction of X, D, and L on the efficiency of the trench 121

Figure 7.1 The architecture of developed ANN 128
Figure 7.2 Performance of the network for training, validation and test datasets . . 129
Figure 7.3 Extracted outputs and targets of all the data 130
Figure 7.4 Results of subsets including training, validation and testing data 131
Figure 7.5 Calculated R-value for the validation data 132
Figure 7.6 Predicted and real value of the efficiency of geofoam-filled trench 132

Figure 9.1 Configure remote scripting server window 156
Figure 9.2 Homepage of vibration isolation app 188
Figure 9.3 Homepage of Plot section in the app 189
Figure 9.4 Homepage of prediction section in the app 190
Figure 9.5 Homepage of optimization section in the app 191
Figure 9.6 Homepage of neural network section in the app 192
Figure 9.7 Interaction of D and L on the response of the trench ($X = 0.75$) 195
Figure 9.8 Interaction of D and L on the response of the trench ($X = 2.25$) 196
Figure 9.9 Interaction of D and L on the response of the trench ($X = 3.75$) 196
Figure 9.10 Interaction of D and W on the response of the trench ($X = 2.25$) 197
Figure 9.11 Interaction of D and EPS on the response of the trench ($X = 2.25$) . . . 197
Figure 9.12 Interaction of V_s and L on the response of the trench ($X = 3.75$) 198
Figure 9.13 Interaction of V_s and EPS on the response of the trench ($X = 2.25$) . . . 198

Figure 9.14 Interaction of V_s and X on the response of the trench ($D = 1.75$) 199
Figure 9.15 Interaction of W and EPS on the response of the trench ($X = 2.25$) . . . 199
Figure 9.16 Interaction of W and L on the response of the trench ($X = 2.25$) 200
Figure 9.17 Interaction of W and V_s on the response of the trench ($X = 2.25$) 200
Figure 9.18 Interaction of X and D on the response of the trench ($V_s = 250$) 201
Figure 9.19 Interaction of X and D on the response of the trench ($V_s = 300$) 201
Figure 9.20 Interaction of X and D on the response of the trench ($V_s = 350$) 202
Figure 9.21 Interaction of X and D on the response of the trench ($V_s = 400$) 202
Figure 9.22 Interaction of X and EPS on the response of the trench ($D = 1.125$) . . . 203
Figure 9.23 Interaction of X and L on the response of the trench ($D = 1.125$) 203
Figure 9.24 Interaction of X and L on the response of the trench ($D = 1.125$) 204
Figure 9.25 Interaction of X and L on the response of the trench ($D = 1.125$) 204
Figure 9.26 Interaction of X, D and V_s on the efficiency of the trench 205
Figure 9.27 Interaction of X, L and V_s on the efficiency of the trench 205

List of Tables

Table 2.1 Vibration magnitude and perception (sinusoidal vibration) [Parsons and Griffin, 1988] 13

Table 2.2 Summary of literature review 20

Table 2.3 EPS geofoam properties [D6817-13, 2013] 26

Table 3.1 Defined ranges for the selected parameters 28

Table 3.2 Different types of neural network and their application 41

Table 3.3 Analogy between the human brain and artificial neural network 41

Table 4.1 material properties of Proposed FE model 58

Table 4.2 Properties of near field and far field system for validation 60

Table 4.3 Properties of soil and concrete 81

Table 5.1 The range for different parameters 91

Table 5.2 Optimized dimensions of the trench for different systems (geofoam, 50Hz) 92

Table 5.3 Optimized dimensions of the trench for different systems (concrete, $50Hz$) 92

Table 5.4 Optimized dimensions of the trench for different systems for $\overline{A_r} = 0.75$, geofoam 93

Table 5.5 Optimized dimensions of the trench for different systems (geofoam $50Hz$) 94

Table 5.6 Optimized dimensions of the trench for different systems (concrete $50Hz$) 95

Table 6.1 Ranges of different parameters in the parametric study 103

Table 6.2 Values of different parameters 111

Table 6.3 Comparison of different mathematical model 112

Table 6.4 ANOVA for the quartic model of vibration isolation problem 113

Table 6.5 Result of calculating the efficiency of the trench with the developed model and Plaxis 114

Table 7.1 The selected parameters and their boundaries in the optimization process 123

Table 7.2 Optimized dimensions of the trench for different systems (geofoam, $50Hz$) 125
Table 7.3 Optimized dimensions of the trench for different systems (geofoam, $50Hz$) 125
Table 7.4 Optimized dimensions of the trench for different frequencies 126
Table 7.5 Governing factors and the ranges in ANN 127
Table 7.6 Performance of the network for in training, validating and test data . . . 130

Listings

9.1 Configure remote scripting server window . . . 156
9.2 Start a new project and create borehole . . . 157
9.3 Start a new project and create borehole . . . 157
9.4 Create plate and assign the material . . . 158
9.5 Install the trench and assign the material . . . 159
9.6 Create surface load . . . 159
9.7 Generate mesh . . . 159
9.8 Define different phases and run the model . . . 160
9.9 Open the output page . . . 162
9.10 Calculate the efficiency of the trench . . . 162
9.11 Collect the data . . . 163
9.12 Save the data . . . 163
9.13 Generating random chromosomes for initial population . . . 165
9.14 Defining mutation function . . . 165
9.15 Defining crossover function . . . 166
9.16 Selection . . . 166
9.17 Genetic Algorithm main code . . . 166
9.18 Plaxis automation for layered soil . . . 173
9.19 Main body of the code . . . 175
9.20 Activation functions . . . 176
9.21 Main body of the code . . . 179
9.22 Define operators of GA . . . 181

List of Symbols

Latin Symbols		
ω	[radians]	Circular frequency
T	[s]	Period of vibration
φ	$[-]$	Phase angle
E_d	$[-]$	Energy dissipated
E_s	$[-]$	Peak strain energy
A_0	$[m]$	Initial wave amplitude
ξ	$[-]$	Damping ratio
C	$[-]$	Damping matrix
K	$[-]$	Stiffness matrix
M	$[-]$	Mass matrix
PPV	$[m/s]$	Peak particle velocity
Z	$[-]$	Acoustic impedance
λ	$[m]$	Wavelength
RSM	$[-]$	Response surface methodology
GA	$[-]$	Genetic algorithm
P_m	$[-]$	Mutation probability
P_c	$[-]$	Crossover probability
FS	$[-]$	Safety factor
FEM	$[-]$	Finite element method
AI	$[-]$	Artificial inteligence
ML	$[-]$	Machine learning
ANN	$[-]$	Artificial neural network
ρ	$[Kg/m^3]$	Density of soil
MASW	$[-]$	Multichannel analysis of surface waves
DFT	$[-]$	Discrete fourier transformation
$\overline{A}_r$	$[-]$	Average amplitude reduction ratio
V_p	$[m/s]$	Primary wave velocity
V_s	$[m/s]$	Secondary wave velocity
$\dot{v}$	$[-]$	Normal velocities
$\dot{u}$	$[-]$	Tangential velocities
I_e	$[-]$	Average element size

Abstract

In metropolitan cities, man-made ground vibrations generated by external dynamic sources including traffic, blasting, machine foundations, and other constructional activities have recently become a major concern for the nearby structures and inhabitants. Most of the transmitted vibration energy is propagated by Rayleigh waves close to the soil surface. The rest of the energy is transmitted by body waves. Therefore, implementing a wave barrier in the transmission path is a suitable solution as it allows scattering the ground-borne vibrations.

This study presents the performance of geofoam-filled trenches in mitigating ground vibration transmissions by the means of a comprehensive parametric study. Fully automated 2D and 3D numerical models are applied to evaluate the screening effectiveness of the trenches in the near field and far field schemes. The validated model is used to investigate the influence of geometrical and dimensional features on the trench with three different configurations including single, double, and triangular wall obstacles. The parametric study is based on complete automation of the model through coupling finite element analysis software (Plaxis) and Python programming language to control input, change the parameters, as well as to produce output and calculate the efficiency of the barrier. The main assumption during the parametric study is treating each parameter as an independent variable and keeping other parameters constant.

An optimization model is also presented to optimize the governing factors of geofoam or concrete-filled trenches as a wave barrier. A genetic algorithm code is implemented with coupling the Python software and the finite element program (Plaxis) for optimization of all parameters mutually. Furthermore, three different configurations including single, double, and triangular wall systems are evaluated with the same cross-sectional area for considering the effect of the shape of the barrier in attenuating the incoming waves.

A usual assumption for the study of ground-borne vibration is considering soil as homogeneous, which is unrealistic. Therefore, it is necessary to find the effect of non-homogeneity of the soil on the efficiency of the geofoam-filled trench. A comprehensive parametric study has been performed automatically by coupling Plaxis and Python under the assumption of treating each parameter as an independent variable. The results showed that some parameters have a considerable impact on each other.

Therefore, the interaction of all governing parameters on each other is also evaluated through the response surface methodology method. In addition, a genetic algorithm code is presented for optimizing all parameters mutually in homogeneous and layered soil. The results showed that layered soil requires a deeper trench for reaching the same value of the efficiency as in homogeneous soil. An artificial neural network model and a quartic polynomial equation are developed in order to estimate the efficiency of the geofoam-filled barrier. The agreement between the results of numerical modelling and the developed models demonstrated the capability of the models in predicting the efficiency of the geofoam-filled trench.

Finally, an application has been developed to easily use and share all developed models and data. The user can install and use the app to access all data, predicting the efficiency of the trench and optimizing the governing parameters.

Kurzfassung

In Großstädten und an anderen Stellen sind in jüngster Zeit vom Menschen verursachte Bodenvibrationen, die durch externe dynamische Quellen wie Verkehr, Sprengungen, Maschinenfundamente und andere bauliche Aktivitäten hervorgerufen werden, zu einem großen Problem für die nahe gelegenen Strukturen und Bewohner geworden. Der größte Teil der übertragenen Schwingungsenergie wird durch Rayleigh-Wellen nahe der Bodenoberfläche übertragen. Der Rest der Energie wird durch Körperwellen übertragen. Oberflächennahe Vibrationen können für die umliegenden Gebäude und ihre Bewohner ein großes Problem darstellen. Daher ist die Implementierung einer Wellenbarriere im Übertragungsweg eine geeignete Lösung, da sie eine Streuung der Bodenschwingungen ermöglicht.

Diese Studie stellt die Leistung von schaumgefüllten Gräben bei der Minderung von Bodenvibrationsübertragungen anhand einer umfassenden Parameter Studie vor. Vollautomatische numerische 2D- und 3D-Modelle werden zur Bewertung der Abschirm-Effektivität der Gräben im aktiven und passiven System eingesetzt. Das validierte Modell wird zur Untersuchung des Einflusses von geometrischen und dimensionalen Merkmalen auf den Graben mit drei verschiedenen Konfigurationen verwendet, darunter Einzel- und Doppelwände, sowie dreiecksförmige Wände. Die Parameter Studie basiert auf einer vollständigen Automatisierung des Modells durch die Kopplung von Finite-Elemente-Analyse-Software (Plaxis) und der Programmiersprache Python zur Steuerung der Eingabe, zur Änderung der Parameter sowie zur Erzeugung der Ausgabe und zur Berechnung der Effizienz der Barriere. Die Hauptannahme bei der parametrischen Studie ist, jeden Parameter als unabhängige Variable zu behandeln und andere Parameter konstant zu halten.

Es wird ein Optimierungsmodell vorgestellt, um die bestimmenden Faktoren eines mit Geoschaum oder eines mit Beton gefüllten Grabens als Wellenbarriere zu optimieren. Es wird ein genetischer Algorithmuscode mit Kopplung der Python-Software und der Finite-Elemente-Programm-Plaxis zur gegenseitigen Optimierung aller Parameter implementiert. Darüber hinaus werden drei verschiedene Konfigurationen mit Einzel- und Doppelwänden, sowie dreiecksförmige Wände ausgewertet, um den Einfluss der Form der Barriere auf die Dämpfung der einfallenden Wellen zu berücksichtigen.

Eine übliche Annahme bei der Untersuchung von Bodenschwingungen ist es, den Boden als homogen zu betrachten, was aber unrealistisch ist. Daher liegt das Hauptaugenmerk dieser Studie darin, den Einfluss der Inhomogenität des Bodens auf die Effizienz des mit Geoschaum gefüllten Grabens zu ermitteln. Eine umfassende parametrische Studie wurde durch Kopplung von Plaxis und Python durchgeführt, wobei die Interaktion aller maßgebenden Parameter aufeinander durch die Methode der Response Surface Methodik dargestellt wird. Es wird auch ein genetischer Algorithmuscode zur gegenseitigen Optimierung aller Parameter in homogenem und inhomogenem Boden vorgestellt. Die Ergebnisse zeigten, dass bei inhomogenem Boden ein tief-

erer Graben erforderlich ist, um den gleichen Wert der Effizienz wie bei homogenem Boden zu erreichen. Ein künstliches neuronales Netzmodell und ein Ausgleichspolynom werden entwickelt, um die Effizienz der mit Geoschaum gefüllten Barriere abzuschätzen. Die Trennung zwischen den numerischen Modellierungsergebnissen und den entwickelten Modellen demonstrieren die Fähigkeit der Modelle, die Effizienz des mit Geoschaum gefüllten Grabens vorherzusagen. Schließlich wurde eine Anwendung entwickelt, die eine einfache und gemeinsame Nutzung aller entwickelten Modelle und Daten ermöglicht. Der Benutzer kann die App installieren und nutzen und dabei auf alle Daten zugreifen, um die Effizienz des Grabens vorherzusagen und die variierbaren Parameter zu optimieren.

1 Introduction

1.1. Background

The number of people who are interested in living in big towns is increasing. This growth in population results in construction of more buildings and transport networks in and around the city. Therefore, residences will have more vibration problems from the vibration sources like passing trains, machine foundation, traffic, and other constructional activities. The body and Rayleigh waves produced from these sources result in ground-born vibration.

The vibration is transmitted through the ground surface to the foundation of the building and creates distress to the buildings and their inhabitants. There are some mitigation measures can be applied to either the vibration source or at the receiver. The installation of a wave barrier between the vibration source and the building is an alternative method to mitigate ground vibration. This study deals with mitigation measures in the transmission path through installing a geofoam-filled barrier.

The trench is used to attenuate the incoming waves and through complex effects, considerable mitigation of ground-borne vibration beyond the trench is attained. The incident waves tend to bend around the edge of the trench. Therefore, the barrier must be constructed deep enough to attenuate the incoming waves. Open trenches are the most effective system in terms of mitigating the ground-borne vibration for relatively short wavelength [Esmaeili et al., 2014; **?**; Garinei et al., 2014]. However, open trenches are not applicable in many cases for a longer time due to stability problems. In such case, in-filled trenches are more preferred [Naghizadehrokni et al., 2020].

Vibration isolation is classified into two different categories including the near field scheme, in which the wave barrier is installed near the vibration source and, the far field scheme where the barrier is constructed far away from the vibration source. In the case of the near field scheme, the body waves are more prominent in comparison with the surface waves whereas for the far field scheme, the main purpose is attenuating the surface waves (specially Rayleigh wave). Several studies have been performed in the last years in order to better understand vibration scattering phenomenon by a wave barrier.

Different approaches including experimental and numerical methods have been carried out to solve the problem of vibration isolation by trench. Since experimental tests are expensive and the parameters to be assessed are fixed, a numerical model is an effective alternative method for assessing governing parameters.

Woods conducted a series of field tests for evaluating the efficiency of the open trench for both near field and far field systems and suggested that a 75% reduction in incoming waves is enough to have a successful system [Woods, 1968].

Periodic geofoam-filled trenches were applied for screening train-induced ground vibration and results showed that the proposed periodic geofoam-filled trenches can attenuate surface waves effectively, when the frequencies of surface waves are located in the attenuation zones. In addition, they concluded that increasing the depth of the barrier up to one λ_r is enough to reach the highest value of efficiency and a further increase in depth does not have an effect on isolation capability for both near field and far field systems [Pu et al., 2018].

A full experimental and numerical study were investigated by [Alzawi, 2011] to assess the efficiency of open and geofoam-filled barrier for both near field and far field schemes. In their experiments, barrier dimensions and location from vibratory source on screening efficiency were examined. Results showed that the geofoam filled trench can be used as an effective wave barrier to scatter the induced ground vibration. They concluded that the normalized depth of 0.6 was selected as an optimum depth for both open and geofoam-filled trench. Moreover, a comparison was conducted between the field measurements and numerical results by a two-dimensional (2D) finite element model, and good agreement was found.

In addition, numerical techniques including the finite element method (FEM) and the boundary element method (BEM) can be used as powerful tools to study the screening performance of wave barriers. Beskos et al. [Beskos et al., 1986; Leung et al., 1991] developed a BEM model to determine the screening capability of open and concrete-filled trenches in homogeneous and layered soil for both near field and far field vibration isolation. It was found that open trenches are more effective than infilled trenches but they present wall instability problems. Moreover, it was concluded that in the case of layered soils, deeper trenches are required in continuously nonhomogeneous soils for achieving the same degree of wave screening effectiveness as in homogeneous soils.

Ahmad and Al-Hussaini [Ahmad and Al-Hussaini, 1991] conducted an extensive parametric study to analyse the influence of different geometrical and material parameters on the screening efficiency of rectangular open and concrete-filled obstacles in homogeneous soil. In addition, they developed a simple model for vibration isolation in near field and far field schemes. The results illustrated that the normalized depth D is the governing factor for open trench and normalized width W is not important, except for shallow depths ($D < 0.8$). However, for in-filled trenches, both depth and width are equally important.

The most important parameters for the design of an efficient barrier are the location and the geometry of the barrier, mainly depth and width. However, it is not possible to install an extremely deep and wide trench because of some practical reasons. Therefore, it is necessary to design a trench with acceptable geometry dimensions for improving the performance of the barrier.

Another unclear issue in wave attenuation is evaluating the mutual influence of multiple parameters. Generally, the dimensional and geometrical parameters of the trench are considered to be the most important factors that affect the vibration isolation performance. Most of the previous researches are only involve single parametric studies and they suggest an optimum parameter without considering the effect of other parameters. Therefore, a lack of mutual influence of all parameters is still observed since the most important problem in vibration isolation is that it

is not possible to treat each parameter as an independent variable.

The investigations on the problem of vibration isolation are usually done based on the idealised situation of homogeneous half-space with constant properties of elastic parameters over the depth, which is not realistic. In nature, however, the shear modulus of the soil usually changes with depth while the mass density and other properties of the soil can be considered approximately as a constant value. Dynamic properties and non-homogeneity of the soil play a significant role in transferring dynamic energy. Therefore, evaluating the effectiveness of the geofoam-filled trench as a soft barrier in layered soil provides a more realistic behaviour of the vibration isolation system.

A previous research project conducted by Julian Sprengel [Sprengel, 2017] at the chair of Geotechnical Engineering of RWTH Aachen found Polyurethane (PU) foam as a proper material for filling the trench, due to its low density and stiffness. In addition, an injection technique had been developed for installing the geofoam-filled trench in the transmission area. In this context, the proof of its practicability as well as the efficiency of the geofoam-filled trench had been provided.

1.2. Scope and objectives

To address the aforementioned research gaps, the fundamental objective of this study is to improve the available knowledge on the performance of a geofoam-filled barrier in screening waves generated from the steady-state foundation vibration. The main objectives of this research include:

- Investigating the effectiveness of different configurations of the geofoam-filled barrier including the single, double and triangular wall systems in homogeneous soil as near field and far field systems.
- Finding the effect of a non-homogeneity of the soil on the efficiency of the geofoam-filled trench.

1.3. Structure of thesis

This dissertation has been prepared according to the guidelines of the faculty of civil engineering at RWTH Aachen University for obtaining the degree of Doctor of Engineering. Some parts of these chapters have been either published, accepted, or submitted for possible publication in peer-review journals and international conferences. The dissertation includes 8 chapters, which present a comprehensive parametric study on attenuating incoming waves by a trench in homogeneous and layered soil and provide some recommendations and design guidelines for implementing a successful system.

The dissertation is organized as follows:

Chapter 1 defines the vibration isolation problem and describes the necessity of the present work. In addition, the objectives and the contents of the work are briefly summarized.

Chapter 2 deals with the fundamental theory of wave and wave propagation in an elastic half-space medium and listing different types of vibration sources. In addition, it provides the literature survey of the previous studies on vibration isolation by a wave barrier followed by some information about the the properties of geofoam material properties.

The principal of genetic algorithm, artificial neural network and responce surface methodology are presented in Chapter 3.

Chapter 4 presents the results of a field test and a comprehensive parametric study. The results of the field test for evaluating the efficiency of a geofoam-filled barrier in mitigating the incident waves in the frequency domain are presented. $2D$ and $3D$ finite element models are developed and the validity of the models are compared with the results of the full experimental test. Subsequently, different configurations including single, double, and triangular wall systems are selected to evaluate the performance of vibration screening in the near field and far field schemes, respectively. Various parameters including geometrical parameters and dimensional factors that govern the screening performance are considered for further assessment.

An approach is proposed in Chapter 5 by coupling a FEM, with a genetic algorithm through Python programming language to an optimized configuration of the geofoam and concrete-filled barriers in homogeneous soil. The finite element model is developed and verified. The implementation of the proposed genetic algorithm model is described. Finally, the developed genetic algorithm code is used for finding the optimized parameters of different configurations in the case of near field and far field systems. These results are presented through some diagrams and tables.

In Chapter 6, a comprehensive parametric study is conducted in layered soil to evaluate the efficiency of the geofoam-filled trench as a wave barrier in layered soil. In addition, the governing parameters on the screening performance are introduced through a single parametric study. Finally, the interaction between the key parameters is considered through a response surface methodology and one polynomial quartic model is presented for predicting the efficiency of the trench.

A model is developed in Chapter 7 for mutual optimization of all parameters in layered soil with the help of FEM, Python, and a genetic algorithm model. In addition, the optimized parameters for different frequencies for homogeneous and layered soil are also presented. Finally, a model is developed based on artificial neural networks for predicting the efficiency of the geofoam-filled trench based on the result of extensive parametric study in Chapter 6.

Finally, in Chapter 8, general conclusions on the effectiveness of using a geofoam-filled trench in homogeneous and layered soil along with some guidelines are presented and prospects for future research are outlined.

2 Literature Review

2.1. Wave

In science, a wave is defined as a disturbance involving the transfer of energy from one place to another. A wave requires a medium to travel. For instance, air is a medium for travelling sound waves. The simplest form of vibratory motion is harmonic or sinusoidal motion that can be described mathematically by Eq. (2.1) [E Richart, 1970].

$$z = A\sin(\omega t - \varphi) \tag{2.1}$$

where z is the magnitude of applied load or displacement excitation, A is defined as displacement amplitude from the mean position, ω is circular frequency, φ and t are regarded as phase angle and time, respectively. All the defined coefficients are illustrated in Fig. 2.1.

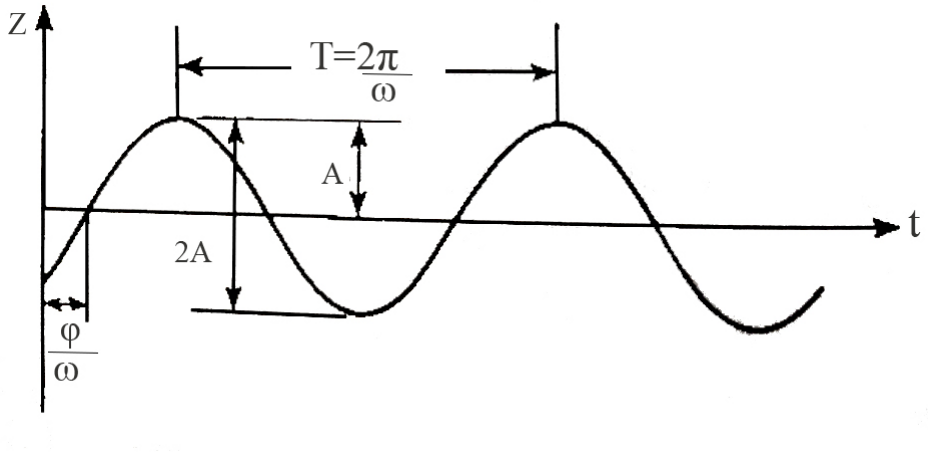


Figure 2.1: Harmonic load as a function of time [E Richart, 1970]

The distance $2A$ represents the peak-to-peak displacement amplitude. Circular frequency (ω) defines the rate of oscillation in terms of radian per unit time and 2π rad is equal to one complete cycle of oscillation. Eq. (2.2) represents the frequency of oscillation in terms of cycles per unit time.

$$f = \omega/2\pi \tag{2.2}$$

The time taken for one complete cycle of vibration to pass a specific point is recognized as a period of vibration and is given by Eq. (2.3).

$$T = 1/f = 2\pi/\omega \tag{2.3}$$

Two independent quantities, which are amplitude and frequency, are required for defining a harmonic motion, which are amplitude and frequency. In some situations, the phase angle (φ)

is required to specify the time relationship between two quantities having the same frequency. However, the phase angle is usually referred to the time origin. Therefore, a harmonically vibrating system can be expressed by Eq. (2.4), too [Das and Luo, 2016].

$$z = A\sin(\omega t) \tag{2.4}$$

However, harmonic motion is generally a result of controlled laboratory conditions. Three types of motion which are harmonic and periodic, random and transient waves are illustrated in Fig. 2.2.

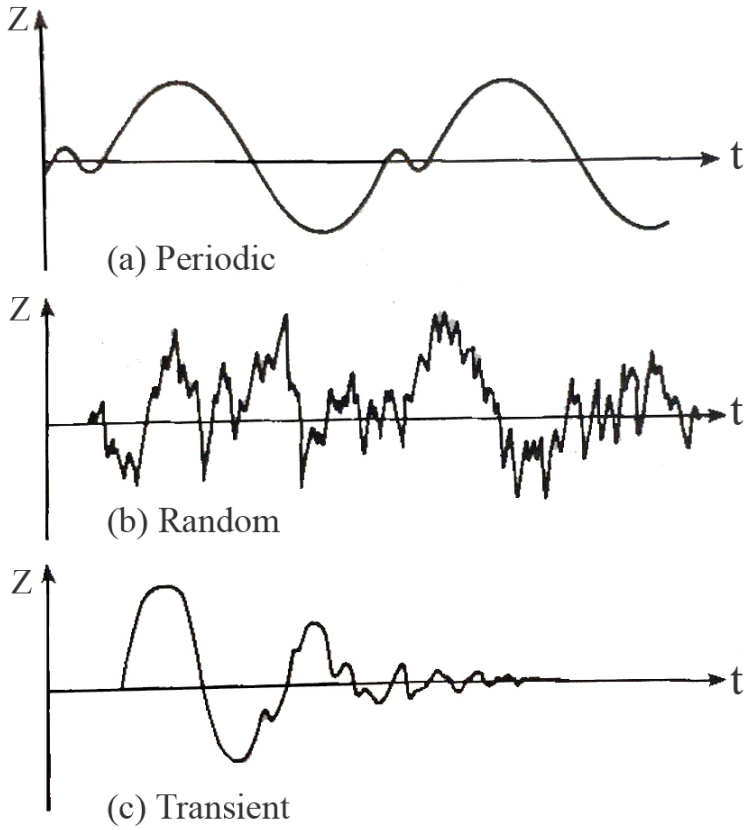


Figure 2.2: Different types of motion [E Richart, 1970]

Harmonic and periodic motion is when the motion of an object continually repeats itself, whereas in random motion, the particle moves in a zig-zag manner and the displacement-time pattern never repeats. Finally, transient motion is associated with a damped system where an impulsive load has been applied for a short-time interval.

The first and second derivatives of the displacement with respect to the time are defined as velocity and acceleration, which are presented in Eq. (2.5) as a harmonic motion.

$$\begin{aligned} Displacement &= z = A\sin(\omega t - \varphi) \\ Velocity &= \frac{dz}{dt} = \dot{z} = \omega A\cos(\omega t - \varphi) \end{aligned} \tag{2.5}$$

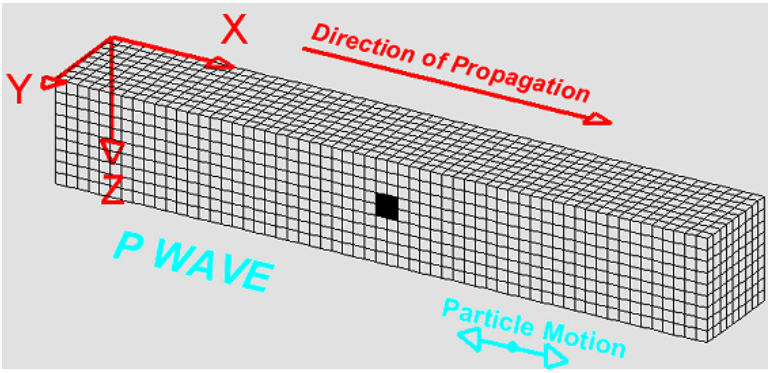
$$Acceleration = \frac{d^2z}{dt^2} = \ddot{z} = -\omega^2 A \sin(\omega t - \varphi)$$

The dot over the quantity indicates derivatives with respect to time. Eq. (2.5) shows that the amplitude of the obtained quantity is the amplitude of the previous quantity multiplied by ω. Therefore, the displacement amplitude and the frequency are necessary values, which are needed to determine the amplitude of the other quantities for harmonic motion.

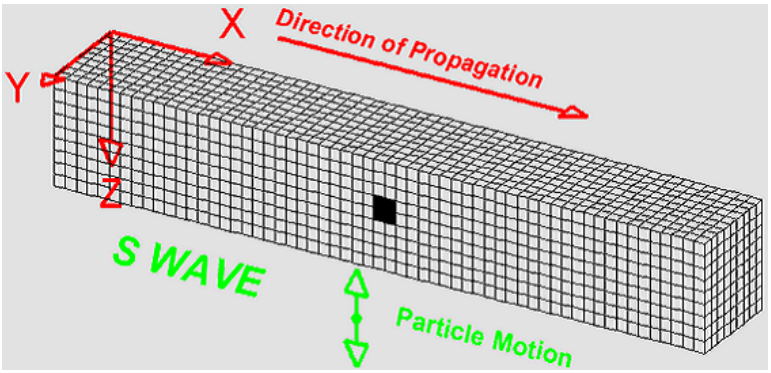
2.1.1. Seismic wave

The elastic wave that propagates through the earth's layer can be the result of an earthquake or any other kinds of man-made activity. The propagation velocity of the waves depends on the density and stiffness of the medium. The velocity of the wave tends to increase with depth.

The seismic waves are divided into two main categories: body and surface waves [Ben-Menahem and Singh, 2012]. Body waves propagate in three dimensions through the interior of the earth and they are categorized as compressional waves (P-wave) and shear waves (S-wave). The particle motion associated with P-waves is parallel to the motion of the wave and it has the highest velocity in comparison with other waves. S-waves travel perpendicularly to the direction of wave propagation. Fig. 2.3 represents the particle motion of body waves.



(a)



(b)

Figure 2.3: Particle motion of body waves; a: P-wave b: S-wave [Developers, 2017]

Having an interface or a surface will result in combining of body waves that can propagate along the surface of half-space, which are called surface waves. The particle motion of surface waves is larger than that of body waves, so surface waves tend to cause more damage. Rayleigh and Love waves are the most common surface waves, which are presented in Fig. 2.4 [E Richart, 1970].

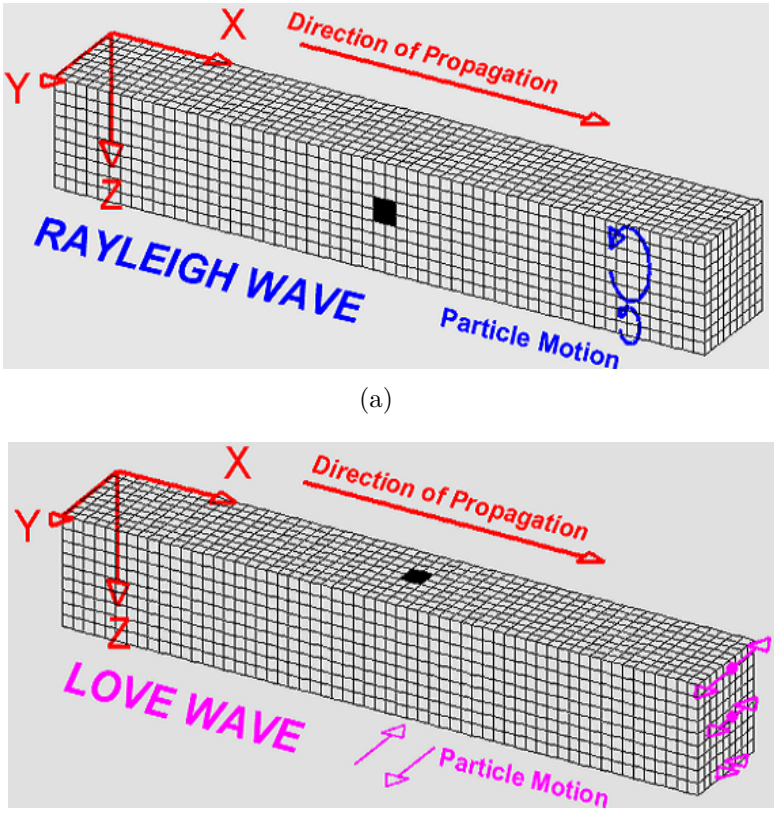


Figure 2.4: Particle motion of surface waves; a: Rayleigh-wave b: Love-wave [Developers, 2017]

The particle motion of R-wave consists of an elliptical shape in the vertical plane and parallel to the direction of the propagation. R-waves are slower than body waves, approximately 90% of the velocity of S-wave for typical homogeneous media. In a layered medium, the velocity of R-wave depends on their frequency and wavelength since the elastic modulus of soil often changes with depth. This phenomenon is called dispersion. However, R-wave in an ideal situation, in homogeneous and flat elastic solids shows no dispersion [Stachowske, 2020; Rahme, 2020]. R-waves with a shorter wavelength (high frequency) travel more slowly than those with a longer wavelength (low frequency), as the speed of waves in the earth increases with increasing depth. In addition, the long-wavelength waves penetrates more deeply into the earth than short-wavelength waves do.

The particle motion of a Love wave is horizontal and transverse to the direction of wave propagation. L-waves are generated in a situation where a soft layer overlay a stiffer layer, whereas R-waves always exist in the presence of a free space [Miller et al., 1955].

R-waves are the most important waves, which are the result of the superposition of two waves, longitudinal and transversal. Both waves propagate almost with the same speed but their energy dissipation, due to the depth, is different. Therefore, the P-wave and S-wave components of the displacement field of R-wave is 90 degrees out of phase from each other, where the vertical component is of higher magnitude than to the horizontal one.

For a vertically oscillating, uniformly distributed, circular energy source on the surface of a homogeneous, isotropic, elastic half-space Miller and Pursey [Miller et al., 1955] determined the distribution of total input energy among the three elastic waves to be 67% for R-waves, 23% and 7% for S-wave and P-wave, respectively.

In wave propagation problems, the vibration source can be considered a circular foundation located at half-space loaded by a harmonic force [Haupt, 1995a]. Fig. 2.5 shows the wave propagation due to the vibration of a circular footing in a half-space. The circular footing generates body waves, which propagate outwards from the source along a hemispherical wave-front. While the generated R-wave propagates radially outward along a cylindrical wave-front.

All generated waves from a circular footing encounter a larger volume of material as they travel toward and this issue results in decreasing the energy of waves with distance from the source. This attenuation in energy or displacement amplitude is called geometrical damping.

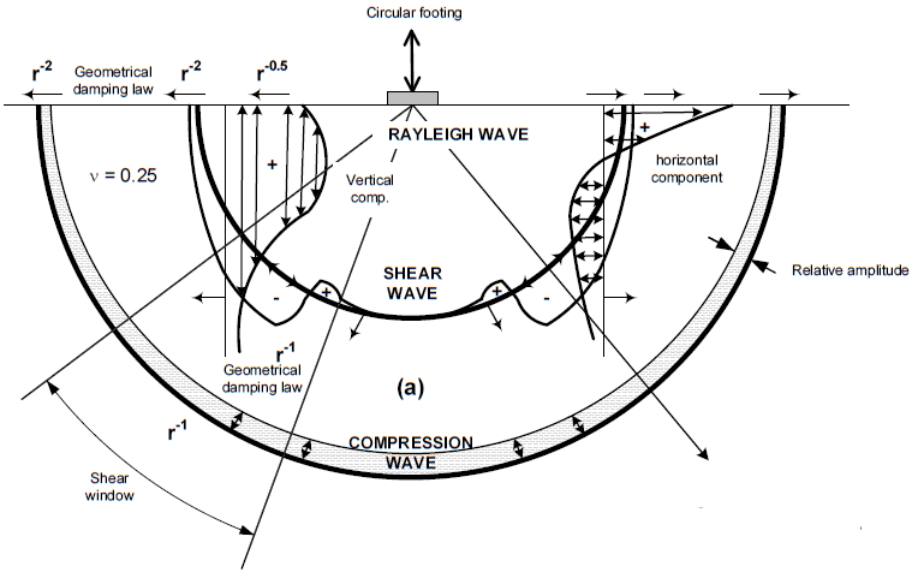


Figure 2.5: Distribution of displacement waves from a circular footing on a homogeneous, isotropic and elastic half-space [Woods, 1968]

The motion of R-waves can be described in vertical and horizontal directions, and both of them decay with depth but according to separate distributions. Wave components with different fre-

quencies (different wavelengths) have different penetration depth and propagate with different velocities. The zone of penetration depth of the R-wave is assumed to be one wavelength L_R from the surface because about 90% of wave energy is transferred in this zone [Haupt, 1995a].

The fact that 2/3 of the energy of the total input energy is carried by the R-wave and the attenuation process of R-wave is much slower with distance than the body waves, indicates that the R-wave is one of the most primary concerns of the vibration isolation problem.

In addition to geometrical damping, material damping, which depends on the viscosity of the soil, wave frequency plays also a significant role in the attenuation of vibration. In a linear, viscoelastic medium, the magnitude of the material damping, which is equal to the fractional elastic energy dissipated during a cycle of oscillation, can be calculated by Eq. (2.6) [Iodice, 2017].

$$\eta = \frac{1}{2\pi}\frac{E_d}{E_s} \tag{2.6}$$

where E_d is the energy dissipated due to viscous damping at each cycle and E_s is the peak strain energy. The quantity is generally frequency-dependent.

The attenuation of the amplitude of a seismic wave in a viscoelastic medium is explained by the complex Eq. (2.7).

$$A = A_0 e^{\left[\frac{-\omega x \eta}{2c_m} + i\omega\left(t - \frac{x}{c_m}\right)\right]} \tag{2.7}$$

where x is the space measured along the propagation direction, A_0 is the initial wave amplitude nitial phase amplitude at reference distance X_0, ω is the angular frequency, c_m and t are wave speed in the medium and the represented time, respectively. A wider expression of wave propagation is presented through Eq. (2.8).

$$A = A_0 e^{i(\omega t - k^* x)} \tag{2.8}$$

where $k^* = (k(1 + i\xi))$ is the complex wave-number and $\xi = \eta/2$ is the damping ratio. For a constant value of η, higher frequencies will attenuate faster, which is because higher frequency waves will go through more oscillations than lower frequency waves in the same time (high-frequency waves have a shorter wavelength). For a constant value of η and ω, due to being the slowest wave, an R-wave undergoes faster intrinsic attenuation than a body wave due to being the slowest wave [Iodice, 2017].

Material damping in dynamic calculations is caused by the viscous properties of soil, friction and the development of irreversible strains. All plasticity models in numerical modelling can generate irreversible (plastic) strains, and may cause material damping. However, this damping is not enough to model the damping characteristic of real soil. Considering very small vibrations, the soil model in numerical modelling does not show material damping, whereas real soils still show a bit of viscous damping [Brinkgreve et al., 2020].

Therefore, additional damping, which is called Rayleigh damping, is required to model realistic damping characteristics of soil in dynamic calculations. Rayleigh-damping is a viscous damping,

which is proportional to a linear combination of a mass matrix (M) and stiffness matrix (K). The damping matrix (C) is given by E.q (2.9).

$$C = \alpha M + \beta K \tag{2.9}$$

where M and K are the mass and stiffness matrices, respectively while α and β are the Rayleigh coefficients.

The parameter α determines the effect of mass in the damping of the soil. Lower frequencies are damped more with a higher value of α. On the other hand, β determines the effect of stiffness in the damping of the soil. A higher value of β results in more damping of higher frequencies. The damping ratio for critical damping is defined as $\xi = 1$, the value of damping to let a single degree-of-freedom system that is released from an initial excitation U_0. The relationship between the damping ratio and R-damping parameters is presented by Eq. (2.10).

$$\alpha + \beta\omega^2 = 2\omega\xi, \qquad \omega = 2\pi f \tag{2.10}$$

where ω is the angular frequency and f is the frequency.

R-damping coefficients can be calculated by Eq. (2.11) through considering two different target frequencies and the corresponding target damping ratio.

$$\begin{aligned} \alpha &= 2\omega_1\omega_2\frac{\omega_1\xi_2 - \omega_1\xi_1}{\omega_1^2 - \omega_2^2} \\ \beta &= 2\frac{\omega_1\xi_1 - \omega_2\xi_2}{\omega_1^2 - \omega_2^2} \end{aligned} \tag{2.11}$$

Fig. 2.6 shows how the mass and stiffness damping terms contribute to the overall damping ratio. Mass proportional damping gives damping due to rigid body motion [Orcaflex, 2010]. The

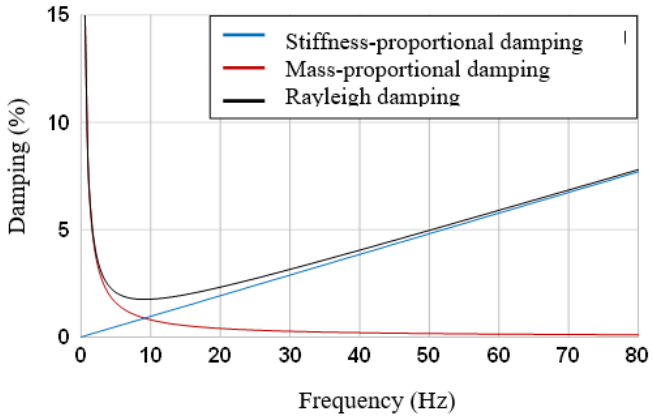


Figure 2.6: Variation of damping ratio with frequency [Orcaflex, 2010]

mass proportional damping is therefore normally neglected for compliant structures undergoing large rigid body motions. In other words, it is suggested to use stiffness-proportional damping.

2.2. Sources of ground-born vibration

Ground-born vibration has been a challenge for large cities in recent years since these vibrations affect surrounding buildings and other structures. The effects range from disturbance of occupants to visible structural damages. Some ground-borne vibration sources include pile driving, road traffic, and railway with different mechanisms of excitations and effects [Stachowske, 2020; Rahme, 2020].

Pile driving is the process of installing a pile into the ground without first excavating. The piles are pushed, driven or otherwise installed into the ground. When the pile driving hammer impacts the pile head, a vibration is created that propagates into the soil and into adjacent structures [Massarsch and Fellenius, 2008].

Woods [Woods, 1997] has concluded that there are two kinds of wave generation mechanisms of seismic waves caused by pile driving. One of the mechanisms is producing shear waves with the interaction of pile shaft surface and surrounding soil. In other mechanisms, shear and compression waves are generated by the interaction between pile bottom and surrounding soil. Ground-borne vibration caused by pile driving is generally affected by three issues [Wang, 2020]:

- The source parameters including driving method, properties of the pile (material area of cross-section) and the penetration depth
- The interaction between the pile and the surrounding soil
- Properties of the soil in transmission area, density and shear wave velocity

Vibration induced by road traffic is mainly generated by the passage of heavy vehicles and divided into static and dynamic components. The static component is due to the mass distribution of the vehicle on the axles while the dynamic component is the result of pavement irregularities. When the vehicle speed is low in comparison with the wave velocity of the soil, the static component contribution is negligible. On the other hand, dynamic components can be up to $50 - 80\%$ higher than static component [Lombaert and Degrande, 2001].

Hao et al. [Hao et al., 2001] measured the ground vibration induced by normal traffic at four different sites, and they found that the largest displacement and velocity responses occur at top floors of the buildings. In addition, they found that ground vibration corresponding to the normal traffic is not strong enough to cause damage to buildings.

Wang et al. [Wang et al., 2019] studied the influence of highway vehicle loads on the vibration of nearby buildings, and both the vehicle induced vibration of ground and adjacent residential are analysed. The results showed that the ground displacement induced by vehicle loads is mainly between 8 to $20Hz$ and the amplitude decreases with increasing distance between measuring points and the highway.

Railway ground vibration is the result of the interaction of the train wheels and the track, which lies on soil [Bahrekazemi, 2004]. The vibration of the wheels depends on the train

system like springs and dampers and the weight of the vehicle whereas the vibration on the rail is dependent on the system below the rail, which is the subsoil. Since neither the wheel nor the rail is perfectly smooth, the train wheel is forced to move in a vertical direction. Since the rail is not completely stiff, it moves also in a vertical direction and this excitation is transferred to the rail pad, sleeper, ballast, and the subsoil under the ballast.

The subsoil under the ballast is usually composed of different layers (non-homogeneous soil), and the elasticity of the soil is also different along the track. Therefore, the interaction of train wheels, and the rail with the track substructure and the subsoil results in generating the vibration with many different resonant frequencies [De Vos, 2017]. Both the train and the rail represent a complex structure, which corresponds to dynamic forces from resonating bodies.

2.3. Effect of vibration

The generated seismic waves can be received by building foundations, and the vibrations are then propagated to other parts of the buildings where they may be amplified and may cause floors and walls to vibrate. This vibration has an impact on the occupants and any sensitive equipment inside a building.

Parsons et al. [Parsons and Griffin, 1988] conducted a series of laboratory experiments concerned with perception thresholds for whole-body vibration. The results have shown that there is a threshold of perception for whole-body vibration and below this threshold, vibration cannot affect human bodies. This threshold is expressed by r.m.s value, which is approximated to $1mm/s$ for the frequency of $1Hz$ and $0.1mm/s$ for $10Hz$. Table 2.1 presents vibration magnitude and perception, which include some indicative information about vibration perception. The table shows that the absolute threshold of perception is equal to 0.015.

Table 2.1: Vibration magnitude and perception (sinusoidal vibration) [Parsons and Griffin, 1988]

r.m.s weighted acceleration (m/s^2)	Perception
< 0.1	Not perceptible
0.015	Threshold of perception
0.02	Barely perceptible
0.08	Easily perceptible
0.315	Strongly perceptible
> 0.315	Extremely perceptible

Damage to buildings from pile driving is divided into two aspects, which are direct and indirect building damage. Direct building damage is caused by seismic surface waves, which are transmitted into the affected buildings. Indirect building damage is caused by the seismic body waves leading to the densification of the ground, which causes settlement in the foundation.

Massarsch et al. investigated the response of buildings to pile and sheet pile driving, especially the differential settlement and total settlement of building foundation. They summarized the

building damage and the settlement of the foundation in four mechanisms [Massarsch and Fellenius, 2014];

- damage caused by static ground movement: possible sources of this kind of damage are instability of surrounded slope and excavations, installation of displacement piles
- structural distortion caused by ground vibration, especially if the length of a building approximately equals half of the wavelength
- damage caused by foundation settlement generated by ground vibration: the reason is loose granular soils
- dynamic effects in a building itself

2.4. Vibration mitigation

Mitigation measures can control vibrations at the source, in the propagation path, and at the receiver. The source can be considered the wheel, track and subsoil for railway and pile material for pile driving. The propagation path encompasses all paths between the vibration source and the building. Finally, the receiver is recognized as the propagation path near the building foundation and the structure. Most of the procedures are frequency dependent [Stachowske, 2020; Rahme, 2020].

2.4.1. Measures at the source

Decreasing the dynamic forces generated by the vibration source results in mitigating the ground-born vibration. The procedure is designed based on the source. Based on the explanation in section 2.2, the combination of train wheels and rail represents a complex dynamic system including masses, springs, and dampers. The response of each element in the system is dependent on how it is coupled with each other. Therefore, the contact between wheels and rail can be improved through keeping both components as smooth as possible. This issue decreases the interaction between wheels and rail and results in reducing vibration.

The heavy mass of the vehicle vibration often represents the dominant source in soft ground and low frequencies. Therefore, soil improvement under a track is another possible reduction method [Andersen and Nielsen, 2005]. RIVAS investigated some mitigation measures for vehicles in order to control the vibration and they suggested the following methods [Müller et al., 2013]:

- Improving wheel roundness:

  Wheels out of roundness is one of the main causes of excessive vibration. This can be treated through good maintenance of wheels.

- Reducing unsprung mass:

This can be achieved for new locomotives and multiple units through improving the suspension of the drive system. Lower levels of vibration are associated with vehicles, which have secondary suspension or smaller wheel diameter. This benefit will be limited to frequencies higher than $20Hz$.

Concerning pile driving, the driving force of the pile plays a significant role in the ground motion. Studies have shown that reducing impact force of the hammer from 8 to $4MN$ results in a decrease in peak particle velocity (PPV) by 18% and 36%, respectively [Farshi Homayoun Rooz and Hamidi, 2017]. Therefore, one solution can be decreasing the hammer impact force when the vibration is greater than the tolerable level.

Another important aspect of the vibration source is the properties of the installed piles. It contains the form of cross-section, elastic modulus, the area of cross-section and the tip angle [Wang, 2020].

Woods [Woods, 1997] has also found that as the pile starts to compact the ground surface, the first generated wave is R-wave and it attenuates more slowly than body waves. As the pile goes deeper, body waves caused by the pile shaft and the pile toe will dominate wave generation. However, body waves attenuate rapidly. Therefore, energy received by the surrounding structure from the driving pile is bigger for a shallow penetration depth than a deep great depth. This means that the PPV received by the surrounding structure has the highest value when the tip of the pile is in a similar depth to the bottom of the foundation.

2.4.2. Measures at the receiver

Since the purpose is to reduce the vibration in protected structures, mitigation procedures to strengthen the ability of structures to withstand the power of vibration are also encouraged. However, since upgrading an existing building is often expensive, measures to improve vibration mitigation in buildings usually have to be implemented beforehand or during its design and construction.

Two different methods of vibration mitigation at the receiver are include [De Vos, 2017]:

- Introducing a vertical elastic layer around the foundation of buildings. This method controls vibration waves to have less effect of vibration. It acts as a protective shell around the foundation, provided that the shell is deep enough to prevent deep waves to reach the foundation.

- A resilient bearing is another practical tool for newly built sensitive buildings. This is a standard method, which consists of steel coil springs bearings. The main advantage of this procedure is that it can be applied to the an existing building.

2.4.3. Measures at the transmission path

All mitigation measures should be implemented either at the source or the receiver during construction of the buildings. However, it is sometimes not possible to use these methods for the constructed source of vibration and building. The installation of a wave barrier between the vibration source and the building can be an alternative method. The trench intercepts the dispatched waves through a complex mode of wave interactions including refection, refraction, diffraction and wave interferences. This results in a considerable reduction in ground motion beyond the trench [Al-Hussaini, 1993].

The problem of vibration isolation for soil structure interaction system is classified into two categories including the near field scheme, in which the obstacle is installed near the source of vibration, and the far field scheme, in which the trench is constructed far away from the vibration source. On the other hand, the applicability of a wave barrier is classified in terms of open or in-filled trenches.

In the case of near field isolation, body waves (P and S-waves) are more predominant in comparison with the surface waves. Increasing the normalized distance between the obstacle and vibration source can lead to making R-waves more prevailing in comparison with body waves. Body waves radiate in all directions whereas R-waves propagate vertically and horizontally in a zone close to the ground surface. In addition, body waves have much higher radiation damping in comparison with R-waves.

2.5. Wave interaction by trench

The reflection phenomenon is the change in the direction of a wave at an interface between two media with different properties so that the wave returns to the first medium. The angle of the value of a reflected wave is equal to the original one. However, the refraction of waves involves a change in the direction of waves as they pass from one medium to another. Refraction, or the bending of the path of the waves, is accompanied by a change in speed and wavelength of the waves.

Seismic waves represent mechanical disturbances that have energy and propagate in the earth at a speed governed by the acoustic impedance of a the medium in which they are moving. An acoustic impedance (Z) is defined through Eq. (2.12).

$$Z = \nu\rho \tag{2.12}$$

where ν is the velocity of the seismic wave and ρ is the density of the soil.

Another theory behind the refraction phenomenon is by considering the wavelength at an interface. When a wave goes from one medium to another at a different speed, the frequency of the wave will stay constant, but the wavelength ($\lambda = \nu/f$) will change. Increasing the speed (ν) results in increasing the wavelength (since the frequency is constant). Therefore, increasing the wavelength results in changing the angle between the incident and transmitted waves at

the interface. The relationship between the angle of incident and transmitted wave and the speed of the first and second materials, which are θ_1, θ_2 and ν_1, ν_2, respectively can be derived by Eq. (2.13), which is known as Snell's law [Sabatier et al., 1986].

$$\frac{\sin\theta_1}{\sin\theta_2} = \frac{\nu_1}{\nu_2} \tag{2.13}$$

Diffraction refers to bending of a wave around the corner of an obstacle into the region of geometrical shadow of a trench when a wave encounters a barrier. When a wave travels in soil, one form of wave energy can be transported into another form through passing the edge of a barrier, which is called mode conversion. Trench bottom corners probably act as additional geometric discontinuities and result in additional mode conversion, in which part of R-wave energy is converted into body waves [Al-Hussaini, 1993]. This phenomenon contributes to the isolation effect by radiating the energy of the wave to the interior of the half-space [Haupt, 1995a].

Finally, the last phenomenon is known as wave interference, in which two waves superposed to form a resultant wave of greater, lower or identical amplitude. Interference usually refers to the interaction of waves that are correlated or coherent with each other, either because they come from the same source or because they have the same frequency.

Constructive interference occurs when a crest of a wave meets the crest of another one of the same frequency at the same point and the result is to make a wave with a larger amplitude. This issue usually results in several unexpected peaks in the result of vibration isolation systems. On the other hand, destructive interference occurs when the maxima of two waves are 180 degrees out of phase, then the amplitude is equal to the difference in the individual amplitude. Fig. 2.7 represents the wave interference phenomenon for constructive and destructive interferences.

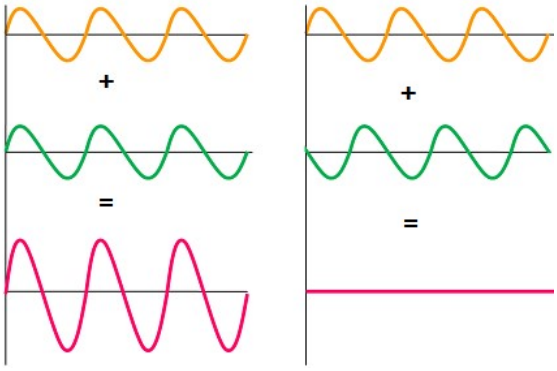


Figure 2.7: Wave interference phenomena

2.6. Vibration isolation through wave barriers

Several studies, including both experimental and numerical, have been carried out in the last few decades in order to improve our understanding of vibration scattering by wave barriers.

However, an analytical method has rarely been used by researchers because of the complexity of a vibration isolation system, specially in the case of layered soil [White, 1958; Mal and Knopoff, 1965].

Woods [Woods, 1968] was one of the first to perform a full experimental test for evaluating the efficiency of open trenches. The field test was suited on a sand and silt deposit and water table was at the depth of $4.5m$. A harmonic load with a constant input excitation load of $80N$ and frequency of $250Hz$ was applied to the soil to generate the vibration. Finally, he introduced a normalized depth of 0.6 with regards to the Rayleigh wavelength (λ_r) to reach 75% reduction in screening of incoming waves.

A series of field tests have been conducted by [Alzawi and El Naggar, 2011; Ulgen and Toygar, 2015] for finding the screening effectiveness of geofoam-filled obstacles as a soft barrier. The soil properties consisted of silty clay, clayey silt and sandy silt [Alzawi and El Naggar, 2011] and clayey sand over clay resting on very stiff clay [Ulgen and Toygar, 2015]. They used a harmonic load with the frequencies in the range of $30 - 70Hz$. The results showed that the vibration amplitude can be reduced up to 68% by installing a geofoam-filled barrier. Moreover, they have found that the performance of a geofoam-filled trench is dependent on the normalized depth. The optimum depths are suggested as $0.6\lambda_r$ and $1\lambda_r$ for near field and far field systems, respectively. In addition, it was concluded that the screening efficiency of the geofoam-filled trenches decreases with increasing the distance between the vibration source and trench.

Celebi et al. [Çelebi et al., 2009] described the results of experimental studies to compute the screening efficiency of stiff and soft barriers in the case of near field and far field schemes under a harmonic load with a frequency range of $20 - 80Hz$. The site soils were characterized as clay, silty clays, silty gravel and gravel. The observations illustrated that far field isolation is more effective than near field isolation and softer backfill materials can be more effective in attenuating the incoming waves in comparison with stiff materials.

In addition, a centrifuge parametric investigation is accomplished by [Baziar et al., 2019; Murillo et al., 2009] to examine the effect of dimensional and geometrical factors on a geofoam-filled trench in the mitigation of ground vibrations induced by high speed railway and traffic. The soil used in both research was sand with density of 1610 and 2640 kg/m^3, respectively. The applied frequencies was in the range of $10-40$ Hz and $50-2000$ Hz, respectively. The results of the study showed that geofoam barrier mitigated ground vibration up to 70%. In addition, the screening performance is dependent on trench depth and the optimum depth of $1\lambda_r$ is suggested to have a successful system.

In addition, numerical techniques including the finite element method (FEM) and the boundary element method (BEM) can be used as powerful tools to study the screening performance of wave barriers. Beskos et al. [Beskos et al., 1986; Beskos, 1987] developed a BEM model to determine the screening capability of open and concrete-filled trenches in homogeneous and layered soil. They used a harmonic loading with a frequency of $50Hz$ and amplitude of $1KN$ as a vibration source. The results showed that open trenches are more effective than in-filled trenches but they present wall instability. It was found that the depth is governing factor in screening effectiveness for open trench. However, for concrete-filled trench, both depth and

width play a role and a significant reduction is noticed by increasing the values of the area of the trench (D and W). From design point of view, for a successful isolation is achieved for $D > 0.6$ for open trench and $DW > 1.5$ for concrete-filled trench in homogeneous soil. In addition, it was concluded that deeper trenches are required in layered soil to achieve the same level of screening as in homogeneous soil. The thickness of the first layer equal to $3\lambda_r$ is enough to ignore the layering effect.

Ahmad and Al-Hussaini conducted an extensive parametric study to analyse the influence of different geometrical and material parameters on the screening efficiency of rectangular open and concrete-filled obstacles in homogeneous and layered soil. The vibration source was considered as a harmonic load with frequency of $50Hz$ and amplitude of $1KN$. They also developed a simple model for vibration isolation in near field and far field schemes [Ahmad and Al-Hussaini, 1991]. The results showed that depth is a governing factor for open trench and width is not important. However, for concrete-filled barrier, both depth and width are equally important. Trench must be installed deeper in layered soil in comparison with homogeneous soil. A minimum normalized depth $D = 2$ is suggested for layered soil to have a successful system.

A FEM is developed in homogeneous sandy soil with density of 1955 kg/m^3 soil to evaluate the efficiency of geofoam-filled trenches by [Ekanayake et al., 2014; Liyanapathirana and Ekanayake, 2016]. A single vertical vibratory force operating at frequency in the range of $30 - 50Hz$ was applied to the driven pile. The influence of dimensional and geometrical parameters of the trench were investigated. They observed that the barrier efficiency can be improved by adopting far field isolation. Efficiency of EPS geofoam wave barriers increase significantly when the depth of the barrier is increased. However,an increase in length of EPS geofoam wave barriers slightly improves the efficiency of the trench. While changes to the width of the wave barrier can either attenuate or amplify the ground vibrations. A summary of the literature review is presented in table 2.2.

Table 2.2: Summary of literature review

Reference	Research type	Trench type	Material for filling the trench	Load type	Frequency	Soil type	Considered parameters	Results
[Yang and Hung, 1997]	Numerical study	open and in-filled	-	harmonic line load	31	Homogeneous	D, X, W, Vs	• D is governing factor for open trench and W is not important except for shallow trench • D and W should meet the conditions of $D > 1$ and $W > 0.3$ • The effect of X can be ignored • For in-filled trench, higher Vs performs better
[Schevenels et al., 2017]	Numerical study	In-filled (stiff)	jet-grout walls and concrete	point load	30 and 60	Homogeneous	T (thickness of trench wall)	• Jet-grout wall barrier performs better that concrete-wall and need less wall-thickness
[Bo et al., 2014]	Numerical study	in-filled	concrete	harmonic line load	50	Homogeneous	X, D, W, ρ	• Increasing the barrier density results in an increase in vibration reduction • Large D contributes to reduce soil motion, but a limiting value exists • Too slender barrier (i.e. barrier with very large depth but very small width) should be avoided
[Majumder and Ghosh, 2016]		Geofoam	Open and in-filled	harmonic load	40-50	Homogeneous	X, D, W	• The dimensions with D = 1.0, W =0.06 and X = 0.15 is found to be most effective • Soil non-linearity significantly enhances the screening efficiency as compared to the linear elastic analysis

[Zoccali et al., 2015]	Numerical study	in-filled	Soil–bentonite, Rubber chip, Concrete	Moving load	-	Homogeneous	L	• Increasing attenuation of the vibration required • longer trenches • the concrete material seems to be the best material for filling the trench
[Ekanayake et al., 2014]	Numerical study	in-filled	Geofoam-Water	point load	40 - 50	Homogeneous	X, D, W, L	• Efficiency of EPS geofoam wave barriers increase significantly when D is increased. • Increasing W and Lhas little impact on the efficiency oft he trench • The barrier efficiency can be improved by adopting far field isolation. • EPS geofoam wave barrier out performs the water-filled wave barrier as the depth of the wave barrier increases
[Esmaeili et al., 2014]	Numerical study	Open	-	harmonic load	4	Homogeneous	X, D, W	• V-shaped trench was more efficient in comparison to rectangular trench
[Saikia, 2014]	Numerical study	In-filled	-	harmonic load	31	Homogeneous	X, D, W, Vs	• X has an ignorable effect on mitigation of vibration • Decrease in Vs results in marked decrease in vibration amplitude • It is suggested that backfill should have Vs within 0.1 to 0.2 times that of surrounding soil • The barrier efficiency consistently increases with increase D up to $0.6\lambda_r$ • No conclusion can be drawn on the effect of W on vibration attenuation

[Leung et al., 1991]	Numerical study	Open	-	harmonic load	50	layered	X, D	• In the case of layered soil, deeper trenches are required in comparison with homogeneous soil for achieving the efficiency
[Thompson et al., 2016]	Numerical study	Open and in-filled (soft)	-	harmonic load	5-100	layered	X, D, W	• For a layered ground with a soft weathered layer above a stiffer substratum, significant reductions can be achieved if the trench cuts through the upper layer • Increasing the width of the open trench has a relatively small effect on the benefit • Filling the trench with a soft barrier material leads to significant reduction in the performance • Finally, it is concluded that the performance of both the open and soft-filled trench varies considerably between locations
[Saikia, 2016]	Numerical study	in-filled (soft)	-	harmonic load	31	Homogeneous	X, D, W, Vs	• In order to achieve a good degree of mitigation, the shear wave velocity ratio, Vb /Vs of backfill should be around 0.3 • The effect of X on its screening effectiveness depends on the barrier depth and width • D= 1.0 can be considered as limiting barrier depth • W= 0.8 can be considered as limiting barrier width

[Motamed et al., 2009]	Numerical study	in-filled	Concrete, Geofoam	harmonic load	40	Homogeneous	D, W	• Increasing D has more influence for stiff barriers in comparison with soft one • Effect of W was found to be noticeable for soft barriers, while this parameter had little impact on stiff barriers • Stiffer materials provide a more effective vibration countermeasure than soft ones
[Sivakumar Babu et al., 2011]	Numerical study	in-filled	Geofoam	vibratory force	30	Homogeneous	X, D, W, L	• X deos not have any influence on vibration mitigation • Changing to D and L of • the wave barrier attenuate ground vibrations • Changing W can either attenuate or amplify the ground vibrations
[Dijckmans et al., 2016]	Field test	sheet pile wall	-	Train load	5	layered	D	• The sheet pile wall is only effective when D is sufficiently large compared to the Rayleigh wavelength in the soil • It is concluded that a sheet pile wall offers potential for vibration reduction in soft soil conditions

[Gao et al., 2018]	Field test	wave impedance block (WIB)	Concrete, Wood	harmonic load	10-100	layered	D, Vs, WIB size	• The vibration mitigation effect of the WIB is improved as the plane size and shear modulus of the WIB increase • Decreasing embedded depth of the WIB results in attenuating more vibration • The installed WIB may amplify rather than reduce the ground vibration when the shear modulus is smaller than a threshold value or the embedded depth is larger than a threshold one
[Murillo et al., 2009]	Centrifuge modelling	in-filled	Geofoam	harmonic load	150-2000	Homogeneous	X, D, W	• For $D > 1$, the vibration mitigation continuously increases. For $0.5 < D < 1$ the acceleration can be amplified. • The influence of W becomes noticeable especially in shallow barriers • Acceleration amplifications behind shallow barriers can be observed when W is less than 0.2 • Barrier is an ineffective isolation system when $X < 0.5$, because of reflected waves.
[Alzawi and El Naggar, 2011]	Field test	Open and in-filled (soft)	Geofoam	harmonic load	20-60	layered	X, D	• The Geofoam barrier protective effectiveness observed in this study was up to 68% or higher • The barriers are found to be generally more effective when $D > 0.6$ • The results show that a deeper trench is required as the X increases

[Çelebi et al., 2009]	Field test	Open and in-filled (soft and stiff)	Water, Concrete	harmonic load	10-100	layered	X, D, W	• D = 0,6 and 1 are suggested for reaching an acceptable amount of mitigation for open and concrete-filled trench, respectively • The minimum W should be 0.3 for both open and concrete-filled trench • Far field system performs better than near field system in attenuating the incoming waves
[Mahdavisefat et al., 2018]	Field test	in-filled	Sand-rubber mixture	harmonic load	10-600	layered	X, D	• Due to the reflection of incident waves on the trench walls and their super positioning, magnified waves are observed in front of the trenches • There is little effect on vibration mitigation for $D > 1.5$ • Increasing X shows negligible effect on its screening effectiveness
[Pu et al., 2018]	Field test	in-filled	Geofoam	harmonic load	50	layered	X, D, W	• For far field isolation, the screening efficiency of trenches consistently increases with increasing D up to 1 • X does not have a big influence on the screening effectiveness

2.7. Geofoam

The term geofoam was proposed by Horvath [Horvath, 1995] to describe all plastic foams used in geotechnical applications. Expanded polystyrene (EPS) geofoam has been used as a geotechnical material since the 1960s. EPS geofoam is approximately 1% the weight of soil and less than 10% the weight of other lightweight fill alternatives material. As a lightweight fill material, EPS geofoam reduces the loads imposed on adjacent and underlying soils and structures [Stark et al., 2012].

ASTM International provides a specification for the minimum properties of EPS geofoam. The relevant ASTM specification for EPS geofoam is ASTM the $D7180$ standard specification for rigid cellular polystyrene geofoam. Other ASTM standards are the $D7557$ standard guide for the sampling of EPS geofoam in geotechnical projects and $D7557$ standard practice for sampling of EPS geofoam specimens. Understanding the standard being used on EPS geofoam project is essential. The technical data of different types of EPS is presented in table 2.3.

Table 2.3: EPS geofoam properties [D6817-13, 2013]

Properties	EPS12	EPS15	EPS19	EPS22	EPS29	EPS39	EPS46
Density (kg/m^3)	11.2	14.4	18.4	21.6	28.8	38.4	45.7
Compressive Resistance at 1%(kPa)	15	25	40	50	75	103	128
Compressive Resistance at 10%(kPa)	40	70	110	135	200	276	345
Flexural Strength (kPa)	69	172	207	240	345	414	517
Elastic Modulus (kPa)	1500	2500	4000	5000	7500	10300	12800

EPS behaves as a linear elastic material up to a strain of about 1% as shown in Fig. 2.8. As a result, the design recommendation for EPS geofoam is to limit loading to the compressive resistance at 1% strain. The stress at a compressive strain of 1% is called the elastic limit stress and is measured in a standard rapid-loading compression test. Except for special compressible applications, higher compressive strain, e.g., 5 or 10%, is not used to estimate the EPS strength because these strains are past the yield strength of the EPS, and this may lead to undesirable permanent strains.

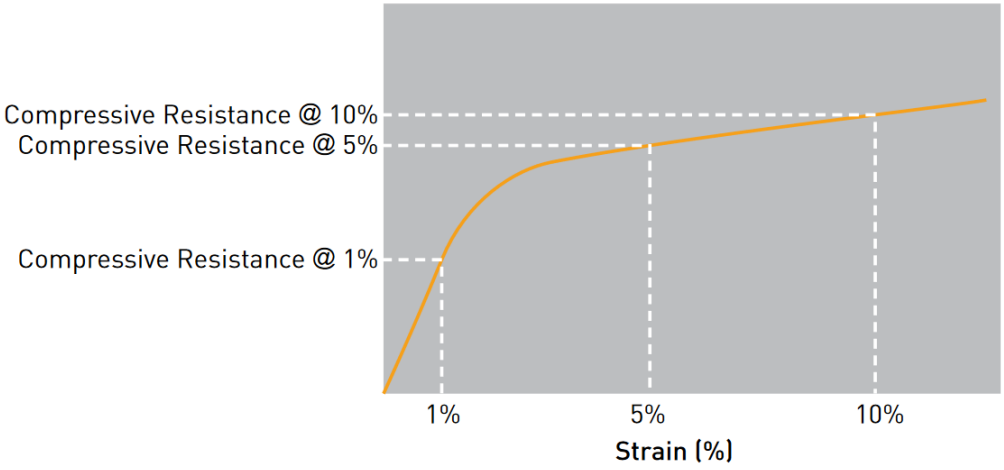


Figure 2.8: Stress-strain response of EPS [Stark et al., 2012]

3 Genetic Algorithm and Artificial Neural Network

3.1. Genetic Algorithm

Optimization consists of studying different aspects of an initial idea and using the gained information to improve it. A computer is a perfect tool for optimization when the factors influencing the idea can be input in a readable format by a computer. The terminology (best solution) in optimization implies that there is more than one solution and the solutions are not of equal value.

A Genetic Algorithm (GA) is a high-level procedure and research-based optimization technique, which is inspired by the genetic and natural selection that belongs to the much larger branch of computation known as evolutionary algorithms [Whitley, 1994]. The principle of search techniques in GA is based on Darwin's theory of evolution [Darwin, 1964].

A GA offers a random search in a complex landscape. One general principle for the implementation of an algorithm for a specific problem is to create a proper balance between explorations and exploitation of the search space. To reach this aim, all operators of GA should be examined carefully [Hansheng and Lishan, 1999].

In a GA, there is a pool of candidate solutions (called individuals) to any given problem which is evolved toward a better solution. A set of properties of each candidate solution can be called a chromosome. A chromosome is composed from genes and its value can be either numerical, binary, symbols or characters depending on the problem want to be solved. The output is generated by a minimizing function from a set of properties of each candidate solution (a chromosome).

The fitness function can be an experimental result or a mathematical function. It calculates the difference between the desired and calculated output. Therefore, determining a proper fitness function and recognizing the most important input variables is really important. The term minimize is used to calculate the output of the fitness function in GA [McCall, 2005].
An attempt has to be made to select an optimal size for the initial population. Too small population will not allow sufficient room for exploring the search effectively, while too large population can increase the computational cost. Therefore, an optimal population should be selected based on the complexity of the fitness function, computational cost, memory, and time.

A try has been done to show the application of a genetic algorithm in vibration isolation for a single-wall trench. The aim is to find the best parameters of a rectangular trench to reach the highest value of efficiency. The considered parameters for optimizing are: location (X), depth (D), width (W) and length of the trench (L). Each parameter of the trench is defined as a gene, which is generated randomly from the defined range from the table 3.1. Each chromosome includes 4 genes, which are the parameters of the trench and the population is a set of all

chromosomes.

Table 3.1: Defined ranges for the selected parameters

Parameters	Min (m)	Max (m)
Location (X)	3	10
Depth (D)	2	6
Width (W)	0.3	1
Length (L)	5	15

Fig. 3.1 shows an example of a population, three chromosomes and randomly-generated genes for a single-wall barrier.

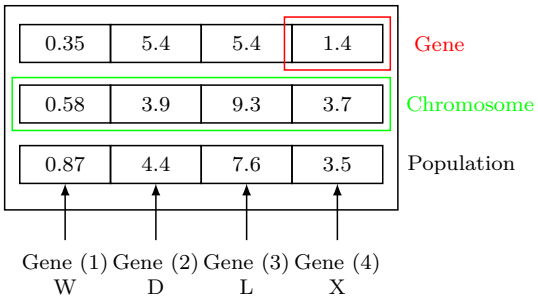


Figure 3.1: Example of gene, chromosome and population in vibration isolation problem

Encoding is the process of representing individual genes. One of the most important decisions to make while implementing a genetic algorithm is to decide a method for representing the solutions. The process of encoding can be performed using binary and floating methods. In binary encoding representation, which is illustrated in Fig. 3.2, each chromosome consists of bit strings. Each chromosome encodes a bit string. Each bit in the string can represent some characteristics of the solution. Every bit string is a solution but not necessarily the best solution. The whole string represents a number.

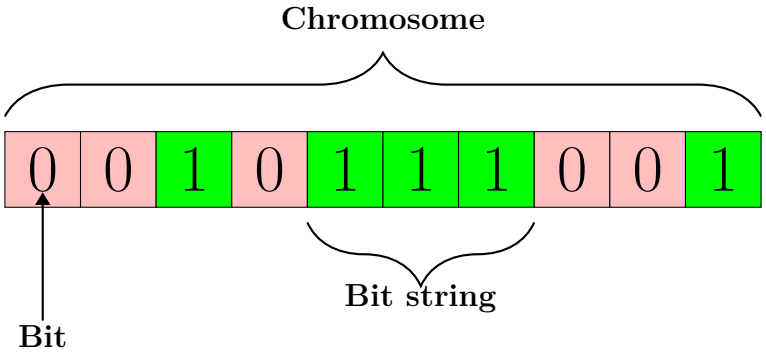


Figure 3.2: Binary encoding representation

In Floating encoding, every chromosome is a string of values and the values can be anything connected to the problem. This encoding method produces the best results for some special

problems, where some complicated values, such as real numbers, are used. For problems with genes using continuous rather than discrete variables, the real-valued or floating-point representation is the best. Fig. 3.3 shows a floating encoding example.

0.5	0.2	0.6	0.8	0.7	0.4	0.3	0.2	0.1	0.9

Figure 3.3: Floating encoding representation

Depending on the solution of the problem, the encoding method can be selected. In vibration isolation, floating encoding is used since all the parameters are real values and can be decimal numbers, too.

As explained, generatin an initial population is one of the first steps in developing a GA model. For this purpose, an initial population in vibration isolation topics with 10 chromosomes are generated randomly and illustrated in Fig. 3.4.

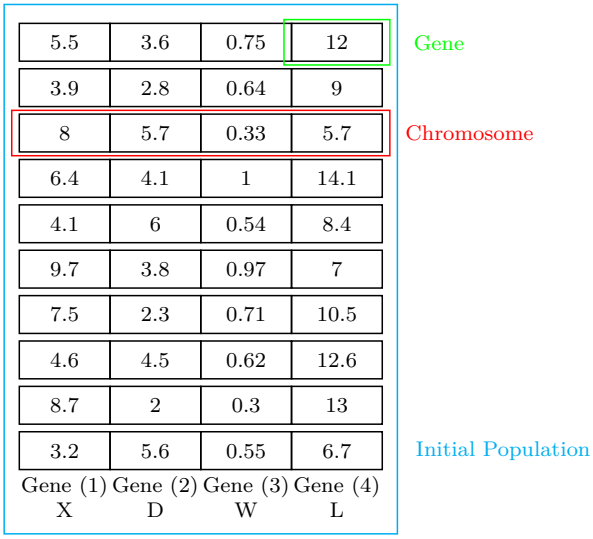


Figure 3.4: Generate an initial population randomly for GA between the defined ranges

3.1.1. Fitness function

The goodness of the chromosome is evaluated as a solution for the problem by the fitness function. In a genetic algorithm, the chromosome and its solution are represented as genotype and phenotype. Calculation of fitness value is done repeatedly in a GA, and therefore it should be sufficiently fast. In most cases, the fitness function and the objective function are the same as the objective is to either maximize or minimize the given objective function. However, for more complex problems with multiple objectives and constraints, an algorithm designer chooses different fitness functions.

The evaluation of the goodness of each chromosome in vibration isolation topic is carried out through a finite element model (Plaxis). It means that the dimensions of the trench as a chromosome will be entered into the Plaxis model. Then, the efficiency of the trench based on each chromosome will be calculated. This process means evaluating the goodness of different parameters. Fig. 3.5 represents the calculated efficiency of each chromosome for the initially generated population. As it can be seen, different efficiencies are calculated for different chromosomes.

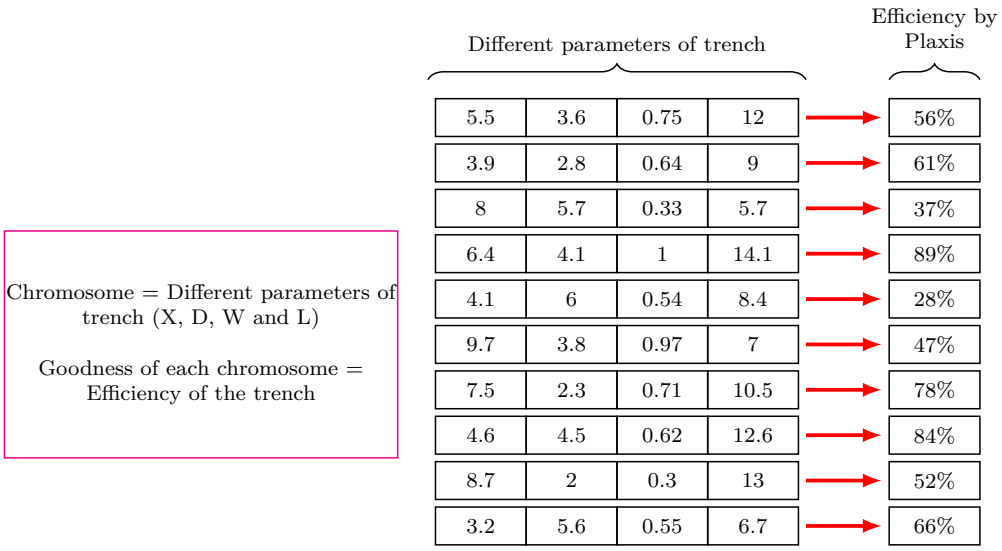


Figure 3.5: Calculated efficiency of each chromosome

3.1.2. Genetic operators

Genetic operators are the heart of a genetic algorithm for guiding the algorithm towards a solution to a given problem. Operators create new and fitter chromosomes [Lim et al., 2017a]. The three main operators are as follows:

1. Selection
2. Crossover
3. Mutation

Genetic operators are used to select the best solutions, called parents, that contribute to the population of the next generation (selection). Combine selected solutions of two parents of children for the next generation (crossover) and create and maintain random population diversity (mutation), which is called recombination.

Selection

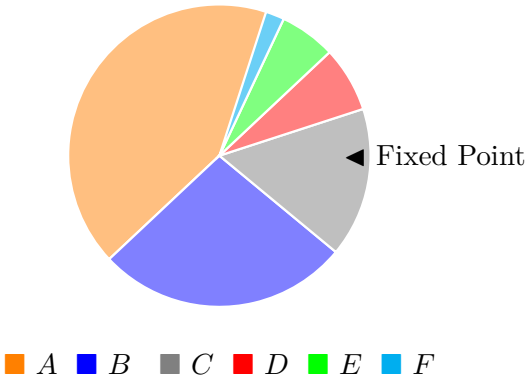
Selection is the process of selecting two parents from the population to create a new population. Following the steps of encoding and evaluating chromosomes with a fitness function, the next step is to decide how to perform a selection. A selection operator aims to emphasize fitter chromosomes in the population. Parents are selected from the initial population. According to Darwin's theory of evolution, the best chromosome survives to create a new offspring [Richards, 2009]. Selection is a procedure to pick chromosomes from the population according to the fitness function evaluation. The chromosome with a higher fitness function has more chance to be selected [Razali et al., 2011].
The process of selecting two parents from the population to apply the crossover is classified as fitness base selection and ranking base selection.

Fitness proportionate selection method

In this method, an individual can become a parent with a probability which is proportional to its fitness. Therefore, fitter individuals have a higher chance of reproduction and propagating their features to the next generation. Two implementations of fitness proportionate selection are Roulette Wheel and Stochastic Universal.

1- Roulette wheel selection method

The principle of Roulette Wheel selection method is to select a chromosome from a pool of population proportional on their fitness value. A wheel, known as roulette wheel is defined for displaying the process with different sections in the wheel, which are based on the fitness value of each chromosome. A fixed point is chosen on the wheel circumference as shown in 3.6. The selection process is based on spinning the wheel. The region of the wheel which comes at the front of the fixed point is chosen as the parent.



Chromosome	Fitness Value
A	8.2
B	3.2
C	1.4
D	1.2
E	4.2
F	0.3

Figure 3.6: Roulette wheel selection

2- Stochastic universal method

In Stochastic Universal method, chromosomes are specified to a segment of line, like the different sections in roulette-wheel selection. N points are considered for the number of chromosomes, and then distance between the points is calculated as ($1/N$ points), and the position of first point is selected through a randomly-generated number. For instance, for 6 individuals to be selected, the distance between the points is $1/6 = 0.167$. The selection process for the example is seen in Fig. 3.7.

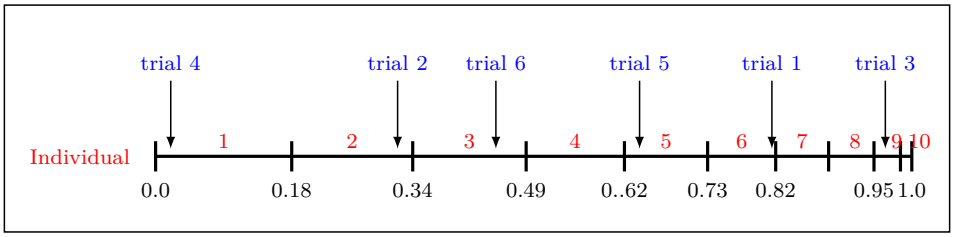


Figure 3.7: Stochastic universal method

Ranking base selection method

In this method, the population is sorted according to objective values. The fitness assigned to each individual depends only on its position in the individuals' rank. Ranking introduces a uniform scaling across the population and provides a simple and effective way of controlling selective pressure. The probability of each individual being selected for reproduction depends on its fitness normalized by the total fitness of the population.
Tournament selection is a ranking base selection method which involves choosing a number of chromosomes randomly from the population and picking out the best individual for the new population. The number of chromosomes in the set is called the tournament size. Assume tournament size = 3, then three chromosomes will be selected from the pool, their fitness will be compared, and fitter chromosomes will be selected to reproduce. Fig. 3.8 shows how the method works.

Tournament selection method is used to select the fittest candidates from the current population in vibration isolation topic.

Crossover

A crossover operator is responsible of taking two parents solutions to produce an offspring for the next generation in order to explore a much wider area of the solution space and find the globally optimal solution for the problem. A crossover selects two or more chromosomes of the population as parents to reproduce one or more offsprings through choosing genes from either the chosen parents or from a combination of both parents.

The duty of a crossover involves sharing information between individuals, where the features of two parent chromosomes are combined to reproduce two children to generate better children.

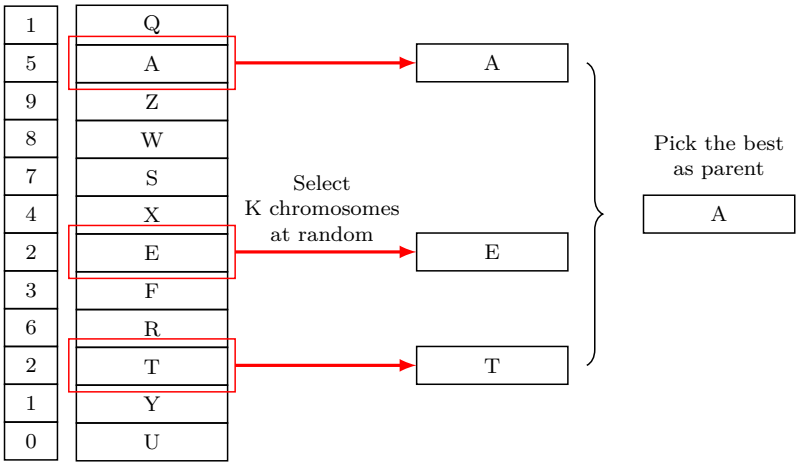


Figure 3.8: Tournament selection method

The crossover probability is a parameter to show how often the crossover will be performed [Lim et al., 2017b].

Summary of the process of crossover operator:

1. Getting the selected parents from the selection operator
2. Selecting a random cross line in the chromosome
3. Finally, changing the value of chromosomes over the cross line

Different kinds of crossover operators include:

1- A single-point crossover (for binary representation)

In this method, a single corresponding point is selected randomly for cutting two parents and then combines the parents at the crossover point to create new children. Fig. 3.9 shows an example of single-point crossover method. The red line shows the crossover points. The contents between these points are swapped between the parents to produce new children to use in the next generation.

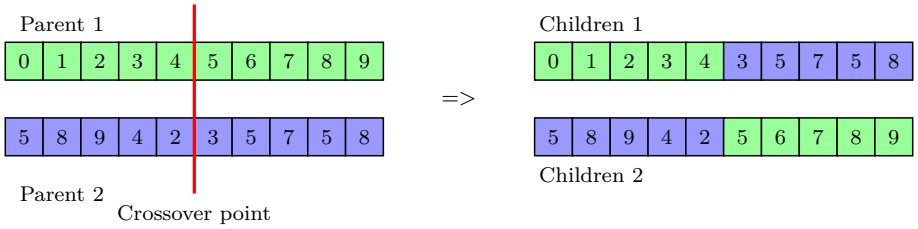


Figure 3.9: Example of single point crossover and create children

2- A two-points crossover (for binary representation)

Two cut-points are selected in this method to provide greater combination of parents and create better children. Fig. 3.10 shows an example of two-point crossover method. The red lines

show crossover points. The contents between these points are swapped between the parents to produce new children to use in the next generation.

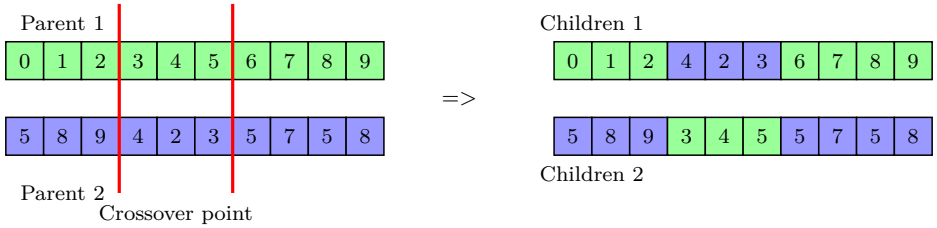


Figure 3.10: Example of two points crossover and create children

3- A uniform crossover (for binary representation)

In this method, each gene is treated separately rather than dividing a chromosome into segments. The operator selects randomly-generated binary crossover, which is called mask, and provides uniformity through swapping genes in parents. The value of children are duplicated from parents as per bits of their mask. When there is 1 in the crossover mask, the gene is copied from the first parent, and when there is 0 in the mask, the gene is copied from the second parent. Fig. 3.11 shows an example of uniform crossover method.

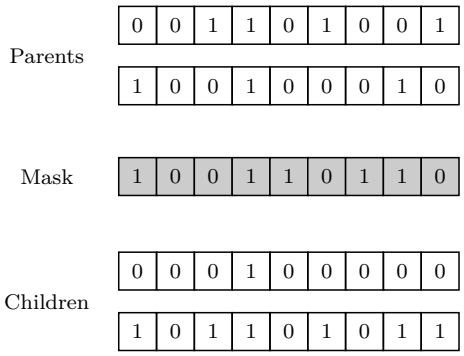


Figure 3.11: Example of uniform crossover and create children

4- An arithmetic crossover (for floating representation)
This operator linearly combines two parents through Eq. 3.1 . In this crossover, two parents are chosen randomly to apply the crossover and through combination of these chromosomes, new children are generated.

$$\begin{aligned} y_i(1) &= \alpha_i x_i(1) + (1-\alpha_i)x_i(2) \\ y_i(2) &= \alpha_i x_i(1) + (1-\alpha_i)x_i(2) \end{aligned} \tag{3.1}$$

where α_i is uniform random number in the range of $[0, 1]$, y_i and x_i are new children and selected parents, respectively.

Arithmetic crossover method is used in vibration isolation topic to generate new parents. As explained, two parents will be selected randomly from the initial population to apply crossover. Chromosomes 1 and 4 are selected randomly to apply the crossover. Before applying crossover, a random value for α_i should be generated in the interval of [0, 1], which is equal to $\alpha_i = 0.3$ for this example. Substituting the value of α_i in the Eq. 3.1 results in Eq. 3.2

$$\begin{aligned} Y_1 &= (0.3)x_1 + (1 - 0.3)x_2 \\ Y_2 &= (0.3)x_2 + (1 - 0.3x_1 \end{aligned} \tag{3.2}$$

Now crossover should be applied based on the Eq. 3.2 to the selected parents from the initial population. Fig. 3.12 illustrates the selected parents and newly generated children after applying crossover.

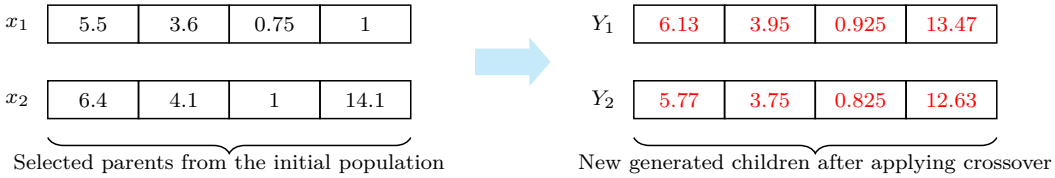


Figure 3.12: Selected parents and new generated children after applying crossover

Mutation

The next step after the crossover is preventing the algorithm to be trapped in a local minimum. This duty is performed by a mutation operator. A mutation operator is insurance for randomly distributing genetic information. If a crossover is considered to perform exploitation in the current solution to find a better one, mutation is viewed as an operator to assist in the exploration of the whole search space. A mutation introduces new structures in the population by randomly changing some of its building blocks and assists in escaping from local minimum traps.

In addition, it tries to maintain genetic algorithm diversity in the new population. Mutation of variables means adding randomly created values to the variables with a mutation probability (P_m). The mutation probability decides how often a chromosome will be mutated. There are many different kinds of mutation operators for different forms of representation including binary and floating (real value) representations. Different kinds of mutation operators are include:

- Flipping (for binary representation)
  Flipping a bit involves changing 0 to 1 and 1 to 0 based on the mutation chromosome, which is generated randomly. Fig. 3.13 shows a parent, a mutation chromosome, which is randomly generated and the children. For a value of 1 in the mutation chromosome, the corresponding bit in parent chromosome is flipped (0 to 1 and 1 to 0) and child chromosome is produced. In this case, the value of 1 occurs at three places of mutation. This

Parent	1 0 1 1 0 1 0 1
Mutation chromosome	1 0 0 0 1 0 0 1
Child	0 0 1 1 1 1 0 0

Figure 3.13: Example of flipping mutation and create child

operator is proper for bit-spring representation, while every variable has only two values.

- Reversing (for binary representation)
  In this method, a randomly-generated position is selected, and the bits next to that position are reversed and a child chromosome is produced. Fig. 3.14 shows a parent, a randomly-generated point and the children.

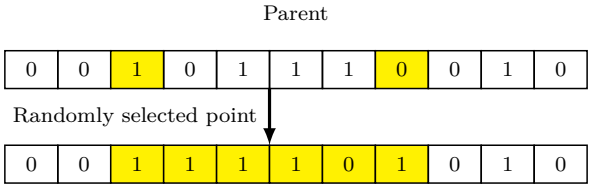


Figure 3.14: Example of reversing mutation and create child

- Uniform (for floating representation)
  Uniform mutation randomly selects one variable from the chromosomes and assigns it to a uniform random value. Fig. 3.15 shows a parent, and randomly selected points to create random changes in the genes.

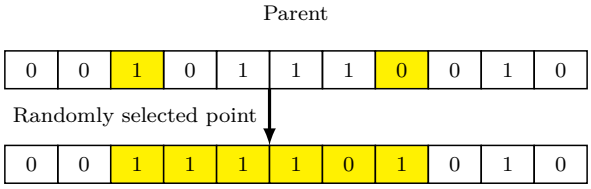


Figure 3.15: Example of uniform mutation and create child

- Gaussian (for floating representation)
  There are two main parameters in Gaussian Mutation, which are the mean and the standard deviation of the Gaussian distribution (σ). As it can be seen in Fig. 3.16, a randomly generated value from the Guassian distribution is added to each element of an individual to produce a new child.

Return to vibration isolation example in Fig. 3.12, there are two selected parents (from the initial population) and two new children (after applying crossover). All of these four chromosomes are transferred to a mating pool in order to be selected to apply mutation. One chromosome

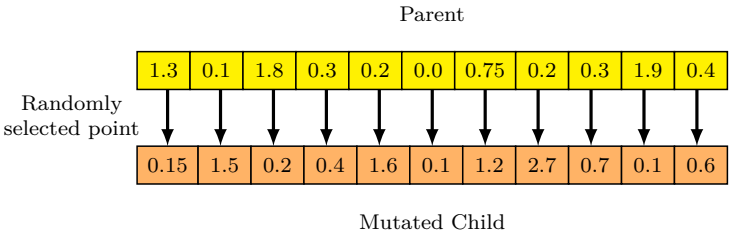


Figure 3.16: Example of gaussian mutation and create child

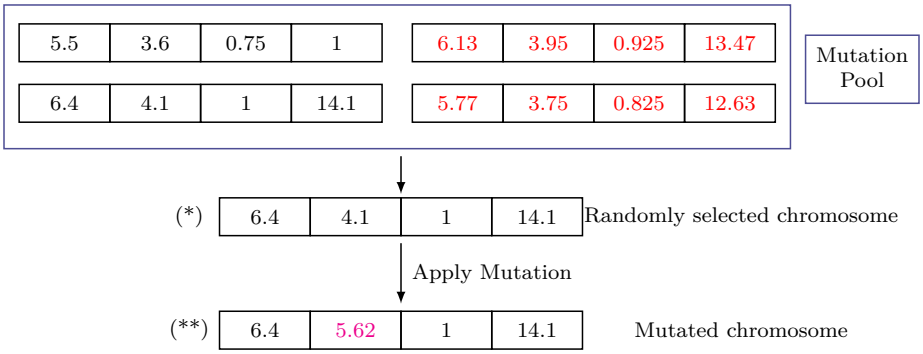


Figure 3.17: Mating pool, selected children for applying mutation and the mutated children

from the mating pool will be selected randomly to apply mutation. Fig. 3.17 shows the mating pool, the selected chromosome for applying mutation and the mutated child.

The mutated child will be substituted by the selected chromosome in the mating pool. Fig. 3.18 demonstrates the new mating pool with new children.

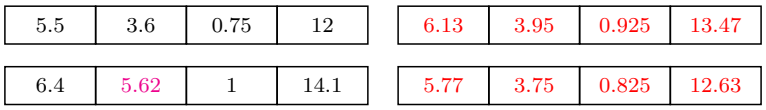


Figure 3.18: New mating pool

3.1.3. Replacement

The last step of an algorithm after recombination is replacement, which is the process of selecting chromosomes from a source of population and substituting them to from a new offspring for a new population. There is a possibility for the optimum solution to be lost after recombination with crossover and mutation since the selection process of a chromosome is completely random. When two new children are produced from two parents of a fixed population, the main problem is which of these newly generated children or parents are allowed to move forward to the next generation, so the two must be replaced.

There are two kinds of replacement methods for creating a new population including steady-state and elitism replacement. In a steady-state method, a small fraction of the population is

replaced in all iterations. This method involves inserting new chromosomes in the population as soon as they are produced. Elitisms replacement is an almost complete replacement except for the best members of each generation which are carried over to the next generation without modification. This method increases the efficiency of the algorithm since it prevents a loss of the best solutions.

Elitism replacement method is selected to generate new population in vibration isolation topic. Fig. 3.19 represents the initial population and the newly generated population.

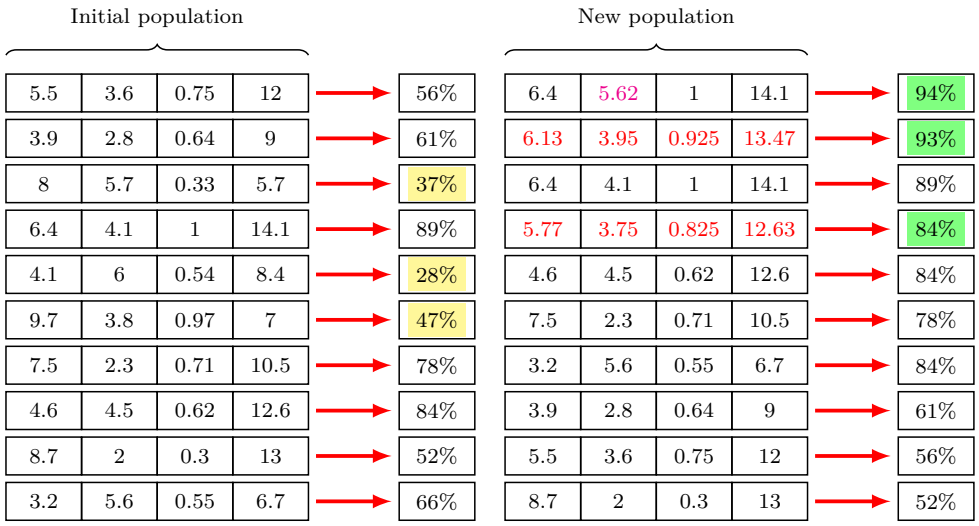


Figure 3.19: Initial population and the new generated population

It can be seen from the figure that the parameters with low efficiencies are substituted with new parameters, which results in better efficiency.

3.2. Application of genetic algorithms

A genetic algorithm (GA) is a well-known method to solve complex geotechnical engineering problems [Gavin and Xue, 2009; Zolfaghari et al., 2005]. Levasseur et al. used a GA to identify constitutive parameters of the Coulomb constitutive model from in situ geotechnical measurements [Levasseur et al., 2008]. A GA is also used for slope stability estimation by [Manouchehrian et al., 2014; Sengupta and Upadhyay, 2009].

The trench dimensions can also be optimized through GA to reach highest amount of efficiency in mitigating the vibration. Yarmohammadi et al. developed a coupled GA-FE methodology for designing single, double, and triple-trench wave barrier systems to reduce train-induced vibrations. They found that open trenches had much higher mitigation capacities when compared with in-filled trenches, and importantly using double-trench barriers instead of single-trench ones increases the mitigation capacity by as much as 20% [Yarmohammadi et al., 2019].

In another attempt, they evaluated the performance of overlapping jet-grouted columns as stiff-wave barrier walls for mitigating train-induced ground vibrations. It was observed that the developed GA/FEM could effectively find the optimal topology of the jet-grouted barriers within the design domain and the barriers with larger heights provided better mitigation [Yarmohammadi et al., 2018].

Attenuation of earthquake-induced vibrations was studied by [Rezaie et al., 2018] through installing buried concrete-filled trenches. A GA model was developed for finding the efficient layout of concrete barriers in a manipulated soil zone around the structure. It was observed that some optimal layouts of limited volume can attenuate the elastic demands of the structures in the range of $30 - 80\%$. In further investigations, they proved that the introduced model could find effective wave barrier layouts with a high potential capacity to mitigate horizontal vibrations, especially for earthquake loadings that have a high-frequency content [Amir Rezaei, 2018].

3.3. Artificial Neural Network

Since modern computers are becoming more powerful, researchers try to use machines to perform calculations of complicated models. Artificial Intelligence (AI) is known as the process of simulating human intelligence in machines for thinking like humans and mimic their actions [Nilsson, 2014]. Artificial intelligence is able to interpret and learn external data and use those learnings to reach specific aims through flexible adaptation. Deep learning is a subset of Machine Learning (ML) that has a network for learning from data. Fig. 3.20 illustrates the application of all three algorithms [Kim, 2017].

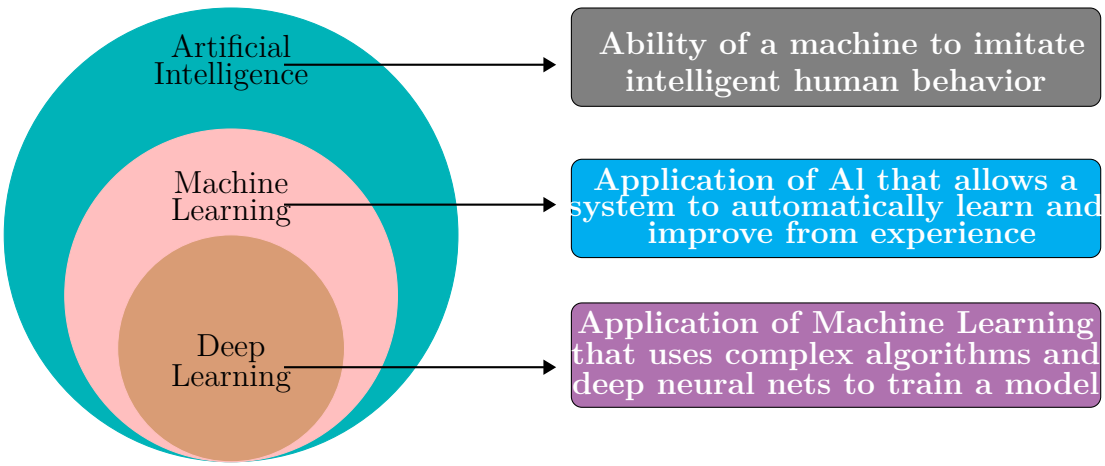


Figure 3.20: Classification of artificial intelligence [Kim, 2017]

Machine learning is a technique to figure out a model from data. After developing the model, it will be applied to real field data. Fig. 3.21 shows the process in which the vertical row indicates the learning process, while the horizontal row demonstrates the trained model [Kim, 2017].

The machine learning technique is categorized into three different groups based on the training

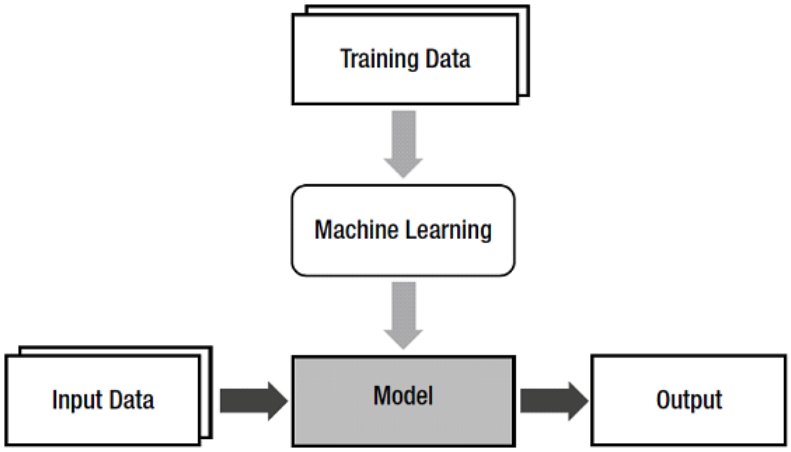


Figure 3.21: Evaluating a model based on field data [Gurney, 1997]

model including [Voyant et al., 2017]

- Supervised learning
- Unsupervised learning
- Reinforcement learning

There is input and ground truth for each training dataset in supervised learning. The main duty of the supervised learning technique is to produce a correct output from the input using training data. Conversely, the unsupervised learning technique contains inputs without ground truth.

Classification and regression are two types of application of the supervised learning technique. Classification is the problem of identifying the classes to which the data belong. In contrast, regression predicts a value. Vibration isolation problem is categorized as a regression problem [Reed and MarksII, 1999].

Machine learning models can be used for different tasks including:

- Artificial Neural Networks (ANN) for regression and classification
- Convolutional Neural Networks (CNN) for computer vision
- Recurrent Neural Networks (RNN) for time series analysis
- Self-organizing Maps for feature extraction
- Deep Boltzmann Machines for recommendation systems
- Auto Encoders for recommendation systems

An Artificial Neural Network (ANN) is a computational model, which is inspired by the structure and functions of biological neural networks in human brains. ANN acts like an artificial human nervous system for receiving, training, and transmitting information. ANN is the most exciting and powerful branch of ML, in which a computer model learns to perform tasks directly from data. ANN is placed as the model in Fig. 3.21 and the learning rules, which are supervised learning with a regression problem is placed as the machine learning. Table 3.2 shows different types of neural network and their application to solve different problems.

Table 3.2: Different types of neural network and their application

Abbreviation	Full name	Problem solver
ANN	Arbificial Neural Network	Pattern recognition
CNN	Convolution Neuval Network	Image processing
BNN	Recursive Neural Network	Speech recognition
DNN	Deep Neural Network	Acoustic modeling
DBN	Deep Belief Network	Cancer detection

3.3.1. Neurons

The principal idea behind a neural network is based on imitating the structure of neurons and the cells in the brain for performing some tasks like recognizing patterns and making decisions.

Fig. 3.22 shows a biological neuron, which is the fundamental unit of the brain and the nervous system. The cells responsible for receiving input from the external world via dendrites, process it through a function and give the output through axons. A neuron does not have any storage for saving data; it just transmits signals from one neuron to another [Gurney, 1997].

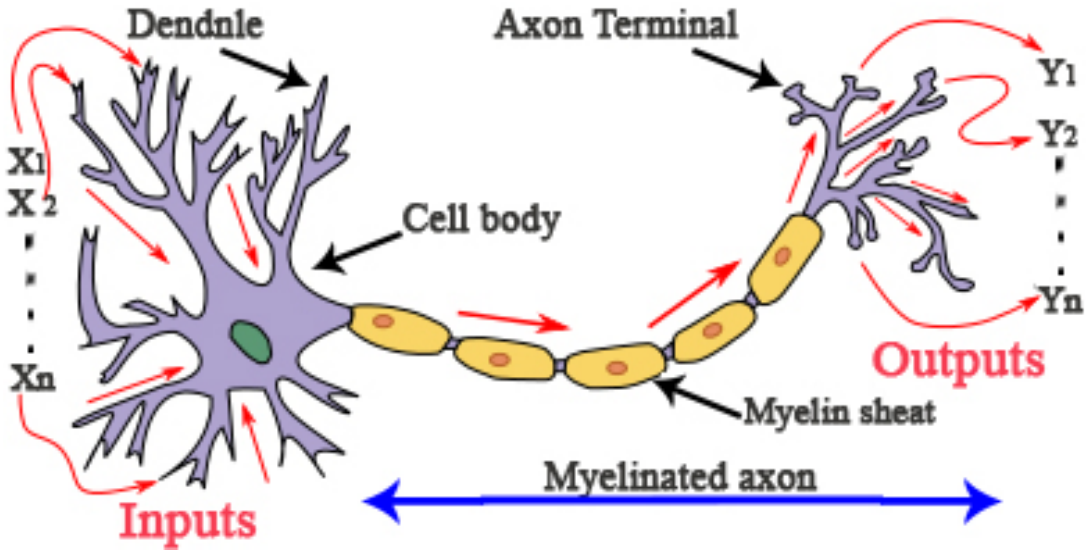


Figure 3.22: A biological neuron [W and WM, 2002]

An artificial neuron is a mathematical function based on biological neurons. Table 3.3 represents the analogy between the human brain and artificial neural network.

Table 3.3: Analogy between the human brain and artificial neural network

Biological Neuron	Artificial Neuron
Cell	Node
Dendrites	Input
Synapse	Weights
Axon	Output

A perceptron is a model based on biological neurons for the supervised learning of binary classifiers. This model enables neurons to learn and process data in a training set once. Single and multilayer are two types of perceptron. A single perceptron with two layers including input and output layers is presented in Fig. 3.23.

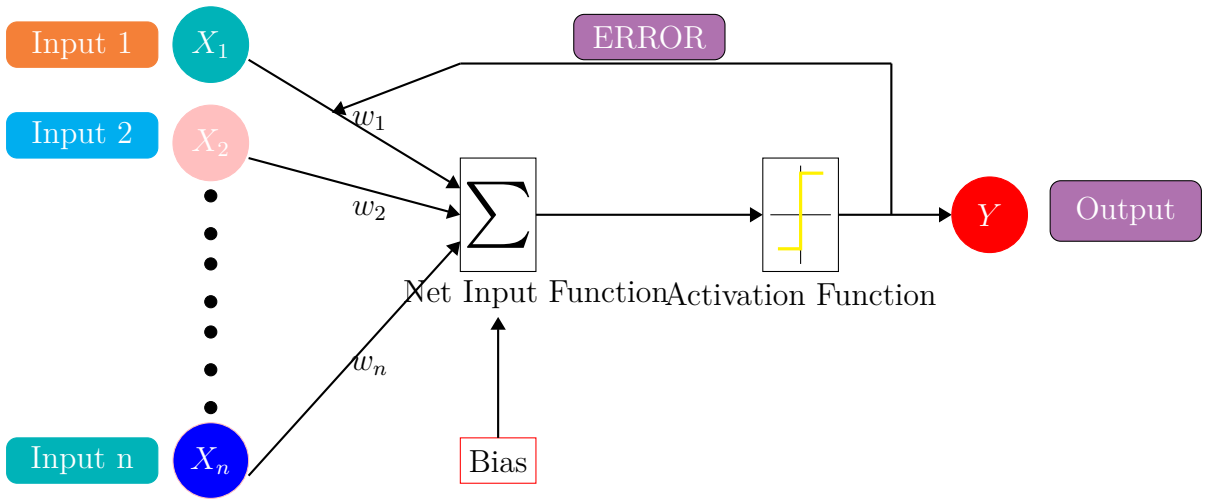


Figure 3.23: A single perceptron [Gurney, 1997]

Nodes X_1, X_2, and X_3 which are called features, are the input, and w_1, w_2 and w_n are the weights for the corresponding features. Weights show the strength of the features. Each feature is multiplied by a connection weight and pulsed through a summation function. Then a bias, which is a constant value, is added to the weighted sum for shifting the result of an activation function.

The summation is passed through the activation function. An activation function introduces non-linearity to the neural network through converting the weighted sum of features into the output signal.

The activation function, which is attached to each neuron in the network, determines the output of a neural network. In addition, it helps to normalize the output of each neuron to a range of $[0, 1]$ or $[-1, 1]$. A neural network without an activation function is a linear regression model. There are two different kinds of activation functions including linear and non-linear functions.

The non-linear activation functions are the most applicable in neural networks. The most popular non-linear activation functions include:

- Sigmoid activation function
- Tanh or hyperbolic tangent activation function
- ReLU (Rectified Linear Unit) activation function

A sigmoid function is an exponential function having a characteristic "S" shape curve and it takes a real value as input and the output value is in the range of $[0, 1]$.

Tanh is an activation function similar to sigmoid in terms of shape but the range of output of this function, is $[-1, 1]$. Therefore, the inputs to the next layers will not always be the same sign. The applicability of the functions is more for classification between two classes. Both Tanh and sigmoid functions are used in feedforwards neural networks.

ReLu, which stands for Rectified Linear Units, is another type of non-linear activation function, which stands for Rectified Linear Units. Mathematically, this function $R(z)$ can be defined using max function over the set of 0 and the input $z, R(z) = \max(0, z)$. Fig. 3.24 represents the pictures of all three activation functions.

In the last step, information will be transferred to output. If the predicted output with ANN is equal to actual output which is called label, the algorithm will be finished; otherwise, there will be an error and it returns to back to neurons for adjusting the weights and bias and this process will continue until the error is minimized.

3.4. Feedforward networks

Feedforward or multilayered perceptrons are an artificial neural network, which combines many layers of perceptrons. A feedforward network leads information only in a forward direction from an input layer through a hidden layer and finally to an output layer. In this network, all nodes are fully connected, and the weights are recognized into layers that feed into each other.

Fig. 3.25 represents a multilayered feedforward neural network in which the first and the last layers are called input and output, respectively. The layers between the input and output are called hidden layers. The number of hidden layers is adjustable based on the complexity of a problem. The application of hidden neurons is to intervene between input and output data. In a feedforward neuron network, every neuron in each layer is fully connected to every other neuron in the next forward layer.

Performing a forward-pass of a network gives us the predicted value. Thus, the goodness of the predicted value should be evaluated by comparing the predicted and actual values. This is the duty of a cost function. Different cost functions are include mean square error (MSE), root mean square error (RMSE) and correlation (corr), which are used to measure the error

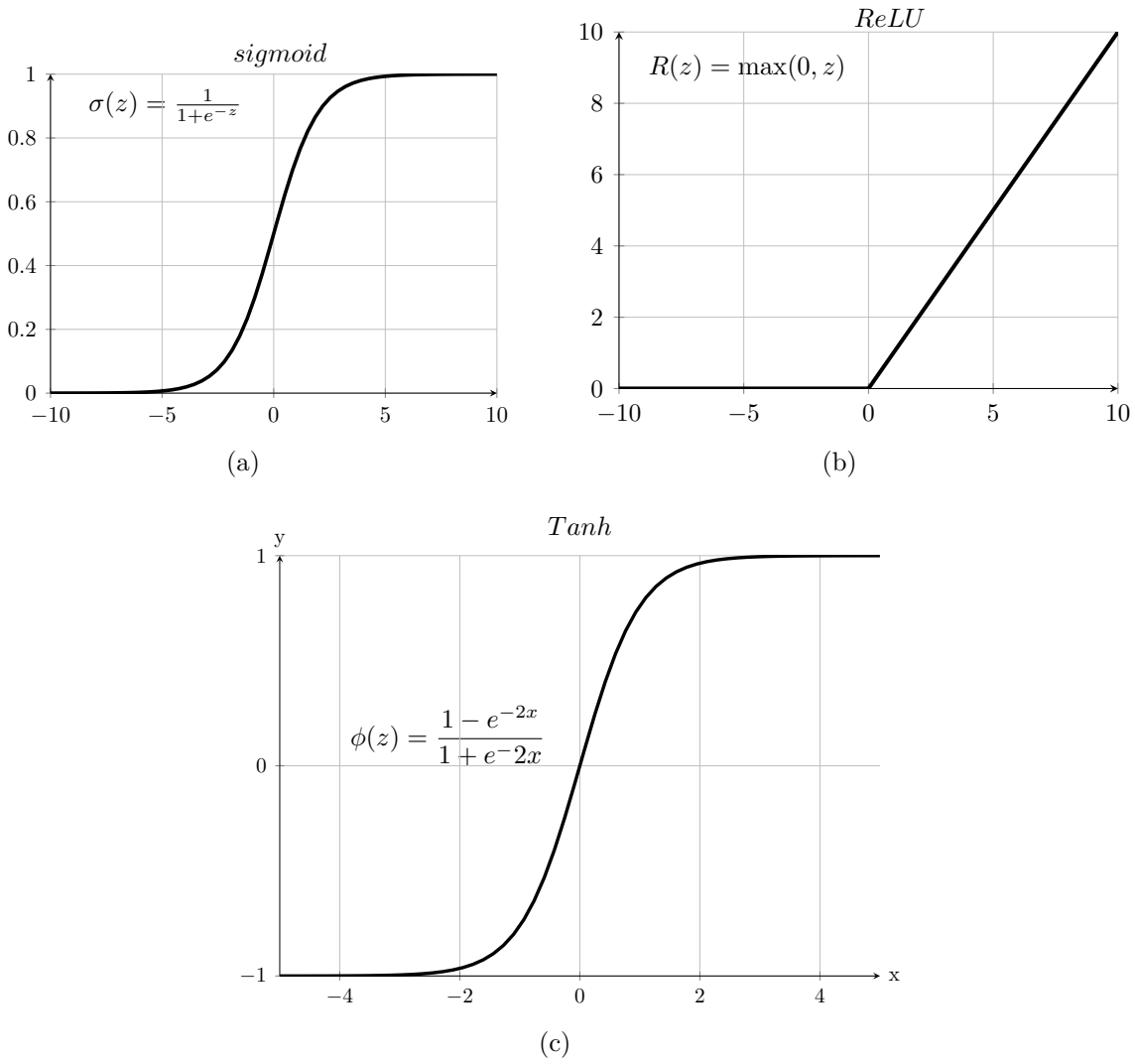


Figure 3.24: Activation functions in artificial neural networks

between the predicted value with a feedforward neural network and the actual value. MSE is the average squared difference between the predicted and actual value. RMSE is the standard deviation of the predicted errors, and it shows how data are concentrated around the line of the best fit. Corr represents how independent variables are related to each other.

The weights W and biases b are the most important factors in converting an input to impact the output. Therefore, training a neural network means finding the proper value for the weights and biases. Generally, the process of adjusting the weights and biases between input data and hidden neurons for minimizing the cost function is called training a neural network.

A neural network can be considered shallow, there is an input layer as well as one hidden layer, which processes the inputs, and an output layer, which presents the final result of the model. On the other hand, a deep neural network usually has between $2 - 8$ hidden layers of neurons.

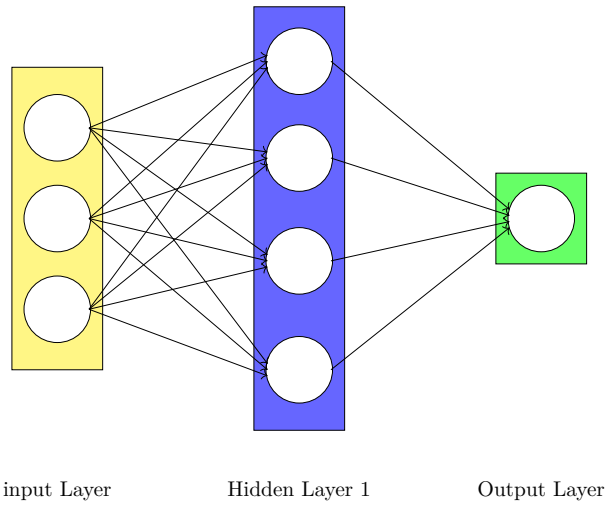


Figure 3.25: A multi-layered feedforward neural network

3.4.1. Backpropagation

A backpropagation algorithm is the most popular learning algorithm in training a feedforward neural network for a supervised problem. In this procedure, the measured error through a cost function is propagated back to all weights and biases in order to decrease error. In summary, backpropagation is adjusting the weights and biases of all connections in a network repeatedly in order to minimize error. An error describes how a set of parameters in a network fits a data set.

There are several algorithms for optimizing errors including:

- Gradient Descent
- Newton Method
- Gauss-Newton Method
- Levenberg-Marquardt Algorithm

The gradient descent method is a first-order iterative optimization technique to adjust the weights and biases in the backpropagation phase to reach the best output. In order to find an appropriate value for weights and biases, a derivative of the cost function should be taken with respect to the weights and biases. A gradient descent algorithm works as follows:

1. Initialize the weights randomly$\sim N(0, \sigma^2)$
2. Loop until convergence:
    a. Computing gradient $\frac{\partial J(W)}{\partial W}$ for all nodes

b. Updating weights, $W = W - \eta \frac{\partial J(W)}{\partial W}$

3. Returning weights

where η is the learning rate, which is one of the most important parameters in the gradient descent technique. The learning rate determines the speed of a neural network training process. A small value of learning rate leads to an optimal set of weights but it may take a long time. On the other hand, a large learning rate results in training the model faster, we may face the risk of missing the optimal weight. Step decay is a proper method for finding the optimal learning rate, in which the learning rate is reduced by some percentages after a set of training epochs. The Newton's method is a second-order algorithm, in which the Hessian matrix is used instead of the Jacobian Matrix. The goal of this algorithm is to find better training directions through using the second derivatives of an error function. The conjugate gradient algorithm can be regarded a method between Newton's and gradient descent procedures. The search process in this method is performed along a conjugate direction which can result in faster convergence than with gradient descent directions.

The Gauss-Newton method, which is used to solve nonlinear least square problems, is a developed model of the Newton method. The assumption in this method is that the objective function in the parameters near the optimal solution is quadratic. The Gauss-Newton method usually converges a medium-sized problem much faster than the gradient descent method.

The Levenberg-Marquardt algorithm is an iterative technique, which is commonly used to solve non-linear Least-squares problems. The LM method can be defined either as a combination of the gradient descent optimization method when the parameters are far from their optimal values or the Gauss-Newton optimization procedures when the parameters are close to their optimal value.

3.4.2. Data preparation

The size of a database plays a significant role in training a neural network. Large database results in a more accurate model but requires a lot of computational time. On the other hand, too small database results in a less accurate model and requires less computational time. Therefore, the database should be big enough to result in an accurate model and optimal computational time, too.
When the input data in the database have different ranges, the database needs to be normalized. Normalization is applied to a neural network in order to produce a set of data values within the same magnitude. When the features are different in terms of magnitude, the fluctuations of some parameters with bigger ranges may decrease the influence of the parameters with smaller ranges. Nevertheless, the features with smaller ranges may be more important in predicting the desired output. Therefore, all the data should be normalized to have the same range to ignore the influence of different ranges in ANN. All features are normalized to be in the range

of $[-1, 1]$ through Eq. (3.3).

$$(X_j)_n = 2\left(\frac{X_j - \min X_j}{\max X_j - \min X_j}\right) - 1 \tag{3.3}$$

where X_j is the feature, $(X_j)_n$ is the scaled input feature, $\min X_j$ and $\max X_j$ are the lower and upper limits of input features, respectively.

3.5. Application of ANN

Over the last few years, ANNs have been widely applied in several areas of geotechnical engineering problems and have demonstrated some degree of success [Shahin et al., 2001a]. The method is able and well-suited to model complex problems where the relationship between model variables is unknown. ANNs have been used successfully in pile capacity prediction [Das and Basudhar, 2006], site characterization [Samui and Sitharam, 2010], earth retaining structures [Ghaleini et al., 2019], estimation of the bearing capacity of shallow foundations and settlement prediction [Ziaee et al., 2015], slope stability [Choobbasti et al., 2009], design of tunnels and underground openings [Lee and Sterling, 1992], liquefaction during earthquakes [Farrokhzad et al., 2012] and soil compaction and permeability [Shahin et al., 2001b].

Jayawardana et al. investigate the use of artificial neural networks (ANN) as a smart and efficient tool to predict the effectiveness of geofoam-filled trenches to mitigate ground vibrations. They used multi-layer feedforward network with a backpropagation algorithm with two hidden layers [Jayawardana et al., 2019].

A comprehensive parametric study has been performed by [Alzawi, 2011] and the results were used to train an ANN model for predicting the efficiency of geofoam-filled trenches. The developed model exhibited a good generalization capacity beyond the training stage as validated by new finite element results within the range of training database.

In addition, soil-ground vibrations induced by moving trains were predicted based on the artificial neural network model [Fang et al., 2019]. The result states that the predicted method can control the maximum error below 6.41% and the average error below 2.29% when it is used to predict acceleration vibration levels.

Hung et al. focused on using multiple neural networks to estimate the screening effect of surface waves by in-filled trenches [Hung and Ni, 2007]. Three artificial neural networks, a backpropagation network (BPN), a generalized regression neural network (GRNN), and a radial base function network (RBF) were used to evaluate the performance of a chosen physical model.

The neural network tool was used to analyze the parametric effects of vibrations versus the surface layer's depth [Eddine, 2017]. Important conclusions were derived from the analysis regarding the mechanical and geometrical properties of multiple layers and their varying effects with regard to the distance from the source.

3.6. Response Surface Methodology

Evaluating the effects of multiple factors and their interactions on one or more response variables is a challenge for researchers in many fields [Khuri and Mukhopadhyay, 2010]. In response surface problems, Y is the response variable of interest and X_1, X_2, ... X_n are regarded as a set of predictors. For instance, in a vibration isolation system, Y is recognized as the efficiency of a trench and X_s are governing factors like depth, location, etc.

In some systems, the nature of the relationship between Y and X_s may be known exactly based on a linear function. Then, Eq. (3.4), which is called mechanistic model can be suggested for fitting the system.

$$Y = g(X_1, X_2, ..., X_n) + \epsilon \tag{3.4}$$

where g is a linear function and ϵ represents the error in the system.

Now consider a system in which a mechanistic model is not suited for the system, so that the model should be approximated by an unknown and non-linear function, which is presented in Eq. (3.5).

$$Y = f(X_1, X_2, ..., X_n) + \epsilon \tag{3.5}$$

where the function f is usually a non-linear polynomial, typically between the first or fourth-order polynomial. This empirical model is called a response surface model.

Response Surface Methodology (RSM) is a statistical method for investigating the interaction and relationship between the independent variables with different responses [Adhikari, 2016]. RSM uses quantitative data from appropriate experiments to determine regression model equations and operating conditions [Sahu et al., 2010]. RSM is a collection of mathematical and statistical techniques to model and analyse problems in which a response of interest is influenced by several variables.

The most extensive applications of RSM are in the industrial world, particularly in situations where several input variables potentially influence performance measures or quality characteristics of a product or a process. These measured performances are called the response. They are typically measured on a continuous scale, although attribute responses, ranks, and sensory responses are not unusual. However, most applications of RSM will involve more than one response. The input variables are sometimes called independent variables, and they are subject to the control of engineers or scientists, at least for purposes of a test or an experiment.

The advantages offered by RSM can be summarized as determining the interaction between independent variables, modelling the system mathematically, and saving time and cost by reducing the number of trials. Another purpose for RSM is to evaluate how a response changes to a given desirable direction by adjusting a process or design variables. The statistical method enables one to optimize responses (dependent variables) which are influenced by various factors (independent variables) [Baş and Boyacı, 2007; Myers et al., 2016].

4 Vibration screening in homogeneous soil

4.1. Problem definition

The mitigation of structures vibration can be accomplished by providing more damping elements in the transmission path of incident waves by means of installation devices like an isolation trench. An advantage of interventions on transmission path is that no change to the track is required, while a big area can be protected from vibration. In addition, the implementation of this system along an existing path can be achieved relatively easy. A wave barrier creates a finite material discontinuity for incoming waves by intercepting, scattering, diffracting, and refracting wave propagation in soil, which can decrease the vibration amplitude beyond the obstacle.

This chapter presents the results of a field test [Sprengel, 2017] and a comprehensive parametric study. The results of the field tests are presented in section 4.2. $2D$ and $3D$ finite element models are developed and validated in section 4.3.1. Subsequently, different systems in terms of the shape of the trench are analysed in near field and far field schemes in sections 4.4 and 4.5, respectively.

4.2. Field test

4.2.1. Site investigation

A full experimental test has been conducted by [Sprengel, 2017] to analyse the efficiency of geofoam-filled trenches in screening dispatched waves. Subsoil properties and the location of the field test are one the most important features. The main criteria for selecting the site location are considered to be homogeneity of the soil, easy accessibility to the test site and possibility of the implementation a trench. For these purposes, the location of the test site has selected in a gravel pit based on a flat area with dimensions of approximately $40m \times 60m$, located in Geilenkirchen, a town in North Rhine-Westphalia, was selected as the location of the test site.

The soil analysis consisted of soil classification using samples from different depths. The result of the laboratory test of the soil demonstrates that the subsoil is a mixture of sand and gravel up to a depth of at least $15m$. According to DIN 18196, the soil is classified as intermittently graded sand. The medium soil density was determined as ($\rho = 2g/cm^3$).

The Multichannel Analysis of Surface Waves method (MASW) was used to determine the dynamic elastic material parameters, which are key factors for describing the dynamic behaviour of the subsoil [Park et al., 2007]. MASW is a geophysical procedure for determining the depth-

dependent profile of propagated shear wave velocity. The data were recorded over a total of 48 geophones, which were laid out at a distance of $1m$ and registered by a seismograph. Fig. 4.1 shows the geophones in the field test and the determined profile of the propagation velocity of the shear wave over the depth as an average value over the entire measuring section.

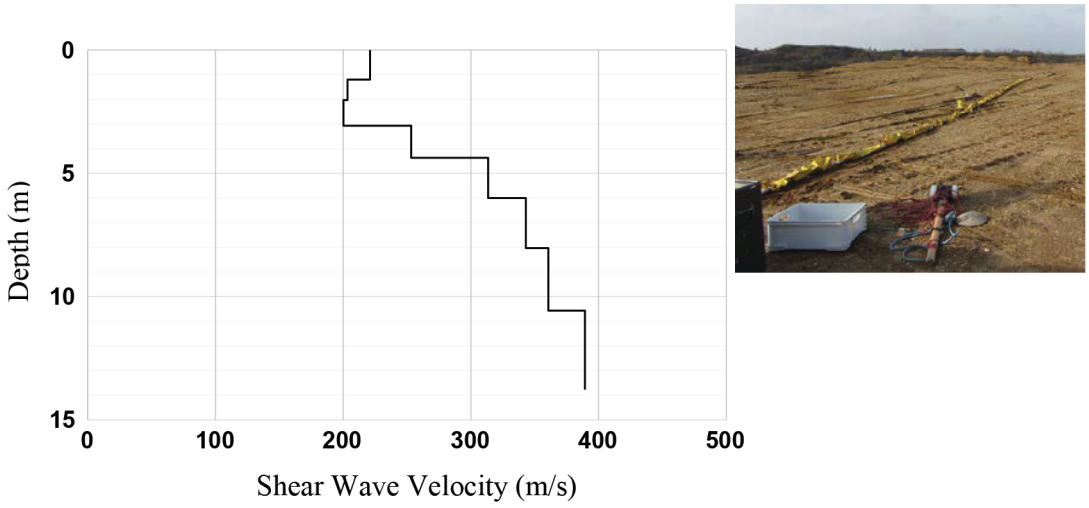


Figure 4.1: Shear wave velocity profile of the site [Sprengel, 2017]

4.2.2. Field test method and equipment

A shaker from Baudynamik Heiland & Mistler GmbH, which allows to produce a harmonic excitation of the ground, was used (see Fig. 4.2 (A)), which allows to produce a harmonic excitation of the ground. The shaker was founded on four steel plates, and the overall dimensions of the shaker were $72 * 72cm$. The servo-hydraulic shaker simulates the requested objects, in this case, harmonic load in the frequency range of theoretically 0.01 to $110Hz$ with a maximum dynamic force amplitude of $20kN$. The force amplitude generated in the field test is constantly $5kN$ in the frequency range from $10Hz$ to $110Hz$, but only the range from $20Hz$ to $80Hz$ was used for trench efficiency evaluation [Sprengel, 2017].

The measurement of vertical soil particle velocity had been done twice; one before installation of the trench and one after the implementation of the geofoam-filled barrier. The measuring chain in the field test consisted of the vibration sensors including geophone and accelerometer shown in Fig. 4.2 (B), which transmitted their data to a measuring computer. The transferred data were analysed by MESSI, a program developed by the Department of Structural Mechanics at RWTH Aachen University for signal acquisition and processing.

Some distinct points are selected to install vibration sensors at different distances from the source of vibration and the obstacle. Fig. 4.3 illustrates the selected measuring arrangement including the positioning of the vibration source, the geofoam-filled barrier and the vibration sensors, respectively.



Figure 4.2: Vibration source: (A) Shaker structural dynamics Heiland & Mistler GmbH, (B) Vibration sensor

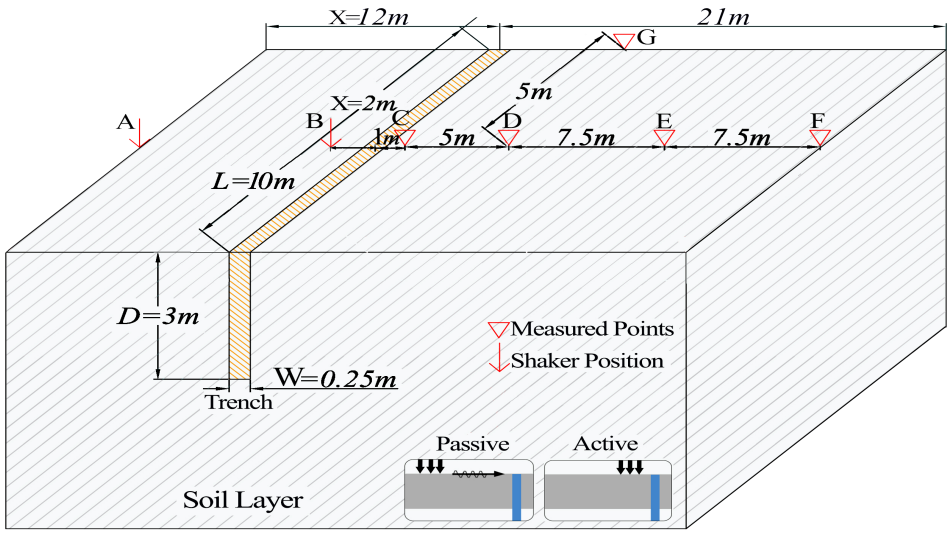


Figure 4.3: Measuring arrangement

The shaker was located at two different distances from the trench. To investigate the effectiveness of the obstacle for both situations, the vibration source has been appropriately positioned relative to the barrier. Due to the limited number of available vibration sensors, seven measuring points were selected per measurement series, where measuring points A and B located directly on the shaker for far field and near field isolation, respectively.

An approximate propagation velocity of the Rayleigh wavelength at the surface of $v_r = 200m/s$ and a minimum and maximum examined frequency of 20 and $100Hz$ leads to a wavelength of

$\lambda_r = 10$ and $2m$. Therefore, the position of vibration source was chosen to be $2m$ for near field isolation and $12m$ for far field isolation, respectively. Excavating a trench to mitigate incident waves is the next step after measuring vertical soil particle velocity in the absence of the barrier. Most of the previous studies [Alzawi and El Naggar, 2011; Ulgen and Toygar, 2015; Gao et al., 2018] state that a normalized depth of $0.8\lambda_r$ is enough to reach an acceptable value of efficiency. Therefore, one attempt was made to reach this depth during the experimental test.

A wheel trencher device was used to dig the trench with the dimensions of $20cm$ wide and $3.2m$ deep and $10m$ long, respectively. However, the excavating process to reach this depth has failed because of hitting rock in some sections. Therefore, the excavated depth of the barrier was between $2.8 - 3.2m$ and an average depth of $3m$ was considered for the whole trench. The final geometry of the trench is included $20cm$ wide, $3m$ deep, and $10m$ long, respectively.

The lack of stability in the trench due to the kind of soil resulted in very short stability of the open trench. Therefore, the foam was injected immediately after excavating the trench. The device used to dig the trench and the final geometry of the injection body are shown in Fig. 4.4. The geofoam material for filling the barrier was a PU from Uretek Company that could be injected in the trench without any resistance and free expansion. All these factors led to a geofoam with very low density. A laboratory test was carried out to find the dynamic properties of the geofoam. The results showed a medium density of $0.61kN/m^3$, shear wave velocity of $330m/s$, and a Poisson's ratio ratio close to zero (0.01).



Figure 4.4: Wheel trench device and injection of geofoam

4.2.3. Test results and discussion

The test results of the field-test were evaluated in terms of the vertical vibration velocities of the soil, which were measured in the time domain and transmitted into the frequency domain by applying Discrete Fourier Transformation (DFT). The results were presented in the frequency domain. An advantage of the representation in the frequency domain is the possibility of visualizing frequently occurring interference influences. The final assessment of the effectiveness of the trench is made by comparing the two measurements before and after the installation of the trench.

The results of full experimental study for all measured points beyond the geofoam-filled trench were analysed, and the results are presented in the following figures. In order to ensure the reliability of the results, the measurements were made twice; once before and once after installing the barrier.

Fig. 4.5 shows a significant attenuation for almost all the measured points for a frequency between 30 and $60Hz$ by implementing the geofoam-filled trench. The results show the highest amount of mitigation for the first point after the trench (point C) in comparison with other points. As the frequency of the applied load increased, the vertical soil velocity amplitude declined dramatically and then gradually reached a stable value after a frequency of $60Hz$. The system effectiveness rose from 37 to 60% by increasing the frequency from 30 to $40Hz$ for point C.

A practical comparison can be drawn between the screening of incident waves for the measured points of D and G, which were located in the line and beside the source in Fig. 4.3, respectively. The results revealed that the highest amount of mitigation was observed in the centreline of the trench in comparison with other areas. The efficiency of the frequency of $40Hz$ for both points D and G were 65 and 35%, respectively, which shows a considerable difference.

There was no attenuation effect for the frequencies less than $20Hz$, and it seems that the isolation system is not practical in lower frequencies. Athanasopoulos stated that the attenuation of R-wave amplitude is frequency-dependent, and it increases exponentially with the frequency of propagating waves due to both geometrical and material damping [Athanasopoulos et al., 2000]. Therefore, low frequency of load results in less attenuation of propagated waves in the soil. This issue impairs the effectiveness of the trench in mitigating waves with a large R-wavelength.

The same statement can be applied to explain the non-practicability of the trench in high frequencies. Higher frequencies result in more attenuation of waves and for these frequencies, the attenuation effect is high enough to let propagated waves disappear. Therefore, there is no difference between amplitude of vertical soil particle velocity before and after installing the trench.

The results of various points for far field isolation are presented in Fig. 4.6. The area immediately after the trench had the highest screening performance. The screening performance in attenuation of incident waves increased for a frequency range between 30 to $60Hz$, whereas the same increase happened for point E for a frequency range of $35 - 50Hz$.

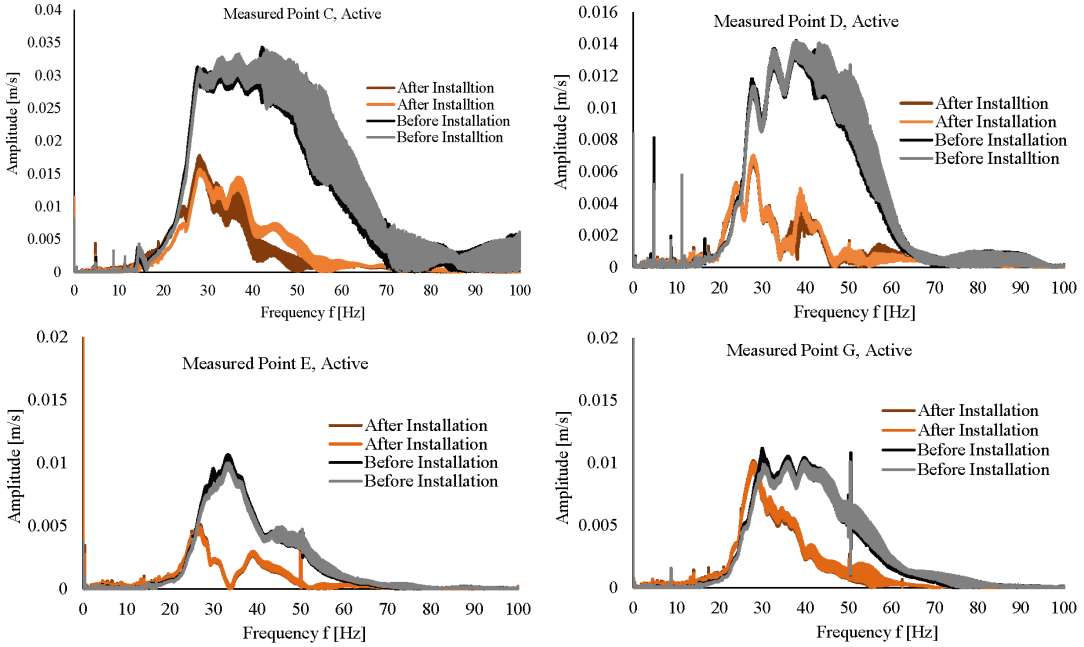


Figure 4.5: Representation in the frequency domain: Measuring points C, D, E, G (Near field Isolation)

However, some unexpected peaks and valleys were observed in vertical soil velocity amplitude of 50 and $40Hz$ for points C and D, respectively.

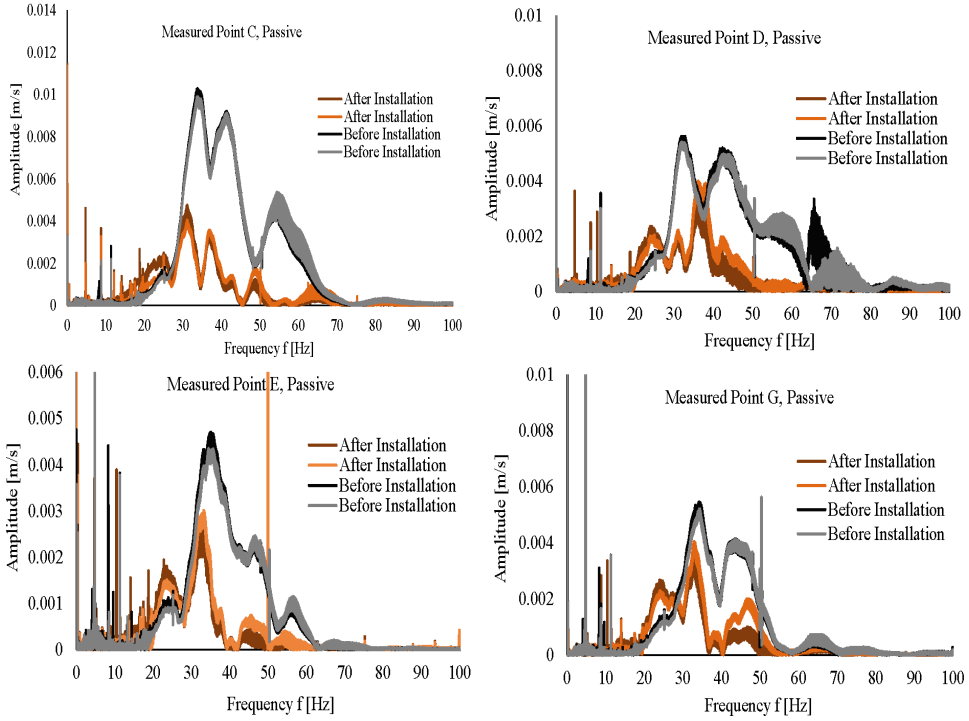


Figure 4.6: Representation in the frequency domain: Measuring points C, D, E, G (Far field Isolation)

Baidya et all. who investigated the amplitude of vibration in layered soil stated that many soils in nature exhibit an increase in shear modulus with depth, and this issue can be recognized as a reason for distinct peaks and valleys [Baidya and Krishna, 2001]. Incoming waves may reflect and refract at the interfaces of soil layer, and they can superpose with surface waves in the same phase and originate a bigger wave, which causes amplification in the vertical response of soil.

As it was already mentioned in section (4.2.2), we hit a rock during the excavation, and for this reason the depth of the trench did not reach the target value ($3.2m$). It means that there were a full reflection of incoming waves after encountering the rock. Therefore, the unexpected discrepancies in the results can be explained by superposition of surface waves and reflected waves from the rock [Mahdavisefat et al., 2018].

Frequency domain analysis of the results provides opportunity to monitor normalized trench depth in terms of R-wavelength. Changing the frequency of the load leads to changing the length of R-wave since the shear wave velocity of the soil is constant. Therefore, the average amplitude reduction ratio of the geofoam-filled trench is presented as a normalized depth in Fig. 4.7 for both near field and far field systems.

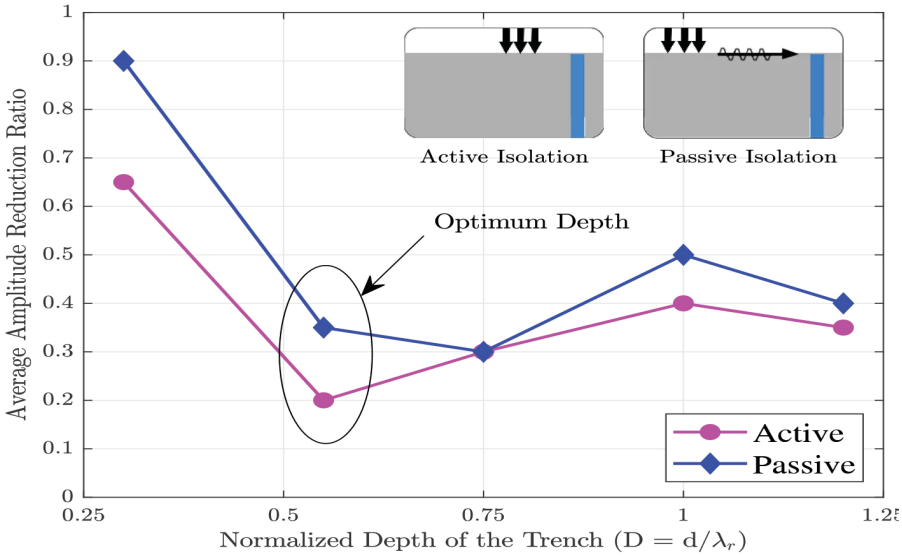


Figure 4.7: Influence of normalized barrier depth on $\overline{A}_r$ ($X = 0.5$)

The results show that increasing D results in decreasing the value of ($\overline{A}_r$), which means increasing the efficiency of the trench. The lowest value of ($\overline{A}_r$) is happened for the normalized depth of approximately 0.6, which is in line with the results of [Alzawi and El Naggar, 2011]. Therefore, this depth can be considered to be normalized depth to reach the highest value of efficiency for both near field and far field isolation.
Average amplitude reduction ratio is expected to decrease with increasing the depth of the trench. However, some amplifications in ($\overline{A}_r$) values are observed after the normalized depth of 0.6. Haupt stated that distinct peak can occur when shear wave velocity of the soil increases proportional with the depth. In addition, Massarsch indicated that refracted waves from the

trench and the transferred waves beneath the barrier can superpose in the same phase and originate a bigger wave, which causes amplification. Since the soil profile in experimental test was non-homogeneous in terms of increasing shear wave velocity, the unexpected fluctuations can be explained by superposition of the surface waves.

4.3. Numerical modelling

A time domain $2D$ and $3D$ numerical models using the finite element package, Plaxis (2019) was developed to examine the efficiency of trench. A comprehensive parametric investigation was carried out to access the effectiveness of different isolation systems of wave barriers for near field and far field isolation due to harmonic load in vertical direction.

Regarding the material for filing the barriers, a stiff barrier is filled with concrete while a soft obstacle is filled with geofoam. The results of the detailed parametric investigation are presented in the discussion section and some applicable recommendations are provided for designing a practical wave barrier.

To maintain the independency of the analysis on the exciting frequency of the dynamic load, geometric parameters (distance between the trench and the vibration source) and dimensional factors (D, W and L), which are the governing factors in the wave attenuation, are normalized by R-wavelength.

Since the model is largely affected by the transmitted and reflected waves from the boundary of the model, it is important to keep the region of interest far enough from the reflecting boundary. Therefore, the dimensions of the model were selected as (50, 20, 20 m)($3D$) and (70, 25 m)($2D$) in the case of near field and far field system, respectively. The soil is modelled as homogeneous, isotropic and half-space. The linear elastic model was selected for the soil since the amplitude of generated vibrations were small and the soil did not experience the development of plastic zone in the region under consideration.

Applying a special boundary condition is one of the most important factors in dynamic calculation to prevent the reflection of waves at the model's boundary, which do not exist in reality. For this purpose, viscous boundaries were applied to the bottom and right sides of the $2D$ and $3D$ models and at right direction of Y axis max direction for $3D$ model, too. A viscous boundary condition, which is introduced by Kuhlmeyer and Lysmer [Kuhlemeyer and Lysmer, 1973], consists of viscous dampers applied in X, and Y axises (for $2D$), and Z axis (for $3D$) direction along the boundary.

Plaxis uses a global meshing parameter, which is called average element size to show the quality of a mesh. This parameter is calculated based on the dimensions of the model and the number of elements. An average element size (I_e) of 0.5 is enough to reach acceptable results and satisfy the criteria of Kuhlemeyer and Lysmer [Kuhlemeyer and Lysmer, 1973] for assuming the average element size less than to one-eight of the wavelength associated with to the maximum frequency component of the input wave.

Vibrating sources can generate either transient (create by blasting) or continuous (created by vibratory pile driving or trains) motions. Some researchers [Woods, 1968; Qiu, 2014; Çelebi et al., 2009] used an oscillatory vibrator to generate a continuous motion. Babu et al. used a vibratory compactor in an experimental test to simulate an operating frequency in the range of 30-70 Hz [Sivakumar Babu et al., 2011].

The vibration source in this study is modelled as a vertical harmonic load with the amplitude of 1 kN and frequency of $50Hz$. The dynamic time interval is considered $0.5s$, which is enough to allow the passage of dynamic load. The steel plate under the shaker is modelled as a plate and the shaker weight is considered a uniformly distributed load with a magnitude of $1kN/m^2$. However, the weight of the steel plate and the shaker is kept constant during the parametric study since it does not play a significant role in the results and the difference for the efficiency of trench between zero and non-zero foundation weight is 1.5%, which can be neglected [Alzawi and El Naggar, 2011; Kattis et al., 1999; Saikia, 2016].

In order to save calculation time, Plaxis remote scripting feature is used to couple the finite element model (Plaxis) with Python programming language. For this purpose, a script is developed to allow the user to control both the input and the output of the model through connecting Plaxis and Python. The main advantage of the automation is accelerating the pace of the parametric study.

In this method, Plaxis connects to Python, and the scripts are imported to the Plaxis as a text file. Thereafter, Python reads the code and evaluates the dimensions and the position of the trench based on the inputs data, and creates a new FE model.

The input of the script corresponds to the values selected for different parameters, including the depth D, width W, length L, and the distance between the walls S and the location X. Three different systems are selected including single, double, and triangular walls to assess the effect of the shape of the trench on the screening performance.

The script starts by creating a borehole and subsequently installs the trench, defines different phases, runs the model, and calculates the efficiency of the trench. The entire process is executed automatically as shown in Fig. 4.8. Different functions are defined to execute the trench with different configurations including single, double and triangular walls.

The vibration screening effectiveness of the wave barrier can be evaluated by comparing the vertical displacement velocity of the ground surface with and without the trench. Studies show that the velocity of vibration is a proper measure of residential structure damage rather than displacement or acceleration [Qiu, 2014]. Therefore, the vertical velocity amplitude is selected to calculate the amplitude reduction ratio for the area beyond the trench. The effectiveness of an isolation system is expressed in terms of an average amplitude reduction ratio factor ($\overline{A}_r$), which is the average value of vertical soil velocity before and after the installation of the trench.

Apparently, a smaller value of ($\overline{A}_r$) means better efficiency has been achieved by the trench. Therefore, two files including the selected points beyond the trench (Points) and the amount of vertical soil particle velocity before installing the trench (Velocity) are imported in order to calculate the efficiency of the trench. Finally, the data for each system are stored in an excel

file. The created Python script for $2D$ and $3D$ model are provided in the Appendix A.

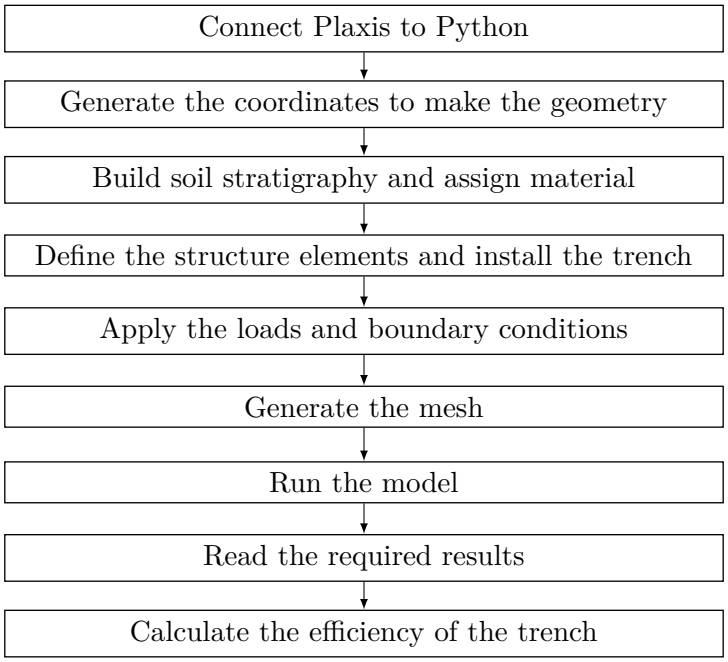


Figure 4.8: Automation process of FE model through connecting Plaxis to Python

The soil properties for the following analysis are considered the same as those measured in the field test, which are presented in Table 4.1. The constant frequency of $f = 50Hz$ is selected for the applied load, which results an R-wavelength equal to $4m$. In addition, the linear elastic behaviour is used for both the geofoam and soil behaviour in further verification. The parameters (α) and (β) are Rayleigh damping coefficients that determine the effect of mass and stiffness in the damping of the system, respectively. In mass proportional damping, damping forces are generated by velocities of the model and simulated the model's movement. Therefore, motion at the points within the model cause damping. It is also worth to mention that the mass proportional would gives damping due to the rigid body motions. However, in stiffness proportional damping, damping is generated by strain rates. Therefore, the damping is more related to the material in comparison with motion of the model. Hence, stiffness proportional damping is used in this finite element model. In addition, in many practical soil related problems, (α) is ignored since it can lead to undesirable results if a large mass has been introduced into the model [Naghizadehrokni et al., 2020].

Table 4.1: material properties of Proposed FE model

	γ (kN/m^3)	Poisson's ratio	Shear wave velocity (m/s)	Elastic Modulus (kN/m^2)	Rayleigh damping coefficient (β)
Soil	20	0.3	216	250000	0.0003183
Geofoam	0.61	0.01	330	13750	-

4.3.1. Validation of finite element method

The developed model has been validated using the results of the field test for near field and far field isolations. The measured and the calculated wave attenuation curves are depicted in Figs. 4.9 and 4.10 using a logarithmic scale for different excitation frequencies including, 20, 35, 50 and $65Hz$, respectively.

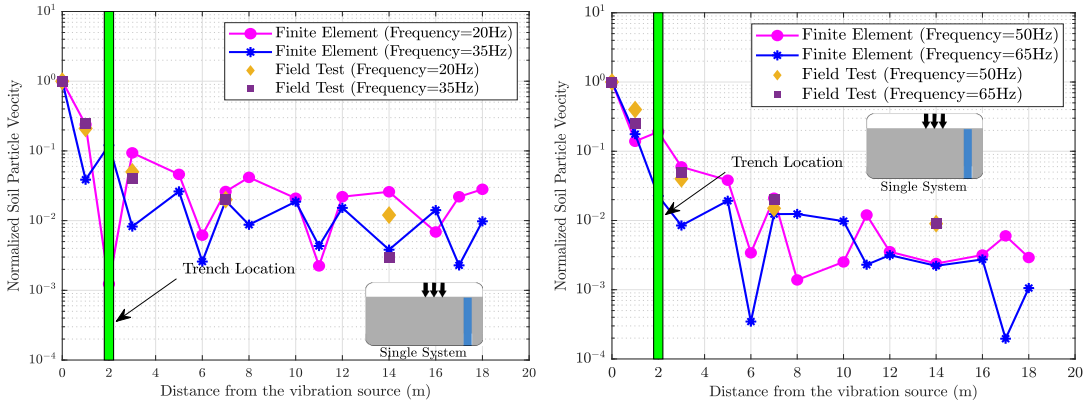


Figure 4.9: Validation of numerical modelling based on the result of field test, near field isolation, (D=3m, W=0.25m, L=10m, X=2m)

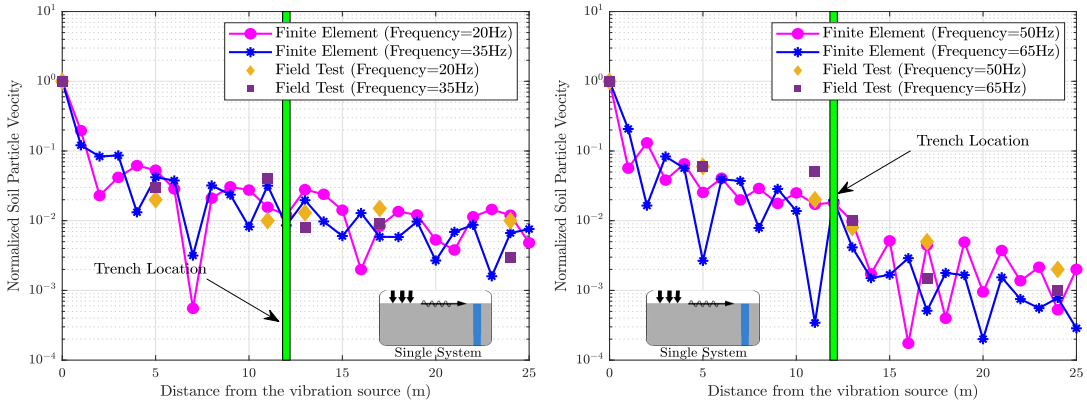


Figure 4.10: Validation of numerical modelling based on the result of field test, far field isolation (D=3m, W=0.25m, L=10m, X=12m)

The FEM results are in line with the trends in the experimental results, and there is a reasonable agreement between the normalized vertical soil particle velocities, obtained for both near field and far field cases. Nonetheless, unexpected valleys are visible in the results, which is the result of the destructive interference of waves [Ekanayake et al., 2014].

Another reason for some irregular peaks in the results is the less normalized distance between the points for presenting the numerical modelling, which is $0.25\lambda_r$. This distance leads to presenting the results as detailed as possible and showing all the irregularities that may happen for the area after the trench. The same figure has been illustrated with a normalized distance of 0.5 and fewer irregularities have been observed with a new distance but the results of this distance are not presented here.

The developed numerical model is also verified by analyzing both near field and far field isolation problems using open trenches to simulate different conditions. For this purpose, the results of Kattis et al. [Kattis et al., 1999] and Ahmad and Al-Hussaini [Ahmad and Al-Hussaini, 1991] are selected for near field and far field cases, respectively. The properties of the soil and the vibration source for both systems are presented in Table. 4.2.

Table 4.2: Properties of near field and far field system for validation

	Soil Properties						Load properties	
	Shear wave velocity (m/s)	Poissons ratio	Rayleigh wave velocity	Mass density (kN/m^3)	Rayleigh damping (%)	Rayleigh wave length (m)	Load amplitude (kN)	Vibration frequency (Hz)
Near field	275	0.25	253	17.5	5	5	1	50
Far field	101	0.25	93	18	5	3	1	31

Figs. 4.11 and 4.12 represent the results of the comparison of the developed model with the published results for an near field and far field isolation, respectively. There is good agreement between the present study and the results obtained by [Kattis et al., 1999] and [Ahmad and Al-Hussaini, 1991].

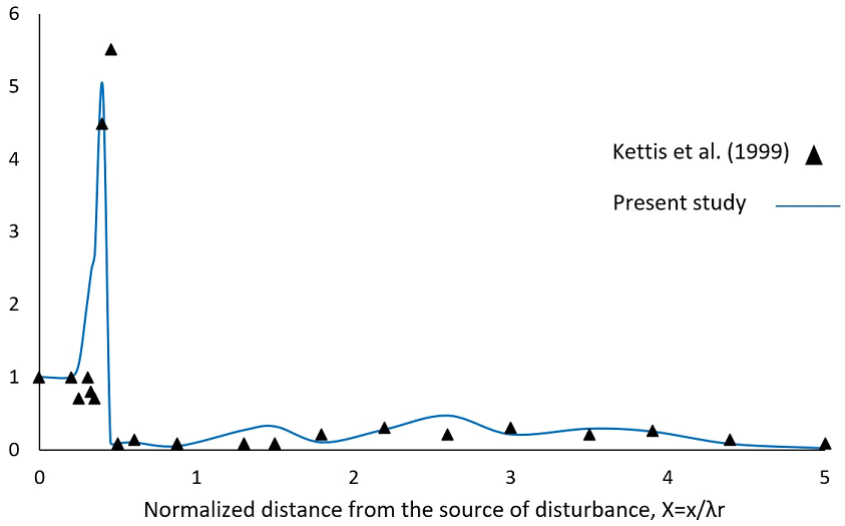


Figure 4.11: Near field isolation case, comparative study of vibration isolation by open trench ($W = 0.06$, $D = 0.5$, $X = 0.4$)

Therefore, the model developed in this study, including the wave absorbing boundary, adequately predicts the vibration propagation problem in the case of the geofoam-filled trench.

4.4. Near field isolation (soft barrier)

The parametric study begins with considering the different normalized values with respect to the R-wavelength for the parameters of the trench including the depth D (from 0.5 to 2.5),

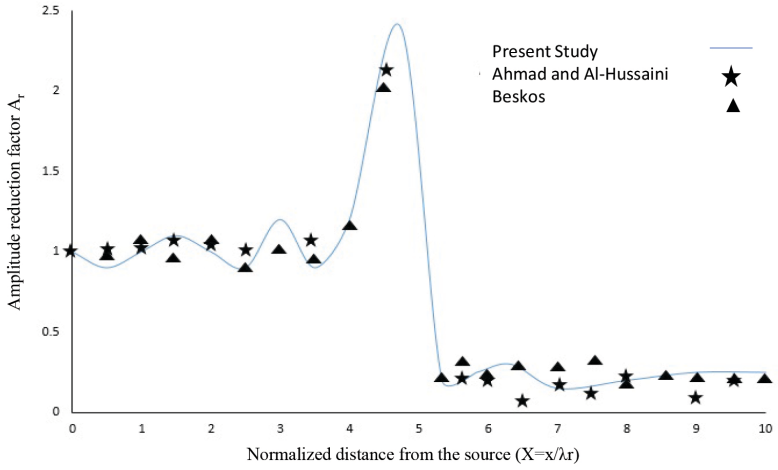


Figure 4.12: Far field isolation case, comparative study of vibration isolation by open trench ($W = 0.1$, $D = 1$, $X = 5$)

the width W (from 0.0625 to 0.25) and the length L (from 0.625 to 5), respectively. Three different normalized locations including 0.5, 1.25 and 2 are selected to compute the efficiency of the geofoam-filled trench. Since the efficiency of the barrier for all the three systems is not affected by the location of the trench, the results of all the locations are not presented here.

4.4.1. Single wall system

This section deals with the efficiency of the rectangular geofoam-filled barrier for blocking incident waves. The single wall barrier is considered to be one of the most practical configurations of filled barriers to scatter waves.

Extent of reduction zone

A study has been performed to find the screened zone to calculate $\overline{A}_r$ in an area after the trench. The results are presented in Fig. 4.13. In this case, only the symmetry line in front of the vibration source is considered. For this purpose, normalized vertical soil particle velocity (normalized with respect to the vertical soil particle velocity at the location of $X = 0.5$ in the absence of the trench) before and after the installation of the geofoam-filled trench against the normalized distance after the trench is depicted to find the difference between two curves.

Some peaks are visible in the results for both curves and the same explanation of section 4.3.1 can be applied to justify the irregular results. Another important reason is the normalized intervals between the selected points to present the results, which is 0.25, whereas this distance is usually selected as 1 or at least $0.5\lambda_r$. Another figure was obtained with the normalized intervals of 0.5 and the results did not show any irregular peaks. However, the results are not presented here.

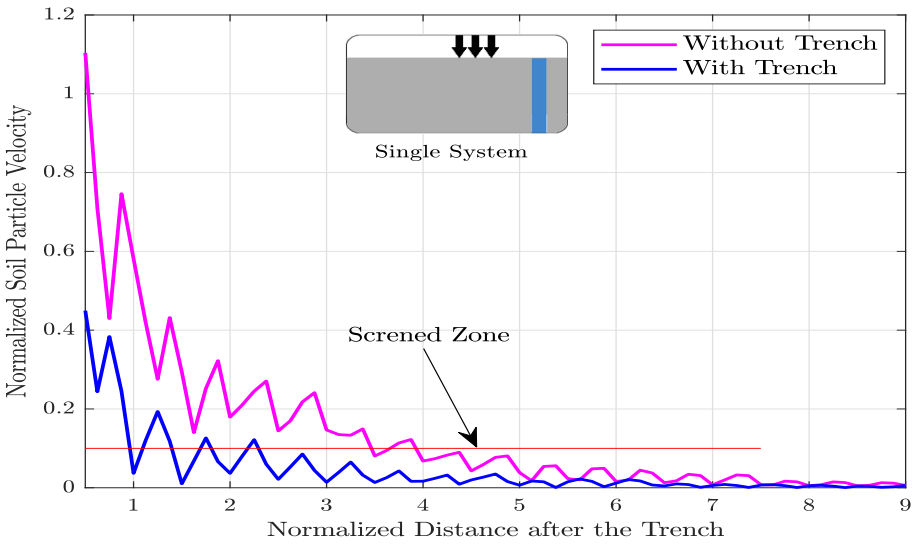


Figure 4.13: Normalized soil particle velocity amplitude of ground surface with and without barrier, at the line parallel to the vibration source ($D = 1, W = 0.075, L = 2.5, X = 0.5$, Frequency$= 50Hz$)

Effect of trench dimensions

A comprehensive parametric study was conducted to find the influence of normalized trench length with different trench dimensions. However, just some results are presented in Fig. 4.14 since there was not a considerable difference between them with respect to the normalized length of the trench. The value of $\overline{A}_r$ decreased dramatically, which was a result of increasing the normalized length from 0.625 to approximately 2.5. Therefore, the normalized length of around 2.5 was selected as the optimum value for this system.

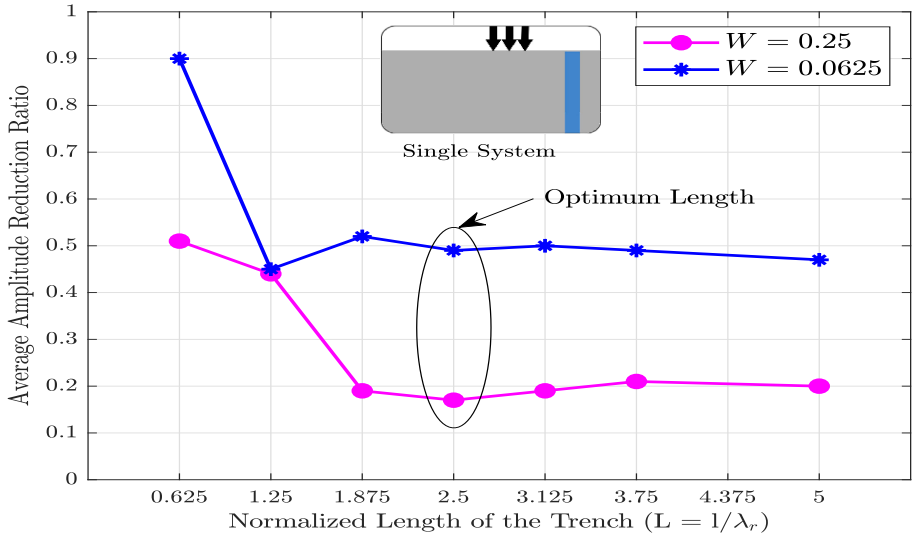


Figure 4.14: Influence of normalized barrier length on $\overline{A}_r$ ($X = 1.25, D = 1.25$)

The influence of varying the depth of wave barriers was studied, and the results are presented in Fig. 4.15. A considerable amount of wave attenuation was achieved by increasing the depth

of the barrier from 0.5 to 1 for all widths. A gradual increase or decrease in wave attenuation was observed by increasing the normalized depth up to 2. Hence, the depth of 1 was defined as the optimum value for all widths. The optimum D had a direct relationship to the width of the barrier.

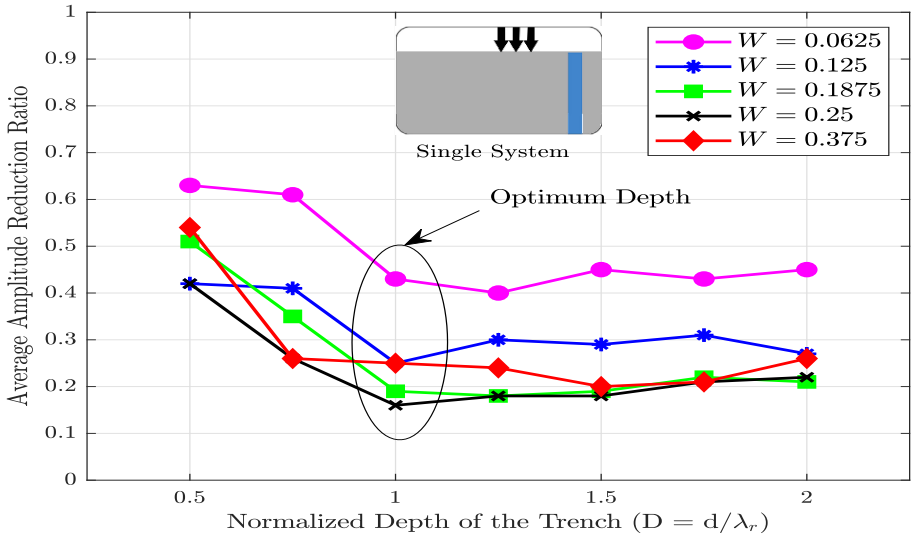


Figure 4.15: Influence of normalized barrier depth on $\overline{A}_r$ ($X = 0.5$)

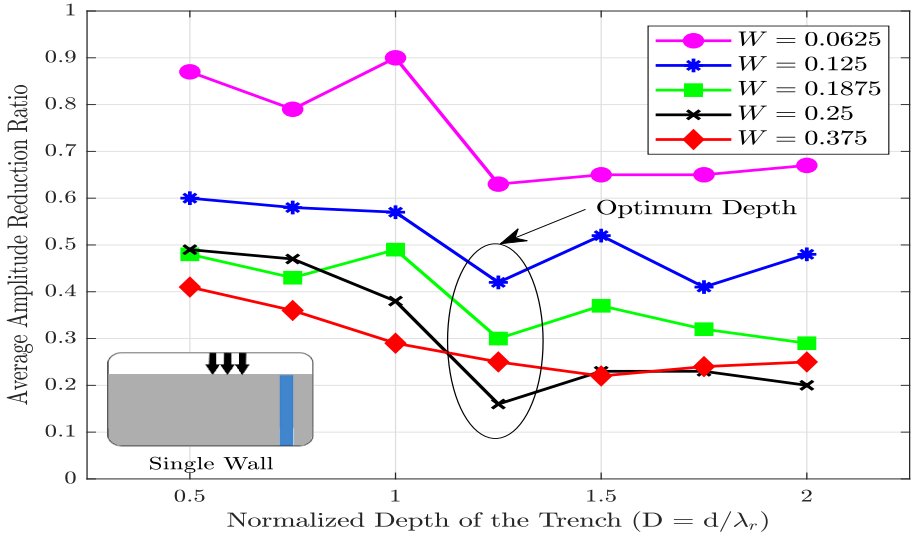


Figure 4.16: Influence of normalized barrier depth on $\overline{A}_r$ ($X = 2$)

The measured average amplitude reduction ratio as a function of normalized barrier depth for normalized location of 2 is presented in Fig. 4.16. The maximum amount of screening effectiveness can be achieved at the maximum amount at the normalized depth D value of around 1.25 for almost all narrow and wider trenches. Also increasing the width of the barrier plays a significant role in increasing the efficiency of the trench.

The results of the parametric study by changing the width of the trench were analysed. Fig.

4.17 shows that wave attenuation reaches its maximum amount at $W = 0.25$. For wider trenches ($W > 0.2$), the effect of W is negligible and can be ignored.

Increasing the width of the barrier means having a larger distance between the two sides of the obstacles, which leads to additional geometric discontinuities in the boundary area and results in a further refraction of incoming R-waves. The effect of W on $\overline{A}_r$ was also analysed at the normalized distance of 2 from the vibration source and the same value for optimum width ($W = 0.25$) was obtained. Therefore, the results are not presented here.

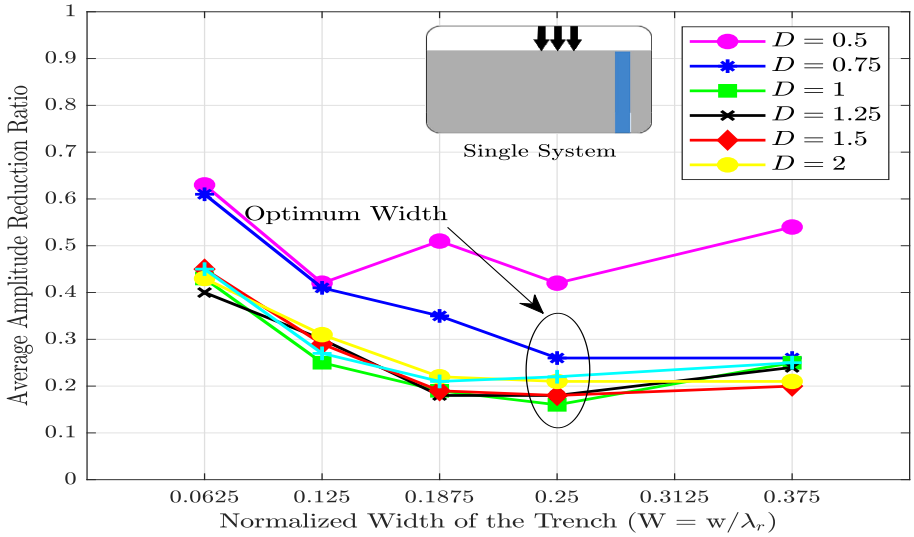


Figure 4.17: Influence of normalized barrier width on $\overline{A}_r$ ($X = 0.5$)

The influence of the normalized distance between the barrier and vibration source was also investigated as a function of trench's depth, and the results are presented in Fig 4.18. Two different widths ($W = 0.0625$ and 0.1875) were selected for analysis. However, the results of only the narrow trench is presented here since the location did not play a significant role in the performance of the trench for wider barriers.

There was an increasing pattern in the value of $\overline{A}_r$, which is resulted in increasing the normalized distance from 1.2 to 2.5 for approximately all depths including shallow and deep trenches. This observation can prove that the performance of trench will decrease by moving away from the vibration source.

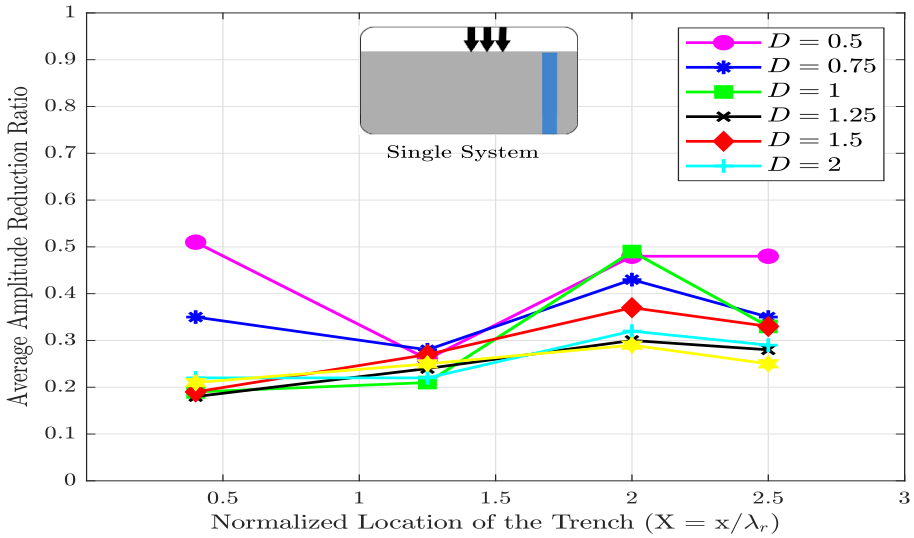


Figure 4.18: Influence of normalized barrier location on $\overline{A}_r$ ($W = 0.1875$)

4.4.2. Double wall system

The attenuation of incident waves through a double-wall system may be advantageous in circumstances where the implementation of a single-wall system is difficult because of unrealistic depth. Using a pair of geofoam-filled barriers may possibly require a lower depth in comparison with the single-wall system. The efficiency of a double-wall system was compared to a single-wall with a thickness of $2W$, and the same width, depth and length as the single-wall obstacle. Therefore, the width of both walls was considered to be one width, which was the normalized width W for both trenches.

At the first step, a parametric study was performed to find the optimum space between the barriers to achieve the best performance. Fig. 4.19 shows that the efficiency of the double-wall system is maximized at the S value of around 0.5. This space was verified with the results of [Alzawi and El Naggar, 2011] for the optimum distance between trenches.

Extent of reduction zone

The normalized vertical soil particle velocity amplitude before and after the construction of the trench was studied to find the protected area after the trench. Fig. 4.20 represents that the amount of normalized vertical soil particle velocity amplitude after a distance of 7.5 from the installed barrier is so small in comparison with a free vibration system. As a consequence, the normalized distance of 7 was selected for any crucial zone that needs wave attenuation.

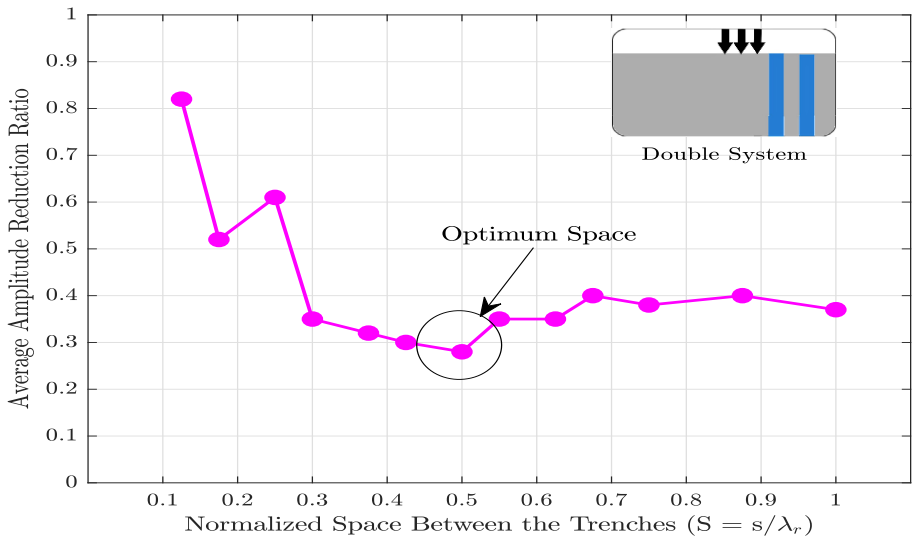


Figure 4.19: Influence of normalized barrier spacing on $\overline{A}_r$ ($D = 1$, $W = 0.075$, $L = 2.5$ and $X = 1.25$)

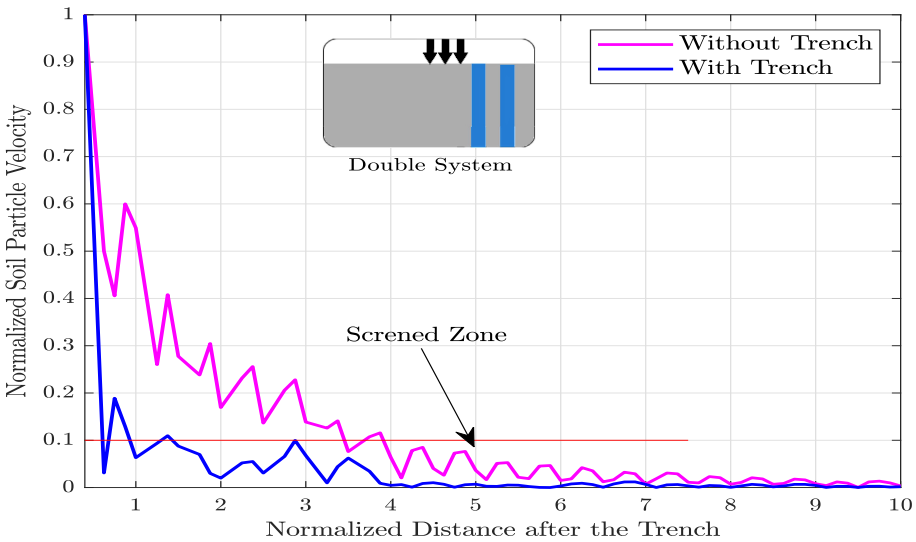


Figure 4.20: Normalized soil particle velocity amplitude of ground surface with and without barrier, at the line parallel to the vibration source ($D = 1$, $W = 0.075$, $L = 2.5$, $X = 0.5$, Frequency$= 50Hz$)

Effect of trench dimensions

The result of the parametric study for the effect of the length of the double-wall trench did not show any specific change in comparison with the result of the single-wall study. Therefore, the result of just one dimension is presented in Fig. 4.21. The normalized length of 2.5 was considered the optimum length for this system.

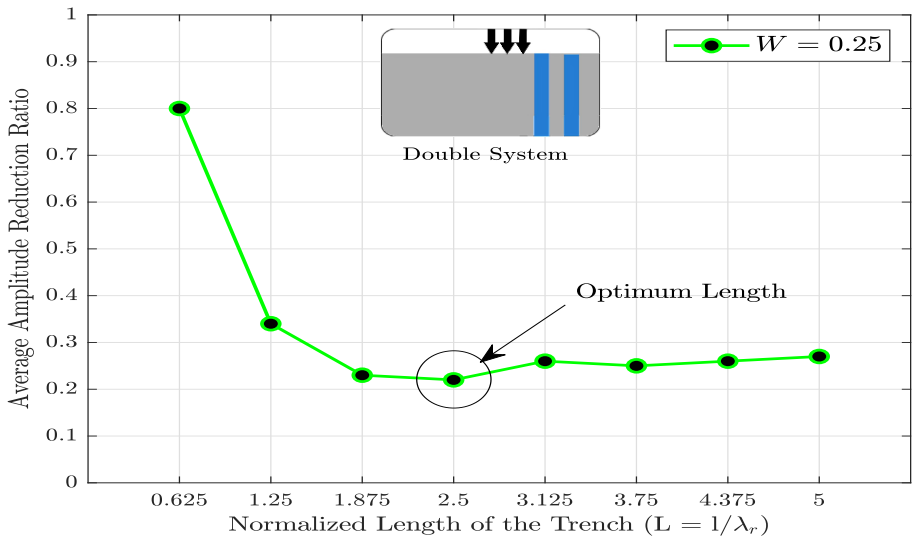


Figure 4.21: Influence of normalized barrier length on $\overline{A}_r$ ($X = 1.25$, $D = 1.25$)

The information of Fig. 4.22 shows that D governs wave screening at the normalized depth between 0.5 and 1.25 for all widths. The optimum depth of almost 1.25 was selected for all barriers. The results show that D plays a more significant role in narrow trenches than in wider trenches. The same parametric study was performed for a normalized location of 1.25 and 2 but the results are not presented here since no significant changes are observed in the results.

In the corners of the trench, mode conversion, which is converted R-wave to body waves, occurred because incoming waves pass through the edges of the obstacle into the region behind this. Since the diffraction effect was low for a narrow trench ($W = 0.0625$), due to the small distance between the two corners of the obstacle, the effect of D was more visible. For wider trenches ($W > 0.0625$), the influence of diffraction phenomenon was greater than the effect of D. All of these issues indicate that diffraction phenomenon plays an important role in the wave attenuation process for double-wall systems [Naghizadehrokni et al., 2020].

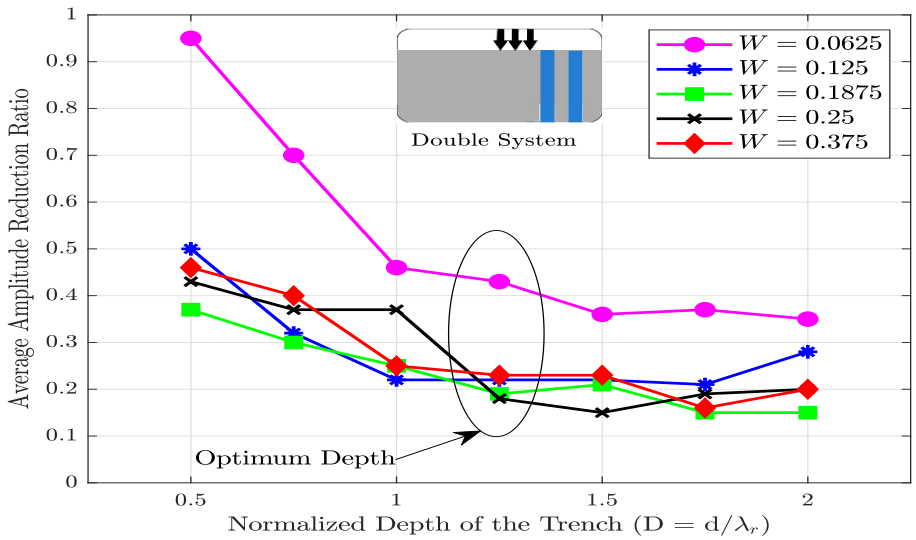


Figure 4.22: Influence of normalized barrier depth on $\overline{A}_r$ ($X = 0.5$)

As seen in Fig. 4.23, $\overline{A}_r$ decreased dramatically by increasing the normalized width of the trench from 0.0625 to around 0.2. Thereafter, it remained approximately at a constant value until $W = 0.375$. An optimum width of almost 0.2 was selected to achieve the efficiency of approximately 70% and 80%. In addition, the influence of W was lower for barriers with D higher than 0.75 and the graphs of deeper trenches depict lower slopes to reach the optimum width (0.2) from the start point ($W = 0.0625$).

According to the developed theory after Dolling, the energy of R-wave in a region between the ground surface and the R-wavelength is partially reflected at the zone of wave shadow. The R-wave energy passing beneath the obstacle creates a new R-wave at some distance beyond the barrier. The energy of the passed R-waves create vibration in the crucial zone. Increasing the width of the trench blocks more incoming waves and lead to passage of fewer incident waves [Dolling, 1970].

Fig. 4.24 shows that increasing the normalized distance between the trenches and vibration source to 1.25 can let the difference disappear between the graphs of shallow and deep trenches and all the graphs follow the same pattern in achieving the optimum width ($W = 0.25$).

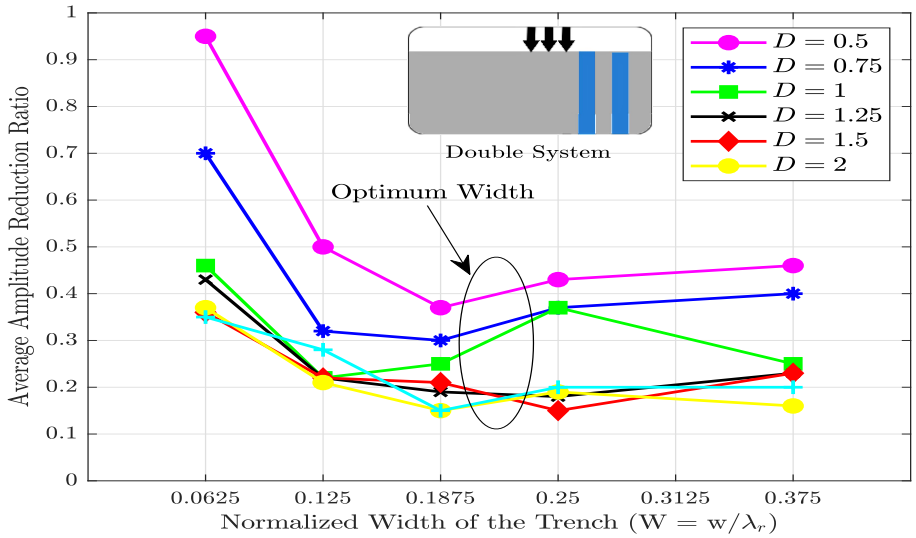


Figure 4.23: Influence of normalized barrier width on $\overline{A}_r$ ($X = 0.5$)

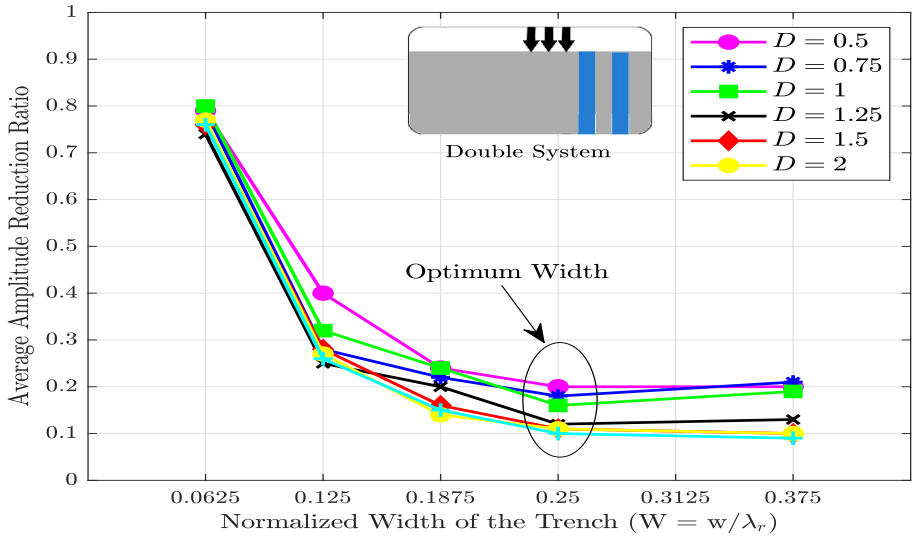


Figure 4.24: Influence of normalized barrier width on $\overline{A}_r$ ($X = 1.25$)

To measure the effect of normalized distance of a wave barrier from the vibration source, three different W including 0.0625, 0.125 and 0.1875 with various D were considered. However, only the result of the narrow trench ($W = 0.0625$) is presented here since X did not play a significant role in wave attenuation for wider trenches ($W > 0.0625$).

Fig. 4.25 demonstrates an obvious amplification for $\overline{A}_r$ from 0.4 to 0.75 (which is a roughly 47% increase in the amount of $\overline{A}_r$) by increasing the distance then this value decreases again to approximately 0.55 by increasing the normalized distance from 1.2 to 2.

The exact reason for this phenomenon is not clear to the author. However, one possible theory can be the border between the near field and far field system, where has the least efficiency ($X = 1.25$). This amplification shows that in an near field system, the trench should be installed

as close as possible to the vibration source while for the far field system, it should be installed as far away as possible to achieve the highest efficiency.

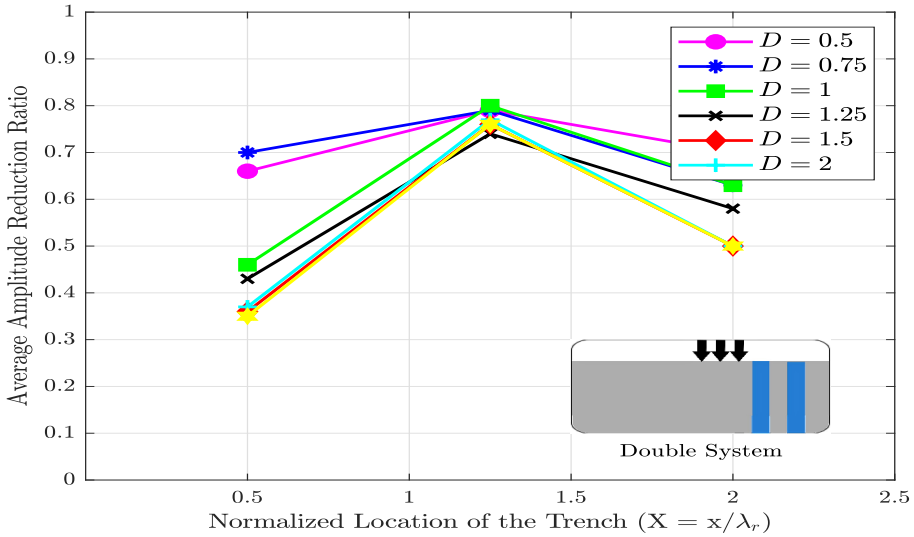


Figure 4.25: Influence of normalized barrier location on $\overline{A}_r$ ($W = 0.0625$)

4.4.3. Triangular wall system

A large part of the energy of a dispatched wave is in the form of R-waves. In addition, the amount of transferred energy by incident waves from an interface to the screened zone is a function of the incident angle. The ratio of the reflected to the transferred R-wave energy is a function of the corner angle of the trench. The angle of the barrier wall and the ground surface is recognized as one of the most important factors in distributing energy among the waves.

Moreover, as discussed in sections 4.4.1 and 4.4.2, the normalized width of the barrier appears to be an important parameter that affects the screening effectiveness of the trench as we achieved more wave attenuation by increasing the width of the trench even in the case of shallow trenches.

For a proper comparison between all configurations, the triangular system was considered with the same depth and the same cross-sectional area as the single-and double-wall trenches; however, the width of the trench was different from that of the other two systems.

The normalized soil particle velocity before and after installing the trench was compared for the area beyond the trench in a triangular wall system. The results, which are not presented here showed that, there wasnot any considerable difference after a distance of $6.5\lambda_r$ for both with and without the trench. This led to using $6\lambda_r$ for the screened zone to calculate $\overline{A}_r$.

An investigation was carried out to find the influence of the normalized length on wave attenuation like for single and double wall systems. The result of the parametric study did not show any specific change in comparison with the results of the single and double wall studies. Therefore, avoid presenting unchanged results, the normalized length of 2.5 was selected as the optimum length for this system.

Effect of trench dimensions

As shown in Fig. 4.26, increasing the normalized depth of the trench from 0.5 to almost 1.25 for the narrow trench led to an increase in the efficiency of the trench. However, when the width of the trench increased ($W > 0.25$), a smaller decrease in $\overline{A}_r$ was visible in comparison with the narrow trenches. A normalized depth of 1 and 1.25 was considered to be the optimum depth to achieve an acceptable amount of wave attenuation in narrow and wider trenches, respectively.

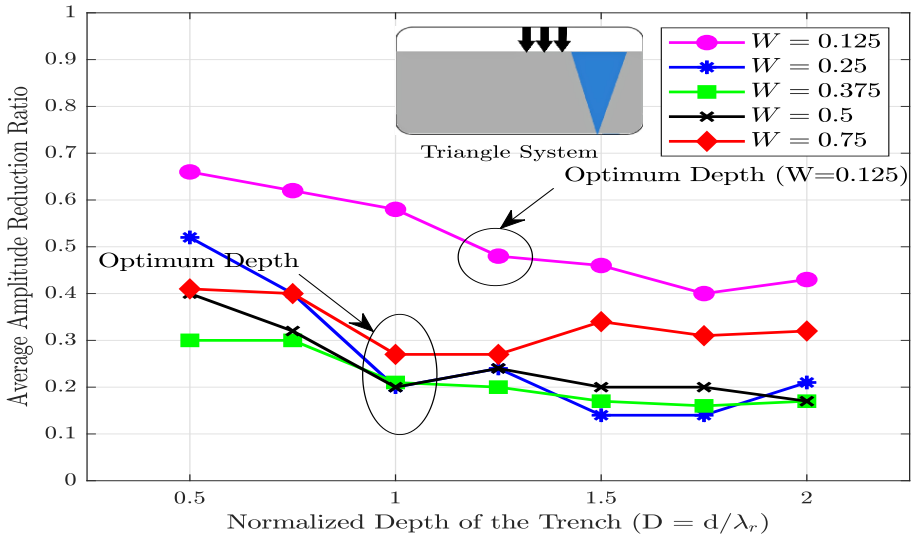


Figure 4.26: Influence of normalized barrier depth on $\overline{A}_r$ ($X = 0.5$)

The results obtained at the normalized location of 2, which are represented in Fig. 4.27 reflect that in general a normalized depth D of almost 1.5 appeared to be the optimum depth to achieve at least 70% of system effectiveness except for the narrow trench ($W = 0.125$). An approximately 50% reduction for almost all barriers with different normalized widths was observed by increasing D from 0.5 to 1.5.

Fig. 4.28 shows the influence of W on screening performance. A wider trench ($W = 0.375$) was needed (for $D < 0.75$) to reach an acceptable level of screening performance (around 75%), while by increasing the normalized depth of the trench ($D > 0.75$), a slender barrier was needed for an effective trench ($W = 0.25$).

According to Fig. 4.29, vibration screening performance reached the highest value when the normalized trench width was approximately 0.5 for shallow trenches ($D = 0.5$), which was considered the optimum W for shallow barriers. However, increasing the normalized depth ($D > 0.5$) led to the highest value of wave attenuation when W is around 0.25.

Increasing the depth of the trench means hindering more incoming waves. Regarding shallow trenches, as the corner of the barrier is near the ground surface, the role of mode conversion of R-waves into body waves becomes apparent. However, in the case of deeper trenches, the corner of the trench moves further into the soil. Therefore, the effect of diffraction,which results from waves passing around the trench edge, (trench corner) becomes smaller. Thus, a slender

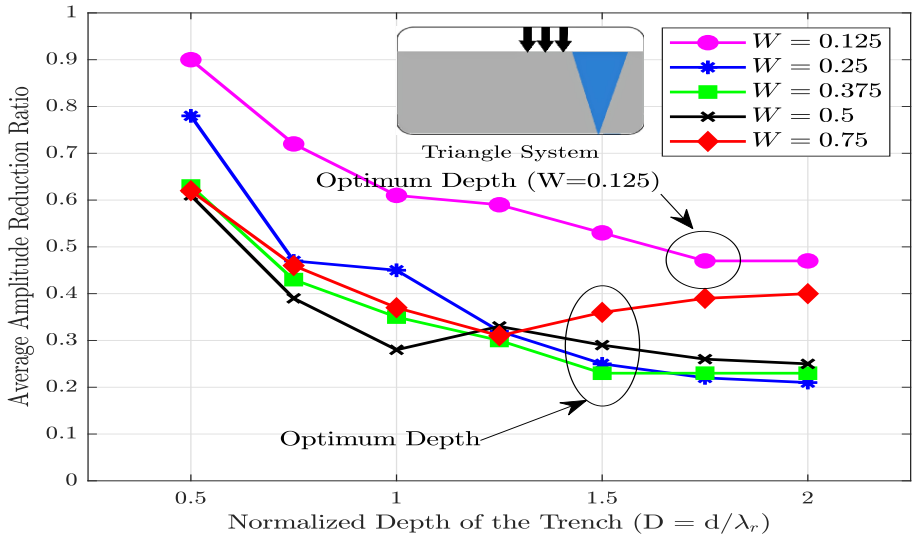


Figure 4.27: Influence of normalized barrier depth on $\overline{A}_r$ ($X = 2$)

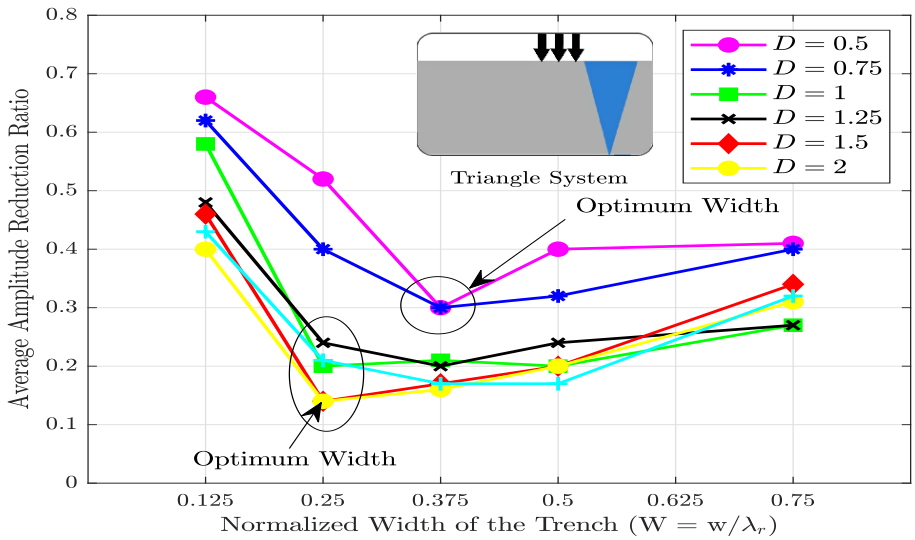


Figure 4.28: Influence of normalized barrier width on $\overline{A}_r$ ($X = 0.5$)

obstacle is needed to achieve an admissible amount of vibration for deep trenches.

The effect of normalized location (X) from the vibration source was investigated for three different normalized widths ($W = 0.125$, 0.375 and 0.75) and different depths. The results showed that the effect of normalized distance on wave attenuation could be recognized small enough to be ignored.

4.4.4. Comparison of different systems

A comparison was performed between all the proposed systems through calculating the screening performance as a function of D, and the results are depicted in Fig. 4.30. The results showed that the efficiency of the trench went up by increasing D for both widths ($W = 0.0625$

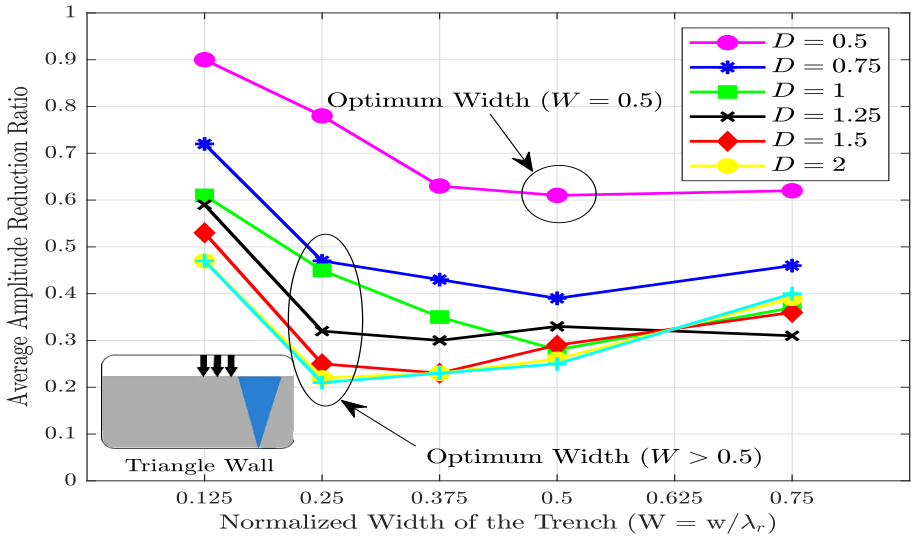


Figure 4.29: Influence of normalized barrier width on $\overline{A}_r$ ($X = 2$)

and 1). There was a considerable gap between the value of $\overline{A}_r$ for narrow and wide trenches, which showed the significance of W.

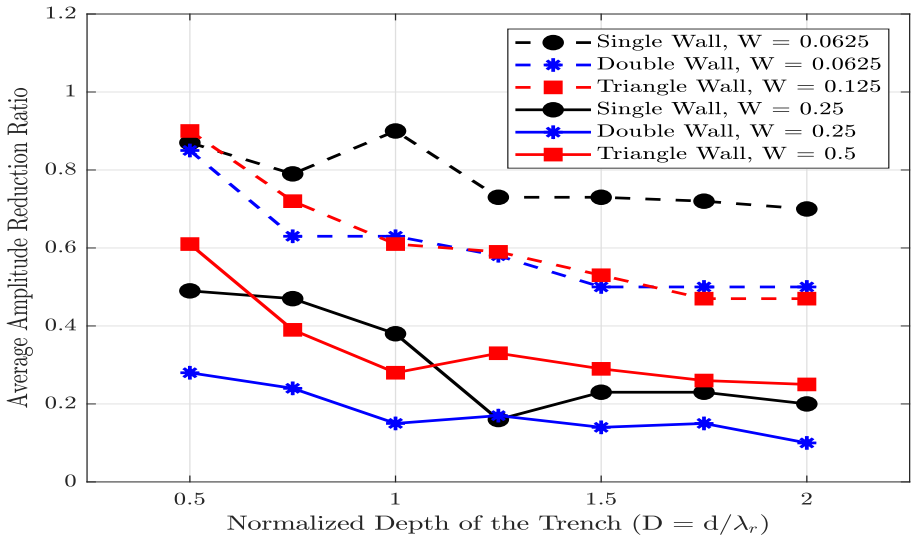


Figure 4.30: Comparison between different systems ($X = 2$)

Regarding the narrow trench, double wall systems had the highest value of screening efficiency for the normalized depth until 1. After this depth, double and triangular wall barriers also had almost the same efficiency for all depths. However, the single-wall systems had the lowest value of the efficiency in comparison with the other systems.

As the width of the systems increases, the efficiency of all the systems grew, too. However, the double wall system still performed better than the other systems in attenuating incoming waves. There was a remarkable decrease in the amount of $\overline{A}_r$ for the single wall barrier when the depth rises from 1 to 1.25.

4.5. Far field isolation (soft barrier)

A $2D$ time domain finite element model was established to perform the parametric investigation. Increasing the normalized distance between the obstacle and vibration source can lead to making R-waves more prevailing in comparison with body waves [E Richart, 1970; Ahmad and Al-Hussaini, 1991]. If the barrier encounters plane waves (in X and Y direction), a plane strain model can present reliable results to calculate average amplitude reduction ratio.

Another reason is saving computational time. Since the geometry of a far field model is bigger than an near field one. analysing several models would require a lot of time. In addition, several studies [Alzawi and El Naggar, 2011; Bo et al., 2014] showed that the results of $2D$ and $3D$ models are in acceptable agreement. Different parameters including trench depth, width, and location are considered to study the effectiveness of the trench.

The variation of the barrier's dimensional factors (including depth and width) was determined in the same way as in the near field isolation scheme. However, the geometric factor (including distance between the obstacle and vibration source) was determined to be 3, 4 and 5. Since the efficiency of the barrier for all the three systems was not affected by the location of the trench, the results of all locations are not presented here.

4.5.1. Single-wall study

The influence of different parameters on the wave attenuation of geofoam-filled trenches was investigated. The properties of soil were considered the same as for near field isolation.

Extended of the reduction zone

It is essential to find a screened zone for a single-wall barrier which could be protected by the trench. Fig. 4.31 depicts the normalized ground displacement amplitude before and after constructing the barrier. A considerable reduction was created in vertical ground displacement after the construction of the geofoam-filled trench. However, there was a small difference between the normalized vertical soil particle velocity before and after the installation of the trench beyond the normalized distance of 13. Hence, a normalized distance of 10 after the barrier was suitable to calculate $\overline{A}_r$.

Effect of trench dimensions

The amplitude of dispatched waves through the trench was measured and the representative $\overline{A}_r$ as a function of D is presented in Fig. 4.32. The results showed that increasing D from 0.5 to 1.25 increased the effectiveness of the barrier from approximately 20% for the narrowest trench to about 50% for the widest barrier, respectively.

The importance of the normalized width for $\overline{A}_r$ is presented in Fig. 4.33. A reduction of

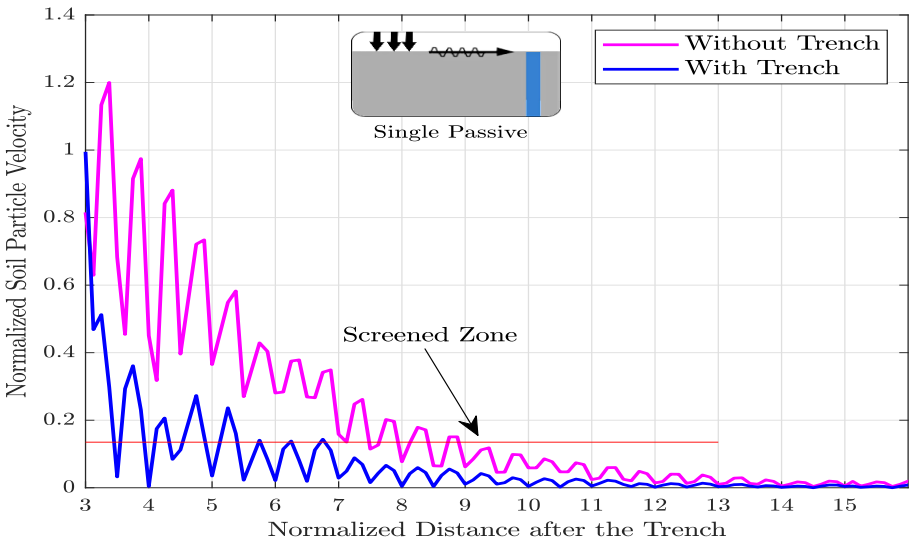


Figure 4.31: Normalized soil particle velocity amplitude of ground surface with and without barrier, along the line parallel to the vibration source ($D = 1$, $W = 0.075$, $X = 3$, Frequency$= 50Hz$)

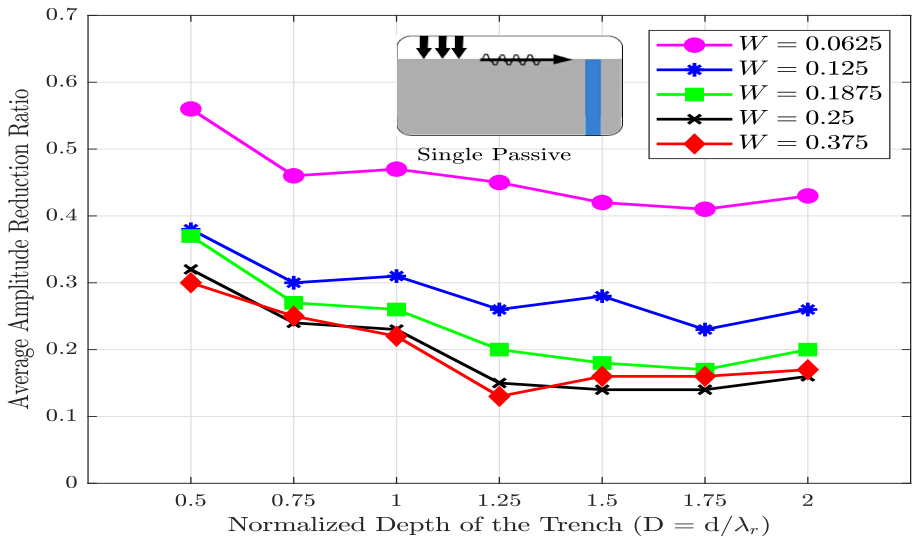


Figure 4.32: Influence of normalized barrier depth on $\overline{A}_r$ ($X = 4$)

approximately 60% was achieved by increasing W from 0.0625 to 0.25 for almost all trench depths and it seemed that $W = 0.25$ was the optimum width to achieve a reasonable amount of wave attenuation. An increase in the width of the trench creates more discontinuity at the ground surface with different dynamic properties and this difference creates a diffraction in the indicident waves.

The amplitude of dispatched vibrations for normalized trench location at 4 and 5 from the vibration source was calculated. The results, which are not presented here, showed the same pattern like $X = 3$ and $W = 0.25$ could be considered to be the optimum width to achieve a reasonable amount of wave scattering.

The results of the parametric study for a normalized distance between the trench and vibration

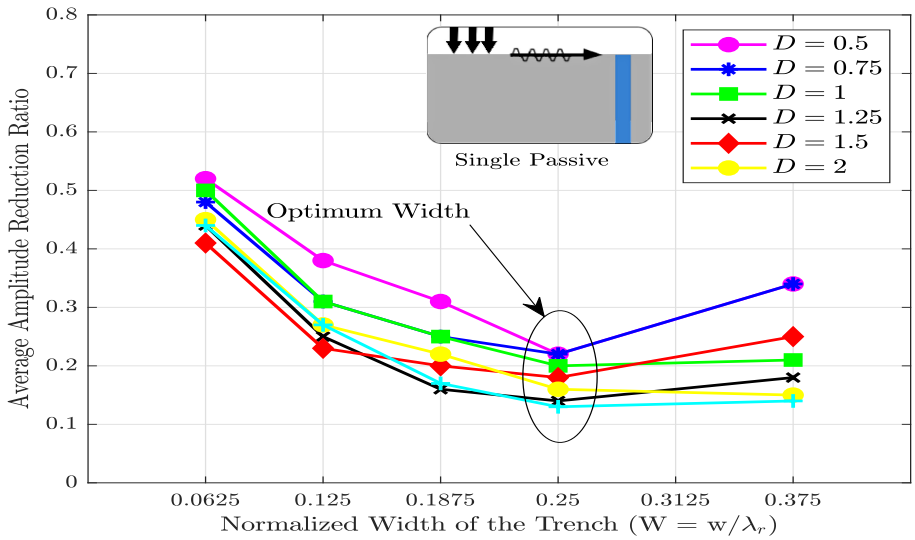


Figure 4.33: Influence of normalized barrier width on $\overline{A}_r$ ($X = 3$)

source (X) proved that $\overline{A}_r$ remained basically unchanged with respect to the trench location and the efficiency of the trench was independent of its location for both thin and wide barriers in almost all depths.

4.5.2. double-wall barrier

A pair of geofoam-filled barriers were installed at points far from the vibration source and the normalized distance between the walls was considered 0.5. A parametric study was carried out to find the reduction of zone of double-wall systems and the same results as those of single-wall systems were obtained. Therefore, the normalized location of 10 beyond the trench can be considered to calculate the average amplitude reduction ratio.

Effect of trench dimensions

Fig. 4.34 shows a slight dependence of $\overline{A}_r$ on the trench depth for $D = 1$, and even increasing W cannot create any change in the influence of D on $\overline{A}_r$. Changing the location of the trench did not create any change in the effect of D on the performance of the trench, too.

Some incident R-waves reflected downward to the left side of the obstacle after encountering the left side of the first wall and the remaining one is transmitted to the right side of the barrier. Subsequently, the transmitted R-waves reflected again through the discontinuity at the second wall. In fact, the diffraction and mode conversion due to the corners of a pair of the trenches played a more significant role in decaying the incoming R-waves in comparison with the depth, and this issue outweighed the role of trench depth.

Fig. 4.35 represents the computed value of $\overline{A}_r$ by changing the width of the trench. Wider barriers led to better screening effect, and W seems to govern the screening process. After the optimum width ($W = 0.2$), increasing the thickness of the barrier hardly affected the screening

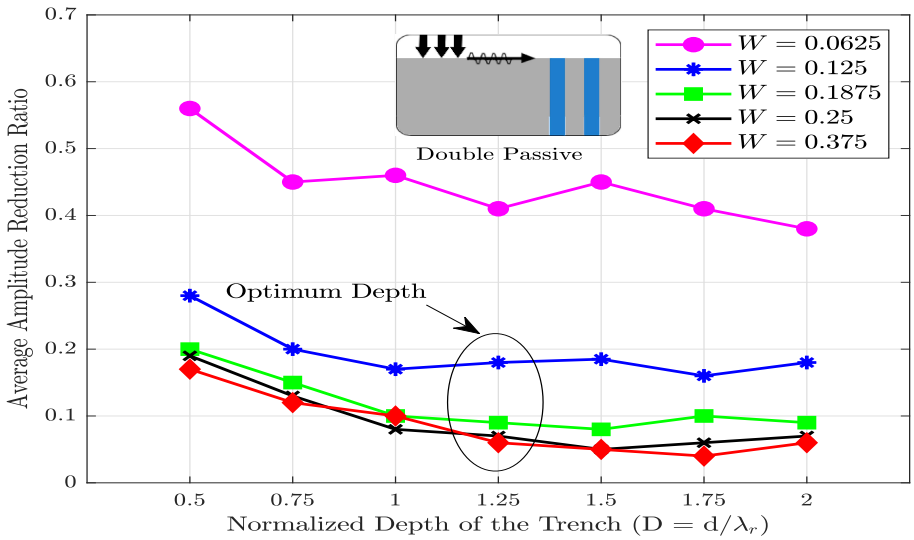


Figure 4.34: Influence of normalized barrier depth on $\overline{A}_r$ ($X = 4$)

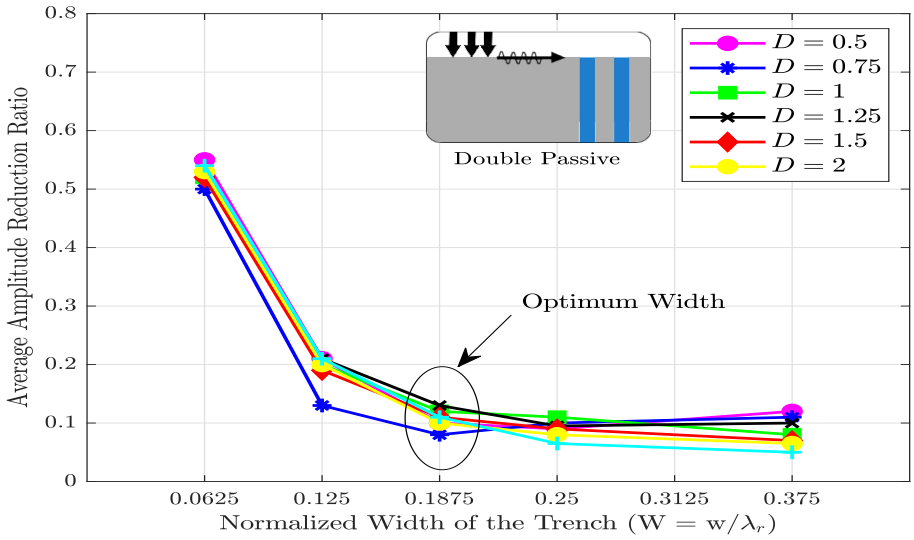


Figure 4.35: Influence of normalized barrier width on $\overline{A}_r$ ($X = 3$)

vibration for almost all depths. Since the thickness of the obstacle reached an optimum value, increasing W did not change in the performance of the trench.

Increasing the normalized width means having more discontinuity at the ground surface with different shear modulus, resulting in hindering more ground-born vibration. However, since W continuously increases, the probability of having wave interferences among the transmitted R-waves through and beneath the trench decreases. This phenomenon may be one of the reasons for reaching a stable value of the normalized width beyond almost 0.2.

The calculated efficiency of the filled barrier against different locations for the narrow and wide barriers showed that $\overline{A}_r$ remained approximately intact with respect to the barrier's location.

4.5.3. Triangular wall barrier

A range of 0.5 to 2 for normalized depth and a range of 0.125 to 0.75 for normalized width were selected, respectively for determining the efficiency of triangular wall trenches. In addition, the parametric study of reduction zone for the triangular wall trench, which is not presented here, showed that a normalized length of 10 after the trench could be enough to be considered the crucial zone.

Effect of trench dimensions

As it can be seen in Fig. 4.36, the efficiency of the trench increased gradually and continuously by increasing the normalized depth for approximately all widths, implying that D governed the scattering influence. It is apparent from the figure that the barrier width had an a negligible influence on the scattering of incoming waves. Considering the corner of the triangular wall barrier, its shape can be the reason for observing no mode conversion or diffraction phenomenon that changed R-waves into body waves.

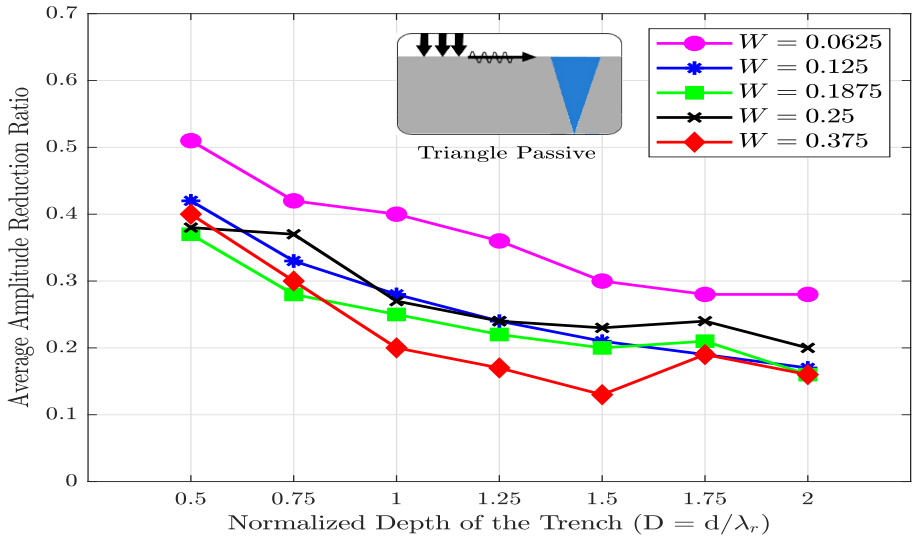


Figure 4.36: Influence of normalized barrier depth on $\overline{A}_r$ ($X = 3$)

Increasing the normalized distance X between the source and the trench led to some new results, which are plotted in Fig. 4.37. The results imply that changing D had a direct relation to the scattering of dispatched waves for $0.5 < D < 1.5$. The results regarding the normalized location of 5 are not presented here as changing the normalized location to $X > 4$ did not bring any increase in the efficiency of the barrier.

The representative $\overline{A}_r$ as a function of W for various depths are presented in Fig. 4.38. An unnoticeable improvement in the performance of the trench was observed, which was around 25% by increasing W from 0.0625 to 0.25 for all depths. Little dependence was observed for vibration attenuation when the normalized width of the trench is wider than 0.25.

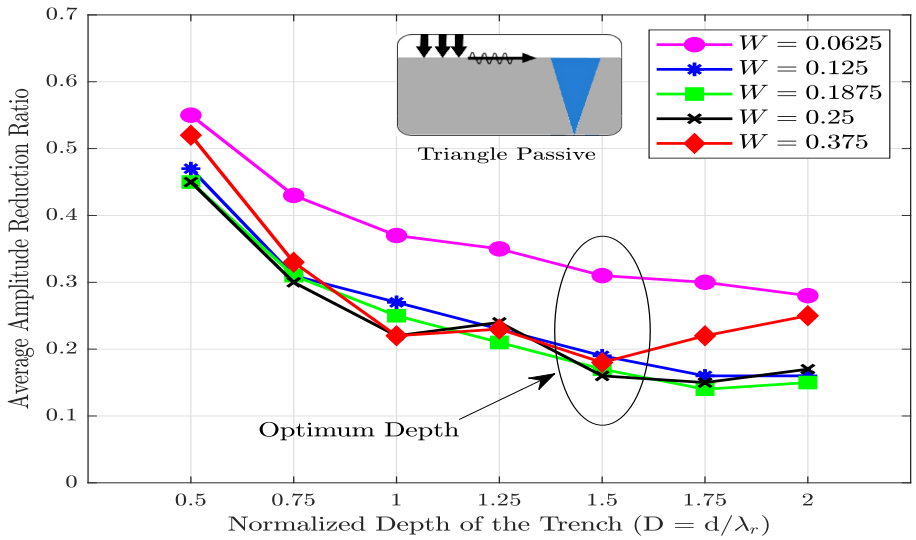


Figure 4.37: Influence of normalized barrier depth on $\overline{A}_r$ ($X = 4$)

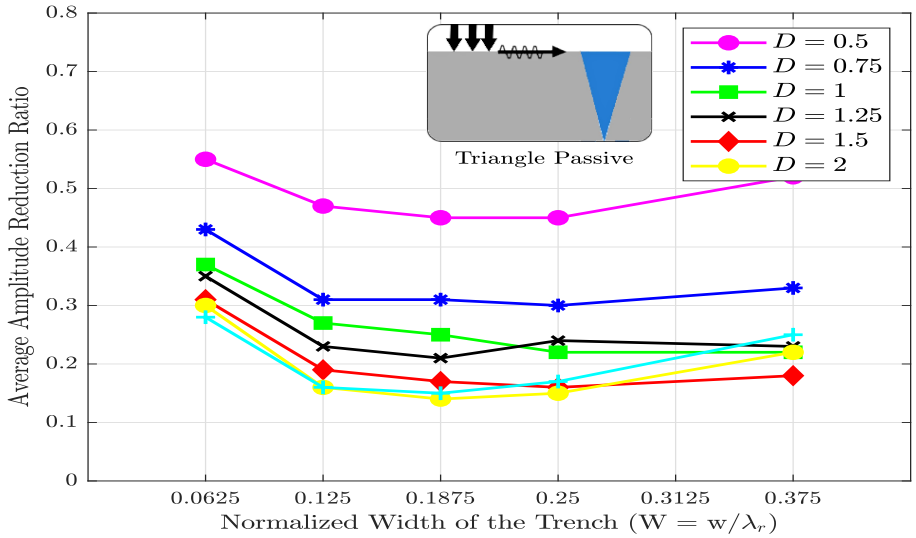


Figure 4.38: Comparison of different systems

The results of the parametric study for the location of the trench, which are not presented here, proved that screening performance of the barrier was independent of the location of the trench.

4.5.4. Comparison of different systems

A comparison between the screening performance of all the proposed configurations was carried out, and the results are illustrated in Fig. 4.39. There was still a significant difference between the efficiency of narrow and wide barriers like section 4.4.4. This issue proves the significance of W for both near field and far field systems. In addition, the results revealed that for all the systems except for the double-wall one ($W = 0.0625$), the effectiveness increased as the depth of the trench went up until to $D = 1.5$. This depth was considered to be as an optimum depth for both narrow and wide barriers.

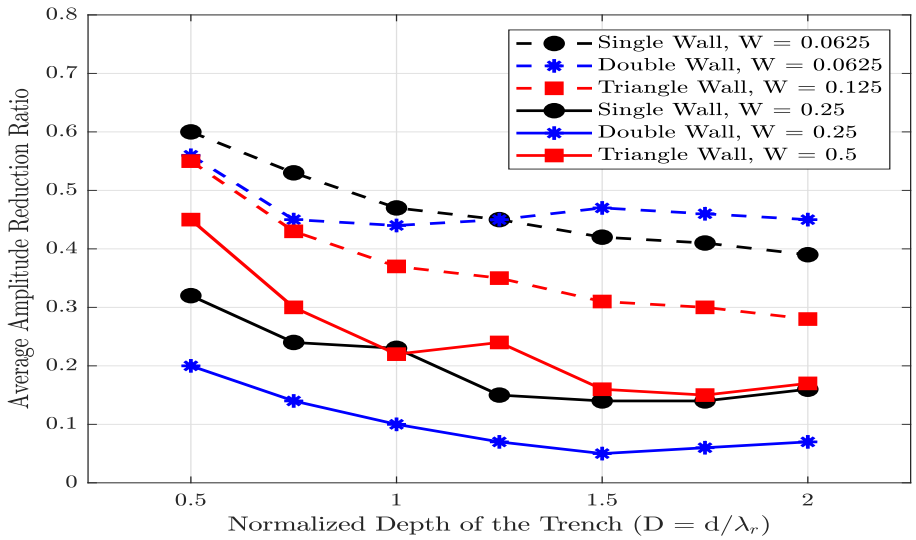


Figure 4.39: Influence of normalized barrier width on $\overline{A}_r$ ($X = 4$)

Concerning narrow trenches, the triangular system performed most efficiently with a considerable difference (around 50%) in efficiency in comparison with the single- and double-wall systems at the optimum depth ($D = 1.5$). Single and double wall systems behaved almost the same in attenuating incoming waves.

Increasing the width of all the systems ($W = 0.25$) resulted in more mitigation of incoming waves. However, the double-wall system was clearly the most effective system regardless of its depth. The performance of the single-wall system was almost the same as the triangular one for all the values of D.

4.6. Near field isolation (stiff barrier)

In this section, the influence of different parameters associated with the wave attenuation of an in-filled trench with concrete is presented by developing a $3D$ finite element model. Three different systems (single, double and triangular wall) were considered to measure the screening performance of an in-filled barrier. The properties of soil medium and concrete are presented in Table 4.3.

Table 4.3: Properties of soil and concrete

	Youngs Modulus (kN/m^2)	Poissons Ratio	Unit Weight (kN/m^3)
Soil	$250,000$	0.3	20
Concrete	$35 * 10^6$	0.2	24.5

The normalized length of 2.5 was considered for both stiff and soft studies.

4.6.1. Single wall barrier

Extended of reduction zone

Fig. 4.40 depicts the normalized ground displacement amplitude before and after construction of the barrier. As it can be observed, there was a small difference between the normalized vertical soil particle velocity before and after the installation of the trench after the normalized distance of 5.5. Hence, it can be concluded that a normalized distance of 5 after the barrier can be a proper distance to calculate $\overline{A}_r$. This distance was selected for all the systems in the near field scheme.

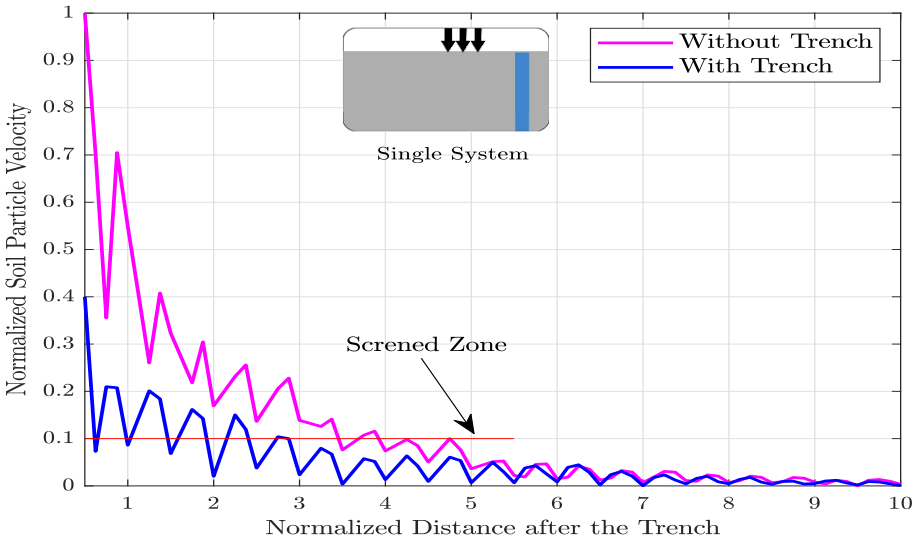


Figure 4.40: Normalized soil particle velocity amplitude of ground surface with and without concrete barrier, at the line parallel to the vibration source ($D = 1$, $W = 0.075$, $L = 2.5$, $X = 0.5$)

Effect of trench dimensions

The effect of normalized depth of the concrete-filled barrier on $\overline{A}_r$ is depicted in Fig. 4.41. Increasing the normalized depth to around 2 resulted in reaching the highest wave attenuation, which was approximately 67% for wider barriers ($W \geq 0.125$) and almost 33% for narrow trenches ($W = 0.0625$).

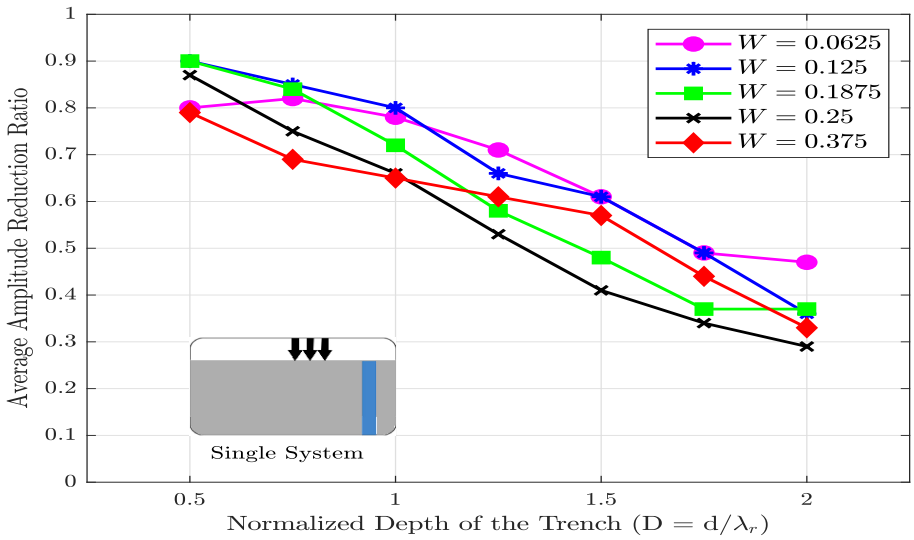


Figure 4.41: Influence of normalized barrier depth on $\overline{A}_r$ ($X = 0.5$)

It is apparent from Fig. 4.41 that the normalized width of the barrier had a small effect on system effectiveness since there was no considerable difference in trench efficiency for various widths.

Concerning the location of the trench, the results, which are not presented here, showed that the location of the barrier had no effect on wave attenuation, and its influence can be ignored.

4.6.2. Double wall barrier

As it can be observed from Fig. 4.42, vibration screening reached the highest amount for the normalized depth of 1 for narrow trenches ($W = 0.0625$ and 0.125). However, the normalized depth became an insignificant parameter by increasing when the width of the barrier rises ($W = 0.1875$ and 0.25). It can be concluded that increasing the width of the trench ($W > 0.1875$) nullifies the effect of depth on the performance of the trench.

It is clear from the results in Fig. 4.43 that the width of a concrete-filled trench played a significant role and $W = 0.25$ was considered to be an optimum width. For instance, system performance increased from approximately 45% to 70% by increasing thickness from 0.0625 to 0.25 for deeper trenches ($D > 0.75$).

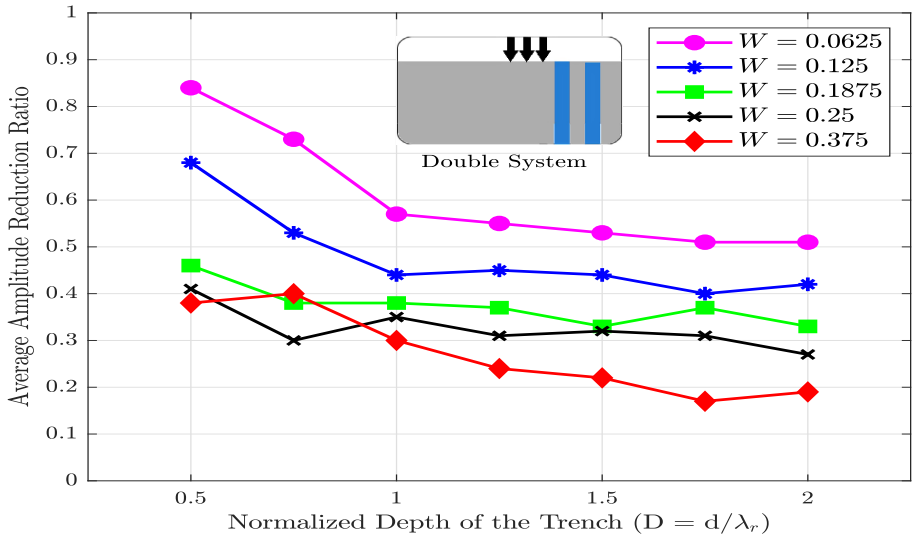


Figure 4.42: Influence of normalized barrier depth on $\overline{A}_r$ ($X = 0.5$)

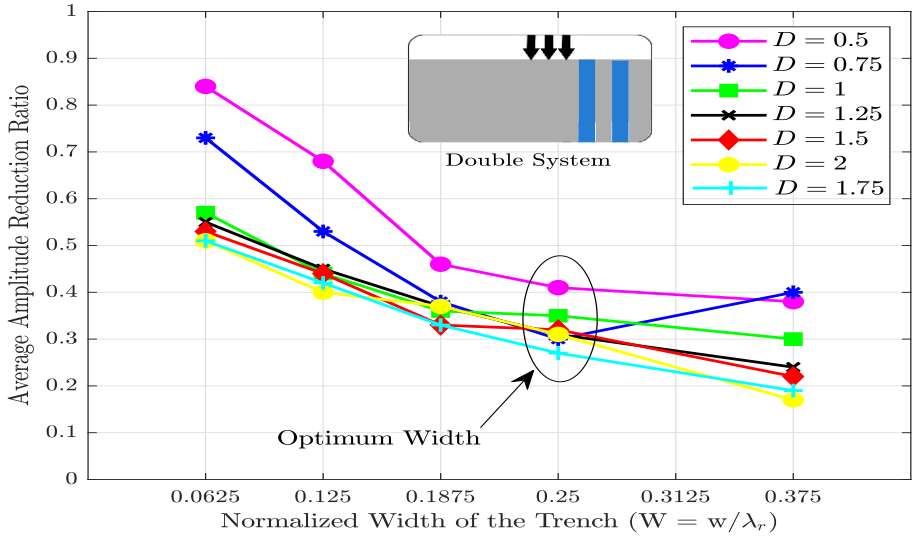


Figure 4.43: Influence of normalized barrier width on $\overline{A}_r$ ($X = 0.5$)

4.6.3. Triangular wall barrier

The influence of the normalized depth of triangular wall barrier on wave attenuation is plotted in Fig. 4.44. A significant increase in vibration mitigation can be seen by increasing the normalized depth of the barrier from 0.5 to 2 for almost all normalized widths. Three different locations were considered to investigate the effect of trench depth; however, the results did not show any considerable changes.

Fig. 4.45 demonstrates the obtained results of studying the effect of W on wave attenuation. $\overline{A}_r$ remained constant by increasing W from 0.125 to approximately 0.4 for almost all depths. However, as W increased from 0.4 to 0.5, $\overline{A}_r$ firstly grows for deeper barriers ($D \geq 1.25$) and then attenuate dramatically by increasing the normalized width from 0.5 to 0.75.

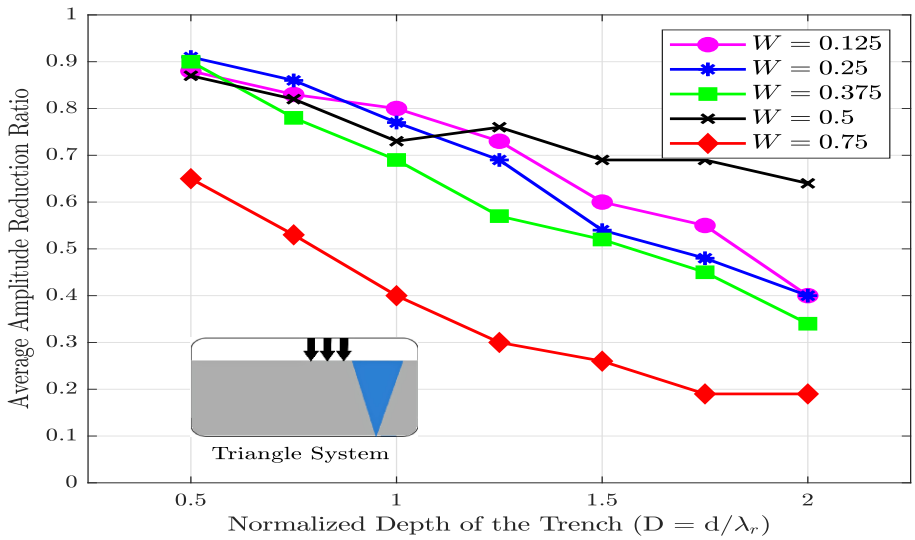


Figure 4.44: Influence of normalized barrier depth on $\overline{A}_r$ ($X = 0.5$)

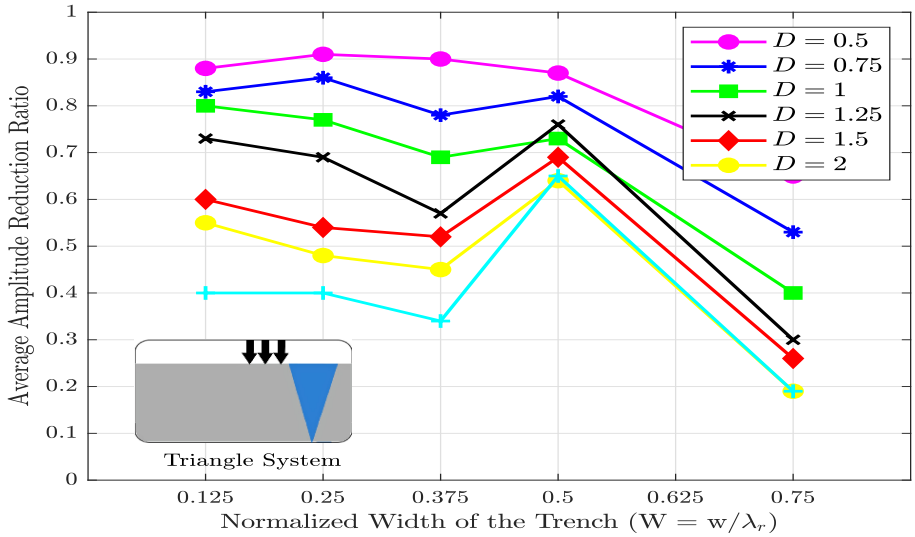


Figure 4.45: Influence of normalized barrier width on $\overline{A}_r$ ($X = 0.5$)

4.7. Conclusion

A comprehensive parametric study for evaluating the efficiency of barriers was performed for near field and far field systems. The conclusions drawn from the results can be summarized as follows:

- Near field isolation can be a better solution to hinder incident waves in comparison with far field isolation based on the results of the field test. However, the results also showed that the first point after the trench had the highest amount of mitigation and a normalized depth of $0.6\lambda_r$ was enough to reach the highest value of efficiency for both near field and far field isolation systems.
- The performed numerical parametric study of the near field and far field isolations showed

the zone of $7\lambda_r$ and $10\lambda_r$ to be crucial zones for an area after the trench to compute $\overline{A}_r$. This finding proves that a vibration isolation system should be divided into near field and far field systems during analysis.

- Analysing the results of the near field scheme demonstrated that the optimum length could be considered to be $2.5\lambda_r$ for all the three systems to reach the highest value of efficiency. The depth of $1\lambda_r$ was considered to be the optimum depth for the single, double, and triangular wall systems, respectively. Concerning the effect of the width of a geofoam-filled trench, it was concluded that a value of $W = 0.25$ was enough to be considered the optimum W for single, double and triangular wall systems, respectively. In addition, the comparison of all the systems revealed that double wall was the best system for both narrow and wide barriers.

- On the other hand, the evaluation of far field isolation illustrated that the depth of a barrier hardly affected the efficiency of the obstacle for single and double wall systems, while D was a key factor in scattering incoming waves for the triangular wall system. However, an optimum depth could not be determined for this system as the efficiency of the system increases gradually and continuously by increasing D. The comparison of all the three systems showed that double wall is the most effective systems for narrow and wide trenches, respectively.

- The normalized width had to be increased to approximately 0.25 and 0.2 to have successful single and double wall systems, respectively. The barrier's width had a negligible effect on scattering dispatched waves for the triangular wall system. In addition, the parametric study of the trench location for both near field and far field schemes demonstrated that this factor was not an important parameter that influenced the efficiency of the geofoam-filled trenches.

- Concerning stiff barriers, a normalized reduction zone of 5 beyond the trench was to consider for calculating $\overline{A}_r$, which showed that reduction zone was an important parameter in calculating the efficiency of a trench. There was no optimum D for single and triangular systems since efficiency increased continuously when depth goes up, while D hardly affected $\overline{A}_r$ for double-wall systems. The normalized width was an important parameter only for double system and the value of 0.25 was considered to be the optimum value. However, for single and triangular systems, it either did not affect $\overline{A}_r$ or had a significant influence on $\overline{A}_r$, respectively.

- The result of this chapter is presented based on single parametric study and the mutual effect of the parameters are not considered here. Therefore, it is necessary to design a trench with considering the mutual effect of all parameters.

5 Shape optimization of the trench by genetic algorithm

5.1. Introduction:

The results in chapter 4 showed that the most important parameters for the design of an efficient barrier is the location and the geometry of the barrier, mainly depth and width. The same FEM coupled with a genetic algorithm presented in Chapter 4 was used to obtain the optimized configuration of geofoam and concrete-filled barriers. The finite element model is developed and verified in section 5.3. The implementation of the proposed genetic algorithm model is described in section 5.5. Finally, the developed genetic algorithm code is used to find the optimized parameters of different configurations for both near field and far field systems, respectively. These results are presented in sections 5.6 and 5.7.

5.2. Problem definition

The main purpose of this chapter is the optimization of different configurations including single, double and triangular wall barriers, which are shown in Fig. 5.1 to reach an acceptable barrier efficiency, which is 75% reduction in vibration screening. An equal cross-sectional area is considered for all three systems to make a proper comparison.

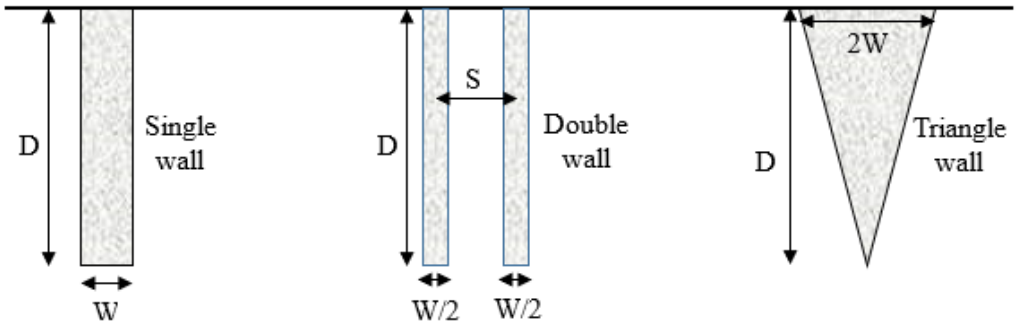


Figure 5.1: Different shapes of trench

5.3. Finite element model

A time domain $2D$ and $3D$ numerical models are developed to assess the efficiency of the trench in attenuating incoming waves for far field and near field isolation systems, respectively. Since the model is largely affected by the transmitted and reflected waves from the boundaries, it is important to keep the region of interest far enough from the reflecting boundary. Therefore, the dimensions of the model are selected as $(50 * 20 * 20\ m)$ for 3D dimensions and $(70 * 25\ m)$ for

2D dimensions in the case of near field and far field systems, respectively. Viscous boundaries are applied to the bottom and right sides of the $2D$ and $3D$ models and at $Ymax$ direction for $3D$ model, too. A viscous boundary condition, which is introduced by Lysmer & Kuhlmeyer [Bahrekazemi, 2004] consists of the viscous dampers applied in X and Y (for $2D$) and Z (for $3D$) axis in a Cartesian coordinator system along the boundary. In this theory, a damper is used, and the absorbed components by the damper are normal and shear stresses, which are obtained by Eqs. (5.1) and (5.2).

(50*20*20 m) for 3D dimensions and (70*25 m) for 2D dimensions in the

$$\sigma = C_1 \rho V_p \dot{w} \tag{5.1}$$

$$\tau = C_2 \rho V_s \dot{u} \tag{5.2}$$

where V_p and V_s are primary and secondary wave propagation respectively, $\dot{w}$ and $\dot{u}$ denote normal and tangential velocities, ρ is material density, and C_1 and C_2 are relaxation coefficients to change the effect of absorption. It is proved that applying the two relaxation coefficients equal to one leads to the highest efficiency in absorbing any waves reaching the boundary, which is sufficient for practical applications [Saikia, 2014].

Plaxis uses a global meshing parameter, which is called average element size (I_e) to show the quality of the mesh. This parameter is calculated based on the dimensions of the model and the number of elements. In Plaxis this parameter is calculated from the outer geometry dimensions ($x_{\min}, x_{\max}, y_{\min}, y_{\max}, z_{\min}, z_{\max}$) acording to Eq. (5.3) [Brinkgreve et al., 2020].

$$I_e =< \frac{r_e}{20} * \sqrt{(x_{\max} - x_{\min})^2 + (y_{\max} - y_{\min})^2 + (z_{\max} - z_{\min})^2} \tag{5.3}$$

where r_e is relative element size factor.

A convergence analysis to compare different local element sizes in local refinement areas is illustrated in Fig 5.2 for the geofoam-filled trench at the location of $5m$ and length, depth and width of 10, 5 and $0.5m$, respectively. The result shows that the black line with average element size (I_e) of 0.5 is enough to reach acceptable results.

The properties of the soil and geofoam are selected from the full experimental test in section 4.2 to be used in Plaxis and evaluate the efficiency of the geofoam-filled barrier.

The vibration source is modelled as a vertical harmonic load with the magnitude of $1KN$ and frequency of $50Hz$ with the dimensions of $0.36 * 0.36\ m$. In addition, the dynamic time interval of 0.5 s is selected for each frequency. The proposed $3D$ FE model of the vibration isolation system and the defined parameters are presented in Fig. 5.3.

5.4. Effect of cross-sectional area

A parametric study for the single wall system is performed to find the influence of cross-sectional area and the shape of the barrier on average amplitude reduction ratio for the near field isolation

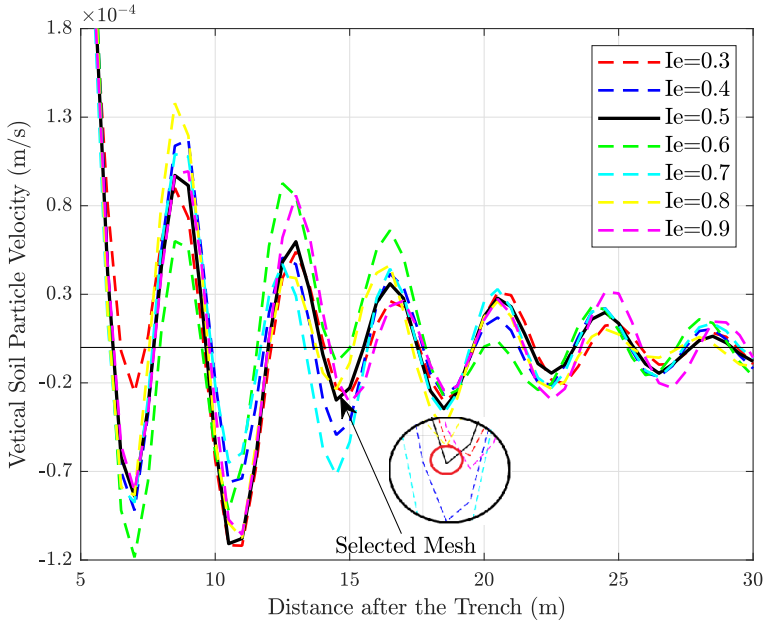


Figure 5.2: Mesh convergence study

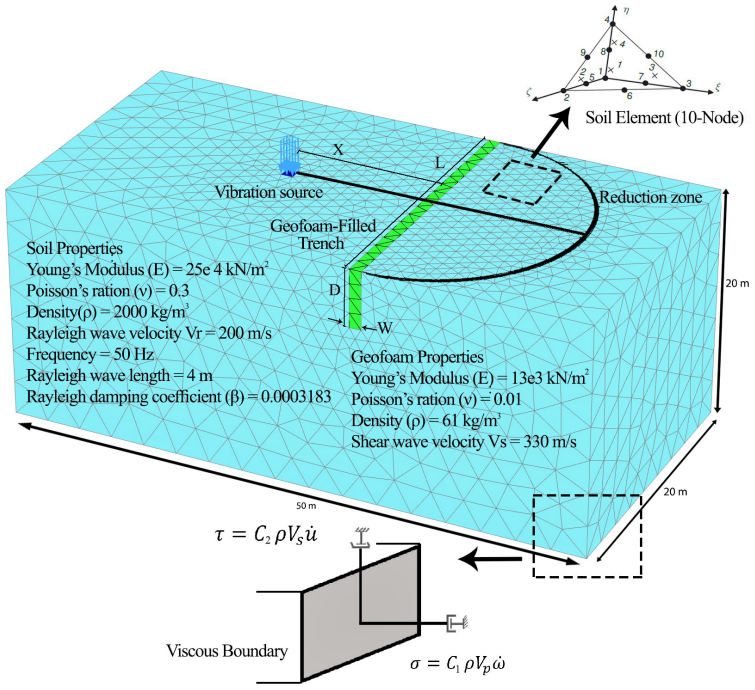


Figure 5.3: Proposed FE model and material properties

system. To better understand the effect of the cross-sectional area, the efficiency of the trench is presented as a percentage, which is calculated by Eq. (5.4).

$$\text{Efficiency} = (1 - \overline{A}_r) * 100 \tag{5.4}$$

For this purpose, a geofoam-filled trench is installed at the location of $5m$ from the vibration

source and with the length of $10m$. The results of calculated A_r are presented in Fig. 5.4.

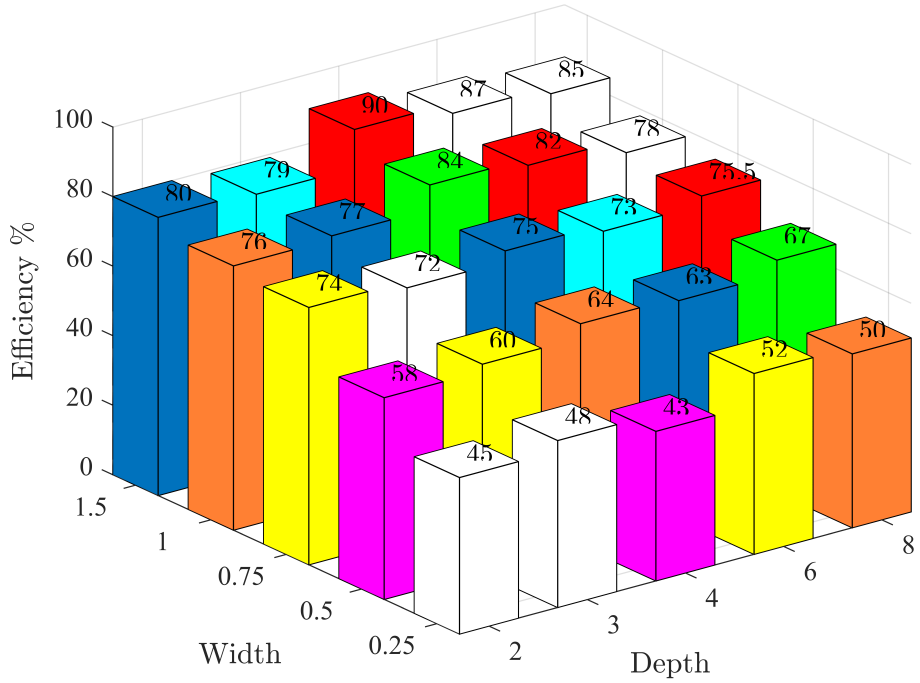


Figure 5.4: Calculated value of efficiency of the geofoam-filled trench for different trench dimensions ($X = 5$ m, $L = 10$ m), near field system

Different colours indicate the trench with the same cross-sectional area. For instance, purple and yellow bars show the cross-sectional area of 1 and $1.5m^2$, respectively. The results demonstrate that increasing the width of the trench leads to an increased efficiency of the trench. For instance, for the trench with the cross-sectional area of $3m^2$ (blue cell), the efficiency of the trench increased by 17% with an increase in the trench width from 0.5 to $1.5m$.

5.5. Genetic algorithm

In Chapter 3, the principles of GA were introduced. The results of the parametric study in chapter 4 showed that the influence of practical ranges of geometric parameters (distance between a trench and the vibration source) and dimensional factors including trench depth (D), width (W), length (L) and the distance between the barriers (S) for a double wall system are the governing factors in wave attenuation. In order to enable a proper comparison of all the three trench shapes, the same depth and cross-sectional area are assumed for all the three systems, while the depth of the trench is the most important factor in increasing the efficiency of the trench. However, the width of all the systems is different from each other. For the double wall system, the width of both two trenches is considered to be one width (W), like the single wall, whereas for the triangular wall system, the width is assumed to be the double value of single and double wall to keep the cross-sectional area constant. For each system, different

boundaries are defined as the maximum and minimum values for various variables, which are presented in table 5.1. The frequency of the applied load is considered to be a fix value to $50Hz$.

Table 5.1: The range for different parameters

Type of system	Location (m)	Depth (m)	Width (m)	Length (m)	Distance (m)
Single	2-20	2-6	0.25-1	5-15	-
Double	2-20	2-6	0.25-1	5-15	2-4
Triangular	2-20	2-6	0.5-2	5-15	-

5.5.1. Implementation of genetic algorithm

The first step is generating an initial population of candidates, which are a group of chromosomes. The population size should be an optimal value. Since small populations do not allow the chromosomes to explore the search effectively, and large population will not be efficient in terms of reasonable computational time. After doing some trials and errors for the initial population, a population size of 30 is found to be optimal for the problems conducted vibration isolation.

Due to the complexity and non-linearity of the vibration isolation problem and extremely large solution space associated with finding the best parameters of the trench with the highest value of the efficiency, a GA-FE coupled methodology is used to calculate the fitness function, which is defined through Eq. (5.5) [Yarmohammadi et al., 2019, 2018; Woods, 1968].

$$\text{Fitness function} = (1 - \overline{A}_r) * 100 \tag{5.5}$$

$\overline{A}_r$ is defined through Eq. (5.6) [Sprengel, 2017].

$$\overline{A}_r = \frac{1}{x} \int_0^x \frac{V_{after}}{V_{before}} \, dx \tag{5.6}$$

where (V_{before}) is the amplitude of the soil particle velocity before installing the trench and (V_{after}) is the amplitude of the soil particle velocity after installing the trench and x is the reduction zone.

5.6. Genetic algorithm model for near field isolation

A computer cluster with 2 central processing units (CPU) and 32 cores at the Chair of Geotechnical Engineering at RWTH Aachen University is used to run the model. The optimal parameters of the geofoam-filled barrier for different systems in the case of near field isolation and for the frequency of $50Hz$ are presented in table 5.2.

Table 5.2: Optimized dimensions of the trench for different systems (geofoam, 50Hz)

System	Location (m)	Depth (m)	Width (m)	Length (m)	Distance between trenches (m)	Efficiency (%)
Single Wall	5.3	2.6	0.9	10	-	78
Double Wall	4.0	2.9	1.2	6.0	2	78
Triangular Wall	2.1	3.3	1.9	8.	-	74

The trench length for the single wall system is calculated as the same value as obtained by the parametric study, so it is concluded that the length of $10m$ for the single wall system is suitable to reach the desired efficiency for $50Hz$. The space between the barriers for the double wall system is also in good agreement with the result of the parametric study.

The results of table 5.2 shows that the single wall system needs the shallowest depth to reach the acceptable value of the efficiency, which is defined as 75% reduction in the screening of incoming waves.

The same optimization is performed by changing the material for filling the trench with concrete. One of the biggest advantages of the GA model is the ability to easily change the properties of the soil and material for filling the trench. The result of the optimization of concrete-filled barrier is summarized in table 5.3.

Table 5.3: Optimized dimensions of the trench for different systems (concrete, $50Hz$)

System	Location (m)	Depth (m)	Width (m)	Length (m)	Distance between trenches (m)	Efficiency (%)
Single Wall	4.3	3.6	0.9	12.3	-	76
Double Wall	5.6	3.9	1.4	5.6	2	74
Triangular Wall	3.5	4.9	1.9	9.4	-	76

The results show that a deeper trench must be excavated to have a successful barrier for all systems. In terms of a stiff barrier, the single wall system has still the most practicability in terms of having the lowest depth and volume. It needs about half the volume of the other systems. The optimized parameters of the triangular wall needs the highest depth in compariosn of other systems for a stiff barrier.

To compare the optimized parameters of the geofoam and concrete-filled trenches as a soft and stiff barrier, there is no considerable difference in the location of the different systems for soft and stiff barriers. For both materials, the triangular wall system should be installed in the nearest location to the vibration source. However, optimized depth of the trench is increased by 28, 25 and 32% for the single, double and triangular wall systems, respectively by changing the system from soft to stiff barrier. The width of the single and triangular wall systems remains almost constant; however, the width of the double wall system increased by almost 20%. Concerning the distance between the trenches, changing the material does not have any effect on this parameter.

5.6.1. Comparison between different systems (near field)

A comparison is drawn to optimize different configurations through calculating $\overline{A_r}$ with different frequencies, and the results are presented in Table 5.4.

Table 5.4: Optimized dimensions of the trench for different systems for $\overline{A_r} = 0.75$, geofoam

	Frequency(Hz)	Depth(m)	Width(m)	Location(m)	Length(m)	Distance(m)
Single	10	4.5	1.3	9.7	14.2	-
Double	10	5.6	1.3	7.4	11.3	2
Triangular	10	5.7	1.9	7.9	12.9	-
Single	20	4.1	1.4	6.1	9.9	-
Double	20	5.5	1.3	7.7	9.8	3
Triangular	20	5.8	1.3	2.6	7.2	-
Single	30	3.2	1.0	5.5	15.7	-
Double	30	4.7	1.2	4.9	18.6	3
Triangular	30	4.7	1.6	3.6	13.6	-
Single	40	2.9	1.1	2.3	9.2	-
Double	40	3.2	1.1	4.9	19.4	2
Triangular	40	4.1	1.3	2.6	14.3	-
Single	50	2.8	0.9	5.3	10	-
Double	50	2.6	1.2	4.0	6.0	2
Triangular	50	2.9	1.9	2.1	8.1	-

A comparison of the optimized depth of different systems shows that increasing the frequency results in requiring a more shallow trench to reach the acceptable amount of efficiency which indicates that the contribution of soil damping is relatively high in higher frequencies. Therefore the system can reach an acceptable amount of efficiency with more shallow trenches. This means that the ground motion is damped both geometrically and materially.

This phenomenon can be more fully explained as follows:
Propagating waves through the ground can lead to transforming some transferred elastic energy into other kinds of energy like heat. The transformation of energy is due to material damping that can be defined through Eq. (5.7) [Beskos et al., 1986; Haupt, 1995a].

$$\psi = e^{-\alpha x} \tag{5.7}$$

Therefore, the amplitude of a harmonic wave can be screened in the form of an exponential function, in which α is the coefficient of attenuation that can be calculated through Eq. (5.8).

$$\alpha = (\psi \cdot f) \,/\, (2 \cdot V) \tag{5.8}$$

By keeping the value of wave velocity (V) constant, α is given directly proportional to the frequency. This can be a reason why high frequency vibrations in a soil is damped much faster with distance in comparison with low frequency [Kolsky, 1963; Haupt, 1995a].

Concerning the optimized width, the single wall system has the lowest value of the optimized width in comparison with other systems for the frequencies of $30-50Hz$. However, double and triangular wall systems are the best systems in terms of the optimized width for the frequencies of 10 and $20Hz$, respectively. A general overview of the optimized locations of all systems represents that trenches should be installed further when the frequency of the load is low. A triangular system has the lowest value of optimized length for all frequencies in comparison with the other systems.

As it can be seen from the results, there is not regular behaviour to explain the effect of different optimized parameters on the efficiency of the barriers for different frequencies. The first reason for this issue is the direct effect of frequency of the applied load on the optimized values of the parameters. The second reason is that vibration isolation is a non-linear problem, and all parameters affect each other.

5.7. Genetic algorithm model for far field isolation

The same GA code is developed for far field isolation with the same properties for the genetic algorithm and the Plaxis model as for the near field optimization scheme. Concerning the dimensions of the barrier, the width and depth of the trench are selected to be identical to those for all the three configurations, the only difference is in the range of normalized distance between the barrier and the vibration source, which is from 12 to $20m$. However, a $2D$ model is used instead of a $3D$ model. The reason for this issue is saving computational time. Since the geometry of the far field model is bigger than of the near field one, analysing several models would require a lot of time. In addition, several research works have shown that Alzawi [2011]; Qiu [2014] the result of $2D$ and $3D$ models are in acceptable agreement.
The results obtained from the genetic algorithm for different combinations of the parameters for all the three systems are presented in Table 5.5. The results reflect that the single wall system needs the lowest value of depth ($2.8m$) in comparison with the other systems. The distance between the pair of trenches should be selected as $3m$, which has increased in comparison with the near field isolation. As it can be seen, the genetic algorithm measured different dimensions for various systems, and it proves that the shape of the trench influences the attenuation of incoming waves.

Table 5.5: Optimized dimensions of the trench for different systems (geofoam $50Hz$)

System	Location (m)	Depth (m)	Width (m)	Distance between trenches (m)	Efficiency (%)
Single Wall	13.9	2.8	0.7	-	74
Double Wall	16.4	3.6	0.5	3	78
triangular Wall	14.6	3.6	1.3	-	74

The optimized parameters of a stiff barrier, which is filled with concrete is presented in Table 5.6. The results show that the width of the trench is independent on its shape of the trenches.

A careful consideration of the importance of both depth and width of the barrier, which is the cross-sectional area of all the systems, can prove that they all have approximately the same cross-sectional area. The general conclusion of the optimized parameters of the stiff barrier is that the efficiency of the trench is independent of the shape of the trench.

Table 5.6: Optimized dimensions of the trench for different systems (concrete $50Hz$)

System	Location (m)	Depth (m)	Width (m)	Distance between trenches (m)	Efficiency (%)
Single Wall	13.2	5.1	1	-	79
Double Wall	13.3	5.5	0.9	2	72
triangular Wall	18.3	5.6	1.9	-	76

The results show that the depth and the width of the trench increase by changing the material from geofoam to concrete. Using the stiff barrier increases the optimized depth by 50, 37 and 34% and the optimized width by 20, 43 and 29% for the single, double and triangular wall systems, respectively in comparison with the soft barrier.

5.8. Conclusion

The most important results are summarized as follows:

- The parametric study of the single wall trench showed that the cross-sectional area of the geofoam-filled trench is one of the most important factors in evaluating the efficiency of the trench.

- The result of the optimization of the near field isolation for the geofoam-filled trench for the frequency of $50Hz$ demonstrated that a depth of approximately $3m$ is enough for all systems but for the rest of the parameters, performing a mutual optimization is needed. A comparison between soft and stiff barrier shows that changing the material of the trench from geofoam to concrete leads to a deeper trench to reach an acceptable amount of efficiency for all the three systems. The frequency analysis of different systems represents that the single wall system is still the most proper solution for mitigating incoming waves for all frequencies.

- The same study is performed for far field isolation for soft and stiff barriers, and the results of the soft trench shows that the single and double wall systems need the lowest depth and width, which are 2.8 and $0.5m$, respectively. The optimized parameters of the stiff trench demonstrate that the depth of the trench is independent of the shape of trenches, while there is not any change in the depth of the trench for different systems. Another important point is that the efficiency of the stiff barrier is independent of the

trench shape since all the systems have approximately the same dimensions and cross-sectional area. However, in terms of depth of the trench, a stiff barrier still needs deeper trenches in comparison with a soft barrier.

- From what has been discussed above, it is concluded the mutual influence of all the parameters is a useful tool for computing the efficiency of a successful trench, since it is apparent that all the parameters can be effective in wave attenuation process when analysing the different parameters together. The developed genetic algorithm code can be used as a reference for engineering applications in vibration isolation problem.

- The result of this chapter is presented based on homogeneous soil, which is an ideal situation and it is uncleared that how a trench will be effective in layered soil.

6 Vibration screening in layered soil

6.1. Problem definition

The investigations on vibration isolation problem are usually done based on the ideal situation of homogeneous half-space with constant properties of elastic parameters over the depth, which is not realistic. In nature, however, the shear modulus of the soil usually changes with depth while the mass density and other properties of the soil can be considered approximately as constant. Dynamic properties and non-homogeneity of the soil play a significant role in transferring dynamic energy [Haupt, 1995a].

Haupt [Haupt, 1995a] stated that shear modulus depends on the mean principal stress of the soil ($\bar{\sigma}_0$), which is calculated through Eq. (6.1).

$$\bar{\sigma}_0 = (\sigma_1 + \sigma_2 + \sigma_3)/3 \tag{6.1}$$

The relationship between the shear modulus and stress of the soil is presented in Eq. (6.2), in which the value of the exponent m is usually considered as 0.5.

$$G \sim (\bar{\sigma}_0)^m \tag{6.2}$$

By considering a uniform ground with no structural inhomogeneity, the overburden pressure ($\bar{\sigma}_0$) increases proportionally to the depth (z). In addition, shear modulus has a direct relationship with shear wave velocity of the soil. Taking Eq. 6.2 into account results in achieving Eq. (6.3).

$$\left.\begin{array}{l} \bar{\sigma}_0 \sim z; \Rightarrow \ \left(G \sim (\bar{\sigma}_0)^m\right) \ \Rightarrow \ G \sim z^m \\ G \sim V_s^2 \end{array}\right\} \Longrightarrow V_s \sim z^{m2} \tag{6.3}$$

where z = depth of the soil.

Therefore, increasing the depth leads to increasing the shear wave velocity and even with a complete uniform ground, the homogeneous soil does not exist in reality in terms of wave propagation issue.

As a consequence of hitting a body wave with an interface between two elastic bodies, not only the wave is partly reflected and refracted to the second medium, but also an other wave type is produced. Fig. 6.1 represents the reflection and refraction process of the incident elastic waves at interface between two elastic media [E Richart, 1970]. The amplitudes of reflected and refracted waves are calculated based on the incident angle, which is determined by Snell's law [Kwan et al., 2002]. The angle of the incoming wave, the ratio of wave velocity and the density in two media are the most important factors in reflecting and refracting of incident waves.

Layering of soil medium is another kind of non-homogeneity, including a stiff soil layer over a soft layer and vice versa. However, the case of a soft layer over a stiff layer is more common in reality.

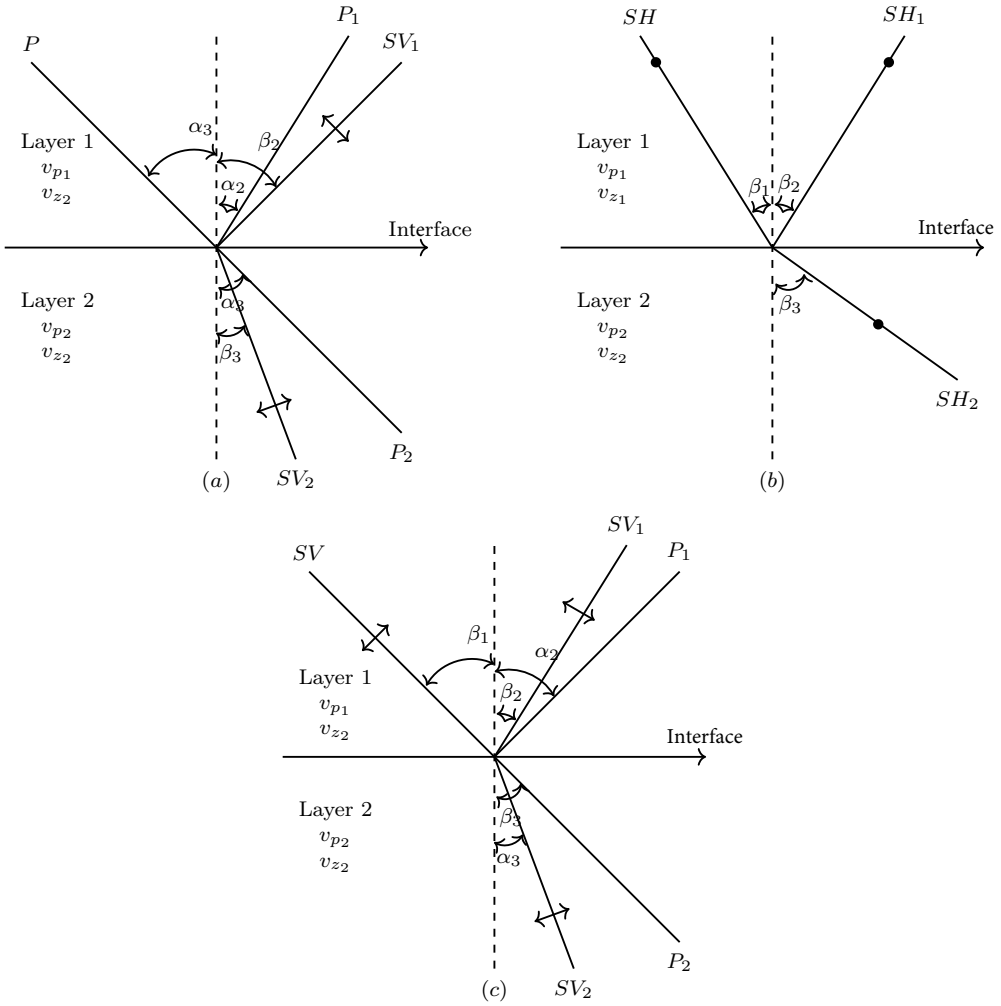


Figure 6.1: Reflection and refraction process of the incident elastic waves

Waves are propagated in all directions in the soil layers with different shear wave velocities and this difference creates numerous reflections and refractions, as well as transformation to the surface [Haupt, 1995a].

The body waves are refracted in a layered soil media, in which we have different layers with various shear wave velocity, and return back to the surface. This phenomenon (refraction), which is observed in layered soil yields more vibration at the ground surface. In terms of R-wave for the case of a soft layer over a stiff layer, increasing the shear wave velocity results in increasing the R-wavelength since the frequency of the load is constant. Therefore, the R-wave penetrates deeper in the soil because of having longer length and this issue has a direct relation in increasing the vibration of the ground surface in layered media. Fig. 6.2 shows penetration of R-wave in different layers.

Love wave is an elastic wave, which is the result of horizontal shear (SH) surface wave. The existence of an elastic surface layer with lower shear wave velocity than the top layer is a necessary condition for propagation of L-waves, since it can be easily shown that on an elastic

half-space alone, SH surface waves cannot exist. The speed of this wave is slower than the body wave and faster than the R-wave.

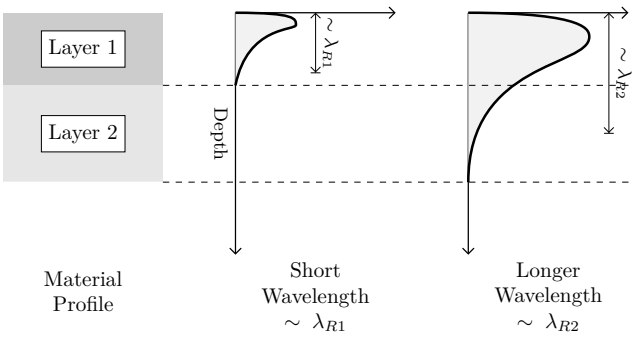


Figure 6.2: Penetration of R-wave in different layers

The second type of non-homogeneity, which is layering of the soil medium is selected for evaluating the vibration screening in layered soil in this chapter.
In this chapter, a comprehensive parametric study is performed to access the efficiency of the geofoam-filled trench as a wave barrier in the layered soil. The effectiveness of the non-homogeneity of the soil is evaluated in section 6.2. The governing parameters on the screening performance are introduced through a single parametric study in 6.3. Finally, the interaction between the key parameters are considered through response surface methodology and one polynomial quartic model is presented for predicting the efficiency of the trench in section 6.4.

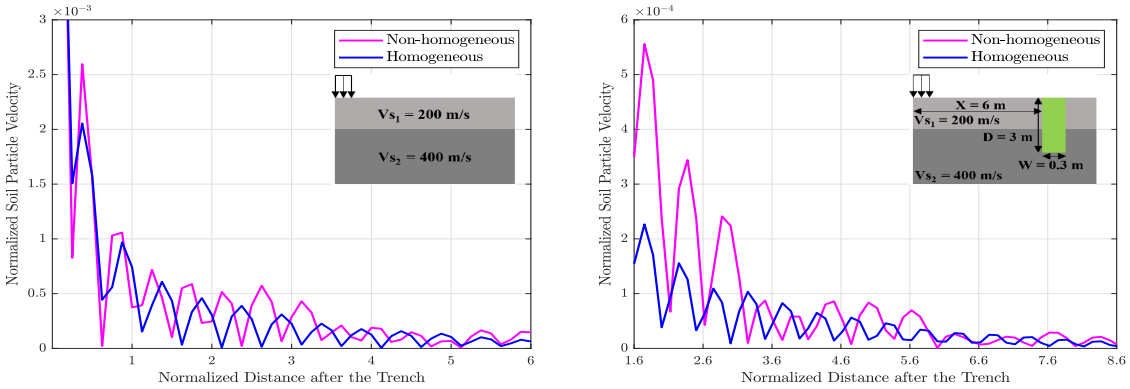
6.2. Homogeneous soil versus layered soil

Rayleigh wave propagates with an independent velocity of the wave length in a homogeneous soil and the amplitude of the displacement of R-wave decays exponentially with depth. However, many soils in the nature are not completely homogeneous and the shear modulus changes usually by the depth [Athanasopoulos et al., 2000; Sahu et al., 2010]. To predict the wave propagation in the soil, it is satisfactory to change the situation to an idealized system. Therefore, the second type of non-homogeneity, which is a layer interface parallel to the ground surface is an acceptable assumption for considering the non-homogeneity of the soil [Haupt, 1995a]. The change of shear modulus in the upper layer is discontinuous.

The lower part of the soil body is usually stiffer than the upper section, since the overburden and confining pressure increases with the depth. Stratifying creates some interfaces in the soil body and the pattern of reflection and refraction in the interfaces of the soil causes the waves to propagate mainly in the horizontal direction and most of the dispersed energy is transmitted in the softer layers close to the surface. R-wave propagates at the ground surface and it carries the highest amount of vibration energy, which is approximately 67% in comparison with the body waves [E Richart, 1970]. Therefore, a higher percentage of the energy from the propagated waves will be carried in the horizontal direction and near the ground surface. Increasing the stiffness of the lower body of the soil medium results in reflecting more waves to the surface.

This phenomenon, which is observed in layered soil yields more vibration at the ground surface [Haupt, 1995a].

In order to better understanding of the effect of non-homogeneity of the soil, a comparison is done between the vertical soil particle velocity of the homogeneous and layered soil with and without a trench. The results are presented in Fig. 6.3. Two layers are considered with different shear wave velocities, which are 200 and $400 m/s$, respectively and constant value for the density and poissons ratio in both layers ($2000 kg/m^3$ and 0.3). The depth of the top layer is $5m$ and the properties of the homogeneous are the same as in the first layer of non-homogeneous soil.



(a) Without Trench

(b) With Trench ($D = 3m$, $W = 0.3m$, $X = 6m$)

Figure 6.3: Vertical amplitude of ground vibration for homogeneous and layered soil

The results show that the response of the layered soil is different from that of the homogeneous soil. One reason of prominent peaks and valleys for layered soil is caused by reflection of the incoming waves from the layer interface to the upper layer, which not happens in homogeneous soil. Another important point is the phase difference between the vertical displacement of homogeneous and layered soil in terms of peaks and valleys in the normalized distance between $2-4$ and $1.6-3.6$ from the vibration source for Figs. 6.3(a) and 6.3(b), respectively. The contribution of R-wave is small near the vibration source, where the body waves are dominant. Therefore, the reflecting of the body waves does not create any difference in the soil response phase and the displacement of both soils is at the same phase until the normalized distance of almost 2. However, increasing the normalized distance between (between $2-4$ or $1.6-3.6$) leads to making R-waves more prevailing in comparison with the body waves.

On the other hand, the R-wave length is dependent on the R-wave velocity and the frequency in the layered medium. The longer R-waves penetrate deeper in the earth and creates more displacements. In addition, the waves in the second layers with higher shear wave velocity move faster than the waves in the first layer. The superposition of R-waves in these two layers leads to constructive and destructive interference and resulting in different phases in the results. It is concluded that the screening of incoming waves in the reduction zone depends on various factors and it is more complicated than homogeneous soil.

6.3. Single parametric study

A time-domain 2D numerical model is developed to assess the efficiency of the trench in attenuating the incoming waves. Since the model is largely affected by the transmitted and reflected waves from the boundary, it is important to keep the region of interest far enough from the reflecting boundary. [Naggar and Chehab, 2005; Yang and Hung, 1997] stated that a zone extending to a minimum distance of $(10\lambda_r)$ from the vibration source is sufficient for wave barrier analysis. With regard to the minimum distance and crucial zone behind the trench, which is $(7\lambda_r)$, the dimensions of the model are selected as $(70 * 25\ m)$[Saikia, 2014].

Viscous boundaries are applied to the bottom and right sides of the model. A viscous boundary condition, which is introduced by [Kuhlemeyer and Lysmer, 1973] consists of viscous dampers applied in X and Y axis in a Cartesian coordinates system along the boundary. In this theory, the absorbed components by the damper are normal (σ_n) and shear stresses (τ), which are obtained by Equations 6.4 and 6.5 [Brinkgreve et al., 2020].

$$\sigma_n = -C_1 \rho V_p \dot{U}_x \tag{6.4}$$

$$\tau = -C_2 \rho V_s \dot{U}_y \tag{6.5}$$

where V_p and V_s are pressure and shear wave velocity respectively, $\dot{U}_x$ and $\dot{U}_y$ denote normal and shear particle velocities derived by time integration, ρ is material density, C_1 and C_2 are relaxation coefficients to change the effect of absorption. It is proved that applying the two relaxation coefficients equal to one leads to the highest efficiency in absorbing any waves reaching the boundary, which is sufficient for practical applications [Saikia, 2014].

The vibration source, which is illustrated in Fig. 6.4, is modelled as a vertical harmonic load with a magnitude of 1 KN,frequency of 50 Hz and a contact length of 0.36 m.

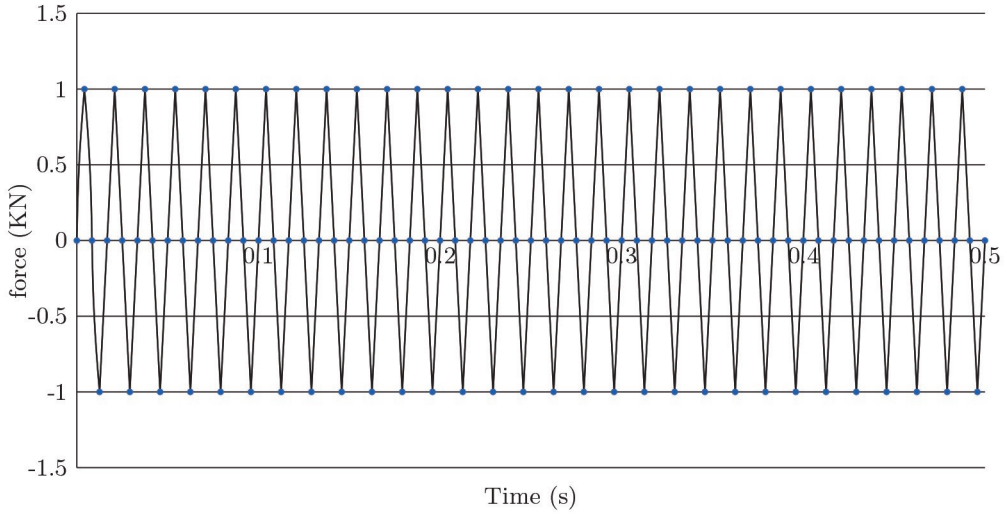


Figure 6.4: Proposed vertical harmonic load as vibration source

The properties of the soil and geofoam obtained from a full experimental test in section 4.2 are used in Plaxis. The proposed FE model of the vibration isolation system and the defined parameters are presented in Fig. 6.5 [Naghizadehrokni et al., 2020].

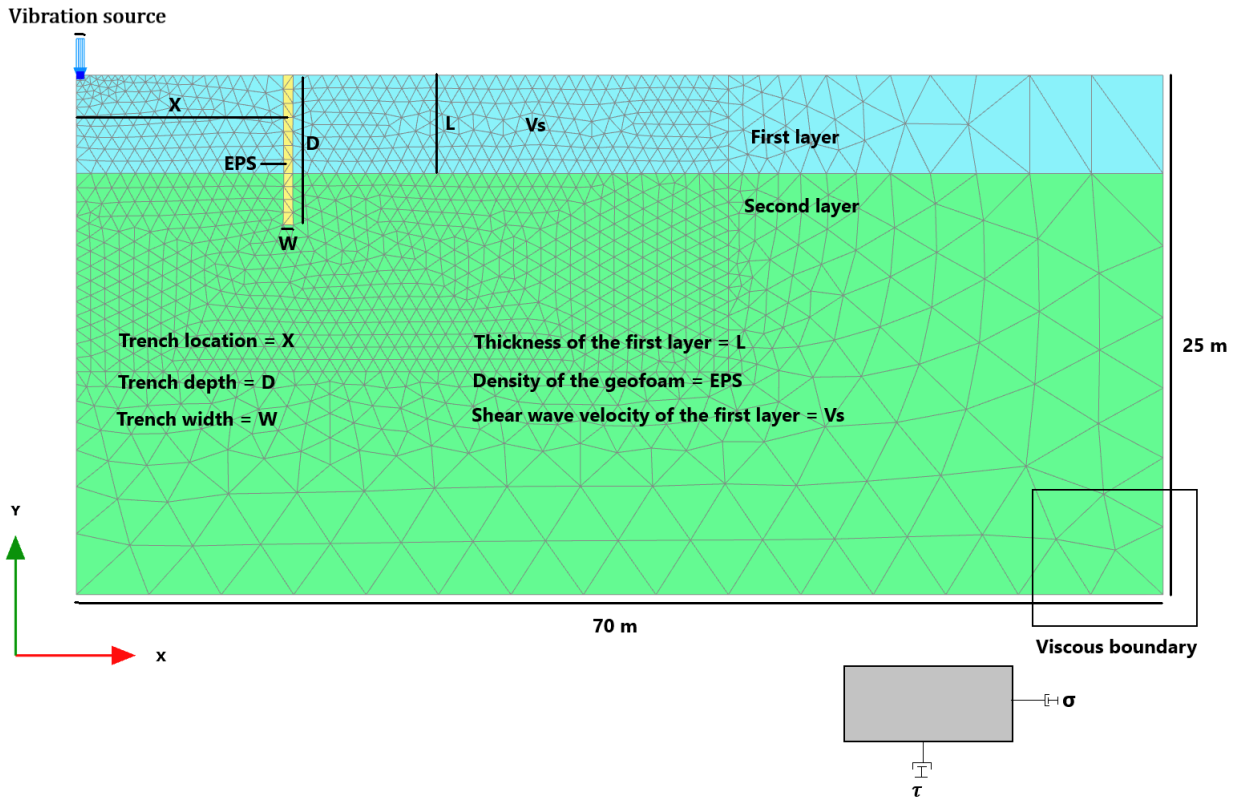


Figure 6.5: Schematic view of Plaxis model and selected parameters

A simplification for the non-homogeneity of the soil is done by considering the layer interface parallel to the ground surface. The first layer is considered as a key layer for creating changes in the parameters. The ranges of parameters in the parametric study are presented in table 6.1. The frequency of the applied load is $50Hz$ and all parameters are normalized with the R-wavelength of the first layer.

[Haupt, 1995a] stated that the limit to distinguish between near (near field) and far (far field) field conditions can be taken as 1.0 to 1.5 of the R-wavelength. Hence, the trench in this study is located at two locations, near ($0.75\lambda_r$) and far ($3.75\lambda_r$) from the source to be considered as an near field and far field isolation system, respectively. Expanded polystyrene (EPS) geofoam material is selected for filling the trench. It has a density of 1% compared to the surrounding soil, making it appropriate for vibration mitigation. It is also accessible in different types with various dynamic properties that can be chosen by the designer for a specific application. In this investigation, EPS 15 with the density of 14.4 kg/m^3 and elastic modulus of 2500 kPa is selected for filling the trench (ASTM).

A parametric study can be time consuming, is prone to human error and requires saving large amounts of data. Altogether, the above parametric study results in 18750 models. Running of all models manually would take several months, even before collecting results and calculating

Table 6.1: Ranges of different parameters in the parametric study

Parameters	The selected value for the parametric study (m)					
Location (X)	3	6	9	12	15	
Depth (D)	2	3	4	5	6	
Width (W)	0.3	0.5	0.7	1	1.5	
Thickness of first layer (L)	2	4	6	8	10	
Geofoam Type (EPS)	EPS12	EPS15	EPS19	EPS22	EPS29	
Shear wave velocity (V_s)	200	250	300	350	400	

the efficiency of the trench. The solution is automation. For this purpose, a script is developed for coupling the finite element model (Plaxis) and Python programming language through Plaxis remote scripting interface in order to run the calculations automatically. All processes are done automatically through five computers for four weeks.

The general purpose of this research is to evaluate the screening effectiveness of the geofoam-filled trench through calculating amplitude reduction ratio (A_r) for different shapes and sizes. The step-by-step plan in numerical model was (1) to set up a harmonic load as a vibration source, (2) to determine the amplitude of vertical ground motion at the selected points with a normalized distance of ($0.125\lambda_r$) at ground surface of the model before installing the trench (V_{before}), (3) to install the trench, (4) to determine the amplitude of ground motion at the same selected points after installing the trench (V_{after}). To evaluate the system effectiveness (screening effectiveness) of the wave barrier system on the ground surface beyond the wave barrier, the averaged amplitude reduction factor, $\overline{A}_r$, was calculated using Equation 6.6.

$$\overline{A}_r = \frac{1}{x}\int_0^x \frac{V_{after}}{V_{before}}\,dx \tag{6.6}$$

where (V_{before}) is the amplitude of the soil particle before installing the trench and (V_{after}) is the amplitude of the soil particle velocity after installing the trench and x is the reduction zone beyond the trench which is equal to 7 Naghizadehrokni et al. [2020].

Therefore, the system effectiveness is calculated using Equation 6.7

$$\text{System effectiveness} = (1 - \overline{A}_r) * 100 \tag{6.7}$$

A comprehensive parametric investigation is carried out to evaluate the effectiveness of the different parameters of the wave barriers for the near field and far field isolation systems in the vertical direction. Results of the detailed parametric investigation are presented, and some applicable recommendations are suggested for designing the wave barriers in layered soil.

6.3.1. Influence of the depth and width of the barrier

To investigate the effect of trench dimensions in screening the vibration, the influence of trench depth is investigated for different values of trench width for near field system and the results are presented in Fig 6.6. The efficiency of the trench in the soft soil (V_s 250m/s) increases with deeper trenches until $D = 1.75$. In addition, it should be noted that the installation of the shallow trench ($D = 0.5$) does not have any practicability in attenuating of incoming waves for shear wave velocity of 200 m/s.

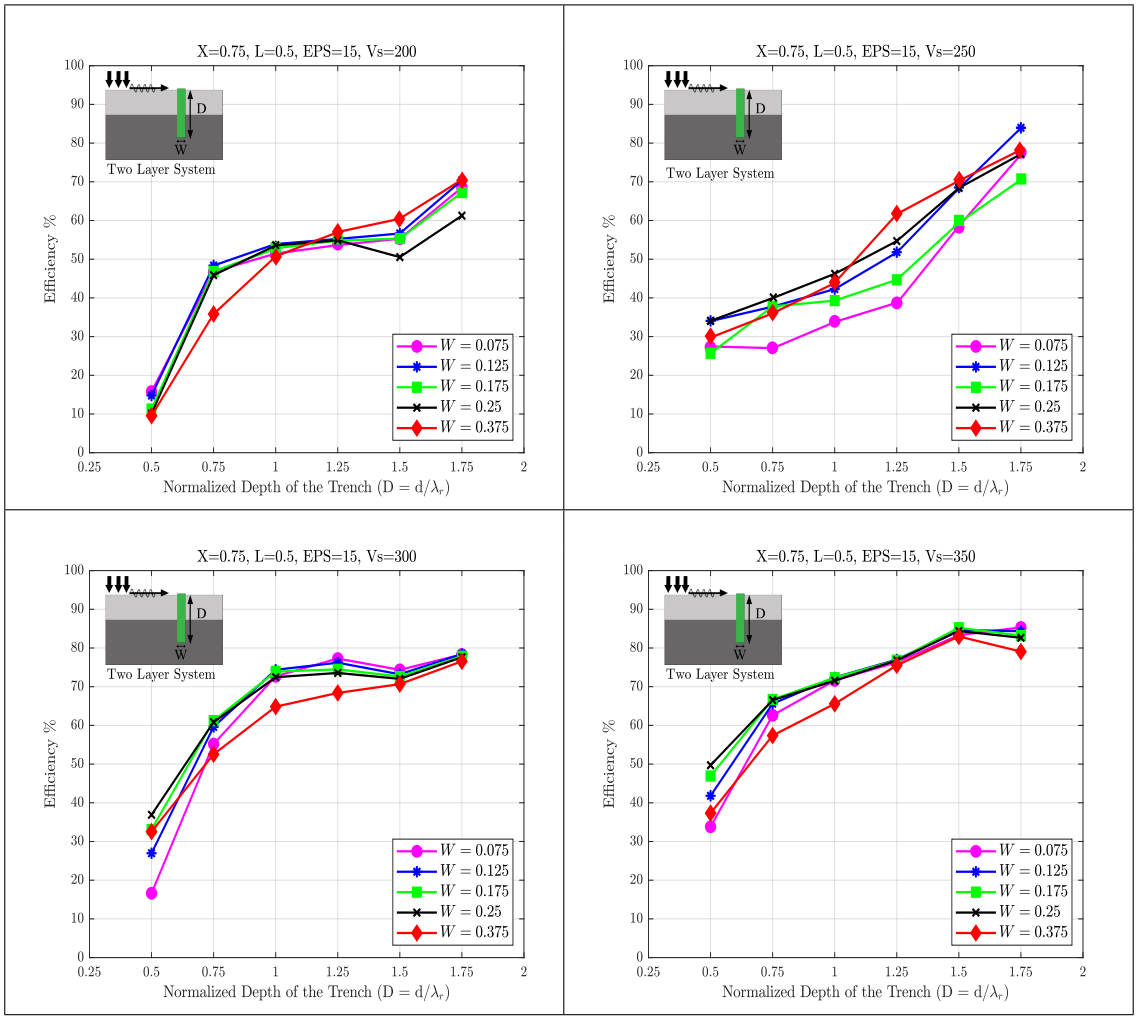


Figure 6.6: Influence of depth on the efficiency ($X = 0.75$, $L = 0.5$, EPS$= 15$)

For stiffer soil (Vs 300m/s), increasing normalized depth improves the efficiency significantly up to $D = 1.0$ and 1.25, beyond this depth the improvement in efficiency is much lower. Owning the fact that as the trench reaches a certain depth, the deeper part of the trench can hardly affect the response of the soil on the free surface. However, this is not the case for the lowest shear wave velocities (V_s 250 m/s) and this issue showed that deeper trenches are needed in softer soil (V_s 250 m/s) for reaching the same screening effectiveness in comparison with the stiffer soil (Vs 300 m/s).

The result of influence of the depth of the barrier for different values of the width are investigated through installing the trench at the normalized location of $X = 3$ for far field scheme and the results are illustrated in Fig 6.7. The efficiency of the trench increases gradually and continuously by increasing the depth of the barrier for approximately all widths, implying that D governs the screening influence. It should also be pointed out that installing a shallow trench with $D < 0.75$ in a layered soil should be ignored while it does not have any practicability (Efficiency $< 30\%$).

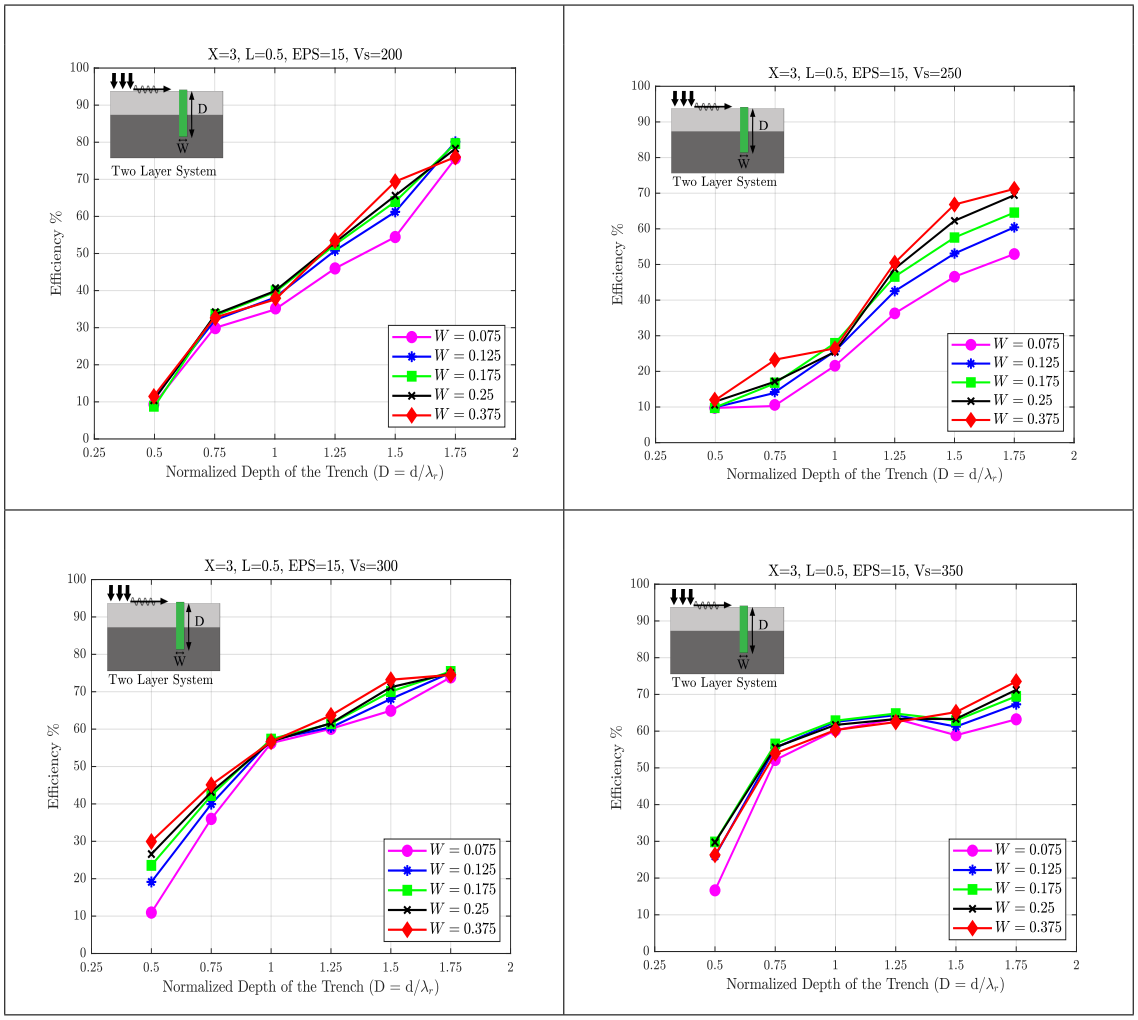


Figure 6.7: Influence of depth on the efficiency ($X = 1.5$, $L = 0.5$, EPS$= 15$)

A general comparison between near field and far field ground vibration isolation with the same parameters showed that for softer soil with $V_s < 250\ m/s$ near field system is more practical as far field one while a higher mitigation is reachable by installing deeper trenches. However, increasing shear wave velocity of the soil ($V_s > 250\ m/s$) results in outperformin the near field system as far field schemes.

It is also apparent from the result of near field and far field systems that the efficiency of the trench is not affected by the width of the trench and even increasing depth and shear wave velocity of the first layer of the soil cannot create any change in the influence of W on screening

effectiveness. Therefore, the normalized width of 0.075 is selected for the rest of the parametric study and the assumption has a good agreement with [Alzawi and El Naggar, 2011].

6.3.2. Influence of the shear wave velocity of the first layer

Fig. 6.8 shows the effect of shear wave velocity of the first layer of the soil on the trench performance as a function of D for near field system ($X = 0.75$). The results clearly demonstrate the significance of V_s on attenuation of incoming waves. As the value of V_s reaches 400m/s, the trench has the highest value of the efficiency for any given D, which means that the barrier has better screening performance in homogeneous soil (remember the bottom layer has a V_s of 400 m/s) in comparison with the layered soil.

As already shown, the effect of the depth is also evident although for $D > 1.25$, the effect is much smaller. For $L = 0.5$ and 1.5, a drop in efficiency is visible for $V_s = 250\ m/s$ for almost all depths, although for larger depths and layer thickness (L), the decrease is less evident.

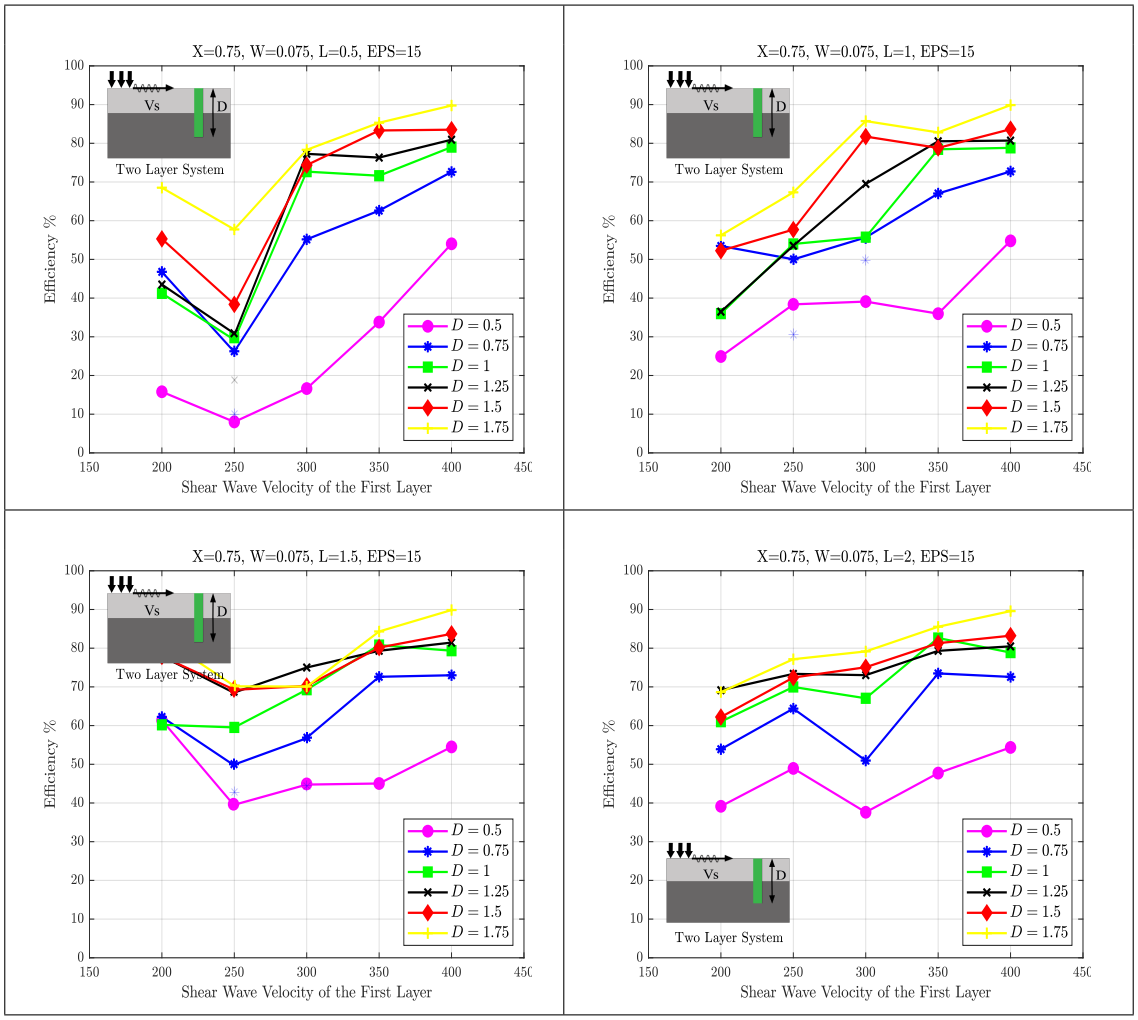


Figure 6.8: Influence of shear wave velocity of the first layer ($X = 0.75$, $W = 0.075$, EPS= 15)

[Haupt, 1995b, 1977] stated that the body waves which radiate from a steady-state oscillation

foundation at the surface to the interior of the half-space in layered soil are bent continuously upwards and return back to the surface. Therefore, a superposition of these body waves and the surface waves occurs yielding an amplification in the amplitude of the vibration that results in some irregularities in FE-calculations.

In addition, according to [Wolf and Obernhuber, 1982], the angle of incidence of the body waves to the interface in layered soil is an important parameter influencing the degree of amplification, as well as the propagation of waves at the surface of the layer. Furthermore, [Naghizadehrokni et al., 2020] observed that the destructive wave interference resulting from the phase difference between the waves is highest for $V_s = 250\ m/s$ which results in the drop of efficiency.

Fig. 6.9 shows the behaviour of the far field system. The results illustrate that for almost all values of L, the efficiency of the trench increases with increasing the value of V_s when $D > L$ (i.e., when the trench depth is greater than the thickness of the first layer) the behaviour is more non-linear showing the more complex interactions. For $D <= L$, the system behaves more in a linear manner This is confirmed for $L = 2.5$ that has the lowest amount of fluctuations in the results for all values of D. It also indicates that this value is large enough for ignoring the effect of layering of the soil. The results also show that for $V_s > 300\ m/s$, the effect of L is limited.

6.3.3. Influence of the thickness of the first layer

The results of the soft soil with shear wave velocity of 200 and 250 m/s are presented in Fig. 6.10. As shown in the last section, there is not a significant influence of L on the efficiency for stiff soil ($V_s > 300$). For $X = 0.075$ the results show a general trend where the efficiency increase with thickness. For X=1.5,the trend disappears. In general, though a singular point occurs for $L = 1.5$ except for $V_s = 250\ m/s$ for the reasons already explained. For $X = 1.5$ the nonlinear behaviour is clear for $D <= L$ especially for low values of $Vs = 200\ m/s$.

6.3.4. Influence of the location of the barrier

Fig. 6.11 and 6.12 show the effect of normalized location of the trench as a function of D for soft soil ($V_s = 200\ m/s$) and stiff soil ($V_s = 350\ m/s$). As expected, the effect of layering is once again clear. For the softer layer the bahviour is much more nonlinear than for the stiffer soil which shear wave velocity is closer to the underlying layer. With only some exceptions, the efficiency does not seem to improve or change significantly for $X > 2.25$ for the softer soil, whereas the stiffer soil continues the linear trend where trench distance to the source reduces the efficiency. However, in the stiffer soil for $X < 2.25$, there seems to be also not significant differences in the efficiency, owning the fact that the position of the layer close to the barrier is not significant for all other parameters constant.

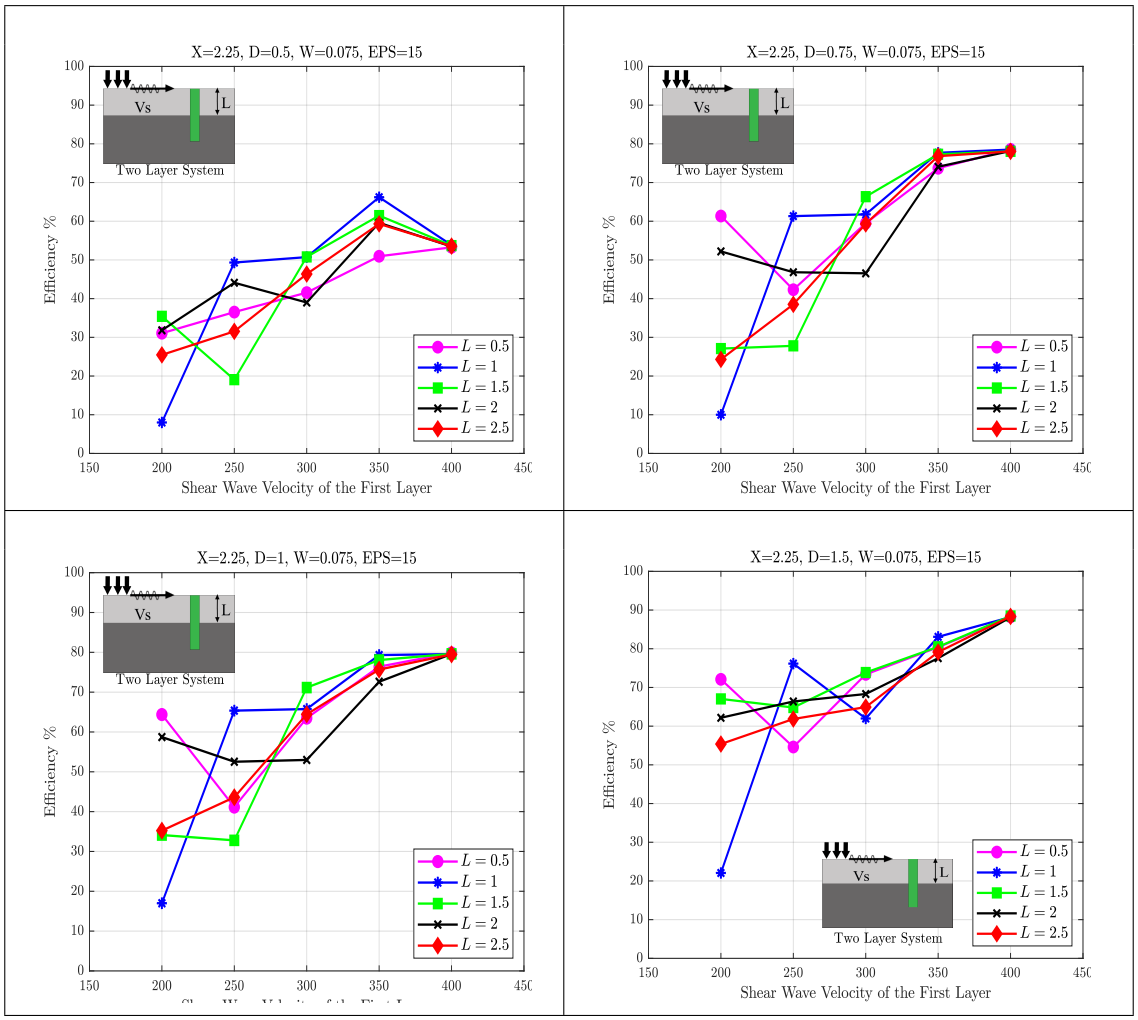


Figure 6.9: Influence of shear wave velocity of the first layer ($X = 2.25$, $W = 0.075$, EPS$= 15$)

After reviewing all depicted diagrams, it can be concluded that the highest attenuation of incoming waves is obtained when installing the barrier near to the vibration source ($X = 0.75 - 2.25$) regardless of the thickness of the first layer and normalized depth , which is in agreement with [Alzawi, 2011].

6.3.5. Influence of the density of the geofoam

Until now, only the results of EPS 15 are represented with varying different parameters. However, in this parametric study, five different geofoams with various density are used. Therefore, the influence of the density of the geofoam for soft and stiff soils ($V_s = 200$, 250 and $300 m/s$) is analysed. The result, which are not presented here does not show any considerable change for stiff soils ($V_s > 250$). However, the results of soft soil ($V_s = 200$) showed that increasing the density of the geofoam results in decreasing the efficiency of the trench for approximately all depth.

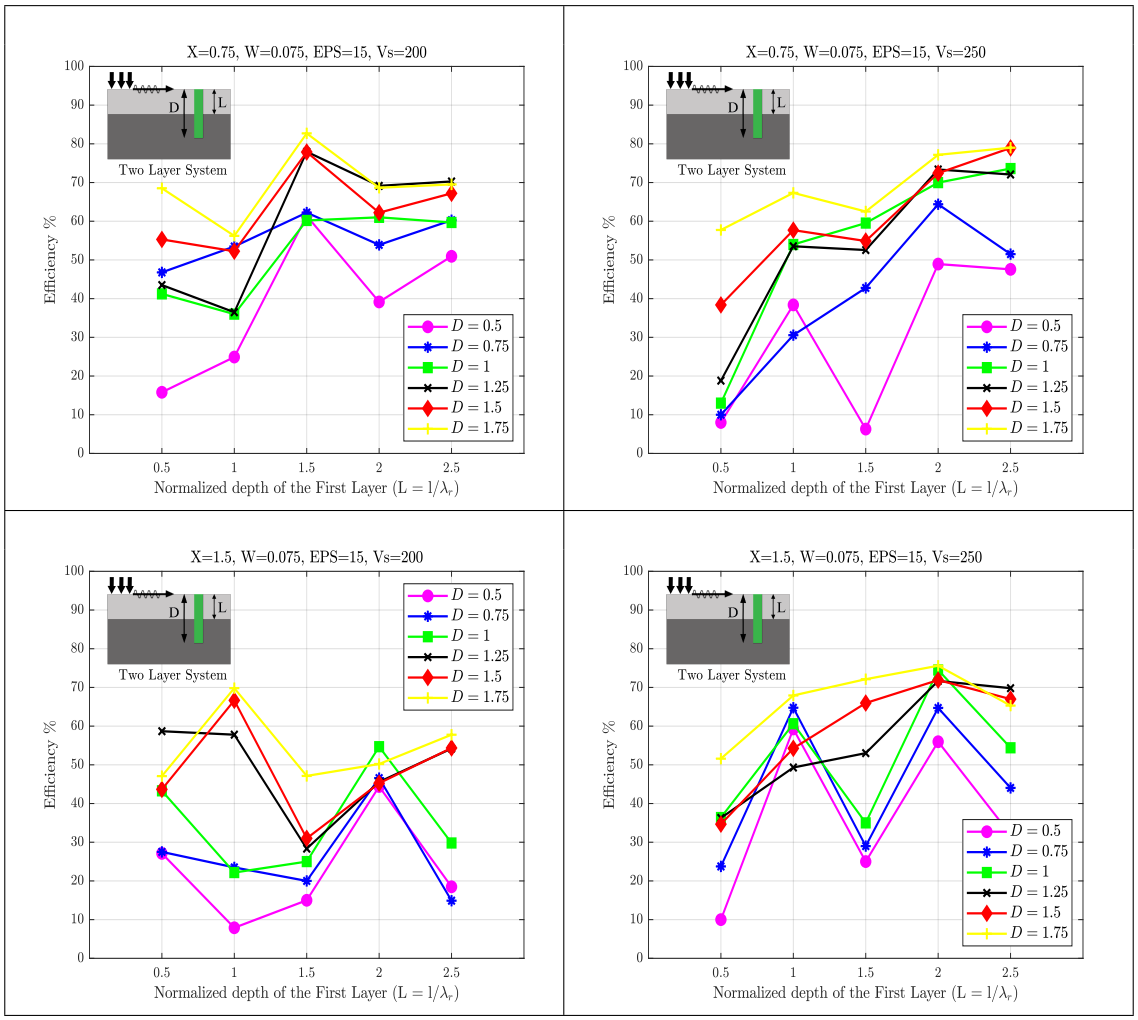


Figure 6.10: Influence of normalized thickness of the first layer ($W = 0.075$, EPS$= 15$)

6.4. Interaction between different parameters

Based on the single parametric study, approximately $100,000$ data were collected after analysing all models based on different parameters. The single parametric study of the results showed that there is a remarkable interaction between some parameters when considering the effect of several factors simultaneously. The presence of interactions has considerable influence for interpreting the trench effectiveness in attenuating the incoming waves in different situations. For instance, if the shear wave velocity and the thickness of the first layer have an interaction, the relationship between the interacted parameters (like X and D) depends on the value of interacting variable of V_s and L.

Therefore, it attempted to present either all interaction between the parameters or at least some part of them. For this purpose, the Response Surface Methodology (RSM), a statistical approach is selected to present the interaction between different parameters and predict the efficiency of the geofoam-filled trench [Khuri and Mukhopadhyay, 2010]. RSM contains a collection of statistical and mathematical techniques for developing and optimizing a process. The

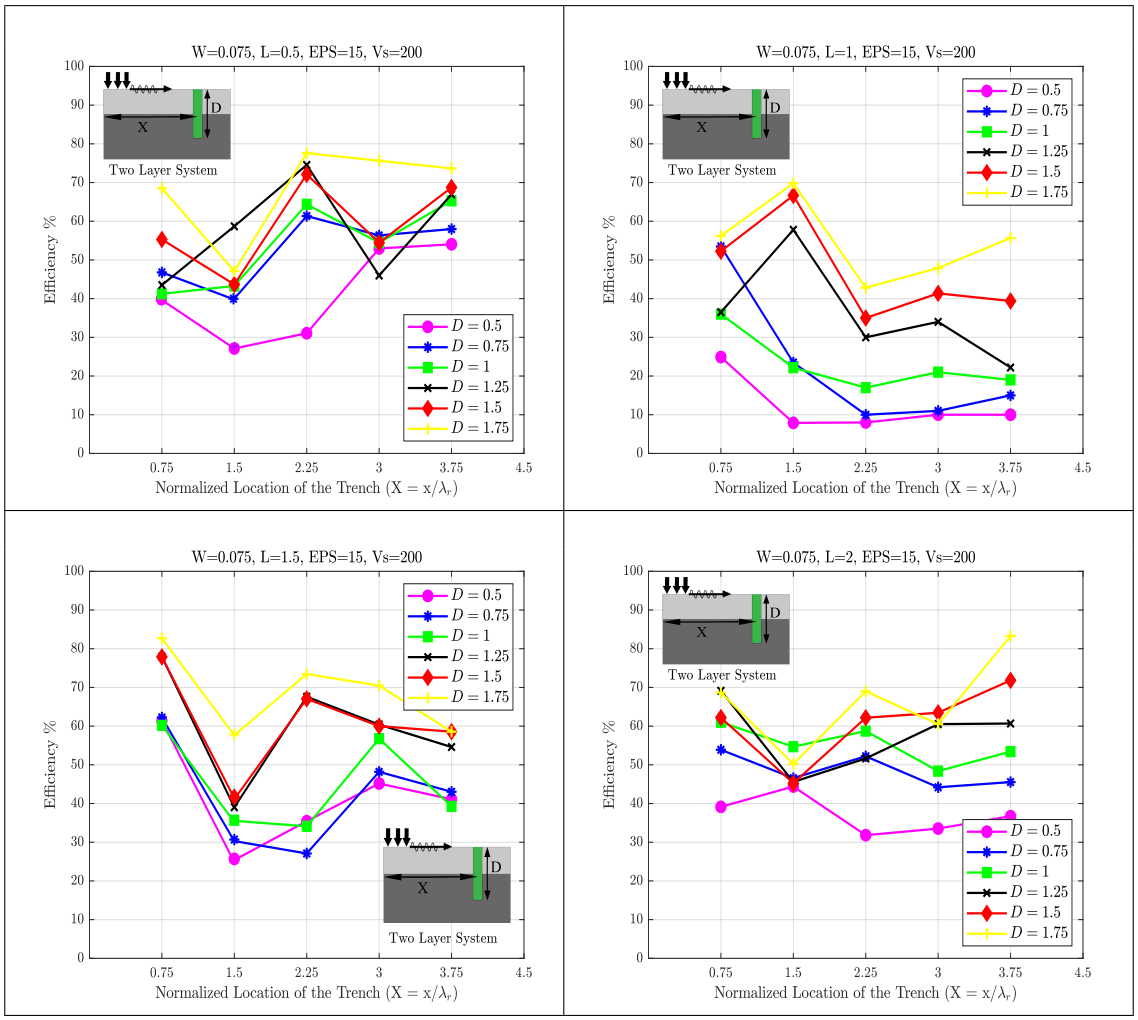


Figure 6.11: Influence of normalized location of the trench ($W = 0.075$, $V_s = 200m/s$, EPS$= 15$)

most extensive application of RSM is the situation in which several independent variables potentially influence the performance of the target variable. The measurement of this interaction between the parameters are called the response. Normally, the highest amount of screening performance happens at particular values of the parameters. However, some changes in the values of these parameters, like location and the depth of the trench simultaneously might create better screening performance. The main duty of RSM in this study is to obtain the relationship between different parameters that affect the efficiency of the barrier.

Identifying the independent parameters and a specific range for each of them that affect the dependent factor is the first step in implementing RSM. This step is already done through a parametric study which are presented in section 6.3. The independent parameters and their corresponding level for finding the interactive effect between them, as well as mean and standard deviation of all parameters are presented in table 6.2. The standard deviation is a measure of the amount of variation or dispersion of a set of values. A low standard deviation indicates that the values tend to be close to the mean of the set, while a high standard deviation indicates that the values are spread out over a wider range.

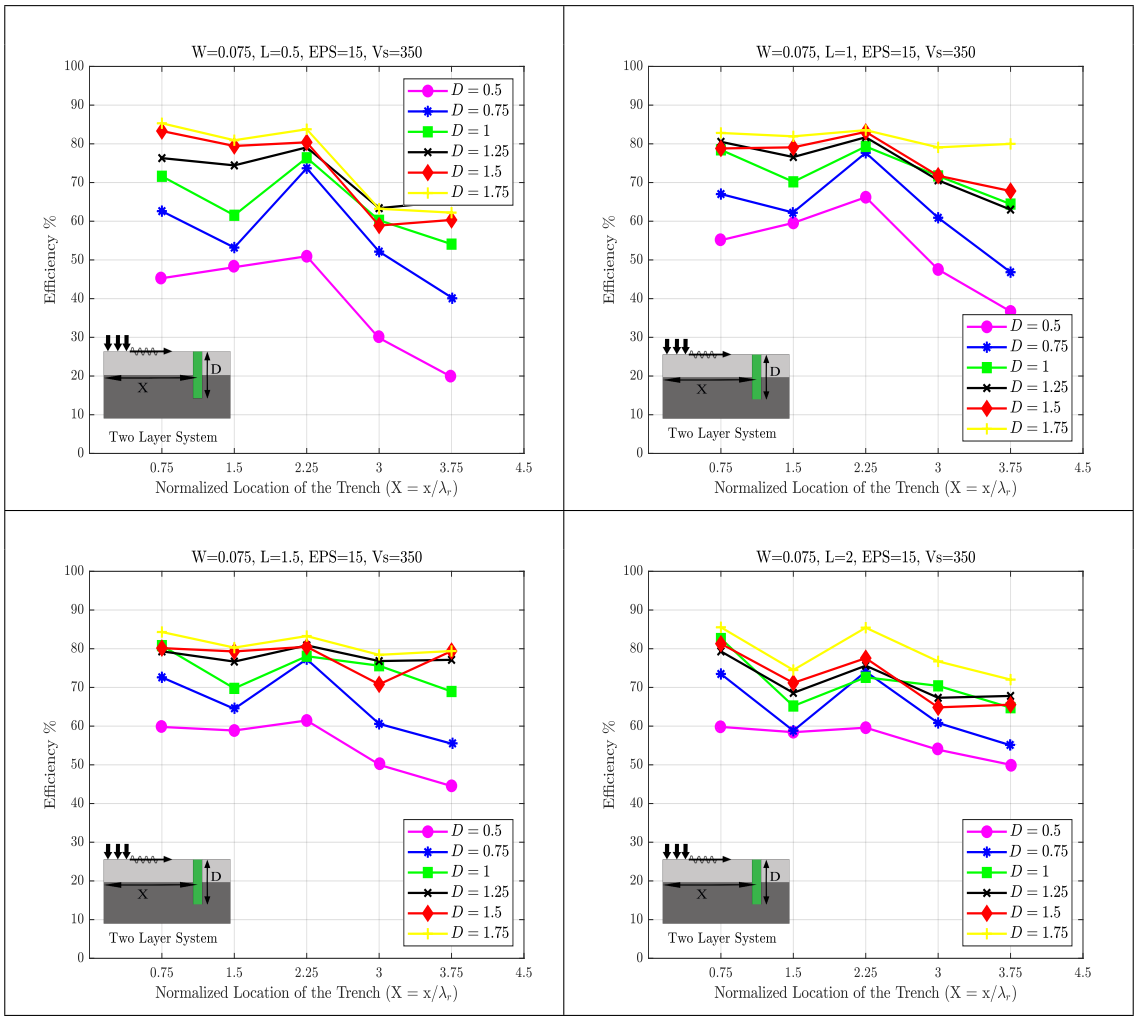


Figure 6.12: Influence of normalized location of the trench ($W = 0.075$, $V_s = 350m/s$, EPS= 15)

Table 6.2: Values of different parameters

Independent variables	Min	Max	Coded Low	Coded High	Mean	Std. Dev.
Trench location (X)	0.75	3.75	-1 ↔ 0.75	+1 ↔ 3.75	2.24	1.07
Trench depth (D)	0.5	1.75	-1 ↔0.50	+1 ↔ 1.75	1.14	0.426
Trench width (W)	0.08	0.38	-1 ↔ 0.08	+1 ↔ 0.38	0.2008	0.105
Thickness of first layer (L)	0.5	2.5	-1↔ 0.50	+1 ↔ 2.50	1.51	0.713
Density of geofoam (EPS) (Kg/m^3)	12	29	-1 ↔ 12.0	+1 ↔ 29.0	19.38	5.89
Shear wave velocity (Vs) (m/s)	200	400	-1 ↔ 200.	+1 ↔ 400.	302.75	70.27

A mathematical model should be fitted with all analysed data. This process is done through coding all data (from -1 to $+1$) and regression. R-squared (R^2) coefficient are used for finding the best mathematical model. Probability value (P-value) is the probability of obtaining test results at least as extreme as the results actually observed during the test [Khuri and Mukhopadhyay, 2010]. This coefficient is another parameter that can help to find fitter mathematical model to the analysed results. The border of 0.05 is recognised for understanding the significance of the result. If the P-value of a parameter is greater than 0.05, it means that

the parameter has enough influence on the vibration efficiency to be considered, otherwise that parameter can be neglected.

Several polynomial models are generated for analysing all data and measuring R^2 and P-value of the parameters. It has been concluded that quartic model with $R^2 = 0.84$ has the highest fit with the vibration isolation system and this shows the complexity of the system. The results of different models are presented in table 6.3. The most important criteria for selecting this model are the lowest amount of P-value, highest value of adjusted R^2 and the highest agreement between adjusted and predicted R^2.

Table 6.3: Comparison of different mathematical model

Source	Sequential P-value	Adjusted R^2	Predicted R^2
Linear	< 0.0001	0.5967	0.5965
2FI	< 0.0001	0.6337	0.6332
Quadratic	< 0.0001	0.6601	0.6595
Cubic	< 0.0001	0.7364	0.7353
Quartic	< 0.0001	0.8451	0.8435

The next step is to find the significance of the results through an analysis of variance (ANOVA). ANOVA shows the interaction between different parameters and make a comparison between the means of parameters. ANOVA for the quartic model of vibration isolation problem is presented in table 6.4. It should be noted that this table present just the interaction of three parameters and the full version of ANOVA for all parameters is available in the APPENDIX. The table contains some practical information including the F-value, which is based on the ratio of mean square and P-value. The P-value should be used in combination with the F-value for finding the significant parameters. A large F-value shows that the parameter plays a significant role in the system, while a large P-value means the results are insignificant. The results in ANOVA table shows that most of parameters have P-value$<$ 0.001 indicating a high significance for parameters. However, a better comparison for determining the importance of the parameters can be done through comparing the F-value. The coefficients for the quartic equation are used to make predictions about the response for given levels of each factor. Positive sign of a coefficient shows a direct affect and negative sign indicate a inverse affect. The equation is presented in terms of coded factors. By default, the high levels of the factors are coded as $+1$ and the low levels are coded as -1. The coded equation is useful for identifying the relative impact of the factors by comparing the coefficients.

The actual parameters that should be used in the presented equation should be converted to the codded scale (between -1 and +1) through Eq. (6.8).

$$Coded = \frac{2 * (actual\,value\,of\,parameter\; - average\,of\,actual\,parameter)}{substraction\,of\,highest\,and\,lowest\,value\,of\,the\,parameter} \tag{6.8}$$

The presented results show that there is a high interaction between some parameters. The most significant factors in terms of single parametric study include X, D and V_s of the first layer with having high values of coefficient and F-value. However, X with a negative coefficient

Table 6.4: ANOVA for the quartic model of vibration isolation problem

Source	F-value	p-value	Coefficient	Source	F-value	p-value	Coefficient
Location (X)	1325.43	< 0.0001	-13.25	X^2	3192.12	< 0.0001	-53.45
Depth (D)	688.38	< 0.0001	9.29	W^2	120.54	< 0.0001	-2.6
Width (W)	13.56	0.0002	1.51	L^2	48.73	< 0.0001	6.56
Layer (L)	1.61	0.2049	-0.4533	V_s^2	204.55	< 0.0001	4.31
EPS	15.96	< 0.0001	-1.09	$X - D - W$	57.37	< 0.0001	1.42
Vs	6832.91	< 0.0001	30.13	$X - D - L$	55.02	< 0.0001	1.37
X-D	68.75	< 0.0001	2.55	$X - D - Vs$	19.78	< 0.0001	0.8507
X-W	38.56	< 0.0001	-3.88	$X - W - Vs$	54.61	< 0.0001	1.37
X-L	112.92	< 0.0001	-6	$X - L - Vs$	1115.82	< 0.0001	5.96
X-EPS	14.89	0.0001	-1.52	$X - EPS - Vs$	41.38	< 0.0001	-1.21
D-L	11	0.0009	1.89	$D - W - L$	25.02	< 0.0001	-0.934
D-Vs	292.22	< 0.0001	-9.88	$D - W - Vs$	103.76	< 0.0001	-1.93
L-Vs	222.94	< 0.0001	-8.88	$W - EPS - Vs$	48.23	< 0.0001	-1.3

has an inverse effect on the efficiency of the geofoam-filled trench. W, L and geofoam density (EPS) separately does not play a significant role in the results.

The interaction of double parameters shows that $D - V_s$, $L - V_s$ and $X - D$ have the highest interaction on the mitigation of incoming waves. However, the influence of all double parameters is inverse and it means that increasing the value of these mixed parameters decreases the efficiency of the trench.

Comparing the P-value of of the second power of parameters shows that the significance of W and L increases remarkably. On the other hand, the results show an increase in the importance of X, while the F-value and coefficient of X^2 have been increased. However it has still inverse influence.

The highest interaction of three parameters is related to $X - L - V_s$ and $X - V_s^2$ with the highest value of coefficient and F-value. Finally, the interaction of four parameters reveals that X^4, $X - V_s^3$ and $L^3 - V_s$ have the highest interaction on each other in comparison with the other combinations of the parameters.

The results show that the screening of incoming waves are completely a non-linear and complicated phenomenon and parameters have either direct or inverse interaction on each other. On the other hand, it can be concluded that the vibration isolation problem cannot be analyzed through a single parametric study.

The developed polynomial quartic model is used to predict the efficiency of the geofoam-filled trench in layered soil with defining the key parameters including trench depth (D), width (W), location (X), thickness (L) and shear wave velocity (V_s) of the first layer and the kind of EPS geofoam. The rest of the parameters including V_s of the second layer ($V_s = 400m/s$), poison's ratio of soil (0.3) and frequency of the vibration source ($F = 50Hz$) remain constant during the comparison. Since there is not any similar vibration isolation model considering the effect

of geofoam-filled trench in layered soil in the literature, finite element model (Plaxis) is used to assess the accuracy of the proposed model. Table 6.5 represents the result of calculating the efficiency of the trench with the developed model and Plaxis.

Table 6.5: Result of calculating the efficiency of the trench with the developed model and Plaxis

Number	X	D	W	L	V_s (m/s)	EPS (Kg/m^3)	Mathematical Model (%)	Numerical Model (%)
1	1	1.6	0.16	1.3	360	12	76.4	85
2	2	0.9	0.3	0.75	230	15	52.8	60
3	0.75	0.5	0.175	2.5	400	22	59	45
4	1.4	1.3	0.1	1.2	330	19	70	79
5	3.2	0.7	0.23	2.1	280	22	78.55	70
6	3.75	1	0.25	0.5	250	12	52.3	60
7	2.1	0.55	0.3	1.1	385	12	41.6	31.8
8	3.15	0.85	0.2	1.65	340	19	53	57
9	3.5	1.15	0.09	2.3	320	29	75	71
10	1.5	0.85	0.3	1.45	350	15	70	60
11	2.25	1.25	0.25	0.5	250	12	69	83
12	3	0.75	0.25	1	350	22	59.8	60
13	1.9	1.74	0.21	0.72	388	22	75.9	72
14	0.75	1	0.172	2.4	289	12	76.6	78
15	3.3	0.6	0.317	2.3	260	29	13	15
16	2.25	1.5	0.075	1	300	22	63	54.6
17	1.6	1.2	0.25	1.7	310	19	65	61
18	2.5	0.85	0.28	1.1	270	22	65.8	59
19	2.3	1.4	0.2	2.15	330	29	42.6	43.4
20	1	0.7	0.35	0.75	370	22	58.5	60.7

R-square coefficient is used to compare the accuracy of the proposed quartic model. Fig. 6.13 shows the calculated efficiency of the geofoam-filled barrier obtained by the numerical and mathematical models. The obtained R^2 from the results, which is 0.831 indicate an acceptable correlation between the parameters. Therefore, the developed mathematical model has a sufficient accuracy to predict the screening performance of the trench in layered soil.

The results are used to visualize the effect of different parameters on the efficiency of the barrier as a percentage to provide some recommendations for implementation best barriers in layered soil.

6.4.1. Interaction of D and V_s

Fig. 6.14 illustrates the interaction of these two factors on the efficiency of the trench. Increasing D and V_s result in attenuating more incoming waves in parallel. The contour diagram at the bottom, which is the reflection of the interaction of two parameters on the screening effectiveness shows that efficiency of the trench follows the same pattern for different D and V_s.

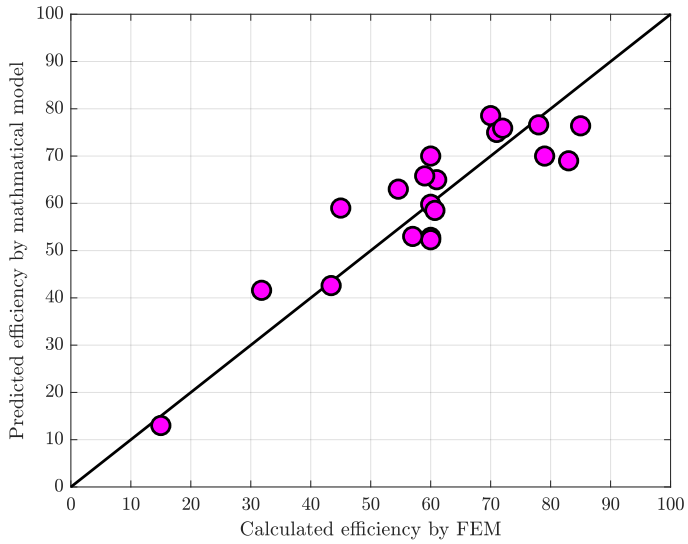


Figure 6.13: Calculated results obtained by FEM versus predicted results obtained by model

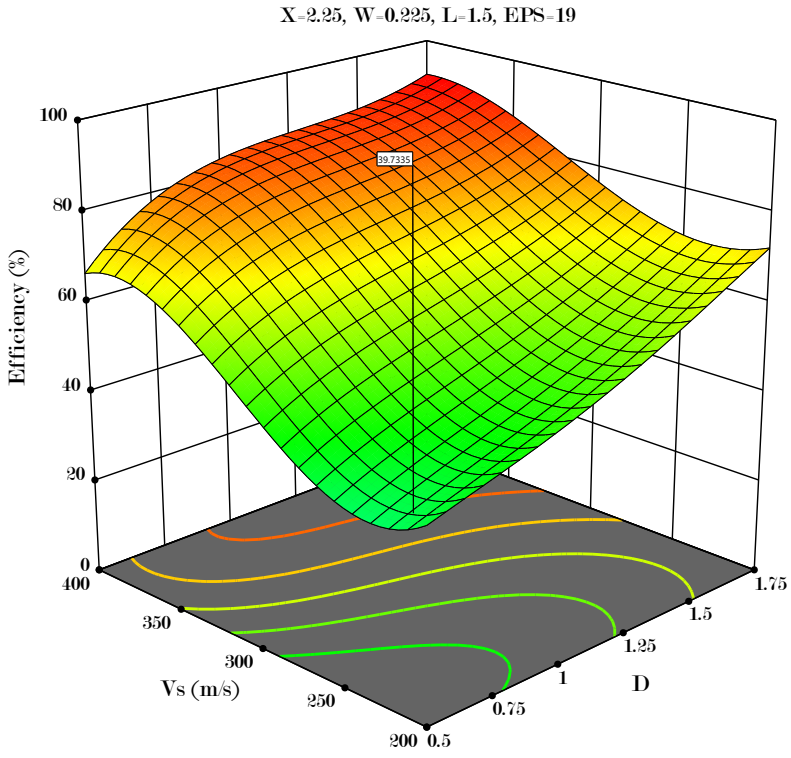


Figure 6.14: Interaction of D and V_s on the response of the trench ($X = 2.25$)

Fig. 6.15 is depicted for interaction of D and V_s at the location of $X = 3.5$ and the results show that the influence of these parameters are the same as for $X = 2.25$. The difference is the value of efficiency, which is considerably decreased for all value of D and V_s in comparison with $X = 2.25$. For instance, there is 50% reduction in the efficiency of the trench for lowest value of efficiency with increasing the distance from $X = 2.25$ with efficiency of 39.7% to furtherer

location $X = 3.5$ with the efficiency of 19.2%. This issue proves that an near field trench has more capability in screening of incoming waves in comparison with a far field trench with having the same value for D and V_s.

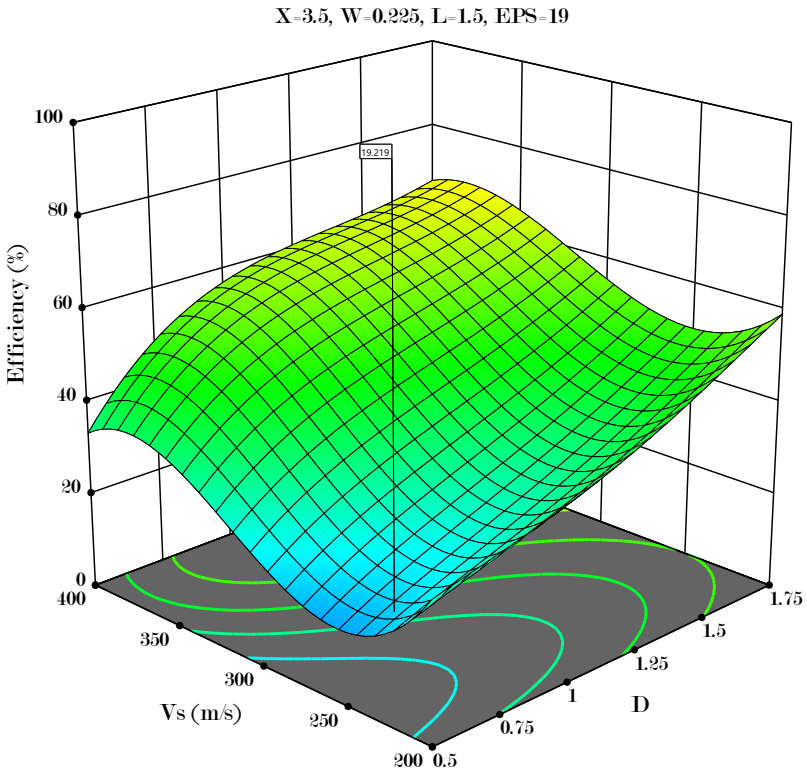


Figure 6.15: Interaction of D and V_s on the response of the trench ($X = 3.75$)

Another remarkable point from the results is that there is not any local maximum in the figure and the efficiency of the barrier increases continuously with increasing both parameters. This argue is matches completely with the result of the ANOVA table since $D - Vs$ has the highest interaction based on the ANOVA result, regarding the F-value.

6.4.2. Interaction of V_s and L

The influence of V_s and L at the location of $X = 0.75$ on the attenuating of incoming waves is presented in Fig 6.16. The screening effectiveness of the trench increases with increasing the thickness of the first layer for lower V_s ($200 < V_s < 300$). However, for stiffer soil ($V_s > 300$), increasing L does not have any effect on the efficiency and the efficiency is almost constant for all values of L. Making the soil stiffer results in increasing homogeneity of the soil, therefore changing the value of L will be meaningless because the soil is homogeneous.

Fig. 6.17 shows that increasing the normalized distance to 2.25 leads to disappearing the significance of L for soft soil and the influence of L can be neglected. The contour diagram at the bottom of the graph, including approximately strait lines shows the same results. However, V_s has still a considerable influence on the efficiency of the trench for $L > 2$.

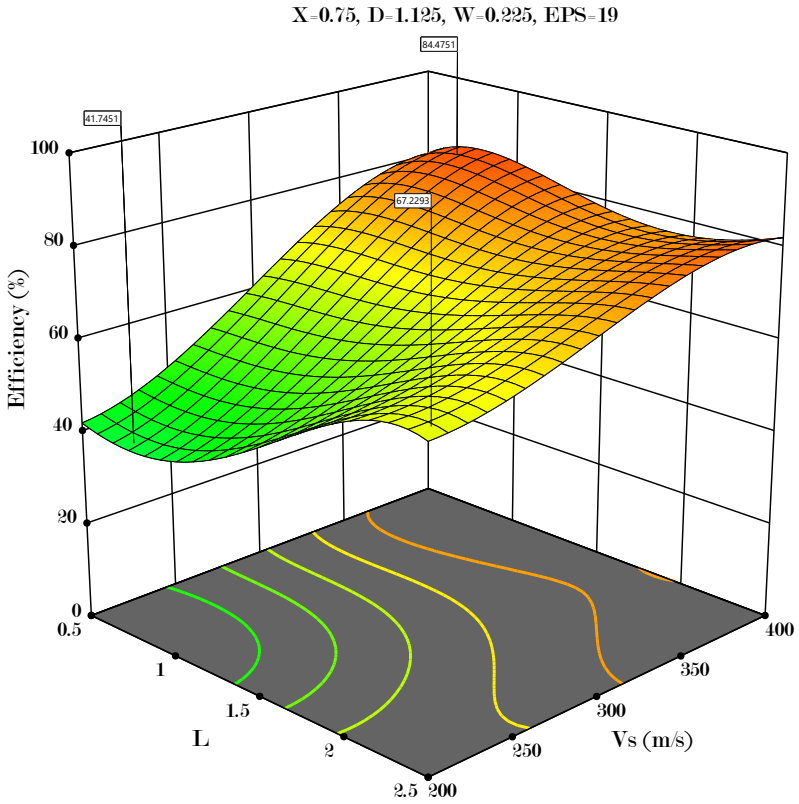


Figure 6.16: Interaction of V_s and L on the response of the trench ($X = 0.75$)

The effect of D has also been considered and the results, which are not presented here showed that increasing D from 0.5 to 1.25 results in increasing screening effectiveness of the trench for all values of V_s and L. It seems that $D = 1.25$ is the optimum depth for stiff soil because the efficiency remains almost constant after this depth. However, there is not any optimum D for soft soil since the efficiency increases continuously with increasing D.

6.4.3. Interaction of X and V_s

One of the most complicated interaction is related to $X - V_s$, which is depicted in Fig. 6.18. The location of the barrier seems to affect the efficiency in such a complex way that the results of wave propagation in layered media are unpredictable. The trench response in terms of location is including several peaks and valleys. These fluctuations result in distinct feature of wave attenuation in layered soil. The superposition of reflected and passed waves from and underneath the trench and new generated waves from the effect of layering results in constructive or destructive interference, depending on the phase of the wave. The constructive feature creates a peak and the destructive feature creates a valley.

The interaction of $X - V_s$ is also analysed for the deepest barrier and lowest thickness of the first layer ($D = 1.75$ and $L = 0.5$). The results, which are not presented here showed that increasing D and decreasing L cannot detach the influence of layering of the soil, in terms of several maximums and minimums in the efficiency of the trench.

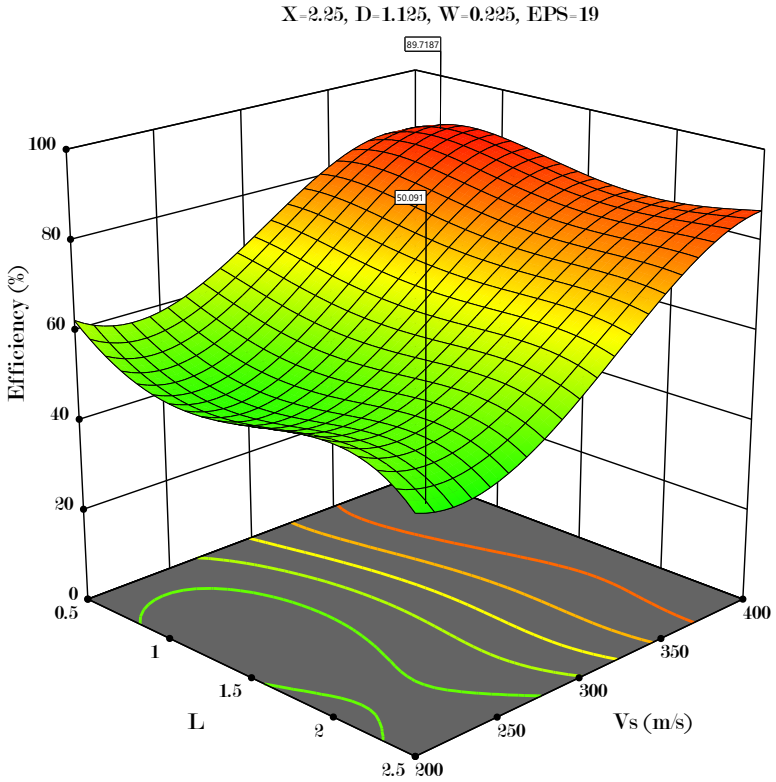


Figure 6.17: Interaction of V_s and L on the response of the trench ($X = 2.25$)

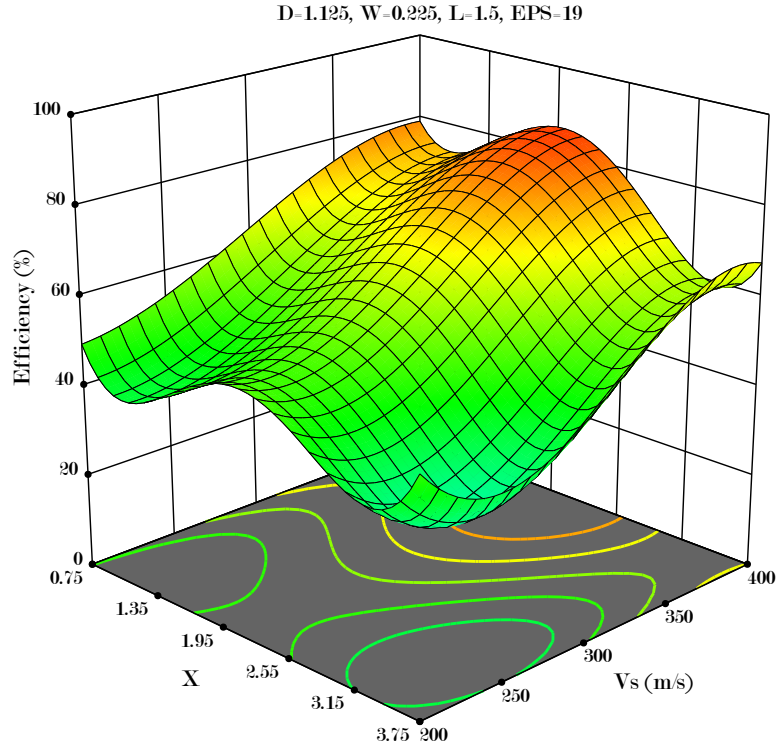


Figure 6.18: Interaction of V_s and X on the response of the trench ($D = 1.125$, $L = 1.5$)

6.4.4. Interaction of X and D

Based on the result of ANOVA table, $X - D$ has a relatively high interaction on the response of trench efficiency. Fig. 6.19 shows still several peaks and valleys, which results in changing the location of the trench for each value of D. However, efficiency remains approximately unchanged with respect to the location. A remarkable reduction in the vertical displacement of ground surface is visible, when increasing the value of D and this issue proves that D can be recognized as the governing parameter to reduce ground born vibration.

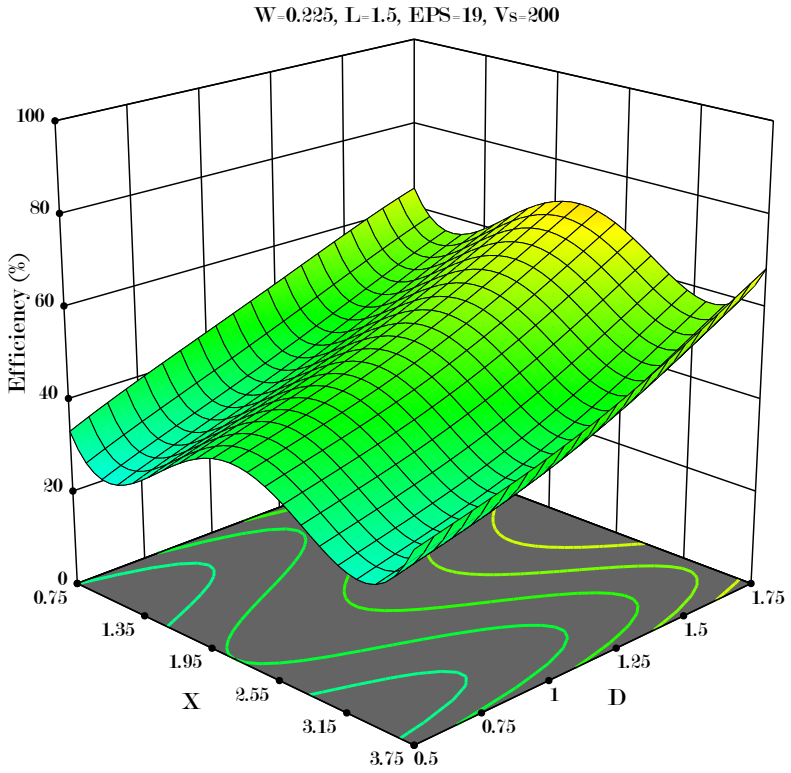


Figure 6.19: Interaction of X and D on the response of the trench ($V_s = 200m/s$)

The same pattern for the trench's response is obtained for the result of $V_s = 350m/s$, which is not presented here. There is not a considerable difference in the behaviour of the trench in terms of changing the location and the depth. However, increasing V_s leads to shifting the whole diagram approximately 20% upper wards of vertical axis.

6.4.5. Interaction of X and L

Fig. 6.20 is depicted for better understanding of the effect of layering for soft soil. The complexity of the result with changing L shows the unpredicted influence of L. However, varying the value of L and X cannot create considerable change in the efficiency of the trench and the screening performance of the trench for all values of $X - L$ is approximately between $40 - 60\%$. Increasing stiffness of the first layer is an effective factor that can diminish the

influence of layering. However, the result of stiff soil is not presented here because L does not play any role in changing the efficiency of the trench. The reason is that increasing V_s means increasing the homogeneity of the soil and this issue result in diminishing the influence of L on efficiency.

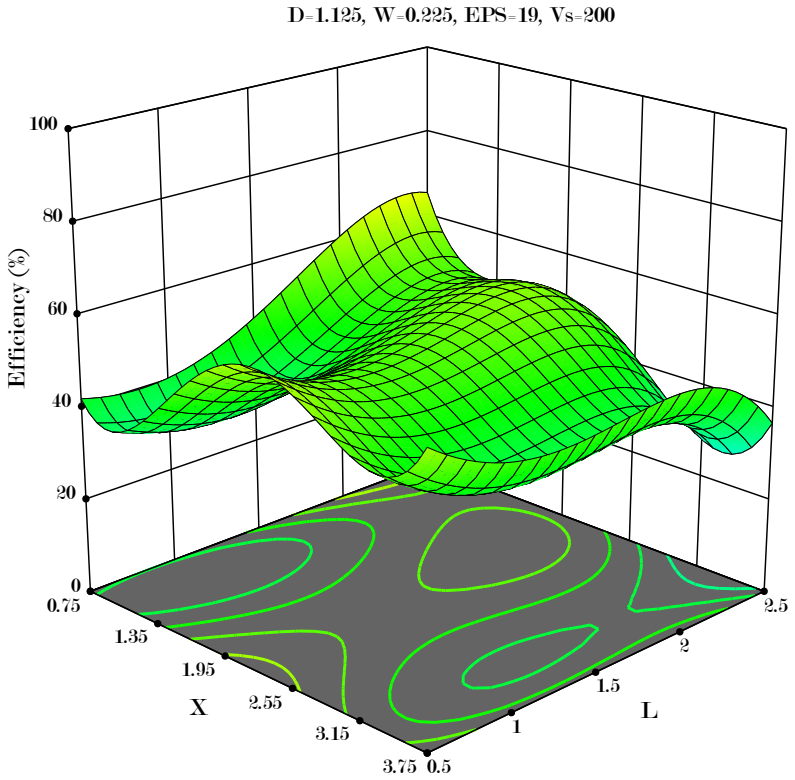


Figure 6.20: Interaction of X and L on the response of the trench

6.4.6. Interaction of three parameters on each other

The cube plot is presented for analysing the interaction of three parameters on each other since the ANOVA table represents that there is really strong interaction between some triple parameters like $X - D - L$ (location-depth-thickness of the first layer). Whereas the single parametric study shows that L does not have a significant influence on the efficiency of the trench.

Fig. 6.21 shows the interaction of the three parameters including $X - D - L$ while keeping constant the rest of parameters ($V_s = 300m/s$, $W = 1.125$, EPS $= 19$). Layer thickness (L) plays a significant role in decreasing the efficiency in the situation of shallow trench, when it is installed near the vibration source ($D = 0.5$, $X = 0.75$).

Evaluating the effect of D represents a considerable influence on the efficiency and the highest impact is related to increasing D from 0.5 to 1.75 for $L = 0.5$ and $X = 3.75$. The least increase in the efficiency (approximately 10%) happens for the largest thickness and nearest location ($L = 2.5$, $X = 0.75$). Increasing the distance between the vibration source and the trench has

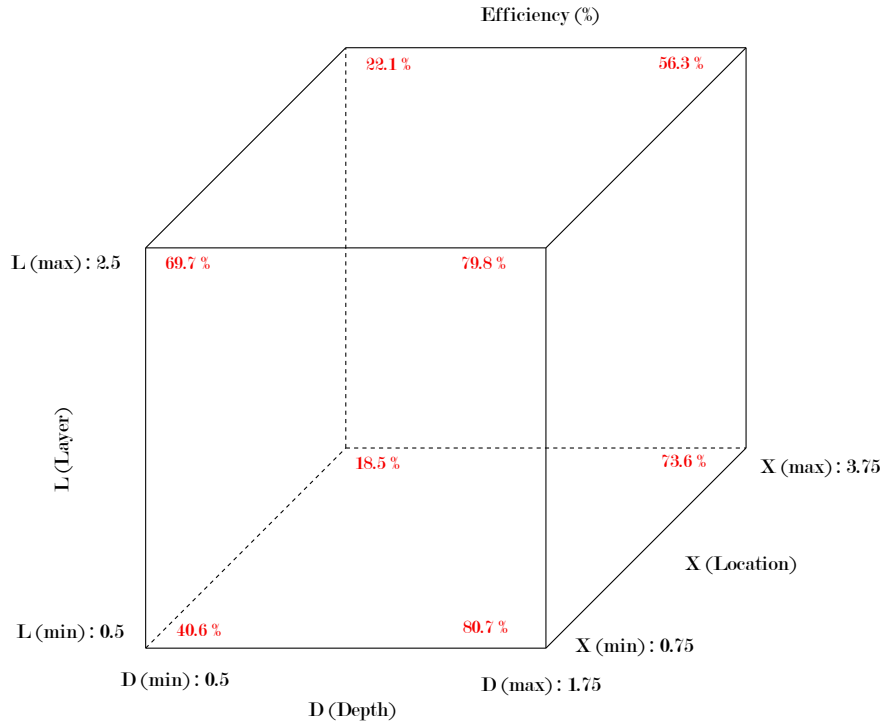


Figure 6.21: Interaction of X, D, and L on the efficiency of the trench

an inverse effect on the efficiency. The biggest and smallest impact of the location, which are 47% and 7%, respectively are related to the shallow trench with the highest thickness ($D = 0.5$, $L = 2.5$) and deep trench with the thin layer ($D = 1.75$, $L = 0.5$), respectively.

6.5. Conclusion

The conclusions drawn from the result of parametric study can be summarized as follows:

- The response of the layered soil increases in comparison with the homogeneous in terms of creating several peak and valleys in the normalized distance between $2 - 4$. It shows that the superposition of constructive and destructive interference of the waves in layered soil is high. This phenomena results in some irregular results in the trench's efficiency with having less practicability to mitigate the incoming waves.

- In layer soils, the depth of the trench compared to the layer thickness is a critical parameter that determines the behaviour of the system. It shows a significant non-linear behaviour when the soil layer is deeper than the trench, especially in the case of softer soils overlying stiffer soils. As the stiffness of the upper layer nears the bottom layer, these nonlinearities smooth out and the situation clearly resembles more of a homogeneous soil, as expected.

- In fact, the clearest trends appear on the influence of the shear wave velocity of the

overlying layer, where, in general, the efficiency of the trench increases for increasing shear wave velocities for all other parameters, except when $D < L$.

- Analyzing the influence of D on the screening effectiveness based on the single parametric study showed that barriers with $D >= 1$ and 1.25 is enough to have an optimum depth for near field system as long as $D > L$. For far field system, the results do not show any optimum depth and the screening effectiveness increases gradually and continuously with increasing D.

- Concerning the location, the highest attenuation of incoming waves is shown when installing the barrier near to the vibration source ($X = 0.75 - 2.25$) regardless of the thickness of the first layer and normalized depth. For softer soils when $X > 2.25$ the efficiency does not change whereas for the stiffer soils ($V_s > 250\ m/s$), the position of the trench is not greatly influential as long as $X < 2.25$.

- The developed polynomial quartic model for predicting the efficiency of the trench was compared with the result of numerical modelling and an accuracy of 83% has been obtained for predicting new data, which shows the practicability of the developed mathematical model.

- The result of interaction between all governing parameters demonstrated that the depth (D) and shear wave velocity of the soil (V_s) are the most important parameters. Considering the interaction of double parameters, $D - V_s$, $L - V_s$ and $X - D$ have the highest influence on the effectiveness of the efficiency of the trench. All of these points show that the vibration isolation topic is a non-linear problem and single parametric study of the trench is not sufficient for finding the impact of different factors.

7 Optimization and Prediction of the Trench in layered Soil

7.1. Implementation of genetic algorithm

This section deals with the optimization of various parameters in layered soil. The result of the parametric study in chapter 6 showed that there is considerable interaction between different parameters and the pattern of how the factors influence each other was completely unpredictable. Therefore, the developed genetic algorithm model in chapter 5 is used to optimize all parameters together in layered soil.

The selected parameters and their values for optimization are presented in table 7.1. The optimized parameters are include the dimensional features of the trench and the properties of the first layer to consider non-homogeneity of the soil. The literature review revealed that the efficiency of the trench is almost independent from the variations of the Poissons ratio of backfill material with respect to the surrounding soil. Therefore, the shear modulus of the first layer of the soil (G), which has a direct relationship with shear wave velocity (V_s) and density (ρ) is selected as a parameter to consider the non-homogeneity of the soil. The shear modulus of the soil is defined through Eq. (7.1).

$$G = (V_s)^2 \cdot \rho \tag{7.1}$$

Table 7.1: The selected parameters and their boundaries in the optimization process

Parameters	Minimum	Maximum
Location [gene (0)]	3 (m)	15 (m)
Depth [gene (1)]	2 (m)	7 (m)
Width [gene (2)]	0.3 (m)	1.5 (m)
Thickness of the first layer [gene (3)]	2 (m)	10 (m)
Shear modulus of the first layer [gene (4)]	81549.4 (kN/m^2)	326198 (kN/m^2)
Geofoam [gene (5)]	12 (kN/m^3)	29 (kN/m^3)

Since the dimensions of the barrier, as the input genes in the genetic algorithm code, is changeable, a function is used to calculate the efficiency of the geofoam-filled trench ($\overline{A}_r$) over a distance of $30m$ beyond the trench, which is defined in section (5.5.1). The main duty of this algorithm is optimizing the input parameters to reach the highest value of attenuation. Woods suggested that reaching 75% mitigation in scattering of incoming waves is enough to consider a vibration isolation system as a successful system. Therefore, a new minimizing function is

defined for the system to reach the efficiency of 75% [Woods, 1968]. In addition, it has been proved that the depth of the barrier plays a significant role in vibration isolation in comparison with other parameters to achieve an acceptable amount of efficiency. On the other hand, excavating a trench with a depth of 5 or $6m$ is sometimes difficult in reality. Therefore, the depth of the trench should be added to the minimizing function, too.

A multiobjective optimization is used for optimizing the value of A_r and the depth of the barrier simultaneously. The multiobjective optimization solves the optimization problem that possesses more than one objective parameter. Weight approach is used for assigning a weight to each objective in the minimizing function by introducing two new coefficients including γ and Δ. The weight interprets the emphasis of each object in comparison with other objects. The efficiency and depth of the trench are two objectives in the minimizing function. Since there are not any basic rules for calculating the weights, the value of coefficients $\gamma = 0.99$ and $\Delta = 0.01$ are selected based on several trade-off. The minimizing function is defined through Eq (7.2) to reach the requested efficiency, which is defined as 75% [Woods, 1968]. The coefficient A_r is the calculated efficiency of the geofoam-filled trench through Plaxis and the constant value of 0.75 is a restriction for reaching 75% of the mitigation, respectively. The duty of the developed genetic algorithm code is minimizing the defined function.

$$\text{Minimizing Function } = \gamma\big|A_r - 0.75\big| + \Delta \cdot Depth \tag{7.2}$$

7.1.1. Results

The developed genetic algorithm code is used to optimize the governing factors, which are presented in table 7.1 to reach 75% of the efficiency. The frequency of the applied load is $50Hz$. To consider the effect of non-homogeneity of the soil, the shear modulus of the first layer changes while the shear modulus of the second layer is considered constant, which is $326198kN/m^2$ (equal to $V_s = 400m/s$). One advantage of using coupl of finite element model (Plaxis) and Python programming language through Plaxis remote scripting interface is that the materials and the ranges of the parameters are changeable. This benefit is used to assess the effect of non-homogeneity of the soil on the governing parameters. Therefore, the genetic algorithm code is used to optimize the parameters in homogeneous and layered soil. For this purpose, the value of shear modulus in the second layer is considered to be the same amount as in the first layer. Hence, the shear modulus of the soil in the case of homogeneous soil is the value for the whole soil. The optimized parameters of layered soil are presented in table 7.2.

The most obvious difference between homogeneous and layered soil is in the parameters of depth and shear modulus of the soil, which are the most important factors in vibration isolation topic. This comparison represents that layered soil needs stiffer soil and a deeper trench. The location of the trench remains almost constant, which shows that this factor is independent of the homogeneity of the soil. Concerning the thickness of the first layer for layered soil, the best situation is installing the trench in the first layer.

Table 7.2: Optimized dimensions of the trench for different systems (geofoam, $50Hz$)

System	Location (m)	Depth (m)	Width (m)	Thickness of first layer (m)	Shear wave velocity (m/s)	Geofoam type
homogeneous	3.2	2.8	0.8	-	335	EPS15
layered	3.4	3.4	0.5	4.5	371	EPS19

As table 7.2 shows the value of shear wave velocity is obtained to be over $330m/s$ for both systems since the surface waves decay faster in stiffer soils in comparison with softer soils. However, the most critical situation is having a soft soil above a stiffer soil. Hence, the same GA model is implemented for both systems by changing the range of shear modulus between $81550-183500$ ($V_s = 200-300m/s$). The optimized parameters of the new models are presented in table 7.3.

Table 7.3: Optimized dimensions of the trench for different systems (geofoam, $50Hz$)

System	Location (m)	Depth (m)	Width (m)	Thickness of first layer (m)	Shear wave velocity (m/s)	Geofoam type
Homogeneous	7.4	3.0	0.8	-	278	EPS22
layered	7.4	4.6	0.6	7.5	292	EPS19

The comparison of the parameters between homogeneous and layered soils for the new models follow approximately the same pattern like table 7.2. The depth of the trench and shear modulus of the soil in layered soil are still bigger in comparison with homogeneous soil. Concerning the thickness of the first layer, we need a thicker layer when facing a softer soil since by decreasing the range of the shear wave velocity from $200 - 400m/s$ to $200 - 300m/s$, the thickness of the first layer increases. The reason of this change can be explained as follows:

Seismic waves decay faster in stiffer soils in comparison with softer soils. This means that stiffer soils have greater strength against vibration, and therefore they need less thickness in comparison with softer soils. With the same statement for a softer soil, it can be concluded that softer soils need thicker layers to reach the same value of efficiency like as stiffer soils.

In order to better understand the effect of the frequency, the developed genetic algorithm is used for different frequencies in the range of $(10 - 60Hz)$ for both homogeneous and layered soils. The results are presented in table 7.4. The calculated efficiency based on the optimized parameters is presented in a table since for some frequencies the model could not reach 75% efficiency.

The results show that a rectangle geofoam-filled trench is not able to reach the restriction (75%) due to the external load for low frequency (f = $10Hz$). This means that the restricted value of efficiency should increase for low frequencies. However, the system is more practical for external loads with a frequency above $20Hz$. It is worth reminding that a tried has been done to keep the depth of the trench as shallow as possible and the minimizing function in Eq.

7.2 is includes optimizing efficiency and depth simultaneously. This is another reason for not being able to reach a higher efficiency for low frequencies ($f \leq 10Hz$).

Table 7.4: Optimized dimensions of the trench for different frequencies

Frequency (Hz)	System	Location (m)	Depth (m)	Width (m)	Thickness of first layer (m)	Shear wave velocity (m/s)	Geofoam type	Efficiency (%)
10	Homogeneous	4.7	4.8	0.5	-	372	EPS22	65
10	layered	4.2	5.0	0.5	3.9	285	EPS15	60
20	Homogeneous	6.0	4.6	0.6	-	317	EPS19	70
20	layered	7.6	4.9	0.7	5.3	386	EPS19	65
30	Homogeneous	6.9	4.2	0.7	-	310	EPS19	73
30	layered	7.0	4.7	0.6	8.0	314	EPS19	74
40	Homogeneous	5.2	3.8	0.7	-	373	EPS19	72
40	layered	4.3	4.1	0.5	6.1	350	EPS22	73
60	Homogeneous	5.5	2.8	0.4	-	347	EPS29	74
60	layered	4.4	3.0	0.6	7.8	347	EPS19	73

Concerning the location of the trench, the range of almost all frequencies are between $4 - 7m$. Therefore, this range can be considered to be a trusted location for installing a trench in both homogeneous and layered soil, respectively. The result of the optimized thickness of the first layer shows that increasing frequency of the vibration source results in increasing the thickness of the first layer. The reason for receiving some irregular patterns for some parameters is that the number of input parameters in layered soil is more than for homogeneous soil. In comparison with homogeneous soil, for which the depth of the trench is the most effective parameter, in layered soil, the depth of the trench, shear wave velocity, and thickness are important, too.

The range of an effective width with one exception (frequency of $60Hz$ in homogenous soil)can be considered between $0.5 - 0.7m$ as to be optimum. However, it shows that the least width of the trench should be wider than $0.5m$ whereas the width of the barrier is considered mostly around $0.3m$ in most of the past experimental and numerical studies. Several published studies have shown that the materials with the lowest density result in the highest attenuation of the incoming waves. However, a mutual parametric study through a genetic algorithm does not select the lowest density (EPS12) for the geofoam as the optimized density. As it can be seen, EPS19 is selected for most frequencies. Therefore, the results of the single parametric study are sometimes different from the mutual parametric study.

7.1.2. Implementing feedforward neural network

A multilayered feedforward neural network with the back-propagation training method is developed to predict the efficiency of the geofoam-filled trench. The feedforward network is used for supervised learning tasks with the results of the parametric study in section 6.3. The main goal of the developed ANN in this study is to approximate a regression function to predict the efficiency of the geofoam-filled trench.

The architecture of the network is includes input, output and two hidden layers with 6, 10, 15 and one neuron, respectively. The optimum number of neurons in each hidden layer is selected based on trial and error. The structure of the network represents the full connection of any nodes in one layer to all other nodes in the next layer and the information only moves forward into the network, from the input to the hidden layers and finally to the output node. The input layer receives the features, which govern the parameters in the vibration isolation topic and the output is corresponded to predict the efficiency of the barrier based on the input layer.

The database includes $18,750$ data points from the parametric study as a result of changing key parameters in the vibration isolation topic. The efficiency of the geofoam-filled barrier is presented as a percentage, which is the average of the ratio of vertical velocity of the soil after and before installing the trench, respectively through Eq. (7.3).

$$\text{Efficiency} = (1 - \overline{A}_r) * 100 \tag{7.3}$$

Table 7.5 presents the governing factors and the ranges.

Table 7.5: Governing factors and the ranges in ANN

Feature	Min	Max
Location (X)	3 (m)	15 (m)
Depth (D)	2 (m)	7 (m)
Width (W)	0.3 (m)	1.5 (m)
Thickness of first layer (L)	2 (m)	10 (m)
Geofoam type (EPS)	EPS12	EPS29
Shear wave velocity (Vs)	200 (m/s)	400 (m/s)

There is a full connection between all neurons and each connection between two nodes has a weight, which is assigned to the connection randomly. The weight shows the strength of the connection between two nodes. When the network receives a value for one feature in the input layer, this value is passed to the next node via a connection, and the value will be multiplied by the weight assigned to that connection. Thereafter, a weighted sum for all incoming connections is computed and this sum, after adding the value of bias, is passed to an activation function. The process is represented in Eq. (7.4).

$$Y = Activation\left(\sum(weight * inputs) + bias\right) \tag{7.4}$$

The activation function transfers the inputs to their corresponding output, which is between lower and upper limits. Since the vibration isolation topic is a non-linear problem, sigmoid

function, which is a non-linear activation function, is used for the developed ANN. The principal of Sigmoid function is explained in chapter 3.

Backpropagation algorithm is one of the best supervised learning algorithms for a multilayer feedforward neural network. The backpropagation with Levenberg-Marquardt algorithm, which is explained in 3.4.1, is selected to update the weights and biases values of the developed ANN.

The learning error is calculated through Eq. (7.5).

$$Error = \frac{1}{2}\sum(t_i - \sigma_i)^2 \tag{7.5}$$

where t_i is the calculated efficiency of the trench through FEM and σ_i is the predicted value by a feedforward neural network. In the whole process of training the neural network, the error between predicted and actual value of the efficiency of the trench is measured and used to update the weights and biases of all neurons through the LM algorithm. The architecture of the developed ANN is presented in Fig. 7.1. Several networks with different numbers of hidden layers and neurons are trained in order to optimize the number of hidden layers and neurons in each layer. The main criteria for optimizing the results is minimizing the mean squared error and to prevent under-fitting (with large training and validation errors) and over-fitting (a low training error but a high validation error). Finally, a model with two hidden layers with 10 and 15 neurons, respectively, is selected to predict the efficiency of the geofoam-filled barrier.

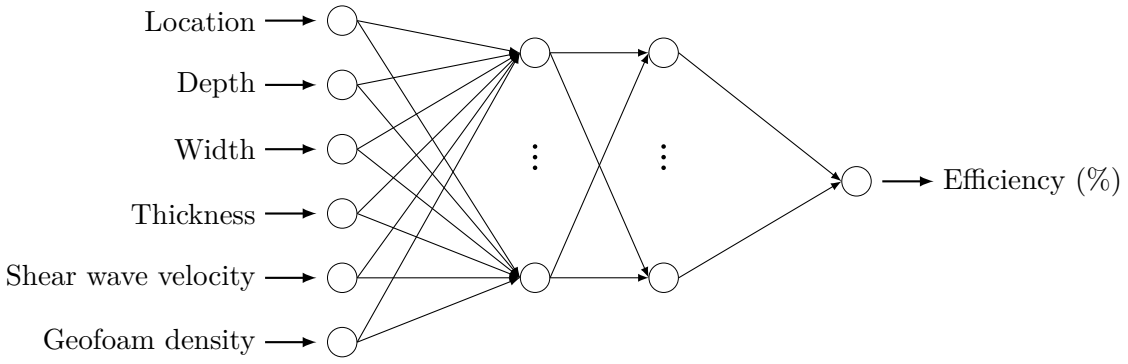


Figure 7.1: The architecture of developed ANN

7.1.3. Results

The developed network is used to predict the efficiency of the geofoam-filled trench using six input variables. Approximately 13000 data are used to train the network and the rest of data are employed to test the model. The magnitude of the gradient, the number of validation checks and epochs are used to terminate the training. The values for these criteria are selected as $1e^{-}7$, 6 and 1000, respectively. The number of validation checks shows the number of successive epochs, in which validation performance fails continuously for more than six epochs. The developed network is terminated by reaching the maximum number of validation checks. The performance of the network in training, validation and test datasets is presented in Fig.

7.2. The best validation performance occurs at epoch 60 and the training continued for more 6 iterations before the training stopped. The results show that the training, validation and test curves decay in a similar way. Since there is no unexpected increase in the result of the test curve, it can be concluded that over-fitting does not occur in the network.

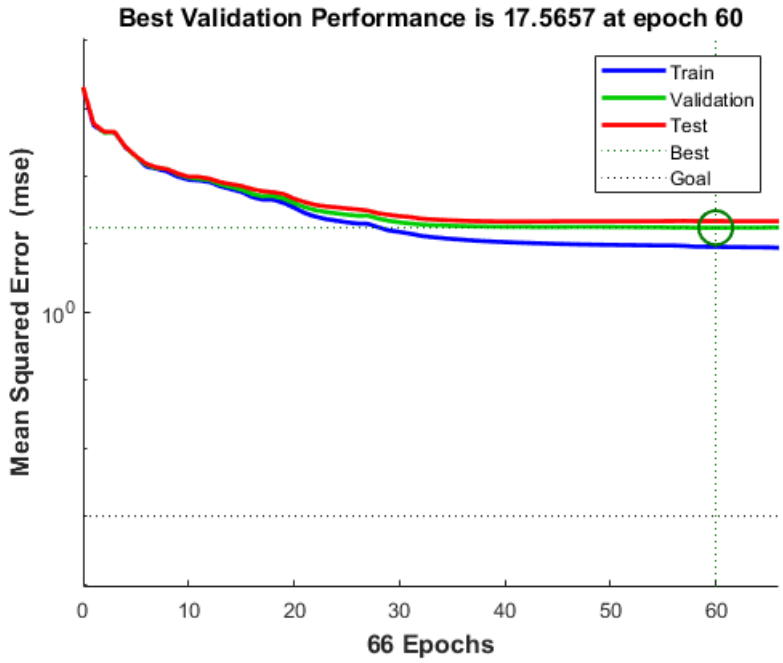


Figure 7.2: Performance of the network for training, validation and test datasets

Creating a regression plot, which shows the relationship between the outputs of the network and the target is another procedure for validating the model. The extracted outputs and targets of all the data are plotted in Fig. 7.3, and the results represent a proper fit. The figure includes a dashed line, which represents the perfect result, (output=target) and a solid line, which is the best fit linear regression line between the output and the target. The regression R-value=0.98 for a total response based on the whole datasets indicates an acceptable performance for the developed network. Most of the points are located on the fitted line and some points are located under and above the fitted line. The computed R-value shows the capability of the network to give a reasonable prediction of the efficiency with a success rate of 98.1%.

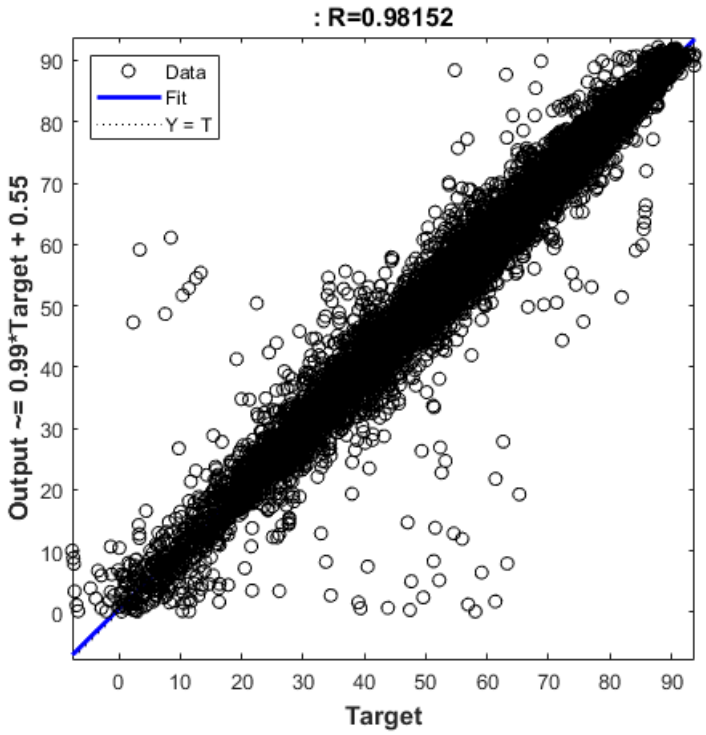


Figure 7.3: Extracted outputs and targets of all the data

To evaluate the prediction capability of the developed network, another linear regression analysis is conducted on the network for three subsets including training, validation and testing data, and the results are presented in the Fig. 7.4. The corresponding coefficient of determination (R^2) for all training, validation, and data testing, which are 0.988, 0, 977 and 0.972, respectively demonstrates acceptable agreement between predicted and actual values of the efficiency of the trench.

Finally, the computed coefficients for assessing the performance of the network in training, validating and testing data are presented in table 7.6. The values of MSE and correlation coefficients for all the data represent that the model predicts the efficiency well.

Table 7.6: Performance of the network for in training, validating and test data

Dataset	R-square	Correlation coefficient	MSE	RMSE
Training test	0.96	0.98	14.47	3.8
Testing test	0.95	0.97	16.61	4.076

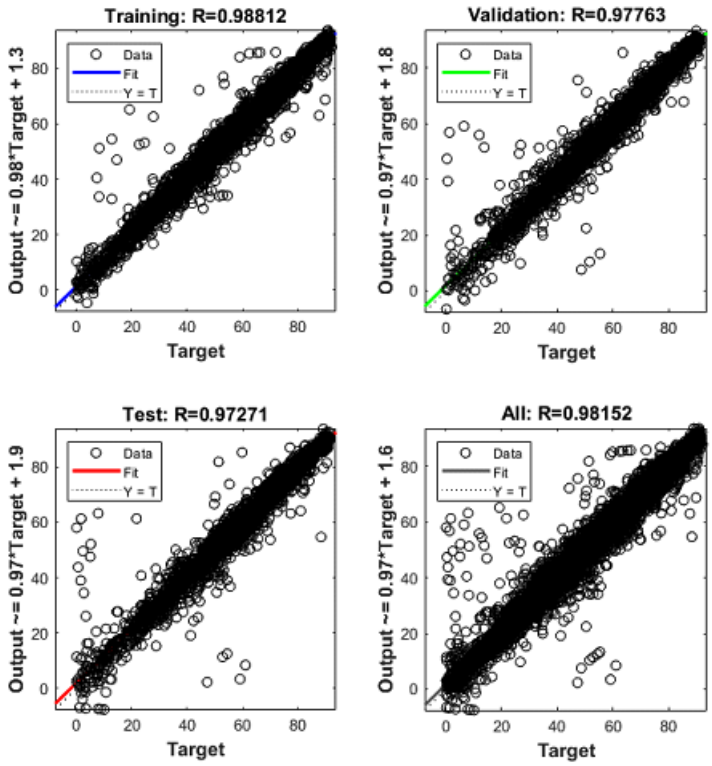


Figure 7.4: Results of subsets including training, validation and testing data

7.1.4. Validating ANN model

In order to demonstrate the capability of the developed network for predicting the efficiency of the geofoam-filled trench, 100 new data with completely new parameters of the trench, which are different from the training and test data for the ANN are analysed through the finite element model (Plaxis), and the results are compared to the predicted value by the trained ANN model. The R-value coefficient is used to compare the predicted and the real value of the efficiency. Fig. 7.5 represents the calculated R-value for the validation data, which is 0.86, and this value indicates an acceptable performance of the ANN model.

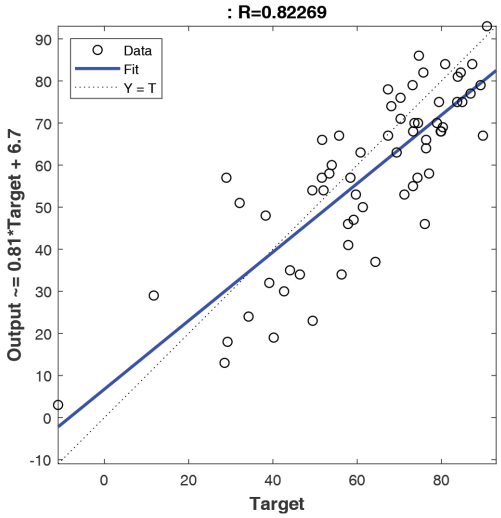


Figure 7.5: Calculated R-value for the validation data

Fig. 7.6 shows the predicted and real value of the efficiency with different parameters of the trench. The result represents that the predicted value by the ANN model follows almost the same pattern like as the real value. In addition, the MSE and RSME coefficients are calculated through measuring the value of error.

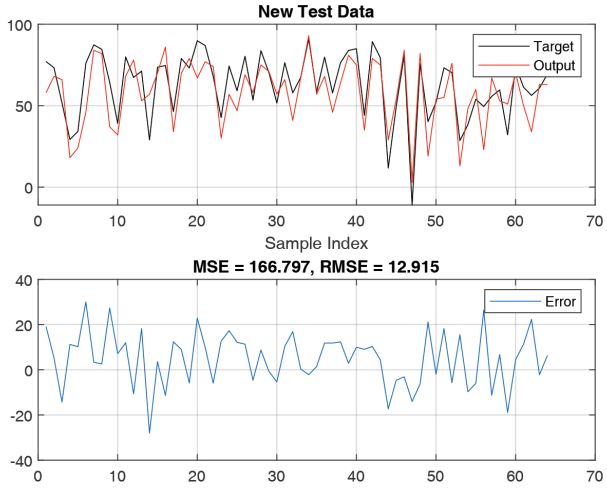


Figure 7.6: Predicted and real value of the efficiency of geofoam-filled trench

The comparison of the results shows acceptable agreement between the predicted and real value of the efficiency, and it shows that the developed ANN model can successfully predict the efficiency of the geofoam-filled barrier in a layered soil based on the new parameters.

7.2. Conclusion

Based on the results, the following conclusion can be drawn:

- The optimization results illustrated that layered soil requires stiffer soil and a deeper trench in comparison with homogeneous soil to reach the same value of efficiency. The location and width of the trench and the geofoam type for filling the trench are independent of the homogeneity of the soil.

- The optimization results for different frequencies revealed that the location between $4-7m$ seems to be the best location for all frequencies. The thinnest width of the trench should be $0.5m$, and the range of $0.5-0.8m$ seems enough for having a successful system. Finally, EPS19 is selected as the best material for filling the trench.

- The training of the artificial neural network showed a high capability to predict the efficiency of the geofoam-filled trench accurately. The regression R-value= 0.98 for a total response based on the whole datasets indicates an excellent performance for the developed network. The computed R-value shows the capability of the network in providing a reasonable prediction of the efficiency with a success rate of 98.1%.

- The developed model is also validated with 100 new data with completely new parameters, which were anaylsed through the finite element model, and the results showed an accuracy of 86% for predicting new data, which is an acceptable performance.

- The developed models can be used as a preliminary design tool to predict the efficiency of a trench based on the existing dimensions without doing any calculations.

8 Summary, conclusions, and recommendations

8.1. Summary and conclusion

A large number of numerical and experimental investigations has been performed in the past few decades to study vibration isolation systems through installing a trench and to improve the understanding of wave attenuation phenomenon. Most of these studies focused on rectangular trenches. On the other hand, few researchers have studied the use of expanded polystyrene (EPS) geofoam material as soft barriers.

Most of the parametric studies in vibration isolation topic have examined the efficiency of barriers based on the single parametric studies. Therefore, a lack of mutual influence of all parameters is still observed. The most important problem in vibration isolation is that it is not possible to treat each parameter as an independent variable.

Investigations on vibration isolation problem are usually done based on the ideal situation of an homogeneous half-space, which is not realistic. In nature, however, the shear modulus of the soil usually changes with depth while the mass density and other properties of the soil can be regarded as approximately as constant value. Since dynamic properties and non-homogeneity of the soil play a significant role in transferring dynamic energy, a comprehensive parametric study is necessary to evaluate governing parameters in layered soil.

Theoretical analysis, numerical simulation, and field experiment are usually used to predict the efficiency of a barrier in attenuating incoming waves. Although these methods can predict vibration with high accuracy, complexity of the models, long calculation time, and inconvenience in practical application are their drawbacks. Therefore, developing a new prediction method which offers high accuracy and spends little time to predict can be really beneficial in this topic.

This dissertation attempts to fill these gaps regarding vibration isolation systems by providing a series of fundamental investigations and numerical modelling on the feasibility of a geofoam-filled trench. In addition, several extra models are developed in this study to better understand the performance of geofoam-filled trenches.

The following understanding and conclusions can be offered based on the results in the previous chapters.

The parametric study performed to evaluate the efficiency of the trench in homogeneous soil based on different configurations offers the following:

- Near field isolation can be a better solution for hindering incident waves in comparison with far field isolation based on the results of the field tests. However, the results also show that the first point after the trench has the highest amount of mitigation, and normalized depth of $0.6\lambda_r$ is enough to reach a high value of efficiency for both near field

and far field isolation systems.

- The parametric study of near field and far field isolations show the zone of $7\lambda_r$ and $10\lambda_r$ to be crucial zones for an area after the trench to compute $\overline{A}_r$. This finding proves that vibration isolation systems should be divided into near field and far field systems during analysis.

- Analysing the result of the near field scheme demonstrated that the optimum length can be considered to be $2.5\lambda_r$ for all three wall-systems in order to reach the highest value of efficiency. The depths of $1\lambda_r$ is considered to be the optimum depths for the single, double and triangular wall systems, respectively. Concerning the effect of the width of a geofoam-filled trench, it can be concluded that the value of $W = 0.25$ is enough to consider the optimum W for single, double, and triangular wall systems, respectively. In addition, the comparison of all systems revealed that double wall can be selected as the best system for both narrow and wide barriers.

- On the other hand, evaluation of the far field isolation revealed that the depth of the barrier hardly affects the efficiency of the obstacle for single and double wall systems while D is a key factor in scattering incoming waves for a rectangular wall system. However, an optimum depth cannot be selected for this system as the efficiency of the obstacle increases gradually and continuously by increasing D. The comparison of all three systems showed that double wall systems are the most effective for narrow and wide trenches, respectively.

- The optimum width for far field system can still be considered as W = 0.25 to achieve greater efficiency with the single and double wall systems. The barrier's width has a negligible effect on the scattering of dispatched waves for a triangular wall system. In addition, the parametric study of the trench location for both near field and far field schemes demonstrated that this factor is not an important parameter that influences the efficiency of a geofoam-filled trench.

- Concerning stiff barriers, a normalized reduction zone of 5 beyond the trench is considered to calculate $\overline{A}_r$, which shows that reduction zone is a key factor in calculating efficiency of a trench. There is no optimum D for single and triangular systems since efficiency increases continuously with increasing the depth while D hardly affects on $\overline{A}_r$ for double wall systems. The normalized width is an important parameter just for double systems and the value of 0.25 is considered to be the optimum value. However, for single and triangular systems, it either does not affect or has a complicated influence on $\overline{A}_r$, respectively.

A new coupled model of $GA - FEM$ is developed for mutual optimization of the governing parameters of vibration isolation for near field and far field systems, considering all three different wall-systems. The most important results based on the developed model are summarized as follows:

- The parametric study of the single wall trench show that the shape of a geofoam-filled trench is one of the most important factors in evaluating the efficiency of the trench.

- The result of the optimization of near field isolation for geofoam-filled trenches for the frequency of $50Hz$ demonstrated that a depth of $3m$ is enough for all systems, but for the rest of the parameters, performing a mutual optimization is needed. A comparison between soft and stiff barriers show that changing the material of the trench from geofoam to concrete leads to a deeper trench to reach an acceptable amount of efficiency for all the three systems. The frequency analysis yields that a single wall system is the best solution for mitigating incoming waves.

- The same study has been performed for far field isolation for soft and stiff barriers, and the results of the soft trench showed that single wall system needs the lowest depth and width, which are 2.8 and $0.5m$, respectively. The optimized parameters of the stiff trench demonstrated that the depth of the trench is independent of on the shape of the trenches, while there is not any change in the depth of the trench for different systems. Another important point of the results is that the efficiency of the stiff barrier is independent of the trench shape since all the systems have approximately the same dimensions and cross-sectional area. However, in terms of depth of the trench, a stiff barrier still needs a deeper trench in comparison with the a soft barrier.

- Finally, the comparison of the near field and far field geofoam-filled barriers represents that near field isolation is more suitable for lower frequencies in comparison with far field isolation. From what has been discussed above, it is concluded that the mutual influence of all the parameters is a useful tool for computing the efficiency of a successful trench, since it is apparent that all the parameters can be effective in the wave attenuation process when analysing the different parameters together. The developed genetic algorithm code can be used as a reference for engineering applications in vibration isolation problem.

A comprehensive parametric study has been performed to evaluate the efficiency of the geofoam-filled trench in layered soil using Plaxis, Python and a Matlab program. The results of the single parametric study show that different parameters have an impact on each other. Therefore, a statistical model through Response Surface Methodology (RSM) has been developed to find the interaction between the governing parameters. The conclusions drawn from the result of the parametric study can be summarized as follows:

- The response of the layered soil increases in comparison with the homogeneous in terms of creating several peak and valleys in the normalized distance between $2 - 4$. It shows that the superposition of constructive and destructive interference of the waves in layered soil is high. This phenomena results in some irregular results in the trench's efficiency with having less practicability to mitigate the incoming waves.

- In layer soils, the depth of the trench compared to the layer thickness is a critical parameter that determines the behaviour of the system. It shows a significant non-linear behaviour when the soil layer is deeper than the trench, especially in the case of softer soils overlying stiffer soils. As the stiffness of the upper layer nears the bottom layer, these nonlinearities smooth out and the situation clearly resembles more of a homogeneous soil, as expected.

- In fact, the clearest trends appear on the influence of the shear wave velocity of the overlying layer, where, in general, the efficiency of the trench increases for increasing shear wave velocities for all other parameters, except when $D < L$.

- Analyzing the influence of D on the screening effectiveness based on the single parametric study showed that barriers with $D >= 1$ and 1.25 is enough to have an optimum depth for near field system as long as $D > L$. For far field system, the results do not show any optimum depth and the screening effectiveness increases gradually and continuously with increasing D.

- Concerning the location, the highest attenuation of incoming waves is shown when installing the barrier near to the vibration source ($X = 0.75 - 2.25$) regardless of the thickness of the first layer and normalized depth. For softer soils when $X > 2.25$ the efficiency does not change whereas for the stiffer soils ($V_s > 250\ m/s$), the position of the trench is not greatly influential as long as $X < 2.25$.

- The developed polynomial quartic model for predicting the efficiency of the trench was compared with the result of numerical modelling and an accuracy of 83% has been obtained for predicting new data, which shows the practicability of the developed mathematical model.

- The result of interaction between all governing parameters demonstrated that the depth (D) and shear wave velocity of the soil (V_s) are the most important parameters. Considering the interaction of double parameters, $D - V_s$, $L - V_s$ and $X - D$ have the highest influence on the effectiveness of the efficiency of the trench. All of these points show that the vibration isolation topic is a non-linear problem and single parametric study of the trench is not sufficient for finding the impact of different factors.

A genetic algorithm model through coupling Plaxis-Python programs has been developed to optimize all the parameters mutually in homogeneous and layered soil. In addition, a multilayered feed-forward neural network with back-propagation training model has also been developed in order to estimate the efficiency of the geofoam-field barriers. Based on the results, the following conclusions can be drawn:

- The optimization results illustrate that layered soil requires a stiffer soil and a deeper trench in comparison with homogeneous soil to reach the same value of efficiency. The location and width of the trench and the geofoam type for filling the trench are independent of the homogeneity of the soil.

- The optimization results for different frequencies reveal that the location between $4 - 7m$ seems to be the best location for all frequencies. The narrowest width of the trench should be $0.5m$ and the range of $0.5 - 0.8m$ seems enough to have a successful system. Concerning the thickness of the first layer, the results show that increasing frequency of the vibration source results in increasing the thickness of the first layer of the soil. Finally, EPS19 is selected as the best material for filling the trench.

- The developed artificial neural network model shows high great capability to predict the efficiency of a geofoam-filled trench accurately. The regression R-value= 0.98 for a total response based on the whole datasets indicates an excellent performance of the developed network. The computed R-value shows the capability of the network to give a reasonable prediction of efficiency with a success rate of 98.1%.
- The developed model is also validated with 100 new data with completely new parameters, which were anaylsed through a finite element model, and the results show an accuracy of 86% for predicting new data, which is an acceptable performance.
- The developed models can be used as a preliminary design tool to predict the efficiency a trench based on the existing dimensions without doing any calculations.

Finally, an application has been developed to access all developed models and data. The user can install the app and use it to access all data, predicting the efficiency of the trench and optimizing the governing parameters.

- The most important feature of the app is the easy use of all sections without having any base knowledge of the artificial neural networks or genetic algorithms. In addition, the app is open to be upgraded in terms of the data and improvement in the developed models.
- A couple of genetic algorithm-artificial neural network models are implemented in order to replace the finite element model as a fitness function.

8.2. Recommendations for future work

Further work to complete the current level of research on vibration isolation by installing a trench is suggested.

- The shape analysis of the trench reveal that soft barriers are shape-dependent. Further explorations need to be conducted for other materials like lightweight expanded clay aggregate (LECA) or expanded clay (exclay), which is a lightweight aggregate made by heating clay. LECA is also used to make lightweight concrete products. This can be done by conducting a full experimental test.
- A moving load as an external vibration source (like a train) needs to be studied. The mutual study of the system shows that the optimized parameters are frequency dependent. Therefore, is it suggested to do the same parametric study with different frequencies since the main frequency of this study was $50Hz$.
- There is a big potential to develop the presented app by adding some more results or developing some extra models for prediction or optimization.

9 Bibliography

Abu-Naser, S. S., **Dawoud, A. M.**, **and Al Sheik Ali, K. M.(2016)**. Design and development of mobile university student guide. journal of multidisciplinary engineering science studies. JMESS, 5(1):193–197.

Adhikari, S.(2016). Development and optimization of Dextromethorphan HBr-2-Hydroxy propyl ß-cyclodextrin inclusion complex based orally disintegrating tablets using response surface methodology. PhD thesis, University of Toledo.

Ahmad, S. and Al-Hussaini, T.(1991). Simplified design for vibration screening by open and in-filled trenches. Journal of geotechnical engineering, 117(1):67–88.

Al-Hussaini, T. M.(1993). Vibration isolation by wave barriers. PhD thesis, State University of New York at Buffalo.

Alzawi, A. and El Naggar, M. H.(2011). Full scale experimental study on vibration scattering using open and in-filled (geofoam) wave barriers. Soil Dynamics and Earthquake Engineering, 31(3):306–317.

Alzawi, A. M. A.(2011). Vibration isolation using in-filled geofoam trench barriers. PhD thesis, The University of Western Ontario.

Amir Rezaei, R. R. D.(2018). Optimally located wave barriers for reducing horizontal vibrations induced by earthquake. In 16TH Europian Conference on Earthquake Thessaloniki Engineering.

Andersen, L. and Nielsen, S. R.(2005). Reduction of ground vibration by means of barriers or soil improvement along a railway track. Soil Dynamics and Earthquake Engineering, 25(7-10):701–716.

Athanasopoulos, G., **Pelekis, P.**, **and Anagnostopoulos, G.(2000)**. Effect of soil stiffness in the attenuation of rayleigh-wave motions from field measurements. Soil Dynamics and Earthquake Engineering, 19(4):277–288.

Bahrekazemi, M.(2004). Train-induced ground vibration and its prediction. PhD thesis, Byggvetenskap.

Baidya, D. and Krishna, G. M.(2001). Investigation of resonant frequency and amplitude of vibrating footing resting on a layered soil system. Geotechnical Testing Journal, 24(4):409–417.

Baş, D. and Boyacı, I. H.(2007). Modeling and optimization i: Usability of response surface methodology. Journal of food engineering, 78(3):836–845.

Baziar, M. H., **Kazemi, M.**, **and Shahnazari, H.(2019)**. Mitigation of ground vibrations induced by high speed railways using double geofoam barriers: Centrifuge modeling. Geotextiles and Geomembranes, 47(6):712–728.

Ben-Menahem, A. and Singh, S. J.(2012). Seismic waves and sources. Springer Science & Business Media, .

Beskos, D., **Dasgupta, B.**, **and Vardoulakis, I.(1986)**. Vibration isolation using open or filled trenches. Computational mechanics, 1(1):43–63.

Beskos, D. E.(1987). Boundary element methods in dynamic analysis. Applied Mechanics Reviews, 40(1):1–23.

Bo, Q., **Ali, L.**, **and Irini, D.-M.(2014)**. Numerical study of wave barrier and its optimization design. Finite Elements in Analysis and Design, 84:1–13.

Brinkgreve, R., **Swolfs, W.**, **and Engine, E.(2020)**. Plaxis users manual. Balkema, Rotterdam (The Neetherlands).

Çelebi, E., **Fırat, S.**, **Beyhan, G.**, **Çankaya, İ.**, **Vural, İ.**, **and Kırtel, O.(2009)**. Field experiments on wave propagation and vibration isolation by using wave barriers. Soil dynamics and earthquake engineering, 29(5):824–833.

Choobbasti, A., **Farrokhzad, F.**, **and Barari, A.(2009)**. Prediction of slope stability using artificial neural network (case study: Noabad, mazandaran, iran). Arabian journal of geosciences, 2(4):311–319.

D6817-13, A.(2013). Standard specification for rigid cellular polystyrene geofoam. ASTM.

Darwin, C.(1964). On the origin of species: A facsimile of the first edition. Harvard University Press, .

Das, B. M. and Luo, Z.(2016). Principles of soil dynamics. Cengage Learning, .

Das, S. K. and Basudhar, P. K.(2006). Undrained lateral load capacity of piles in clay using artificial neural network. Computers and Geotechnics, 33(8):454–459.

De Vos, P.(2017). Railway induced vibration: state-of-the-art report. Paris: UIC International Union of Railways.

Developers, G.(2017). Basics of wave propagation. https://gpg.geosci.xyz/content/seismic/wave_basics.html.

Dijckmans, A., **Ekblad, A.**, **Smekal, A.**, **Degrande, G.**, **and Lombaert, G.(2016)**. Efficacy of a sheet pile wall as a wave barrier for railway induced ground vibration. Soil Dynamics and Earthquake Engineering, 84:55–69.

Dolling, H.-J.(1970). Abschirming von erschitterungen durch bodenschlitze. Die Bautecnic, 5:151–158.

E Richart, F.(1970). Vibrations of soils and foundations. Book, Printed in the United States of America, .

Eddine, A. K. J.(2017). Sources of vibrations and their impact on the environnement. PhD thesis.

Ekanayake, S. D., **Liyanapathirana, D.**, **and Leo, C. J.(2014)**. Attenuation of ground vibrations using in-filled wave barriers. Soil Dynamics and Earthquake Engineering, 67:290–300.

Esmaeili, M., **Zakeri, J. A.**, **and Mosayebi, S. A.(2014)**. Investigating the optimized open v-shaped trench performance in reduction of train-induced ground vibrations. International Journal of Geomechanics, 14(3):04014004.

Fang, L., **Yao, J.**, **and Xia, H.(2019)**. Prediction on soil-ground vibration induced by high-speed moving train based on artificial neural network model. Advances in Mechanical Engineering, 11(5):1687814019847290.

Farrokhzad, F., **Choobbasti, A.**, **and Barari, A.(2012)**. Liquefaction microzonation of babol city using artificial neural network. Journal of King Saud University-Science, 24(1):89–100.

Farshi Homayoun Rooz, A. and Hamidi, A.(2017). Numerical analysis of factors affecting ground vibrations due to continuous impact pile driving. International Journal of Geomechanics, 17(12):04017107.

Gao, G., **Zhang, Q.**, **Chen, J.**, **and Chen, Q.(2018)**. Field experiments and numerical analysis on the ground vibration isolation of wave impeding block under horizontal and rocking coupled excitations. Soil Dynamics and Earthquake Engineering, 115:507–512.

Garinei, A., **Risitano, G.**, **and Scappaticci, L.(2014)**. Experimental evaluation of the efficiency of trenches for the mitigation of train-induced vibrations. Transportation Research Part D: Transport and Environment, 32:303–315.

Gavin, K. and Xue, J.(2009). Use of a genetic algorithm to perform reliability analysis of unsaturated soil slopes. Géotechnique, 59(6):545–549.

Ghaleini, E. N., **Koopialipoor, M.**, **Momenzadeh, M.**, **Sarafraz, M. E.**, **Mohamad, E. T.**, **and Gordan, B.(2019)**. A combination of artificial bee colony and neural network for approximating the safety factor of retaining walls. Engineering with Computers, 35(2):647–658.

Gurney, K.(1997). An introduction to neural networks. Book, CRC press, University of Sheffield, .

Hansheng, L. and Lishan, K.(1999). Balance between exploration and exploitation in genetic search. Wuhan University Journal of Natural Sciences, 4(1):28–32.

Hao, H., **Ang, T.**, **and Shen, J.(2001)**. Building vibration to traffic-induced ground motion. Building and environment, 36(3):321–336.

Haupt, W.(1977). Isolation of vibrations by concrete core walls. In Proceedings of the ninth international conference on soil mechanics and foundation engineering, volume 2, pages 251–256.

Haupt, W.(1995a). Wave propagation in the ground and isolation measures. International Conferences on Recent Advances in Geotechnical Earthquake Engineering and Soil Dynamics, 2:985–1016.

Haupt, W.(1995b). Wave propagation in the ground and isolation measures. University of Missouri–Rolla.

Horvath, J. S.(1995). Geofoam geosynthetic. National Academy of Sciences.

Hung, C.-C. and Ni, S.-H.(2007). Using multiple neural networks to estimate the screening effect of surface waves by in-filled trenches. Computers and Geotechnics, 34(5):397–409.

Iodice, M.(2017). Road and soil dynamic characterization from surface measurements. PhD thesis, University of Southampton.

Jaluria, Y.(2019). Design and Optimization of Thermal Systems: with MATLAB Applications. CRC press, .

Jayawardana, P., **Thambiratnam, D. P.**, **Perera, N.**, **Chan, T.**, **and De Silva, G. S.(2019)**. Use of artificial neural network to evaluate the vibration mitigation performance of geofoam-filled trenches. Soils and Foundations, 59(4):874–887.

Kalevo, M.(2019). Building a graphical user interface with matlab. Metropolia University of Applied Sciences.

Kattis, S., **Polyzos, D.**, **and Beskos, D.(1999)**. Modelling of pile wave barriers by effective trenches and their screening effectiveness. Soil Dynamics and Earthquake Engineering, 18(1):1–10.

Khuri, A. I. and Mukhopadhyay, S.(2010). Response surface methodology. Wiley Interdisciplinary Reviews: Computational Statistics, 2(2):128–149.

Kim, P.(2017). Matlab deep learning. With Machine Learning, Neural Networks and Artificial Intelligence, 130:21.

Kolsky, H.(1963). Stress waves in solids, volume 1098. Book, Dover Press, New York, .

Kuhlemeyer, R. L. and Lysmer, J.(1973). Finite element method accuracy for wave propagation problems. Journal of Soil Mechanics & Foundations Div, 99(Tech Rpt).

Kwan, A., **Dudley, J.**, **and Lantz, E.(2002)**. Who really discovered snell's law? Physics World, 15(4).

Lee, C. and Sterling, R.(1992). Identifying probable failure modes for underground openings using a neural network. In International journal of rock mechanics and mining sciences & geomechanics abstracts, volume 29, pages 49–67. Elsevier.

Leung, K., **Vardoulakis, I.**, **Beskos, D.**, **and Tassoulas, J.(1991)**. Vibration isolation by trenches in continuously nonhomogeneous soil by the bem. Soil Dynamics and Earthquake Engineering, 10(3):172–179.

Levasseur, S., **Malécot, Y.**, **Boulon, M.**, **and Flavigny, E.(2008)**. Soil parameter identification using a genetic algorithm. International Journal for Numerical and Analytical Methods in Geomechanics, 32(2):189–213.

Lim, S. M., **Sultan, A. B. M.**, **Sulaiman, M. N.**, **Mustapha, A.**, **and Leong, K.(2017a)**. Crossover and mutation operators of genetic algorithms. International Journal of Machine Learning and Computing, 7(1):9–12.

Lim, S. M., **Sultan, A. B. M.**, **Sulaiman, M. N.**, **Mustapha, A.**, **and Leong, K.(2017b)**. Crossover and mutation operators of genetic algorithms. International Journal of Machine Learning and Computing, 7(1):9–12.

Liyanapathirana, D. and Ekanayake, S. D.(2016). Application of eps geofoam in attenuating ground vibrations during vibratory pile driving. Geotextiles and Geomembranes, 44(1):59–69.

Lombaert, G. and Degrande, G.(2001). Experimental validation of a numerical prediction model for free field traffic induced vibrations by in situ experiments. Soil Dynamics and Earthquake Engineering, 21(6):485–497.

Mahdavisefat, E., **Salehzadeh, H.**, **and Heshmati, A.(2018)**. Full-scale experimental study on screening effectiveness of srm-filled trench barriers. Géotechnique, 68(10):869–882.

Majumder, M. and Ghosh, P.(2016). Intermittent geofoam in-filled trench for vibration screening considering soil non-linearity. KSCE Journal of Civil Engineering, 20(6):2308–2318.

Mal, A. and Knopoff, L.(1965). Transmission of rayleigh waves past a step change in elevation. Bulletin of the seismological society of America, 55(2):319–334.

Manouchehrian, A., **Gholamnejad, J.**, **and Sharifzadeh, M.(2014)**. Development of a model for analysis of slope stability for circular mode failure using genetic algorithm. Environmental Earth Sciences, 71(3):1267–1277.

Massarsch, K. R. and Fellenius, B.(2014). Ground vibrations from pile and sheet pile driving, part 1-building damage. In Proceedings of the International Conference on Piling and Deep Foundations, pages 131–139.

Massarsch, K. R. and Fellenius, B. H.(2008). Ground vibrations induced by impact pile driving. Missouri University of Science and Technology.

McCall, J.(2005). Genetic algorithms for modelling and optimisation. Journal of computational and Applied Mathematics, 184(1):205–222.

Miller, G., **Pursey, H.**, **and Bullard, E. C.(1955)**. On the partition of energy between elastic waves in a semi-infinite solid. Proceedings of the Royal Society of London. Series A. Mathematical and Physical Sciences, 233(1192):55–69.

Motamed, R., **Itoh, K.**, **Hirose, S.**, **Takahashi, A.**, **and Kusakabe, O.(2009)**. Evaluation of wave barriers on ground vibration reduction through numerical modeling in abaqus. In Proceedings of SIMULIA Customer Conference, pages 402–41.

Müller, R., **Gratacos, P.**, **Mora, P.**, **Nielsen, J.**, **Feng, J.**, **and Cervello, S.(2013)**. Definition of wheel maintenance measures for reducing ground vibration. RIVAS (SCP0-GA-2010-265754): Deliverable, 2:87.

Murillo, C., **Thorel, L.**, **and Caicedo, B.(2009)**. Ground vibration isolation with geofoam barriers: Centrifuge modeling. Geotextiles and Geomembranes, 27(6):423–434.

Myers, R. H., **Montgomery, D. C.**, **and Anderson-Cook, C. M.(2016)**. Response surface methodology: process and product optimization using designed experiments. John Wiley & Sons, .

Naggar, M. H. E. and Chehab, A. G.(2005). Vibration barriers for shock-producing equipment. Canadian Geotechnical Journal, 42:297–306.

Naghizadehrokni, M., **Ziegler, M.**, **and Sprengel, J.(2020)**. A full experimental and numerical modelling of the practicability of thin foam barrier as vibration reduction measure. Soil Dynamics and Earthquake Engineering, 139:106416.

Nilsson, N. J.(2014). Principles of artificial intelligence. Book, Morgan Kaufmann, .

Orcaflex(2010). Rayleigh damping: Guidance. url-https://www.orcina.com/webhelp/OrcaFlex/Content/html/Rayleighdamping,Guidance.htm.

Park, C. B., **Miller, R. D.**, **Xia, J.**, **and Ivanov, J.(2007)**. Multichannel analysis of surface waves (masw)active and passive methods. The Leading Edge, 26(1):60–64.

Parsons, K. and Griffin, M.(1988). Whole-body vibration perception thresholds. Journal of sound and Vibration, 121(2):237–258.

Pu, X., **Shi, Z.**, **and Xiang, H.(2018)**. Feasibility of ambient vibration screening by periodic geofoam-filled trenches. Soil Dynamics and Earthquake Engineering, 104:228–235.

Qiu, B.(2014). Numerical study on vibration isolation by wave barrier and protection of existing tunnel under explosions. Institut National des Sciences Appliquées de Lyon, PhD thesis.

Rahme, L.(2020). Screening of ground-born vibration by installing a trench in the transmission path. Bachelor, thesis, RWTH Aachen University.

Razali, N. M., **Geraghty, J.**, **and others(2011)**. Genetic algorithm performance with different selection strategies in solving tsp. In Proceedings of the world congress on engineering, volume 2, pages 1–6. International Association of Engineers Hong Kong.

Reed, R. and MarksII, R. J.(1999). Neural smithing: supervised learning in feedforward artificial neural networks. Book, Mit Press, .

Rezaie, A., **Rafiee-Dehkharghani, R.**, **Dolatshahi, K. M.**, **and Mirghaderi, S. R.(2018)**. Soil-buried wave barriers for vibration control of structures subjected to vertically incident shear waves. Soil Dynamics and Earthquake Engineering, 109:312–323.

Richards, R. J.(2009). The meaning of evolution: The morphological construction and ideological reconstruction of Darwin's theory. Book, University of Chicago Press, .

Sabatier, J. M., **Bass, H. E.**, **Bolen, L. N.**, **and Attenborough, K.(1986)**. Acoustically induced seismic waves. The Journal of the Acoustical Society of America, 80(2):646–649.

Sahu, J., **Acharya, J.**, **and Meikap, B.(2010)**. Optimization of production conditions for activated carbons from tamarind wood by zinc chloride using response surface methodology. Bioresource technology, 101(6):1974–1982.

Saikia, A.(2014). Numerical study on screening of surface waves using a pair of softer backfilled trenches. Soil Dynamics and Earthquake Engineering, 65:206–213.

Saikia, A.(2016). Numerical investigation on vibration isolation by softer in-filled trench barriers. Journal of Geo-Engineering Sciences, 3(1):31–42.

Samui, P. and Sitharam, T.(2010). Site characterization model using artificial neural network and kriging. International Journal of Geomechanics, 10(5):171–180.

Schevenels, M., **Lombaert, G.**, **and others(2017)**. Double wall barriers for the reduction of ground vibration transmission. Soil Dynamics and Earthquake Engineering, 97:1–13.

Sengupta, A. and Upadhyay, A.(2009). Locating the critical failure surface in a slope stability analysis by genetic algorithm. Applied Soft Computing, 9(1):387–392.

Shahin, M. A., **Jaksa, M. B.**, **and Maier, H. R.(2001a)**. Artificial neural network applications in geotechnical engineering. Australian geomechanics, 36(1):49–62.

Shahin, M. A., **Jaksa, M. B.**, **and Maier, H. R.(2001b)**. Artificial neural network applications in geotechnical engineering. Australian geomechanics, 36(1):49–62.

Sivakumar Babu, G., **Srivastava, A.**, **Nanjunda Rao, K.**, **and Venkatesha, S.(2011)**. Analysis and design of vibration isolation system using open trenches. International Journal of Geomechanics, 11(5):364–369.

Sprengel, J.(2017). Optimierung der praktischen Anwendbarkeit aufgeschäumter Isolierkörper im Boden zur Erschütterungsreduktion. PhD thesis, RWTH Aachen University.

Stachowske, M.(2020). Mitigation of vibration in a building caused by pile driving with a filled isolation trench and its optimization. Master thesis, RWTH Aachen University.

Stark, T., **Bartlett, S.**, **and Arellano, D.(2012)**. Expanded polystyrene (eps) geofoam applications and technical data. The EPS Industry Alliance, 1298:36.

Thompson, D., **Jiang, J.**, **Toward, M.**, **Hussein, M.**, **Ntotsios, E.**, **Dijckmans, A.**, **Coulier, P.**, **Lombaert, G.**, **and Degrande, G.(2016)**. Reducing railway-induced ground-borne vibration by using open trenches and soft-filled barriers. Soil Dynamics and Earthquake Engineering, 88:45–59.

Turk, I.(2019). Applications with graphical user interfaces. In Practical MATLAB, pages 271–290. Springer, .

Ulgen, D. and Toygar, O.(2015). Screening effectiveness of open and in-filled wave barriers: A full-scale experimental study. Construction and Building Materials, 86:12–20.

Voyant, C., **Notton, G.**, **Kalogirou, S.**, **Nivet, M.-L.**, **Paoli, C.**, **Motte, F.**, **and Fouilloy, A.(2017)**. Machine learning methods for solar radiation forecasting: A review. Renewable Energy, 105:569–582.

W, G. and WM, K.(2002). Biological neuron model. https://en.wikipedia.org/wiki/Biological_neuron_model#cite_note-Gerstner_2002-1.

Wang, G., **Wu, C.**, **and Li, S.(2019)**. Effect of vibration from highway vehicle load on adjacent buildings and its assessment. In IOP Conference Series: Earth and Environmental Science, volume 267, page 052048. IOP Publishing.

Wang, P.(2020). Building vibration attenuation due to plie driving by using geofoam filled barrier in non-homogeneous soil. Master thesis, RWTH Aachen University.

White, R.(1958). Elastic wave scattering at a cylindrical discontinuity in a solid. The Journal of the Acoustical Society of America, 30(8):771–785.

Whitley, D.(1994). A genetic algorithm tutorial. Statistics and computing, 4(2):65–85.

Wolf, J. P. and Obernhuber, P.(1982). Free-field response from inclined sh-waves and love-waves. Earthquake Engineering & Structural Dynamics, 10(6):823–845.

Woods, R. D.(1968). Screening of suface waves in soils. Technical report.

Woods, R. D.(1997). Dynamic effects of pile installations on adjacent structures, volume 253. Transportation Research Board, .

Yakimenko, O. A.(2019). Engineering Computations and Modeling in MATLAB®/Simulink®. American Institute of Aeronautics and Astronautics, Inc., .

Yang, Y.-B. and Hung, H.-H.(1997). A parametric study of wave barriers for reduction of train-induced vibrations. International Journal for Numerical Methods in Engineering, 40(20):3729–3747.

Yarmohammadi, F., **Rafiee-Dehkharghani, R.**, **Behnia, C.**, **and Aref, A.(2018)**. Topology optimization of jet-grouted overlapping columns for mitigation of train-induced ground vibrations. Construction and Building Materials, 190:838–850.

Yarmohammadi, F., **Rafiee-Dehkharghani, R.**, **Behnia, C.**, **and Aref, A.(2019)**. Design of wave barriers for mitigation of train–induced vibrations using a coupled genetic-algorithm/finite-element methodology. Soil Dynamics and Earthquake Engineering, 121:262–275.

Ziaee, S. A., **Sadrossadat, E.**, **Alavi, A. H.**, **and Shadmehri, D. M.(2015)**. Explicit formulation of bearing capacity of shallow foundations on rock masses using artificial neural networks: application and supplementary studies. Environmental earth sciences, 73(7):3417–3431.

Zoccali, P., **Cantisani, G.**, **and Loprencipe, G.(2015)**. Ground-vibrations induced by trains: filled trenches mitigation capacity and length influence. Construction and Building Materials, 74:1–8.

Zolfaghari, A. R., **Heath, A. C.**, **and McCombie, P. F.(2005)**. Simple genetic algorithm search for critical non-circular failure surface in slope stability analysis. Computers and geotechnics, 32(3):139–152.

Publications

Partial results from this dissertation have been published in the following scientific journals and conference proceedings:

Naghizadehrokni, M., Ziegler, M., & Sprengel, J. (2020). A full experimental and numerical modelling of the practicability of thin foam barrier as vibration reduction measure. Soil Dynamics and Earthquake Engineering, 139, 106416.

Naghizadehrokni, M., Ziegler, M. (2020). Effect of Different Configurations of a Geofoam-Filled Barrier in Vibration Scattering and its Optimization by Genetic Algorithm. EURODYN 2020 : Proceedings of the XI International Conference on Structural : Proceedings / M. Papadrakakis, M. Fragiadakis, C. Papadimitriou (Eds.); EADS, European Association for Structural Dynamics. - Volume 2 Page(s)/Article-Nr.: 4069-4084.

APPENDIX

A Guidelines for Python scripting
B Genetic algorithm code for homogeneous soil
C Plaxis script for layered soil
D Artificial neural network
E Genetic algorithm code for layered soil
F Developing an app for predicting and optimizing the vibration
G Diagrams of parametric study for layered soil for frequency $f = 50Hz$

A Guidelines for Python scripting

Since the introduction of the command line in Plaxis 3D and more recently in Plaxis 2D AE, Plaxis offers the ability to quickly build or rebuild models by typing commands, as a more advanced alternative to the user-friendly interface. The command line also gives access to some advanced options which are not available through the user interface. To make Plaxis a more powerful design tool, a remote scripting interface was added to the software.

The remote scripting interface is based on the Python language and allows users to control both the Input and Output program via an external Python handler, for example IDLE, to either directly input commands on-the-fly or to run script files.

In the current appendix no attempt is made at explaining the underlying details related strictly to the discipline of computer science and programming, as it would be outside the project scope. Thus, the reader is reminded that the following sections of this appendix present the developed PYTHON scripting methods and how they were applied to Plaxis.

In order to be able to access the scripting features, a list of prerequisites must be fulfilled, as defined in Brinkgreve et al. (2017).

Remote scripting server

Before running a script, it is always necessary to activate the remote scripting server in Plaxis Input or Plaxis Output (or both, depending on the task). The process of activation is the same for both applications, so Plaxis Input is used as an example.

- Start the Plaxis Input application.
- Start a new project.
- Go to the Expert menu and select Configure remote scripting server. A window as shown in Figure C.1 will open.
- Find a port that is available. The default is given as 10000.
- Depending on the Plaxis version, the user may be requested to define a password for security reasons.
- Start the server and check that all the tick marks on the left side are near field, then close the window.

Fig. 9.1 shows the configure remote scripting server window.

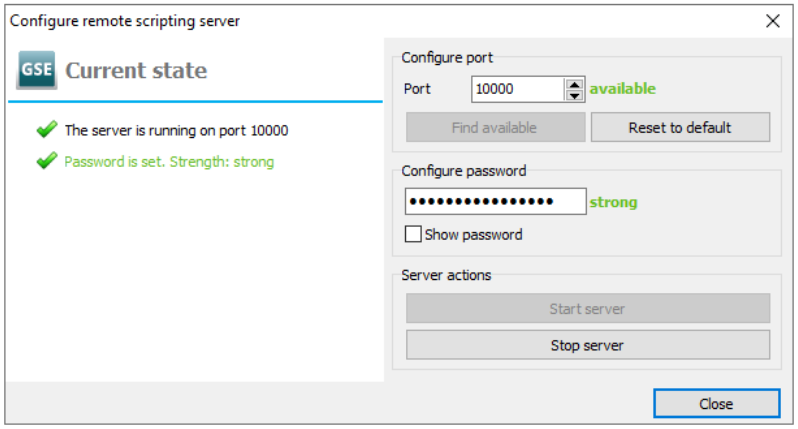


Figure 9.1: Configure remote scripting server window

Libraries and connection to Plaxis application

The first step in using Python wrapper for Plaxis is importing the scripting libraries and establishing the connection with the application. In this example it is assumed that 10000 and 10001 are the port numbers for Plaxis Input and Plaxis Output, respectively. These numbers must be the same as the ones defined earlier in the Configure remote scripting server window. The same applies to the password.

Listing 9.1: Configure remote scripting server window

```
# Define the path to the scripting  libraries
import math
import numpy
import  statistics
from plxscripting.easy import *

# Port info
input_port_i = '10000'
input_port_o = '10001'
input_password = 'gkiePHMehran7075'# PUT YOUR PLAXIS 3D INPUT PASSWORD HERE
save_path = 'C:\Program Files (x86)\Plaxis\PLAXIS 3D' # r'C:\Plaxis\Data' # PUT THE
    FOLDER TO SAVE THE PLAXIS FILES HERE

Connect to PLAXIS application
s_i, g_i = new_server('localhost', 10000, password='gkiePHMehran7075')
s_o, g_o = new_server('localhost', 10001, password='gkiePHMehran7075')
```

The variables s_i and s_o are bound to objects that represent the Plaxis application and they allow the user to control project files, e.g. open projects. On the other hand, g_i and g_o are related to the model. These are the variables that must be used in order to manipulate the current model.

Plaxis Input

The following code opens a new project and defines its properties. The properties are set by using name-value pair arguments. If a certain property is not explicitly addressed in the script, the default value is assumed in the project. The next step is to define the boreholes through specifying X, Y and Z coordinates.

Listing 9.2: Start a new project and create borehole

```
def Calculator(wx, width, depth, length, Dist, s_i, g_i, type):
    # Start a new project
    s_i.new()

    # Set model and element properties
    g_i.Soilcontour. initializerectangular (0,0,40,20)
    borehole = g_i.borehole(0, 0)
    g_i. soillayer (20)
```

Soil menu

Fig. 9.3 shows how to create a soil material set and specifies some of its properties. Unlike model properties, some soil characteristics do not have default values and thus must be defined by the user, otherwise PLAXIS gives a warning and the execution of the script stops. Material properties are set in the same manner (name-value pairs) as model properties.

Listing 9.3: Start a new project and create borehole

```
    # create soil material set
    material1 = g_i.soilmat()
    material1. setproperties (
        "MaterialName", "Soil",

        "Colour", 15262369,
        "SoilModel", 1,
        "gammaUnsat", 20,
        "gammaSat", 20,
        "Gref", 96150,
        "nu", 0.3,
        "cref", 0,
        "phi", 0,
        "RayleighBeta", 0.0003183)

    # create soil material set
    material2 = g_i.soilmat()
    material2. setproperties (
    "MaterialName", "Geofoam",
```

```
    "Colour", 9079434,
    "SoilModel", 1,
    "gammaUnsat", 0.61,
    "gammaSat", 0.61,
    "Gref", 6807,
    "nu", 0.01,
    "cref", 0,
    "phi", 0)

# Assign the soil material to the layer
g_i.setmaterial(g_i.Soil_1, material1)
```

Structures menu

The structural entities, boundary conditions, loads/prescribed displacements and soil polygons are created under the Structures menu. The starting point is to select the actual menu and create the lines which define the geometry of the structure, the interfaces and the distribution of prescribed displacements. Following Script shows the process of defining the plate structure and assigning material properties.

Listing 9.4: Create plate and assign the material

```
# Move to structure tab
g_i.gotostructures()

# Create plate
g_i.plate((0, 0, 0), (0.36, 0, 0), (0.36, 0.36, 0), (0, 0.36, 0))

# Create plate material set
material3 = g_i.platemat()
material3.setproperties(
    "MaterialName", "Plate",

    "Colour", 16711680,
    "IsIsotropic", True,
    "E1", 30000000,
    "E2", 30000000,
    "d", 0.1,
    "G12", 15000000,
    "G13", 15000000,
    "G23", 15000000)

# Assign material
g_i.setmaterial(g_i.plate_1, material3)
```

The next step is to define some surfaces, extrude them and assign the material for installing

the trench. Fig. 9.5 represents three defined functions for creating trenches with various configurations.

Listing 9.5: Install the trench and assign the material

```
# Create trench for different configurations
if (type == 1): #(Function for single wall system)
    g_i.surface(wx-width/2, 0, 0, wx+width/2, 0, 0, wx+width/2, length, 0, wx-width/2,
        length, 0, wx-width/2, 0, 0)
    g_i.extrude((g_i.Polygon_2), 0, 0, 0-depth)
    g_i.delete(g_i.Polygon_2)
    g_i.setmaterial(g_i.Soil_2, material2)
elif (type == 2): # (Function for Double Wall system)
    g_i.surface(wx-Dist-width/2, 0, 0, wx-Dist+width/2, 0, 0, wx-Dist+width/2, length, 0,
        wx-Dist-width/2, length, 0, wx-Dist-width/2, 0, 0)
    g_i.extrude((g_i.Polygon_2), 0, 0, 0-depth)
    g_i.delete(g_i.Polygon_2)
    g_i.setmaterial(g_i.Soil_2, material2)

    g_i.surface(wx+Dist-width/2, 0, 0, wx+Dist+width/2, 0, 0, wx+Dist+width/2, length, 0,
        wx+Dist-width/2, length, 0, wx+Dist-width/2, 0, 0)
    g_i.extrude((g_i.Polygon_2), 0, 0, 0-depth)
    g_i.delete(g_i.Polygon_2)
    g_i.setmaterial(g_i.Soil_3, material2)
elif (type == 3):# (Function for Triangle wall System)
    g_i.surface(wx-width, 0, 0, wx+width, 0, 0, wx, 0, 0-depth)
    g_i.delete(g_i.Polygon_2)
    g_i.setmaterial(g_i.Soil_2, material2)
```

Surface load is also created in structure section.

Listing 9.6: Create surface load

```
# Create a surface load
g_i.surfload(0, 0, 0, 0.36, 0, 0, 0.36, 0.36, 0, 0, 0.36, 0)
```

Mesh menu

The following part of the script in Fig 9.7 is responsible for generating the mesh. Both the global mesh coarseness and the local mesh coarseness factor can be adjusted. It is important to notice that the coarseness factor is not applied to the soil object, but rather to the polygon itself.

Listing 9.7: Generate mesh

```
# Mesh tab
g_i.gotomesh()
```

```
# Define local and global coarsnes factor
g_i.Polygon_1_Polygon_2_Polygon_3_1.CoarsenessFactor = 0.1
g_i.Polygon_3_1.CoarsenessFactor = 0.15
g_i.Polygon_3_2.CoarsenessFactor = 0.2
g_i.Polygon_4_1.CoarsenessFactor = 0.15
g_i.Polygon_4_2.CoarsenessFactor = 0.3
g_i.BoreholeVolume_1_1.CoarsenessFactor = 0.7

# Generate mesh
g_i.mesh(3.15, 256)
```

Staged construction menu

The process of defining a phase follows a specific pattern:

- Add a phase. At the same time the previous phase must be stated.
- Near field the new phase.
- Set the properties of the phase.

This pattern can be observed in Fig. 9.8, where 6 phases are created.

Listing 9.8: Define different phases and run the model

```
# Moved to staged construction
g_i.gotostages()

# Phase 1
phase1 = g_i.phase(g_i.phases[0])
g_i.Polygon_1_Polygon_2_Polygon_3_1.activate(g_i.phase_1)

# Phase 2
phase2 = g_i.phase(g_i.phases[1])
g_i.BoreholeVolume_1_Volume_1_1.deactivate(g_i.phase_2)

# Phase 3
phase3 = g_i.phase(g_i.phases[2])
g_i.Soil_1_Soil_2_1.Material[g_i.Phase_3] = material2

# Phase 4
phase4 = g_i.phase(g_i.phases[3])
g_i.Volume_1.activate(g_i.phase_4)

# Phase 5
phase5 = g_i.phase(g_i.phases[4])
g_i.set(g_i.phase_5.DeformCalcType,"Dynamic")
```

```
g_i.set(g_i.Phase_5.Deform.TimeIntervalSeconds, 0.0005)
g_i.set(g_i.Phase_5.Deform.ResetDisplacementsToZero, True)
g_i.DynSurfaceLoad_1_1.activate(g_i.phase_5)
g_i.set(g_i.phase_5.DeformCalcType,"Dynamic")
g_i.DynSurfaceLoad_1_1.sigz[g_i.Phase_5] = -26
g_i.loadmultiplier()
g_i.set(g_i.LoadMultiplier_1.Signal, "Harmonic")

g_i.set(g_i.LoadMultiplier_1.Amplitude, 1)
g_i.set(g_i.LoadMultiplier_1.Frequency, 50)
g_i.DynSurfaceLoad_1_1.Multiplierz[g_i.Phase_5] = g_i.LoadMultiplier_1
g_i.Dynamics.BoundaryXMin[g_i.Phase_5] = "None"

g_i.Dynamics.BoundaryYMin[g_i.Phase_5] = "None"

g_i.Dynamics.BoundaryZMin[g_i.Phase_5] = "Viscous"


# Phase 6
phase6 = g_i.phase(g_i.phases[5])
g_i.set(g_i.phase_6.DeformCalcType,"Dynamic")
g_i.set(g_i.Phase_6.Deform.TimeIntervalSeconds, 0.005)
g_i.DynSurfaceLoad_1_1.activate(g_i.phase_6)
g_i.set(g_i.LoadMultiplier_1.Signal, "Harmonic")

g_i.set(g_i.LoadMultiplier_1.Amplitude, 1)
g_i.set(g_i.LoadMultiplier_1.Frequency, 50)
g_i.DynSurfaceLoad_1_1.Multiplierz[g_i.Phase_6] = g_i.LoadMultiplier_1
g_i.Dynamics.BoundaryXMin[g_i.Phase_6] = "None"

g_i.Dynamics.BoundaryYMin[g_i.Phase_6] = "None"

g_i.Dynamics.BoundaryZMin[g_i.Phase_6] = "Viscous"


g_i.calculate()
```

The addition of a new phase is carried out by the function phase(), the argument of which is the previous phase. In order to change the properties of objects during a certain phase, the set(object.attribute, (phase), value) command is used. The properties of the phase itself (e.g. ID, calculation type) can be accessed directly through the dot symbol. When the phases are set, the model is ready for calculation. This is done simply with the last command in the figure.

Plaxis output

The next step is extracting the vertical soil particle velocity beyond the trench for calculating the efficiency of the trench.

Listing 9.9: Open the output page

```
# Open output
outpu_port = g_i.view(phase6)

f1 = open("points.txt", "r")

if f1.mode == "r":

    xloc = list(map(float, f1.read().split()))
else:
    print("can't read 'points.txt' file")
f1.close()

f2 = open("VelocityZ.txt", "r")

if f2.mode == "r":

    Vz = list(map(float, f2.read().split()))
else:
    print("can't read 'Velocity.txt' file")
f2.close()
```

The next step is defining a function for calculting the efficiency of the trench.

Listing 9.10: Calculate the efficiency of the trench

```
# Define function for calculating efficiency of trench
thresh = wx + width / 2
value = []
Temp = 0
Npoints = len(xloc)
for k in range(0, Npoints):
    if (xloc[k] > thresh) and (xloc[k] < (thresh + 30)):
        vz = abs(float(g_o.getsingleresult(g_o.Phase_6, g_o.ResultTypes.Soil.Vz, (xloc[k], 0,
            0))))
        value.append(vz / Vz[k])
        #if (vy / Vy[k]<8):
        Temp += vz / Vz[k]

Efficiency = statistics.mean(value)
g_o.close()
return Efficiency
```

The next step is collecting the data.

Listing 9.11: Collect the data

```
#Calculator(wx, width, length, depth, Dist, s_i, g_i, type):

Wx = [3, 6] #Location of the trench
De = [2, 3] #Depth of the trench
Le = [5, 20] #Length of the trench
Wi = [0.3, 0.5] #Width of the trench
Dist= [2, 2.5] #Distance between the wall

List =[]
Iter = 1
type = 1
for i in (Wx):
    for j in (Wi):
        for k in (De):
            for l in (Le):
                if type == 1 :
                    Out = Calculator(i, j, k, l, 1, s_i, g_i, type)
                    List.append([i, j, k, l, Out])
                    continue
                for m in (Dist):
                    Out = Calculator(i, j, k, l, m, s_i, g_i, type)
                    List.append([i, j, k, l, m, Out])
```

The last step is saving the data.

Listing 9.12: Save the data

```
a = numpy.asarray(List)
if type == 1:
    numpy.savetxt("Single_Efficiency.csv", a, delimiter=",")
elif type == 2:
    numpy.savetxt("Two_Wall_Efficiency.csv", a, delimiter=",")
elif type == 3:
    numpy.savetxt("Triangle_Wall_Efficiency.csv", a, delimiter=",")
```

B Genetic algorithm code for homogeneous soil

The used libraries in this code are including:

- Random: this function implements random number generators for various distributions.
- Genetic: this file contains the implementation of the main operators of genetic algorithm including selection, crossover and mutation.
- Math: the mathematical functions are accessible through this function.
- Statistics: this module provides functions for calculating mathematical statistics of numerical data (real-value) since the genetic algorithm code is implemented for real-value representations (floating encoding).
- Pickle: pickling is a converting process of a Python object to a byte stream. This function is used for reading the files of points and velocity.
- plxscripting.easy: this library is called for importing the scripting library of Plaxis program.

Listing 9.13: Generating random chromosomes for initial population

```
import random

class Chromosome:
    def __init__(self, genes, fitness):
        self.Genes = genes
        self.Fitness = fitness

def createPop(popSize, min, max):
    D = len(min)
    pop = []
    for i in range(0, popSize):
        chrom = []
        for j in range(0, D):
            chrom.append(random.uniform(min[j],max[j]))
        fitness = None
        pop.append(Chromosome(chrom, fitness))
    return pop
```

Listing 9.14: Defining mutation function

```
def mutate(chrom, min, max):
    index = random.randrange(0, len(min))
```

```
    newGene = random.uniform(min[index], max[index])
    Genes = chrom.Genes[:]
    Genes[index] = newGene
    return Chromosome(Genes, None)
```

Listing 9.15: Defining crossover function

```
def crossover(chrom1, chrom2):
    index = random.randrange(0, len(chrom1.Genes))
    newChrom1 = Chromosome(chrom1.Genes[:index]+chrom2.Genes[index:], None)
    newChrom2 = Chromosome(chrom2.Genes[:index]+chrom1.Genes[index:], None)
    return (newChrom1, newChrom2)
```

Listing 9.16: Selection

```
def minFit(pop):
    N = len(pop)
    idx = 0
    val = pop[0].Fitness
    for i in range(1, N):
        if pop[i].Fitness<val:
            val = pop[i].Fitness
            idx = i
    return (val, idx)
```

Listing 9.17: Genetic Algorithm main code

```
import MyGenetic
import random
import math
import statistics
import pickle

from plxscripting.easy import *

f1 = open("points.txt", "r")

if f1.mode == "r":

    xloc = list(map(float, f1.read().split()))
else:
    print("can't read 'points.txt' file")
f1.close()

f2 = open("VelocityZ.txt", "r")

if f2.mode == "r":

    Vz = list(map(float, f2.read().split()))
```

```
else:
    print("can't read 'Velocity.txt' file")
f2.close()
doLoad = False
if doLoad:
    with open('GaData.pkl', 'rb') as f:
        pop, f_iter = pickle.load(f)

Npoints = len(xloc)

# var name: wx, width, depth, length
Min = [2, 0.25, 2, 5, 50]
Max = [8, 1, 6, 15, 50]
popSize = 30
maxIter = 50
pm = 0.008 # probability of mutate
pc = 0.8 # probability of crossover

input_port_i = '10000'
input_port_o = '10001'
input_password = 'gkiePHMehran7075'# PUT YOUR PLAXIS 3D INPUT PASSWORD HERE
save_path = 'C:\Program Files (x86)\Plaxis\PLAXIS 3D' # r'C:\Plaxis\Data' # PUT THE
    FOLDER TO SAVE THE PLAXIS FILES HERE

def fitness(gene):
    s_i, g_i = new_server('localhost', input_port_i, password=input_password)
    s_i.new()
    material1 = g_i.soilmat()
    material1.setproperties(
        "MaterialName", "Soil",

        "Colour", 15262369,
        "SoilModel", 1,
        "gammaUnsat", 20,
        "gammaSat", 20,
        "Gref", 96150,
        "nu", 0.3,
        "cref", 0,
        "phi", 0,
        "RayleighBeta", 0.0003183)
    material2 = g_i.soilmat()
    material2.setproperties(
        "MaterialName", "Geofoam",

        "Colour", 9079434,
        "SoilModel", 1,
        "gammaUnsat", 0.61,
        "gammaSat", 0.61,
        "Gref", 6807,
```

```
        "nu", 0.01,
        "cref", 0,
        "phi", 0)
g_i.Soilcontour. initializerectangular (0,0,40,20)
borehole = g_i.borehole(0,0)
g_i. soillayer (20)
g_i.setmaterial(g_i.Soil_1, material1)
g_i.gotostructures()
g_i.plate((0, 0, 0), (0.36, 0, 0), (0.36, 0.36, 0), (0, 0.36, 0))
material3 = g_i.platemat()
material3. setproperties(
        "MaterialName", "Plate",

        "Colour", 16711680,
        "IsIsotropic", True,
        "E1", 30000000,
        "E2", 30000000,
        "d", 0.1,
        "G12", 15000000,
        "G13", 15000000,
        "G23", 15000000)
g_i.setmaterial(g_i.plate_1, material3)

# var name: wx, width, depth, length
wx = gene[0]
width = gene[1]
depth = gene[2]
length = gene[3]

g_i.surface(wx-width/2, 0, 0, wx+width/2, 0, 0, wx+width/2, length, 0, wx-width/2, length,
    0, wx-width/2, 0, 0)
g_i.extrude((g_i.Polygon_2), 0, 0, 0-depth)
g_i.delete(g_i.Polygon_2)
g_i.setmaterial(g_i.Soil_2, material2)

g_i.surfload(0, 0, 0, 0.36, 0, 0, 0.36, 0.36, 0, 0, 0.36, 0)
g_i.surface(0, 0, 0, 35, 0, 0, 35, 20, 0, 0, 20, 0, 0, 0, 0)
g_i.surface(0, 0, 0, 35, 0, 0, 35, 0, -15, 0, 0, -15, 0, 0, 0)

g_i.gotomesh()

g_i.Polygon_1_Polygon_2_Polygon_3_1.CoarsenessFactor = 0.1
g_i.Polygon_3_1.CoarsenessFactor = 0.15
g_i.Polygon_3_2.CoarsenessFactor = 0.2
g_i.Polygon_4_1.CoarsenessFactor = 0.15
g_i.Polygon_4_2.CoarsenessFactor = 0.3
g_i.BoreholeVolume_1_1.CoarsenessFactor = 0.7

g_i.mesh(0.15, 256)
```

```
g_i.gotostages()

phase1 = g_i.phase(g_i.phases[0])
g_i.Polygon_1_Polygon_2_Polygon_3_1.activate(g_i.phase_1)

phase2 = g_i.phase(g_i.phases[1])
g_i.BoreholeVolume_1_Volume_1_1.deactivate(g_i.phase_2)

phase3 = g_i.phase(g_i.phases[2])
g_i.Soil_1_Soil_2_1.Material[g_i.Phase_3] = material2

phase4 = g_i.phase(g_i.phases[3])
g_i.Volume_1.activate(g_i.phase_4)

f = round(gene[4])
phase5 = g_i.phase(g_i.phases[4])
g_i.set(g_i.phase_5.DeformCalcType,"Dynamic")
g_i.set(g_i.Phase_5.Deform.TimeIntervalSeconds, 0.5)
g_i.set(g_i.Phase_5.Deform.ResetDisplacementsToZero, True)
g_i.DynSurfaceLoad_1_1.activate(g_i.phase_5)
g_i.set(g_i.phase_5.DeformCalcType,"Dynamic")
g_i.DynSurfaceLoad_1_1.sigz[g_i.Phase_5] = -26
g_i.loadmultiplier()
g_i.set(g_i.LoadMultiplier_1.Signal, "Harmonic")

g_i.set(g_i.LoadMultiplier_1.Amplitude, 1)
g_i.set(g_i.LoadMultiplier_1.Frequency, f)
g_i.DynSurfaceLoad_1_1.Multiplierz[g_i.Phase_5] = g_i.LoadMultiplier_1
g_i.Dynamics.BoundaryXMin[g_i.Phase_5] = "None"

g_i.Dynamics.BoundaryYMin[g_i.Phase_5] = "None"

g_i.Dynamics.BoundaryZMin[g_i.Phase_5] = "Viscous"


phase6 = g_i.phase(g_i.phases[5])
g_i.set(g_i.phase_6.DeformCalcType,"Dynamic")
g_i.set(g_i.Phase_6.Deform.TimeIntervalSeconds, 0.5)
g_i.DynSurfaceLoad_1_1.activate(g_i.phase_6)
g_i.set(g_i.LoadMultiplier_1.Signal, "Harmonic")

g_i.set(g_i.LoadMultiplier_1.Amplitude, 1)
g_i.set(g_i.LoadMultiplier_1.Frequency, f)
g_i.DynSurfaceLoad_1_1.Multiplierz[g_i.Phase_6] = g_i.LoadMultiplier_1
g_i.Dynamics.BoundaryXMin[g_i.Phase_6] = "None"

g_i.Dynamics.BoundaryYMin[g_i.Phase_6] = "None"

g_i.Dynamics.BoundaryZMin[g_i.Phase_6] = "Viscous"
```

```
    g_i.calculate()

    outpu_port = g_i.view(phase6)
    s_o, g_o = new_server('localhost', input_port_o, password=input_password)

    thresh = wx+width/2
    value = []
    for k in range(0, Npoints):
        if (xloc[k]>thresh) and (xloc[k]<(thresh+25)):
            vz = abs(float(g_o.getsingleresult(g_o.Phase_6, g_o.ResultTypes.Soil.Vz, (xloc[k], 0,
                0))))
            value.append(vz/Vz[k])

    g_o.close()
    AR = 1-statistics.mean(value)
    D_AR = 0.75
    alpha = 0.995
    beta  = 0.005
    Cost = alpha*abs(AR-D_AR) + beta*depth
    return Cost


if __name__ == '__main__':

    if not doLoad:
        pop = MyGenetic.createPop(popSize, Min, Max)
        for i in range(0, popSize):
            pop[i].Fitness = fitness(pop[i].Genes)
        (bestFit, idx) = MyGenetic.minFit(pop)
        print("In iteration 0\t best fitness value is {0:12.9f}".format(
            bestFit
        ))
        f_iter = 0
    iter0 = f_iter
    for itr in range(iter0, maxIter):
        NewPop = []

        # crossover
        idr = random.sample(range(0,popSize),popSize)
        for i in range(0, int(popSize/2)):
            id1 = idr[i*2]
            id2 = idr[i*2+1]
            if random.random()<pc:
                (newChrom1, newChrom2) = MyGenetic.crossover(pop[id1], pop[id2])

                newChrom1.Fitness = fitness(newChrom1.Genes)
                newChrom2.Fitness = fitness(newChrom2.Genes)
```

```
                if newChrom1.Fitness<pop[id1].Fitness:
                    NewPop.append(newChrom1)
                else:
                    NewPop.append(pop[id1])

                if newChrom2.Fitness<pop[id2].Fitness:
                    NewPop.append(newChrom2)
                else:
                    NewPop.append(pop[id2])
            else:
                NewPop.append(pop[id1])
                NewPop.append(pop[id2])

        # Mutate
        pop = []
        for i in range(0, popSize):
            if random.random()<pm:
                newChrom = MyGenetic.mutate(NewPop[i], Min, Max)
                newChrom.Fitness = fitness(newChrom.Genes)
                if newChrom.Fitness<NewPop[i].Fitness:
                    pop.append(newChrom)
                else:
                    pop.append(NewPop[i])
            else:
                pop.append(NewPop[i])

        (bestFit, idx) = MyGenetic.minFit(pop)
        print("In iteration {0}\t best fitness value is {1:12.9f}".format(
            (itr+1),
            bestFit
        ))
        f_iter = itr
        with open('GaData.pkl', 'wb') as f:
            pickle.dump([pop, f_iter], f)

    # var name: wx, width, depth, length
    wx = pop[idx].Genes[0]
    width = pop[idx].Genes[1]
    depth = pop[idx].Genes[2]
    length = pop[idx].Genes[3]
    f = round(pop[idx].Genes[4])
    print("best value obtained with wx = {0:3.2f}, width = {1:3.2f}, depth = {2:3.2f}, length =
        {3:3.2f} and Frequency = {4}.".format(
        wx, width, depth, length, f
    ))
    print("best fittness value is: {0:12.9f} .".format(bestFit))
```

C Plaxis script for layered soil

Listing 9.18: Plaxis automation for layered soil

```
import math
import numpy
import  statistics
from plxscripting.easy import *
import TwoLayer_crossing
import TwoLayer

input_port_i = '10000'
input_port_o = '10001'
input_password = 'gkiePHMehran7075'# PUT YOUR PLAXIS 3D INPUT PASSWORD HERE
save_path = 'C:\Program Files (x86)\Plaxis\PLAXIS 3D' # r'C:\Plaxis\Data' # PUT THE
    FOLDER TO SAVE THE PLAXIS FILES HERE
s_i, g_i = new_server('localhost', 10000, password='gkiePHMehran7075')

f1 = open("points.txt", "r")

if f1.mode == "r":

    xloc = list(map(float, f1.read().split()))
else:
    print("can't read 'points.txt' file")
f1.close()

f2 = open("VelocityY.txt", "r")

if f2.mode == "r":

    Vy = list(map(float, f2.read().split()))
else:
    print("can't read 'Velocity.txt' file")
f2.close()


#VAR Name : X, Width, Depth, first layer depth (line_9), Gref (Line 21), Geofoam (Line 41)


def Calculator(Vector, s_i, g_i,xloc, Vy):
    #Vector=[x, d, l, w, gr, Ep]
    D = Vector[1]
    L = Vector[2]
    if D>L:
```

```
        Out = TwoLayer_crossing.Calculation(Vector, s_i, g_i, xloc, Vy)
    else:
        Out = TwoLayer.Calculation(Vector, s_i, g_i, xloc, Vy)
    return Out

X = [1.4, 4.2, 7.6, 10.5, 13.8]
D = [2.6, 3.5, 4.7, 5.3, 6.8, 7.5]
L = [1.5, 3.3, 5.2, 8.7]
W = [0.2]
Gref = [105756]
Eps = [12]
List =[]
Iter = 1
f=open('Efficiency_In_Process.csv', 'wb')
for x in (X):
    for d in (D):
        for l in (L):
            for w in (W):
                for gr in (Gref):
                    for Ep in range(0, len(Eps)):
                        Vector = [x, d, l, w, gr, Ep+1]
                        Out = Calculator(Vector, s_i, g_i, xloc, Vy)
                        # Out=x+d+l+w+gr+Ep
                        Vector1 = [[x, d, l, w, gr, Eps[Ep], Out]]
                        Vector = [x, d, l, w, gr, Eps[Ep], Out]
                        List.append(Vector)
                        a = numpy.asarray(Vector1)
                        print(a)
                        print(Vector1)
                        numpy.savetxt(f, a, fmt='%1.6e', delimiter=",")
                        Iter = Iter + 1
                        print(Iter)

a = numpy.asarray(List)
print("best value obtained with X = {0:3.2f}, W = {1:3.2f}, D = {2:3.2f}, L = {3:3.2f}, Gref =
    {4:3.2f} and , Geofoam.".format(
        x, d, l, w, gr,
), Eps[Ep])
numpy.savetxt("Efficiency2.csv", a, fmt='%1.6e', delimiter=",")
```

D Artificial Neural Network

Listing 9.19: Main body of the code

```
clc
clear all
close all
warning off
%% Read Data
AllData=xlsread('Results.xlsx');
[Row, Col] = size(AllData);
%% Normalization
Data=AllData(:,1:end-1);
Max_Data=max(Data);
Min_Data=min(Data);
%%
Min_Normal=0;
Max_Normal=1;
Data=mapminmax(Data',Min_Normal,Max_Normal)';
AllData(:,1:end-1)=Data;
%%
RandInd=randperm(Row);
AllData=AllData(RandInd,:);
%% Make Train and Test Set (Train Set = 70%, Test Set = 30%)
TrainInfo=AllData(1:ceil(0.7*Row),:);
TestInfo=AllData(ceil(0.7*Row)+1:end,:);
%%
TrainTarget=TrainInfo(:,end); % Ar
TrainData=TrainInfo(:,1:end-1); % Parameters

TestTarget=TestInfo(:,end);
TestData=TestInfo(:,1:end-1);
% [Row,Col]=size(TrainData);


%% Determine New Data
SelectedParam=[1 2 3 4 5 6];
TrainData=TrainData(:,SelectedParam);
TestData=TestData(:,SelectedParam);
%% Make ANN Model
Plot=1; % 1. show net and Train Result , 0: Don't Show
[ AnnModel,TrResult ] = ANN_regression( TrainData,TrainTarget,Plot );
%%
  Predicted=sim(AnnModel,TestData'); %simulation the network
  TeResult.MSE=mse(Predicted'-TestTarget);
```

```
TeResult.RMSE=sqrt(mse(Predicted'-TestTarget));
TeResult.CORR=corr2(Predicted',TestTarget);
TeResult.R2 = rsquare(Predicted',TestTarget);
figure
PlotResults(Predicted', TestTarget, 'Test Data')
%%
xlswrite('Test_Out.xlsx',[Predicted', TestTarget, Predicted'-TestTarget]);
save('AnnModel','AnnModel','Max_Data','Min_Data','SelectedParam',
    'Max_Normal','Min_Normal');
```

Defining activation functions and neurons of hidden layers

Listing 9.20: Activation functions

```
function [ net,TrResult ] = ANN_regression( TrainData,TrainTarget,Flag )
%UNTITLED2 Summary of this function goes here
%   Detailed explanation goes here
    si=[10 15];
    TF1 = 'logsig';    % {tansig, logsig, purelin} ==> Transfer Function for first hidden layer
    TF2 = 'logsig';    % {tansig, logsig, purelin} ==> Transfer Function for second hidden
        layer
    TF3 = 'logsig';    % {tansig, logsig, purelin} ==> Transfer Function for second hidden
        layer
    BTF = 'trainlm'; % train+{bfg, br, cgb, cgf, cgp, gd, gdm, gda, gdx, lm, oss, r, rp,
        scg}, ==> Train Function
    PF = 'msereg';    % Performance Metric for MLP
   net = newff(TrainData',TrainTarget',si,{TF1 TF3 TF2},BTF,PF);
   net.trainparam.epochs =1000;
   net.trainparam.goal = 0.001;
%     net.trainparam.mu = 0.001;
%     net.trainparam.mu_dec = 0.001;
%     net.trainparam.mu_inc = 0.001;
%     net.trainparam.mu_max = 0.001;
%     net.trainparam.mem_reduc = 0.001;
%     net.trainparam.Max_perf_inc = 1.004;

%     net.trainparam.Lr = 0.02;
%     net.trainparam.Lr_dec = 0.05;
%     net.trainparam.Lr_inc = 1.05;
     net.divideparam.trainRatio = 50;
     net.divideparam.valRatio = 25;
     net.divideparam.testRatio = 25;

     net.performParam.regularization=0.01;

   net.performFcn=PF;
```

```
    net=init(net); % initialising the weight and bias wectors
    net=train(net,TrainData',TrainTarget'); %training the network
    Predicted=sim(net,TrainData'); %simulation the network
    TrResult.MSE=mse(Predicted'-TrainTarget);
    TrResult.RMSE=sqrt(mse(Predicted'-TrainTarget));
    TrResult.CORR=corr2(Predicted',TrainTarget);
    TrResult.R2=rsquare(Predicted',TrainTarget);
    if Flag
        view(net)
        figure
        PlotResults(Predicted', TrainTarget, 'Train Data')
    end
end
```

E Genetic algorithm code for layered soil

Listing 9.21: Main body of the code

```
import Genetic2
import random
import math
import  statistics
import pickle
import TwoLayer_crossing
import TwoLayer

from plxscripting.easy import *

f1 = open("points.txt", "r")
if f1.mode == "r":
    xloc = list(map(float, f1.read().split()))
else:
    print("can't read 'points.txt' file")
f1.close()

f2 = open("VelocityY.txt", "r")
if f2.mode == "r":
    Vy = list(map(float, f2.read().split()))
else:
    print("can't read 'Velocity.txt' file")
f2.close()
doLoad = False
if doLoad:
    with open('GaData.pkl', 'wb') as f:
        pop, f_iter = pickle.load(f)

Npoints = len(xloc)

#VAR Name : Location of the trench, Width of the trench, Depth of the trench, Thickness of the
    first layer (line_9), Gref (shear modulus of the first layer) (Line 21), Geofoam (Line 41)

Min = [2, 0.25, 2, 2, 81549, 0.5]
Max = [8, 1, 6, 10, 326198, 5.5]
popSize = 40
maxIter = 50
pm = 0.2 # probability of mutate
pc = 0.8 # probability of crossover

input_port_i = '10000'
```

```
input_port_o = '10001'
input_password = 'gkiePHMehran7075'# PUT YOUR PLAXIS 3D INPUT PASSWORD HERE
save_path = 'C:\Program Files (x86)\Plaxis\PLAXIS 3D' # r'C:\Plaxis\Data' # PUT THE
    FOLDER TO SAVE THE PLAXIS FILES HERE


def fitness(gene, xloc, Vy):
    D = gene[2]
    L = gene[3]
    if D>L:
        Out = TwoLayer_crossing.Calculation(gene, xloc, Vy)
    else:
        Out = TwoLayer.Calculation(gene, xloc, Vy)
    return Out

doLoad = False
if __name__ == '__main__':

    if not doLoad:
        pop = Genetic2.createPop(popSize, Min, Max)
        for i in range(0, popSize):
            pop[i].Fitness = fitness(pop[i].Genes, xloc, Vy)
        (bestFit, idx) = Genetic2.minFit(pop)
        print("In iteration 0\t best fitness value is {0:12.9f}".format(
            bestFit
        ))
        f_iter = 0
    iter0 = f_iter
    ConvergenceCurve = []
    NumberOfParent = 10
    K = 5
# Main loop for Genetic Algorithm
    for itr in range(iter0, maxIter):
# Parent Selection with K-tournament selection
        idr = Genetic2.ParentSelection(pop, popSize, NumberOfParent, K)
# Now we apply crossover on Parents
        NewPop = []
        for i in range(0, NumberOfParent, 2):
            id1 = idr[i]
            id2 = idr[i+1]
            if random.random() < pc:
                (newChrom1, newChrom2) = Genetic2.crossover(pop[id1], pop[id2])
                newChrom1.Fitness = fitness(newChrom1.Genes, xloc, Vy)
                newChrom2.Fitness = fitness(newChrom2.Genes, xloc, Vy)
                if newChrom1.Fitness<pop[id1].Fitness:
                    NewPop.append(newChrom1)
                else:
                    NewPop.append(pop[id1])
```

```
                if newChrom2.Fitness<pop[id2].Fitness:
                    NewPop.append(newChrom2)
                else:
                    NewPop.append(pop[id2])
            else:
                NewPop.append(pop[id1])
                NewPop.append(pop[id2])

# Now we apply Mutate on New population (NewPop)
        for i in range(0, NumberOfParent):
            if random.random() < pm:
                newChrom = Genetic2.mutate(NewPop[i], Min, Max, itr+1)
                newChrom.Fitness = fitness(newChrom.Genes, xloc, Vy)
                if newChrom.Fitness < NewPop[i].Fitness:
                    pop[idr[i]] = newChrom
                else:
                    pop[idr[i]] = (NewPop[i])
            else:
                pop[idr[i]] = (NewPop[i])
# find the best Chromosome in each Iteration
        (bestFit, idx) = Genetic2.minFit(pop)
# Print the best Result
        print("In iteration {0}\t best fitness value is {1:12.9f}".format(
            (itr+1),
            bestFit
        ))
        ConvergenceCurve.append(bestFit)
        f_iter = itr
        with open('GaData.pkl', 'wb') as f:
            pickle.dump([pop, f_iter], f)

    # var name: Location, Width, Depth, Thickness of the first layer,
    X = pop[idx].Genes[0]
    W = pop[idx].Genes[1]
    D = pop[idx].Genes[2]
    L = pop[idx].Genes[3]
    Gref = pop[idx].Genes[4]
    Geofoam = pop[idx].Genes[5]


    print("best value obtained with wx = {0:3.2f}, width = {1:3.2f}, depth = {2:3.2f}, length =
        {3:3.2f}, Gref = {4:3.2f} and , Geofoam = {5:3.2f}.".format(
        X, W, D, L, Gref and Geofoam
    ))
    print("best fittness value is: {0:12.9f} .".format(bestFit))
#print (Convergence Curve)
Genetic2.PlotResult(ConvergenceCurve)
```

Listing 9.22: Define operators of GA

```
import random
from matplotlib import pyplot as Plt

# The function is used for defining the chromosome, the function considered two concept for each
    chromosome, first the genes, which are in the chromosome and the fitness value for each
    chromosome
class Chromosome:
    def __init__(self, genes, fitness):
        self.Genes = genes
        self.Fitness = fitness

# Function for creating the initial population
def createPop(popSize, min, max):
# The number of genes (or dimensions), which is equal the minimum length of variables that in
    this algorithm is equal 5 because we have 5 variables
# We can using the funcion of len(max), which is equal to len(min), too, because it creates a
     flexibility to change the number of of valuebles automatically in Genetic file.
# More explanation, for instance if we change the number of variables in our code, we don't need
    to change in Genetic file, too. It can be done automatically because we didn't put a number
    for our chromosome length
    D = len(max)
    pop = []
# The random population is generated in the interval of [0, popSize], in which popSize is
    population size
    for i in range(0, popSize):
        chrom = []
# j is a coefficient for for specifying the specific gene that we are using (for instance depth
    or width etc.). This Gene is selected from (0, D), which D is the number of our gene
#In fact, j coefficient will say us that now we are working on which gene.
        for j in range(0, D):
# random.uniform function is used for creating a random number in the interval of [Min, Max]
    value of the specific gene that we randomly selected (in line 22)
# For instance in line 21, we randomly selected width as a gene for j, in this function we
    randomly select a value in the interval of Max and Min for width
            chrom.append(random.uniform(min[j],max[j]))
# Fitness function=0, because the fitness function in Main file is defined
        fitness = None
        pop.append(Chromosome(chrom, fitness))
    return pop

# Mutation Operator Function (Arithmetic method)
# The input in crossover function is chromosome1 and 2 (parent 1 and 2), which are selected
    parents by selection operator (K-Tournament selection method)
def crossover(chrom1, chrom2):
    newChrom1 = []
    newChrom2 = []
```

```
# Alpha is the coefficient of Arithmetic method, which is a random number in the interval of [0,
    1]
    Alpha = random.uniform(0, 1)
# Applying crossover and generating new children
    for i in range(0, len(chrom1.Genes)):
        newChrom1.append(Alpha*chrom1.Genes[i] + (1-Alpha)*chrom2.Genes[i])
        newChrom2.append((1 - Alpha) * chrom1.Genes[i] + Alpha * chrom2.Genes[i])
# The generated children after applying crossover (newChrom1 and newChrom2)
    newChrom1 = Chromosome(newChrom1, None)
    newChrom2 = Chromosome(newChrom2, None)
    return (newChrom1, newChrom2)

# Mutation Operator Function (Gaussian method)
# Input in mutation function is chromosome, Min and Max amount of variables and number of
    iterations, because sigma in the Gaussian mutation operator is defined based on these
    parameters
def mutate(chrom, min, max, Iter):
# Function for creating a random number in the interval of [0, len(min)], len(min) is the number
    of variables in the algorithm (5)
    index = random.randrange(0, len(min))
    Genes = chrom.Genes[:]
# Defining two main parameters in Gaussian mutation method (Mu, Sigma)
    Mu= Genes[index]
    Sigma = ((max[index]-min[index])/Iter)
    newGene = random.gauss(Mu, Sigma)
# Boundary Check, because the random generated number (random.gauss) may be out of interval
    of [Min, Max], so we need a boundary check
    if newGene>max[index]:
        newGene=max[index]
    if newGene<min[index]:
        newGene = min[index]
# The amount of Gene for random generated index in line 44, is the amount of new Gene
    (newGene)
    Genes[index] = newGene
    return Chromosome(Genes, None)

def minFit(pop):
    N = len(pop)
    idx = 0
    val = pop[0].Fitness
    for i in range(1, N):
        if pop[i].Fitness<val:
            val = pop[i].Fitness
            idx = i
    return (val, idx)

def PlotResult(Vector):
    Plt.plot(Vector)
    Plt.show()
```

```
def ParentSelection (pop, popSize, NumberOfParent, K):
    PrID = []
    for i in range(0, NumberOfParent):
        Canidate = random.sample(range(0, popSize), K)
        Fit = []
        for j in range(0, K):
            Fit.append(pop[Canidate[j]].Fitness)
        ID = Fit.index(min(Fit))
        PrID.append(Canidate[ID])
    return PrID
```

F Developing an app for predicting and optimizing the vibration

Problem definition

The process of organizing, storing, presenting and sharing of data is called research data management. The main aim of this process is to ensure the reliability and accessibility of research data for other users. In addition, it is an assurance that research data and results remain useful in the long term as users can easily access the data. It allows for reliable verification and permits new innovative research built on the existing information.

In this study, an artificial neural network, a quartic equation and a genetic algorithm model are developed to estimate the efficiency of trenches and optimize the governing parameters in vibration isolation in layered soil. In addition, almost $20,000$ models with different parameters are created in Plaxis, and the results are used for training and estimating the artificial neural network and the quartic equation.

There are some challenges in using the developed ANN model and genetic algorithm. The user should have access to the required software used for developing the models. In addition, the user should be able to read the code and operate the software. This will take a relatively long time when the user does not have any previous knowledge. In addition, in order to share the developed models, a long and complicated code should be shared. Generally speaking, easy accessibility, usability and capability of sharing the developed models are missing in the literature.

A software program is a set of machine-readable instructions, which are executed in a computer to perform specific operations. An application, which is labelled as app is a piece of computer software or a program that can be downloaded and installed on a computer or smartphone with a single action. Apps have become a powerful and easy method to help the user to perform specific tasks. Stand-alone applications can be installed and run on a computer or any device with a windows operating system. These apps include all necessary functions and do not need any extra license to be installed [Kalevo, 2019]. App development needs a programming language and a source code control to share an app with the source code of other developers and researchers to make it available for updating in the future. Matlab®, which is a numerical computing environment is used to develop the app. Matlab is used not only in academic and research institutions, but also in industries. Matlab App Designer allows for the plotting of data and the implementation of artificial neural network and genetic algorithm required for predicting and optimizing the parameters.

User interface (UI), in the industrial design field of human-computer interaction, is a tool, which assists humans to have better communication with a machine [Kalevo, 2019]. UI design

generally refers to the visual layout of the elements, in which a user might interact in an app. Basically, all apps are displayed to users by UI design, which plays a significant role in the usability of an app. An app with a complex UI design may confuse its users so they may not be able to find the information or services that they are seeking. The design of an app should lead the user directly to operate the app as quickly and easily as possible. The two procedures in Matlab which are employed to create a user interface include Graphical User Interface Development Environment (GUIDE) and App designer [Abu-Naser et al., 2016].

GUIDE is an interactive graphical system for designing and generating graphical user interfaces. It provides flexibility to the system designer while minimizing the amount of code which the designer must write [Turk, 2019]. App Designer is an interactive development environment for designing an app layout and programming its behavior. It provides a fully integrated version of MATLAB® editor and a large set of interactive UI components. It also offers a grid layout manager to organize one's user interface and automatic reflow options to make the app resizeable and respond to change in screen size. It lets you distribute apps by packaging them into installer files directly from the App Designer toolstrip, or by creating a standalone desktop or web app (requires MATLAB® Compiler™) [Yakimenko, 2019].

The main aim of developing the app is to create easy usability of the developed model without requiring advanced technical knowledge. An application is created with the help of Matlab App Designer in order to provide easy access to the developed artificial neural network, the estimated quartic equation, and genetic algorithm code.

MATLAB App Designer

Matlab contains development tools as step by step simulations and code checkers to analyze code and its functionality. Also, it is possible to record the time of code execution and to do directory reports, which find the differences and dependencies of the files as well as the efficiency and coverage of the code. In addition, it is possible to make Graphical User Interfaces (GUI) in Matlab. GUIs are possible to make programmatically with GUIDE (Graphical User Interface Developer Environment) and with the newest method, i.e. App Designer environment (published in 2016). Each of these methods of building apps have their differences in functionalities and building processes. The choice of a method depends on project needs or the preference of the working. GUIs can be used to show one's algorithms and to provide a better user experience. GUIs are also possible to deploy for standalone applications with the deploy tool [Kalevo, 2019].

In App Designer, the file mode is difference from other versions. While, in programmatical way, the file mode is (*.m*), whereas in App Designer the file mode is (*.mlapp*). The working environment is external and the code of an application is written with an external editor that is integrated with a layout view. The layout windows is called 'Design View' and the editor is called 'Code View'. In the layout section, the visual components are added with the drag-and-drop method. The application gives hints in alignment to get a precise layout [Jaluria, 2019].

Developing Anti-Vibration App

In this study, an app is designed and developed to predict efficiency and optimize different values for reaching the required efficiency. Recently, the availability of data and results of parametric studies are of interest for researchers so that they can use them to validate the developed models or to update the results. For this purpose, all used data for training ANN model are attached in the App. Therefore, all results are usable for validating the developed finite element model by other researchers.

The main aim of this app is measuring the efficiency of the installed trench in layered soil for mitigating the vibration at ground surface. In summary, the efficiency, which is presented in percentage means how successful is the trench in mitigating the vibration. Some key factors influence the efficiency of the trench including the dimensions of the trench (depth and width), location, material for filling the trench (density of the material) and the properties of the soil (thickness of the first layer and shear wave velocity of the soil). In conclusion, there are six different parameters to evaluate, which are, depth (D), width (W), location of the trench (L), the density of the material for filling the trench (EPS), thickness and shear wave velocity of the first layer of the soil (L and V_s). The main advantages of the developed App are:

1. We don't need any finite element program for calculating the efficiency of the trench. The efficiency will be calculated directly with the app
2. The app is easy to understand and to use
3. There is a possibility to import new data to the app, so it can be used for every researcher in this field when using Artificial Neural Network and Genetic Algorithm
4. This app can be upgraded by other users, too. It means that the user can add some sections or create some changes in different sections to improve the app
5. Installing the app is easy and does not need any extra license

There are four different parts in the developed app.

Fig 9.2. shows the home page of the app, which includes tabs and a short summary of the app and its application. There are four sections based on the available tabs and clicking on any of the tabs leads the user to reach the requested section. A callback function is defined for each button to lead the program to the selected section. A callback function is a function that passes an argument to another function, to be called back at a later time. In addition, a summary of the app is presented in the homepage section, in which the user gets an overview of the app and the different sections.

The first part, which is called 'Plot Section', presents the result of the parametric study for calculating the efficiency of the geofoam-filled trench in layered soil. The collected data are the result of running approximately $20,000$ Plaxis Models. Fig. 9.3 represents the plot section of the app.

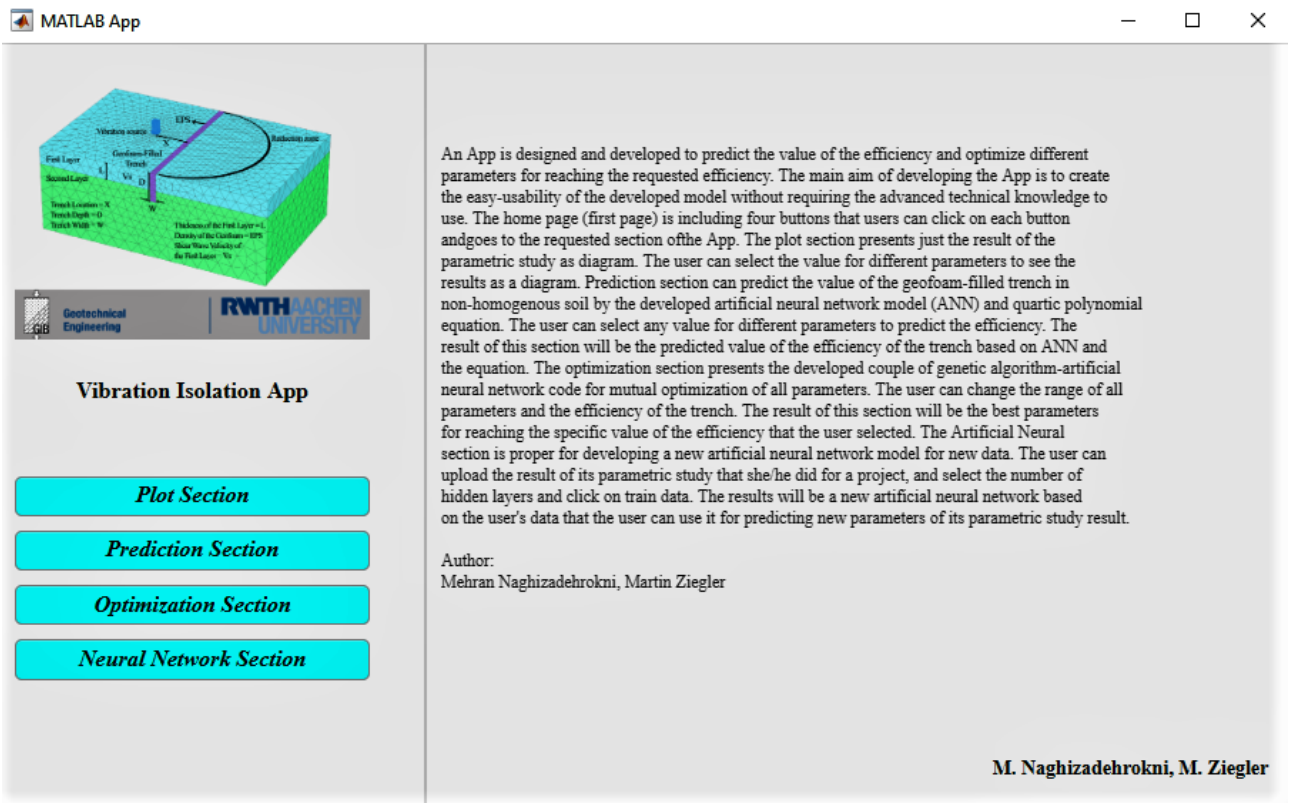


Figure 9.2: Homepage of vibration isolation app

Six different drop-down lists enable the user to select different variables for drawing a diagram. The parameters to be defined are the same as the ones in the parametric study including the location, depth and width of the trench. In terms of properties of the soil, the thickness and shear wave velocity of the first layer, which are known as L and V_s, can be selected. Finally, EPS geofoam for filling the trench can be selected with different densities. Selecting the main variable specifies the value on the X axis in the diagram. The Y axis always represents THE efficiency. The rest of the parameters are considered fixed, which are kept constant during each plot. A plot function is defined in order to auto-draw diagrams after changing each value of the parameters. However, the operation of drawing the diagram for the first time is executed by clicking on the (Plot) button. This section can be used by other researchers for validating a newly developed model in vibration isolation topic in homogeneous and layered soil since the whole properties of the used soil in the parametric study is presented in this section as an extra information by clicking on question mark.

All data are located into the app and this is an advantage of the developed app, which is open source. Therefore, the app can be be upgraded by other researchers by adding some extra data in other ranges, which are not included in this version (from version 1.0 to upper version).

In each part of the app, some extra information is presented through defining a help calback function, which is visible as a question mark. These question marks give some extra information about different parts.

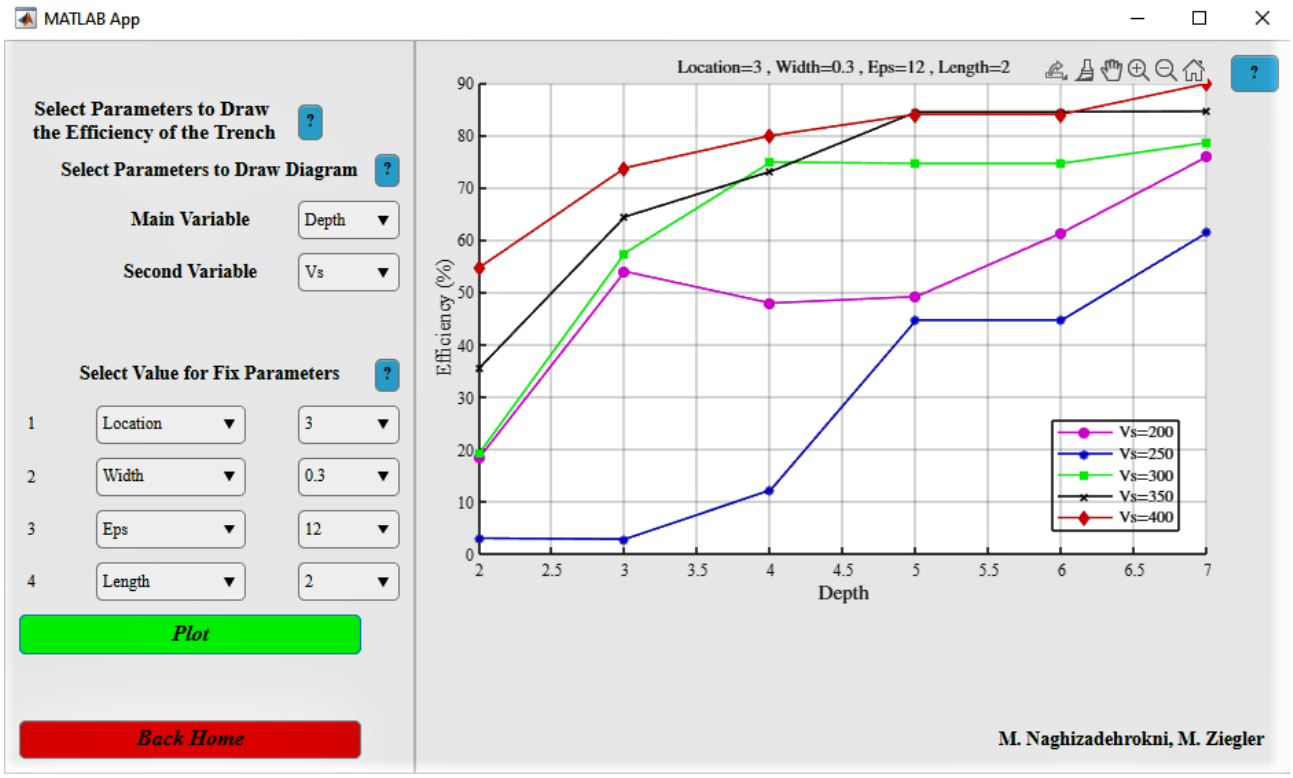


Figure 9.3: Homepage of Plot section in the app

There are different methods to measure the efficiency of a trench, which include developing a numerical model, experimental or laboratory tests or an analytical method. However, all of these procedures need a lot of time to understand the topic and sometimes would be really expensive. In order to overcome this disadvantage, the second part, which is prediction tab for predicting the efficiency of the geofoam-filled trench in layered soil is added to the app. Several functions are defined in the predict section, which is illustrated in Fig. 9.4 for executing different orders.

There are two methods for importing data from the (Data Source) drop up, which are (costume data) or (read from the file), respectively. For custom data, the user is able to insert the values for different parameters. Since the ANN model and quartic polynomial equation are developed based on the results of the parametric study, a function is defined to create a specific limit for each parameter to prevent setting a parameter out of range. The user should pay attention to keep the range of all parameters in the same range as in the parametric study, which is presented in the 'Plot Section'. Concerning importing method (read from the file), unfortunately, there is not any possibility to write the same function for the uploaded Excel file. Therefore, the user should pay attention to keep the range of all parameters in the same range as in the parametric study, which is presented in the Plot section. In addition, the order of putting all input parameters in a row in the Excel file should be the same order as the custom data.

After importing the requested data either through custom data or uploading a file and pushing the 'Predict' button, the app predicts the value of the efficiency based on the percentage. For

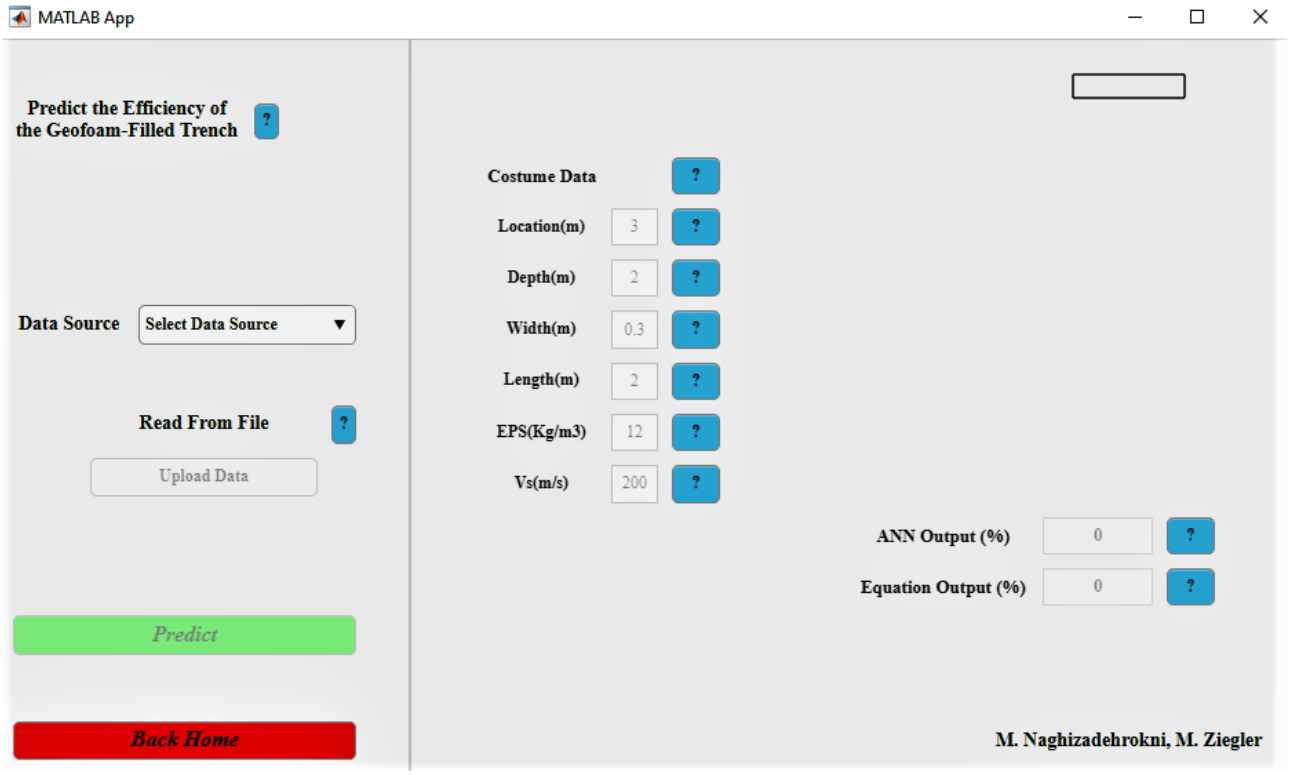


Figure 9.4: Homepage of prediction section in the app

this purpose, the app uses the developed ANN model and quartic polynomial equation. The implemented ANN model and equation are defined as two different functions in the app. Finally, the app will calculate the efficiency of the geofoam-filled trench based on the input parameters and the results are shown in the output box.

Fig. 9.5 shows the homepage of 'Optimization Section'. The most important problem of the developed GA in the parametric study is evaluating the goodness of the chromosomes since the developed algorithm should use a finite element program like Plaxis or Abaqus for calculating the efficiency of the trench. The drawback of using FEM is the calculation time since using Plaxis in optimization process of input parameters takes several hours. In addition, the user should develop a script for automating the model and this leads sometimes to define some extra functions, which is challenging. In order to deal with all of these challenges, a couple of genetic algorithm-artificial neural network code is implemented for the third section of the app for mutual optimization of all the parameters. The developed ANN model is used for evaluating the goodness of the chromosomes.

The only parameters, which should be inserted in the app is the range of input parameters as the minimum and maximum value of each parameter. In addition, a restriction value for the efficiency of the trench is defined, which can be changed by the user. Since the main purpose of the app is easy use of the developed models, the rest of the adjustments including the number of iterations and functions of genetic algorithm operators are considered to be default values. However, all different operators of the GA code are changeable in the code

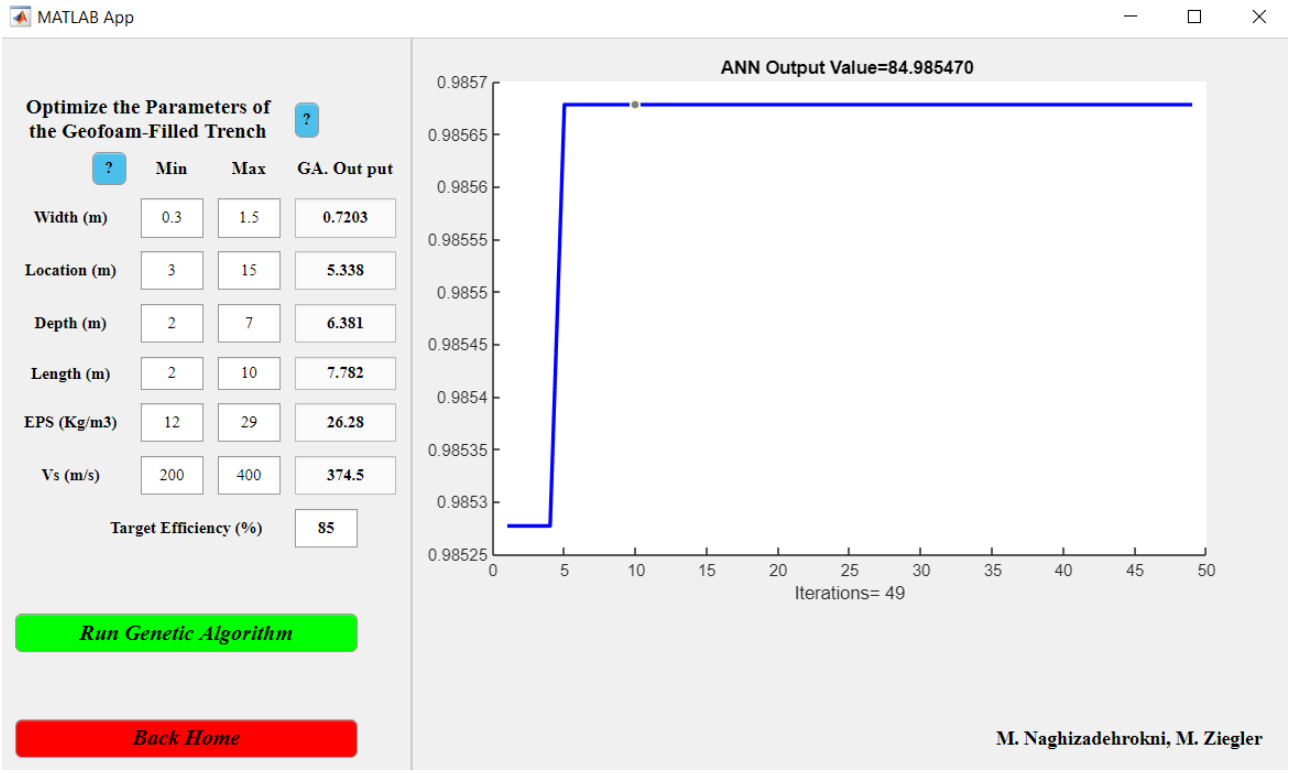


Figure 9.5: Homepage of optimization section in the app

section. The process of optimizing the parameters for different iterations can be monitored by the convergence curve. Finally, the optimized parameters are presented in the GA output section. In addition, some callbacks functions are defined as question marks for explaining different sections of the optimization section.

Applying an Artificial Neural Network to new data needs understanding the principle of neural networks and implementing an ANN including activation and training functions. Fig. 9.6 illustrates the last section of the app, which is available for training new data through the ANN model.

This model can be used either for vibration isolation or any other topic. The user just needs to prepare an excel file, which includes the input data and the result. There are two different kinds of data, which are independent and dependent. All input parameters are independent data and the result of the parametric study is dependent data. The order of the parameters is not important but the last column should be the result of the parametric study, which is the dependent parameter in ANN. All adjustments of the ANN model including the fitness and training function, categorizing of the train and test data and coefficients for evaluating the performance of the model are fixed. The number of hidden layers and number of neurons in each layer are the only changeable section of this part of the app since the number of hidden layers and number of neurons are problem-dependent. The activation function of all hidden layers and training function are considered Logsig and Tranlm functions. In addition, the ratio of distributing the train, validation and test data is 50, 25, and 25%, respectively. A function is

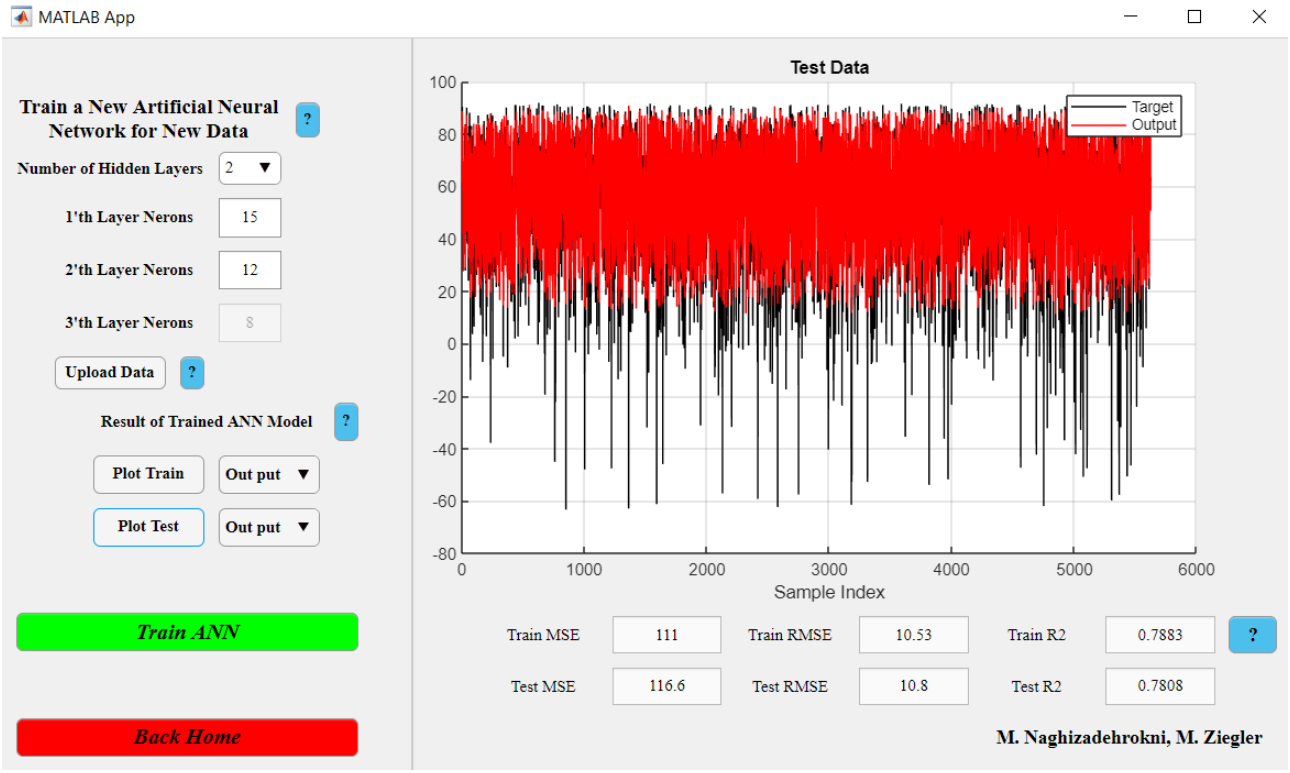


Figure 9.6: Homepage of neural network section in the app

defined to upload the original data which is supposed to be trained by the user through 'Upload data' button. 'Train ANN' button is a callback function for activating the training process of new data with the ANN model. The result of the developed ANN model for the new data is stored at in the same folder path that the user used for uploading data.

The last step is evaluating the performance of the ANN model. This is done through defining coefficients that show the performance of the developed ANN model, which are MSE, RMSE, and R-value for train and test data. A function is defined for each coefficient to calculate the value of the error of the new ANN model. In addition, the output, error, and regression of the train and test data can be plotted through plot train in order to get an overview from the new model.

Conclusion

The most important challenge of scientific research is the accessibility and reachability of data and results. Practical research data and results allow for reliable verification to other users and permit new innovative research built on the existing models. To deal with this challenge, an application has been developed for easy use and sharing of all the developed models and data. The user can install the app and use it in order to access all data, predicting the efficiency of the trench and optimizing the governing parameters.

- The most important feature of the app is the easy use of all sections without having any base knowledge of artificial neural networks or genetic algorithms. In addition, the app is open to be upgraded in terms of data and improvement of the developed models.
- A couple of genetic algorithm-artificial neural network models are implemented in order to replace the finite element model for assessing the goodness of each chromosome and calculating the efficiency of the trench.

G Diagrams of parametric study for layered soil

Diagrams of parametric study for layered soil for frequency of 50 Hz

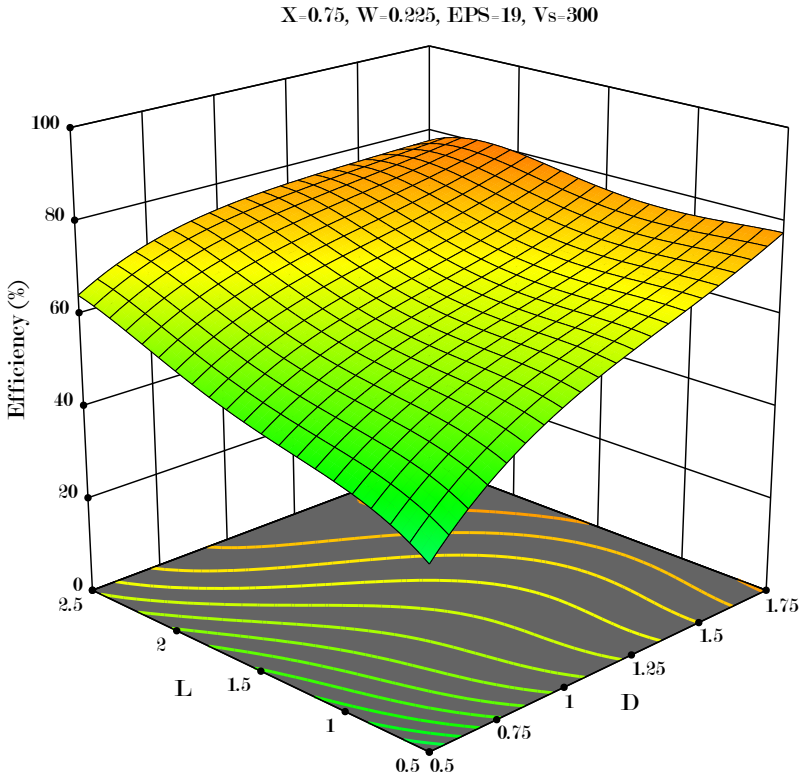


Figure 9.7: Interaction of D and L on the response of the trench ($X = 0.75$)

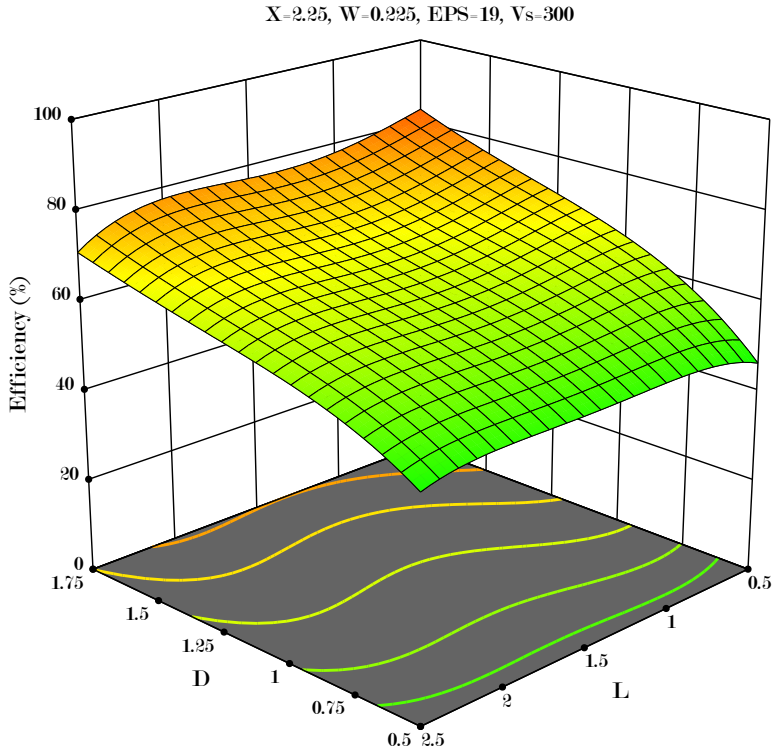


Figure 9.8: Interaction of D and L on the response of the trench ($X = 2.25$)

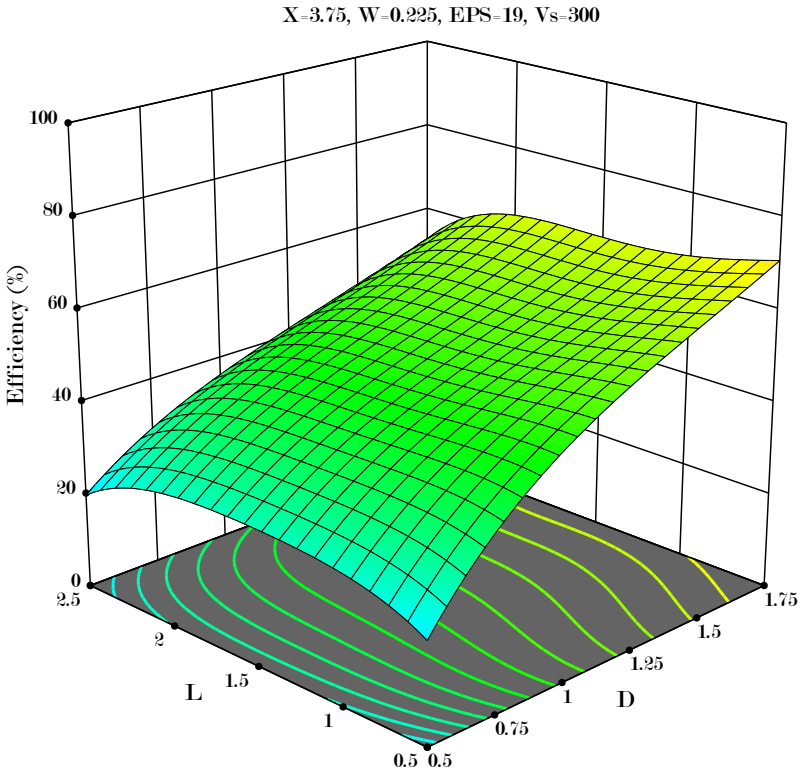


Figure 9.9: Interaction of D and L on the response of the trench ($X = 3.75$)

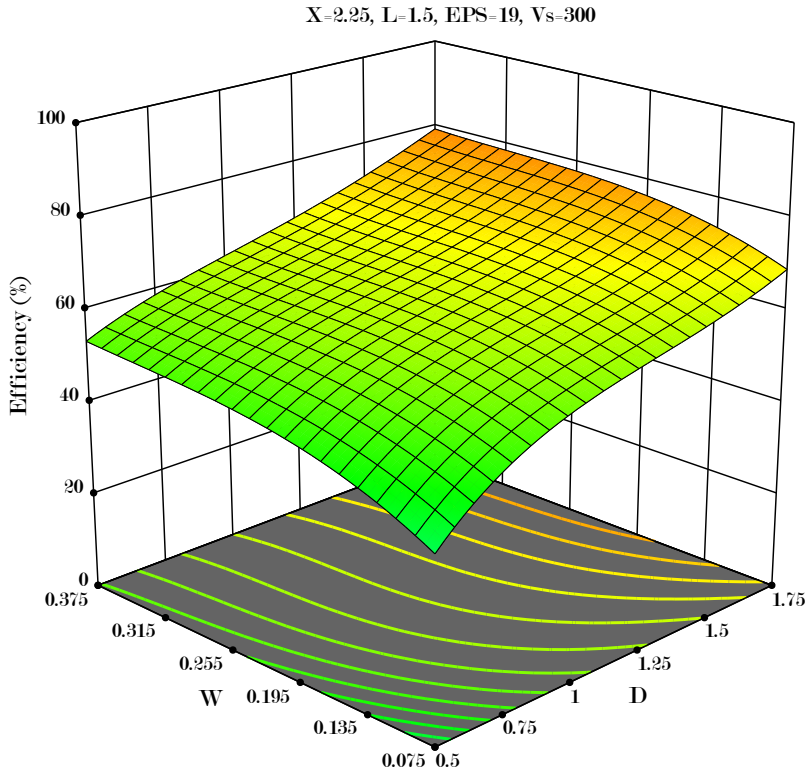


Figure 9.10: Interaction of D and W on the response of the trench ($X = 2.25$)

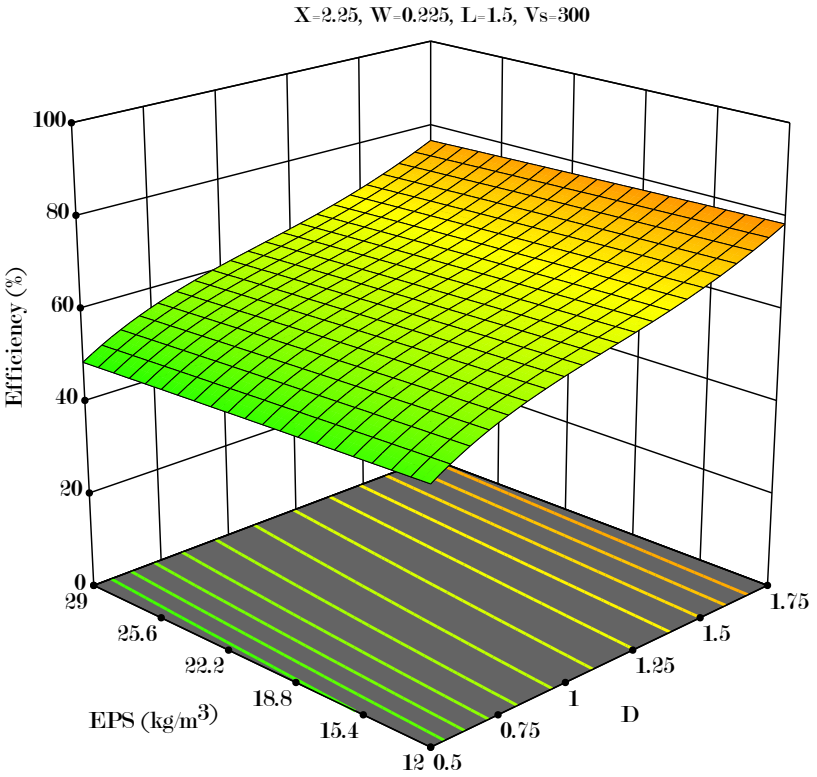


Figure 9.11: Interaction of D and EPS on the response of the trench ($X = 2.25$)

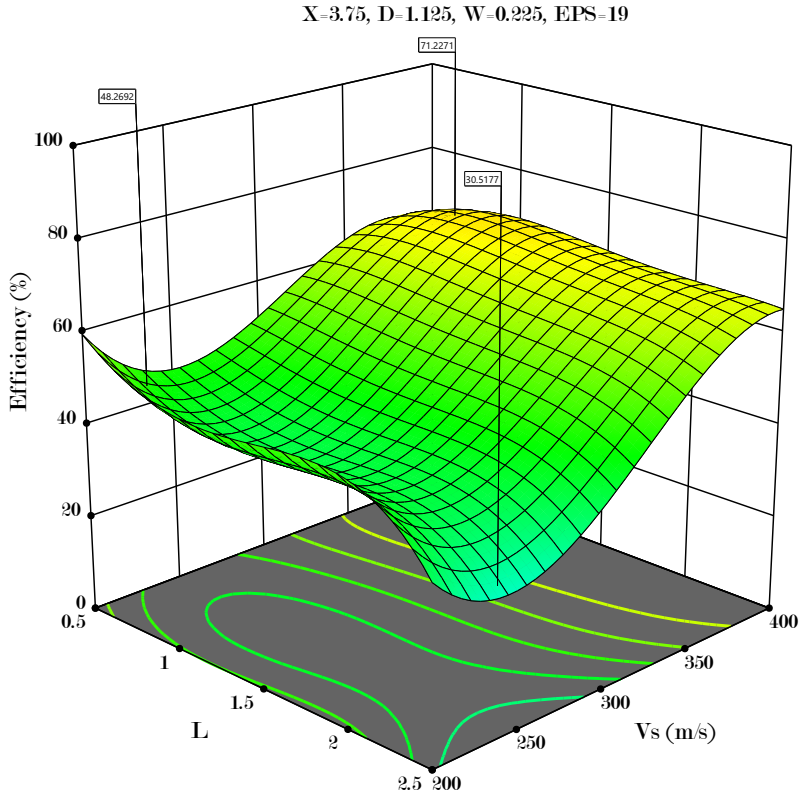


Figure 9.12: Interaction of V_s and L on the response of the trench ($X = 3.75$)

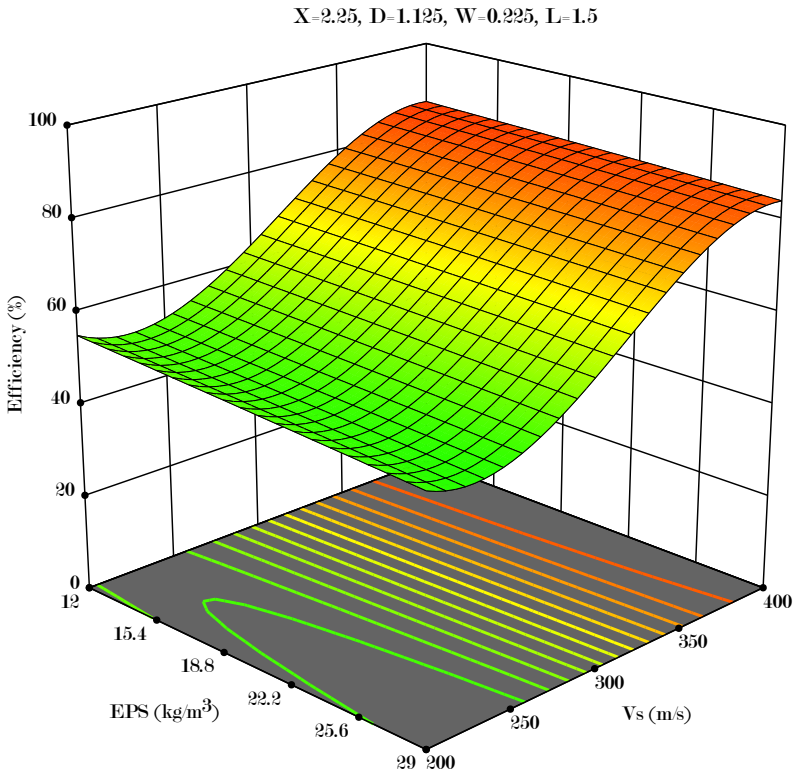


Figure 9.13: Interaction of V_s and EPS on the response of the trench ($X = 2.25$)

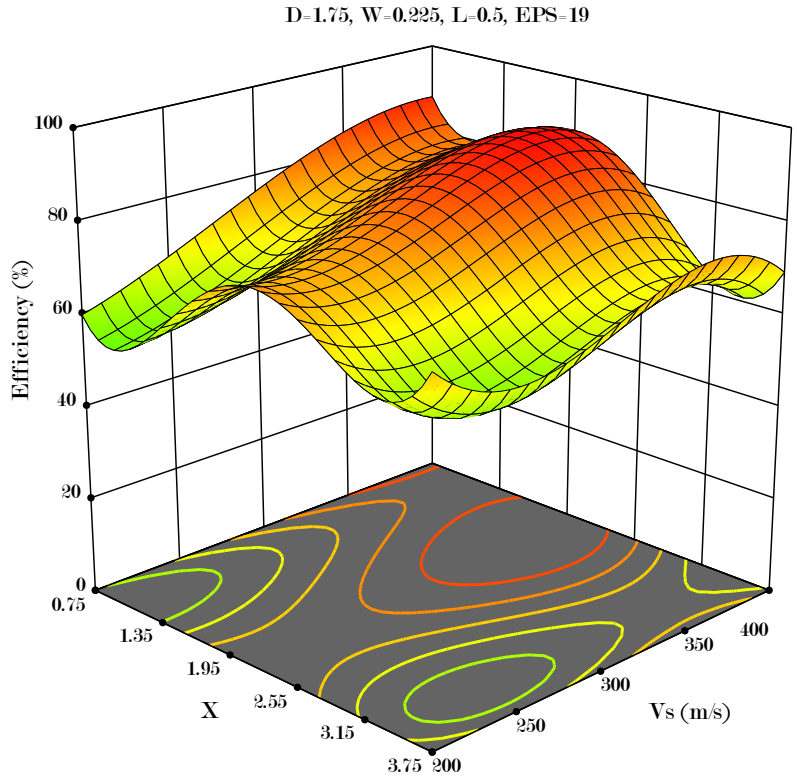


Figure 9.14: Interaction of V_s and X on the response of the trench ($D = 1.75$)

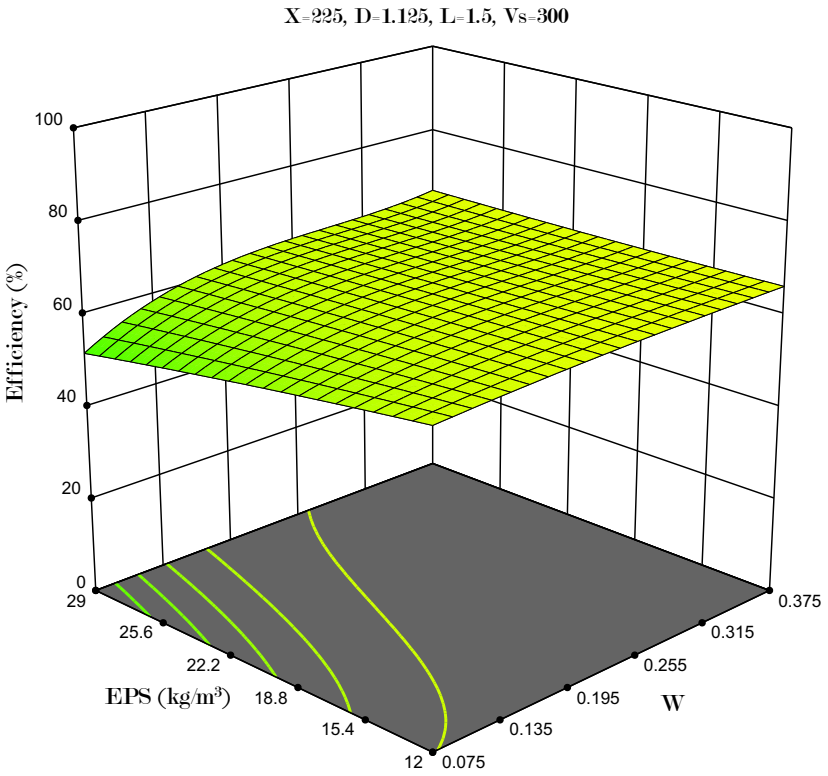


Figure 9.15: Interaction of W and EPS on the response of the trench ($X = 2.25$)

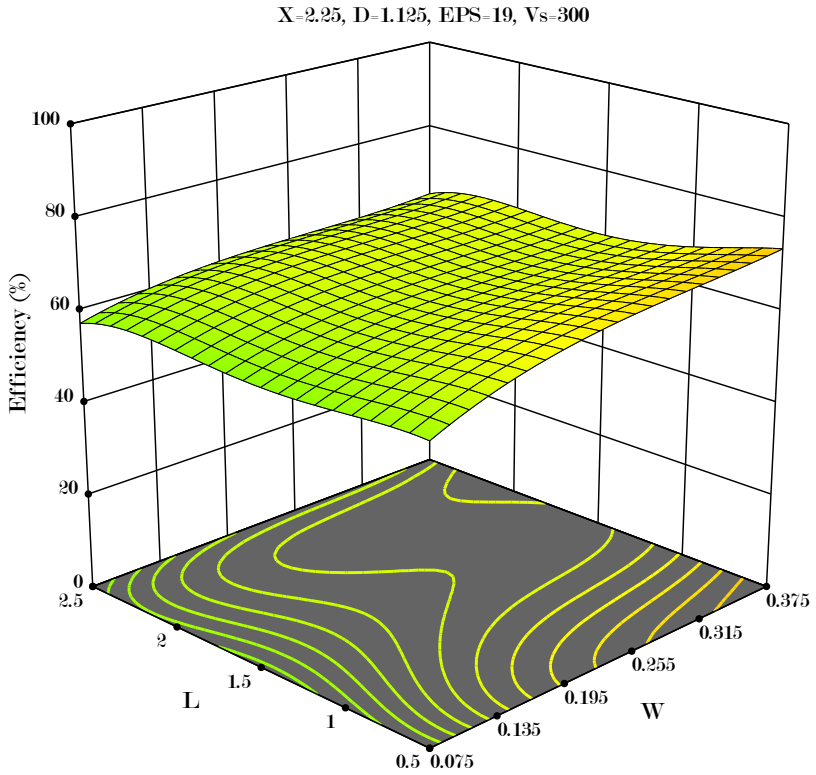


Figure 9.16: Interaction of W and L on the response of the trench ($X = 2.25$)

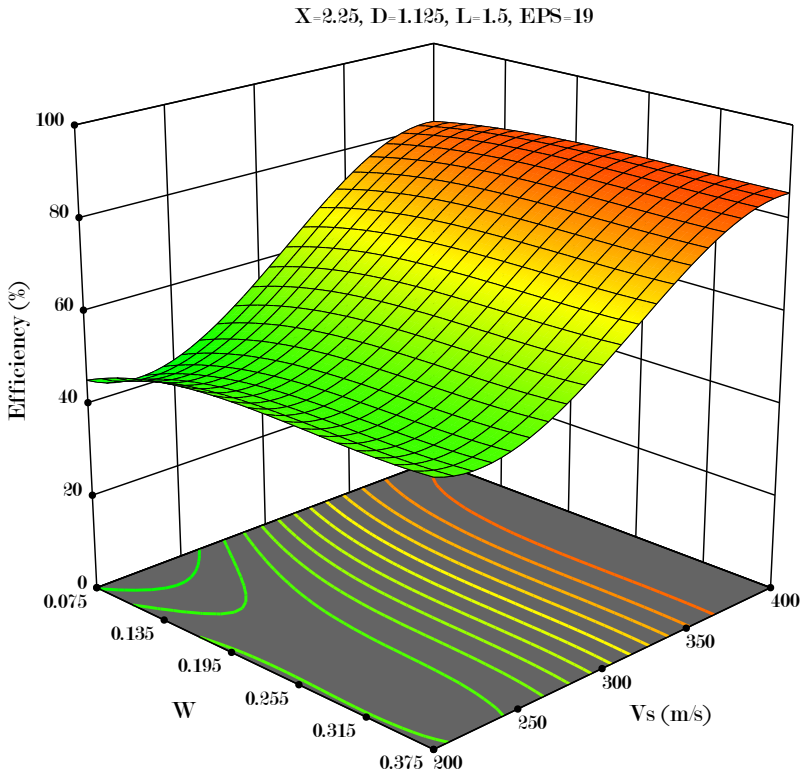


Figure 9.17: Interaction of W and V_s on the response of the trench ($X = 2.25$)

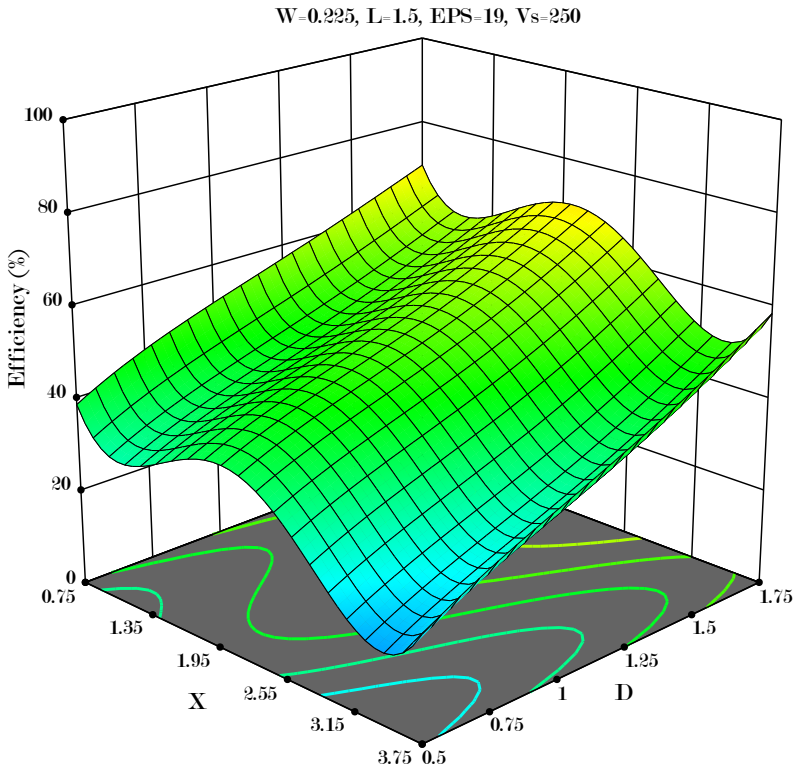


Figure 9.18: Interaction of X and D on the response of the trench ($V_s = 250$)

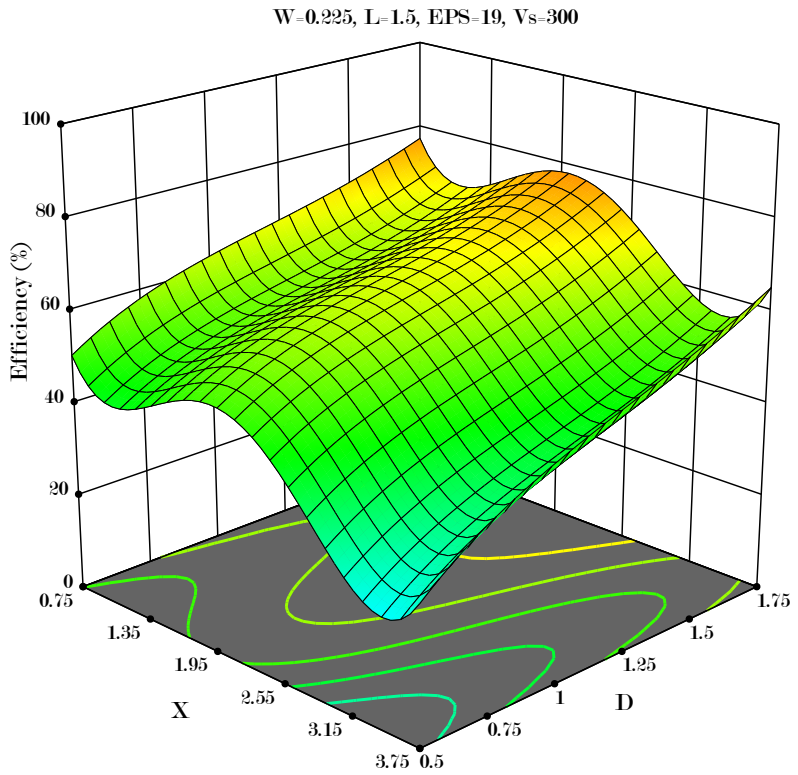


Figure 9.19: Interaction of X and D on the response of the trench ($V_s = 300$)

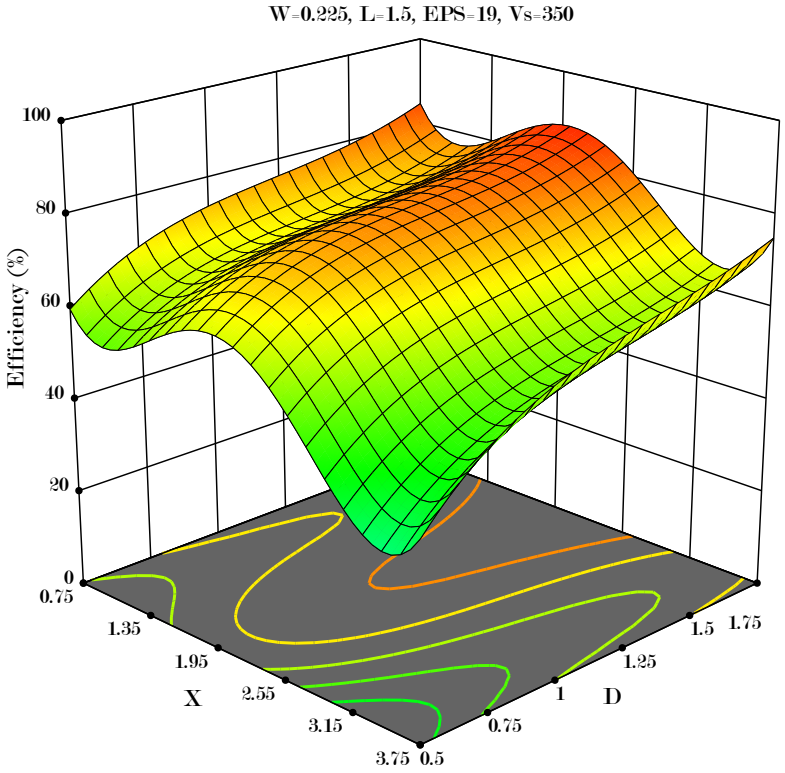


Figure 9.20: Interaction of X and D on the response of the trench ($V_s = 350$)

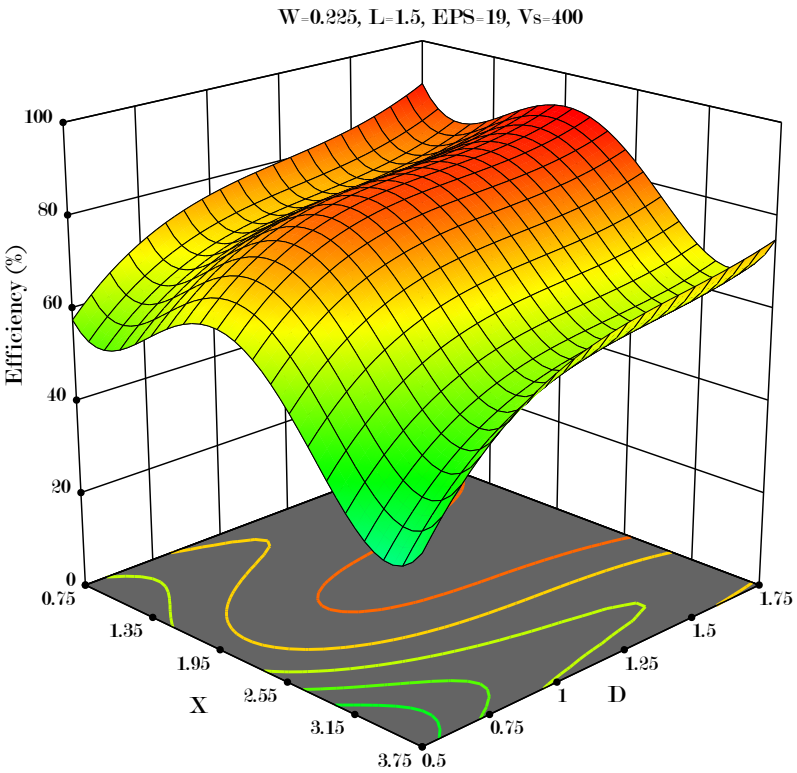


Figure 9.21: Interaction of X and D on the response of the trench ($V_s = 400$)

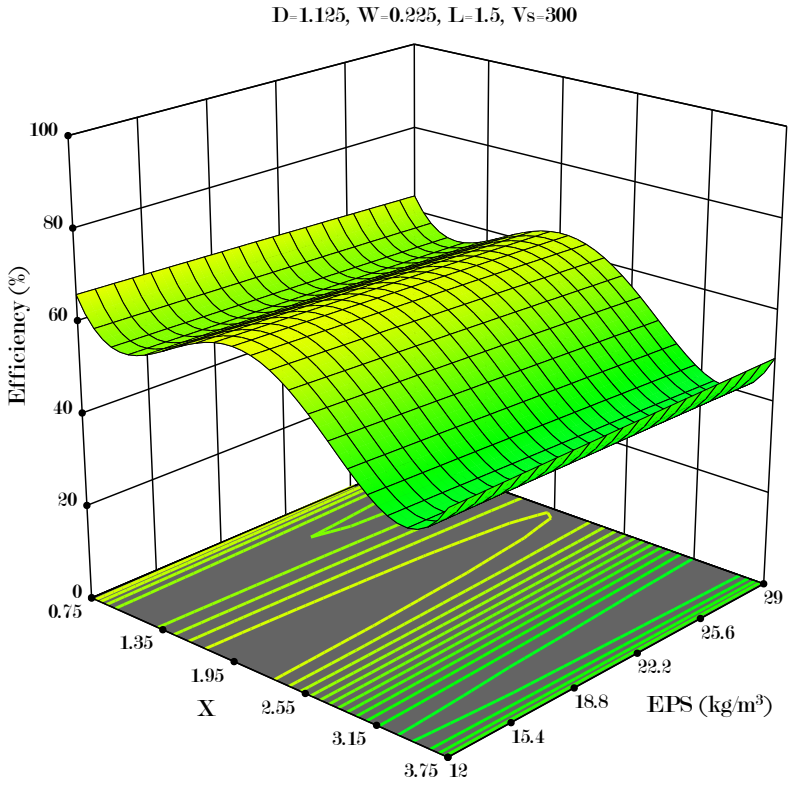


Figure 9.22: Interaction of X and EPS on the response of the trench ($D = 1.125$)

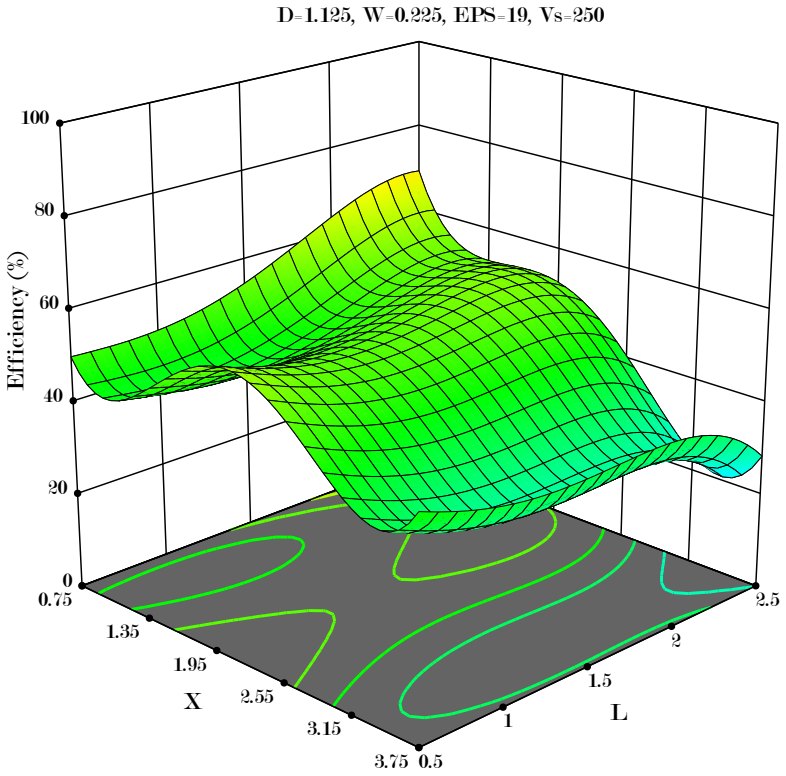


Figure 9.23: Interaction of X and L on the response of the trench ($D = 1.125$)

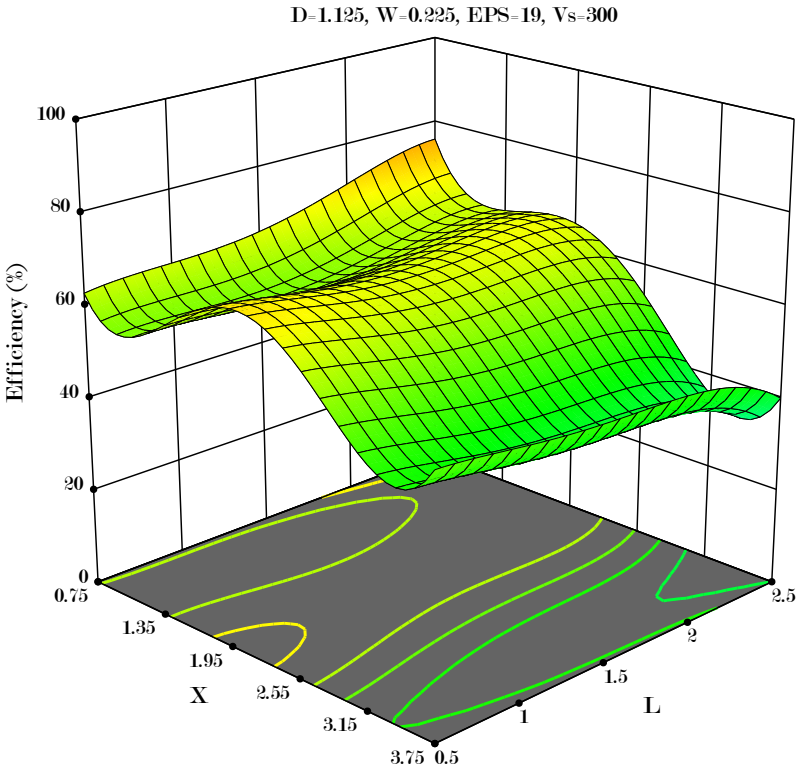


Figure 9.24: Interaction of X and L on the response of the trench ($D = 1.125$)

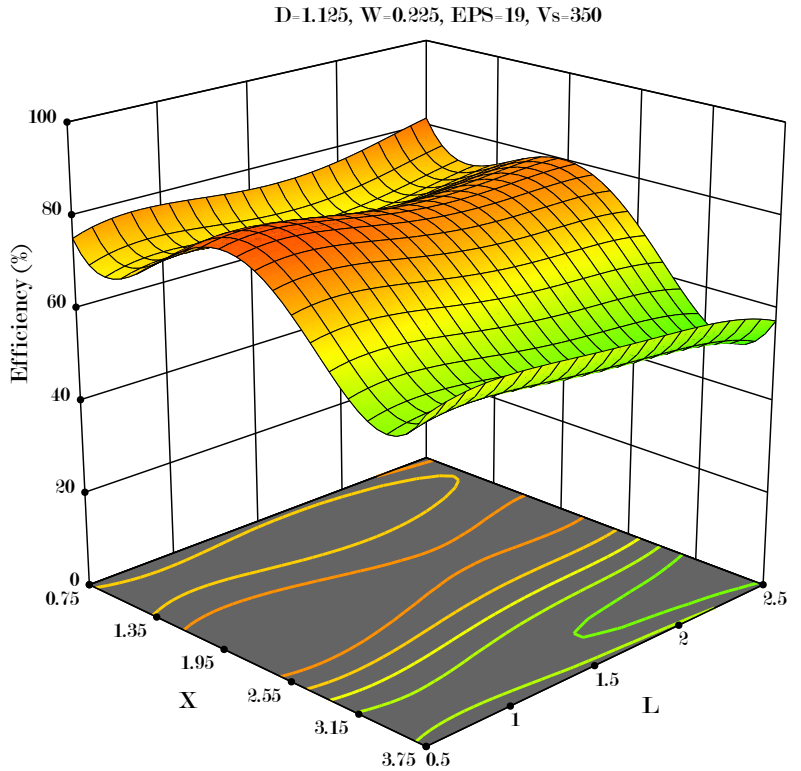


Figure 9.25: Interaction of X and L on the response of the trench ($D = 1.125$)

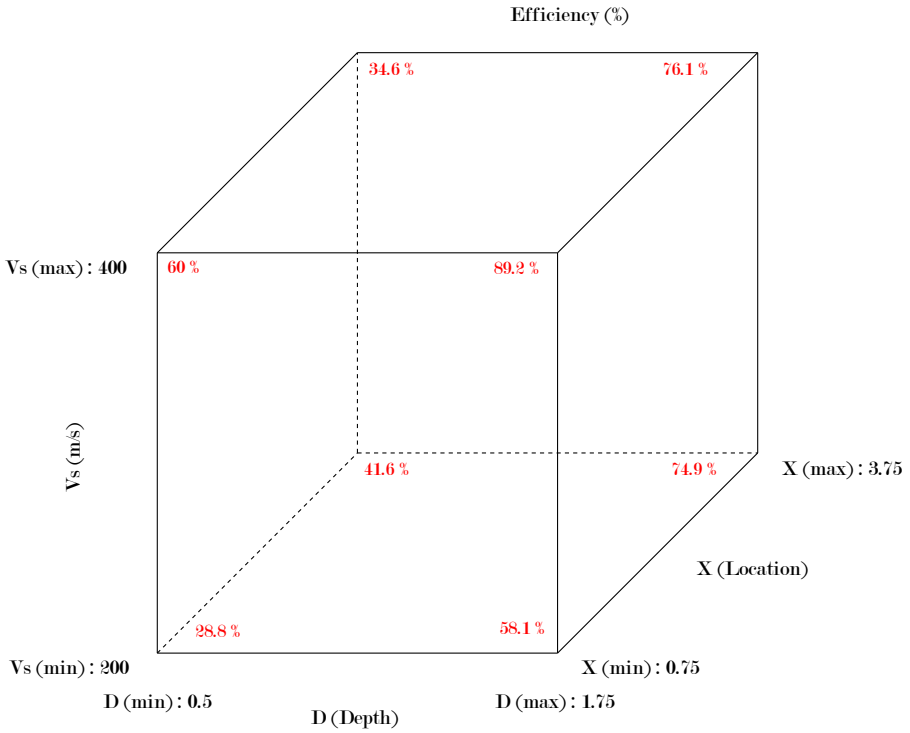


Figure 9.26: Interaction of X, D and V_s on the efficiency of the trench

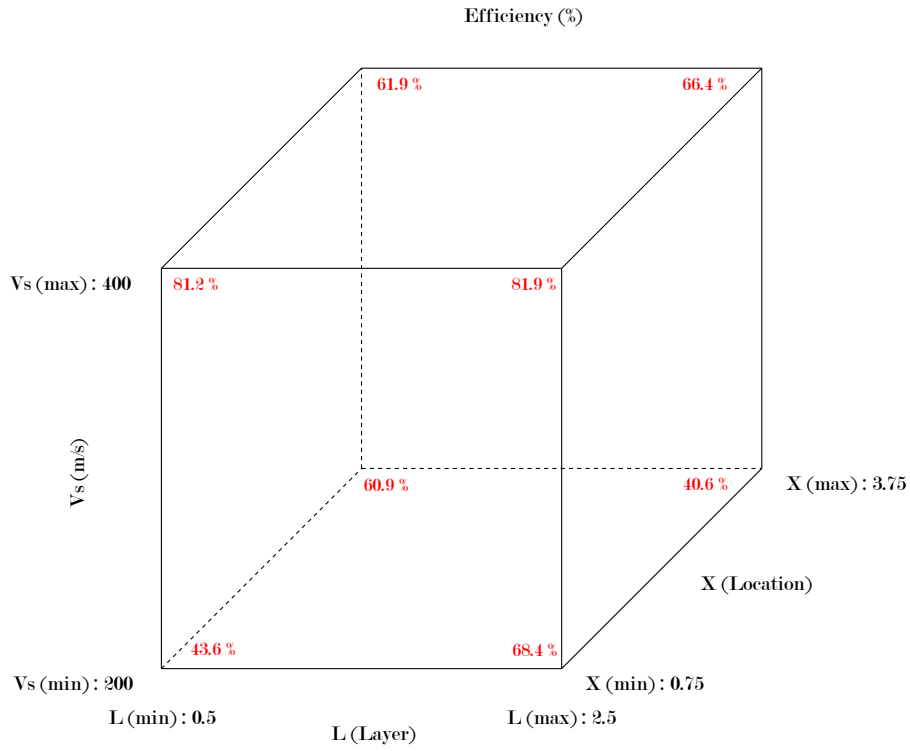


Figure 9.27: Interaction of X, L and V_s on the efficiency of the trench